Calibration of Fatigue Design Factors and Fatigue Life Reliability of Steel Highway Bridges Using WIM Databases

by

Ahmed Mostafa Tawfik Farag

A thesis submitted in partial fulfillment of the requirements for the degree of

Doctor of Philosophy

in

Structural Engineering

Department of Civil and Environmental Engineering
University of Alberta

ABSTRACT

Fatigue life assessment of steel highway bridges is crucial to maintain their safety. Researches are required to quantify uncertainties in loading, resistance, fatigue life prediction and improvement techniques. This study calibrates some fatigue code parameters and models fatigue loading probabilistically using truck data in Canada. Fatigue life improvement by weld toe grinding is assessed experimentally and numerically. Finally, the remaining fatigue life using reliability-based method for cruciform bridge welded detail is predicted.

Truck data screening is vital to ensure its quality in calibration and load history prediction. Three different fatigue truck factors and equivalent number of cycles are proposed, using single and dual slope curves, for three bridge span ranges. Span length and fatigue category affected the calibration in short spans and dual slope curves. Using Ontario and Quebec data, probabilistic distributions for stress-range histograms for bridge spans and configurations are developed.

Weld toe grinding improved the fatigue life by 60% for category E joint compared to the non-ground specimen. Still, weld imperfections might adverse grinding effect. In deterministic fatigue life prediction, energy-based approach is used for crack initiation, while linear elastic fracture mechanics is used for crack propagation. An initial spherical flaw size of 0.1 mm with no residual stresses leads to the most precise prediction of fatigue resistance for test specimens.

For the probabilistic fatigue life prediction of cruciform detail of 6.4 mm fillet weld size, the fatigue life of the concave weld profiles are usually larger than the convex ones. The study developed a method to convert the probabilistic stress range into number of cycles for remaining fatigue life reliability of steel detail. The generated reliability illustrates the fatigue repair and inspection management.

ACKNOWLEDGEMENTS

The thesis work presented herein was carried out at the Markin/CNRL Natural Resources Engineering Facility and the I.F. Morrison Laboratory of the University of Alberta. This research was mostly funded by the Natural Sciences and Engineering Research Council of Canada and AMEC Infrastructures in Edmonton through doctoral industrial postgraduate scholarship (IPS2). Scholarships from the Faculty of Graduate Studies at the University of Alberta (Provost Doctoral Entrance Award for two consecutive years), Citizenship award from Government of Alberta and Transportation Association of Canada are acknowledged with gratitude.

I would like to thank Dr. Samer Adeeb. Without his support, guidance and help, this work won't be carried out. The gratitude is also offered to Dr. Roger Cheng, the department head of the civil and environmental engineering.

I would also like to sincerely thank the examining committee, which consisted of: Prof. Han-Ping Hong, Prof. Roger Cheng, Prof. Jozef Szymanski, Dr. Marwan El-Rich, Dr. Mustafa Gul (chairman) in addition to Dr. Samer Adeeb for their comments that are greatly appreciated.

In addition, I would like to extend a big "thanks" to my family back in Egypt for their understanding and support during these last six years. These years saw difficult times especially with the passing of my father. My last big "thank you" is also a personal one to my wife for her support, patience, understanding, care and encouragement throughout this study.

TABLE OF CONTENTS

LIST OF FIGURES

LIST OF TABLES

LIST OF SYMBOLS

a_{init}	initial flaw size
a_0	initial crack size
a_f	final crack size
$(a/c)_{init}$	initial crack aspect ratio
ADTT	average daily truck traffic
b	fatigue strength exponent
c	fatigue ductility exponent
C	fatigue crack growth parameter
CAFL	constant amplitude fatigue limit
CHBDC	Canadian Highway Bridge Design Code
CL-625	fatigue design truck for bridges of GVW 625 kN
CL-800	fatigue design truck for bridges of GVW 800 kN
C_L	reduction factor
CJP weld	complete joint penetration weld
$\frac{da}{dN}$	crack propagation rate
D_{code}	fatigue damage due to design truck
D_{real}	fatigue damage due to real truck
E	WIM weight error (%)
FHWA	Federal Highway Association
FTF	fatigue truck factor
GVW	gross vehicle weight

G(Z)	limit state function
K_i	stress intensity factor
L	bridge span length
LEFM	linear elastic fracture mechanics
LN	lognormal distribution
m	S-N slope
MCS	Monte Carlo Simulation
MOU	Memorandum of Understanding on vehicles weights and dimensions
n’	cyclic hardening exponent
N	number of stress cycles to failure
N_a	number of applied cycles due to loading
N_C	total cycles to failure using single or dual slope fatigue design curves
N_d	number of stress cycles experienced for each passage of the design truck
N_{init}	fatigue crack initiation life
N_{prop}	fatigue crack propagation life
N_r	number of cycles due to fatigue resistance
N_{total}	total fatigue life
NWT	Northwest Territories
p_f	probability of failure
pdf	probability density function
r_i	random number
R	stress ratio and resistance factor
S	load effect

S-N curves stress range versus number of cycles curves

SWT Smith-Watson-Topper model for strain energy approach

TAC Transportation Association of Canada

T_N total number of design trucks

TIG tungsten inert gas

UIT ultrasonic impact treatment

WIM weight in motion

W_{WIM} weight recorded by the WIM system

W_{static} weight recorded by the static scale

x_i sample input value

X_i basic random variable

β reliability index

β_G stress gradient correction factor

γ fatigue life constant

$\Delta\varepsilon^p$ plastic strain range

ΔK_{th} threshold stress intensity factor range

ΔK stress intensity factor range

ΔW^p plastic strain energy density per cycle

ΔW total strain energy density

ΔW^T plastic plus tensile elastic strain energy density per cycle

$\Delta\sigma$ stress range

$\Delta\sigma_{\max,des}$ maximum stress range induced from the load history due to design truck

$\varepsilon_f^{'}$ fatigue ductility coefficient

σ_ε standard deviation of standard WIM error

$\sigma_f^{'}$ fatigue strength coefficient

$\sigma_{\max}$ maximum local stress accounting for plasticity

$\sigma_{\max,app}$ maximum applied stress at weld flaw vicinity

$\sigma_{\min,app}$ minimum applied stress at weld flaw vicinity

σ_{res} residual stresses

σ_R standard deviation of resistance

σ_S standard deviation of load

σ_z WIM accuracy standard deviation

σ_Z standard deviation of G(Z)

μ_R mean value of resistance

μ_S mean value of load

μ_Z mean value of G(Z)

1. INTRODUCTION

1.1. Motivation

Infrastructure is a major cornerstone for the development of any country. In many cases, these infrastructure were designed and constructed many decades ago, when the loading condition and design standards were different from those that are currently used. Therefore, it is important to assess their present status from a structural perspective to ensure their safety under operating conditions. This assessment should comprise loading, material properties, fatigue and corrosion effects, etc. Among various types of infrastructure, steel highway bridges are in great need to apply such assessments.

Throughout the service life of many bridges in Canada, traffic loading and volume increased tremendously. This increase has a detrimental effect on the current status of these bridges as it increases the stress cycles that might lead to fatigue failures at critical locations i.e. welded details. Steel bridge failures could cause human fatalities in addition to catastrophic economic losses. The human losses have a shocking impact on the society since it is related to the public safety, whereas the economic losses require financial plans to cover the cost of the rehabilitation in some cases, and the replacement of the entire structure in other cases.

In a study considering the cause of damage and type of structures, Oehme (1989) found that fatigue is ranked to be the first cause of damages for bridges with 38.3% for 128 reported damages in the period of 1955 to 1984. For bridges in Canada in the period of 1987 to 1996, Carper (1998) stated that the failure causes of structural components of bridges are: 8 failures due to overloads, 12 failures due to fatigue, and 18 failures related to deterioration other than fatigue. For that reason, it is crucial to seek innovative methodologies and develop advanced technologies to reduce the fatigue effect phenomenon. Equally important, recent studies should carryout reliable assessment of the remaining fatigue life for critical welded details in steel bridges which are considered to be vital components serving the transportation infrastructure in Canada.

One methodology to reduce the fatigue effect in steel bridges is to calibrate the fatigue related parameters in the current bridge design code in Canada, CSA-S6-06 (CSA 2006). This calibration should be based on actual truck load data collected from various sources to allow the

comparisons between a range of results and to propose the most accurate values for fatigue-related parameters in the code.

For existing steel bridges, several methodologies are used to strengthen or rehabilitate welded details, where fatigue cracks might be present due to high stress concentrations. The fatigue life of critical welded details could be improved by imposing post-weld treatment techniques: weld geometry improvement methods and residual stress methods. Although many investigations were carried out using these techniques in the past, more experimental programs are required to investigate post-weld treatment effect on fatigue life improvement.

The assessment of the remaining fatigue life of critical welded details in bridges requires the knowledge of different uncertainties involved in the loading, fatigue resistance and fatigue life prediction methods. In spite of the different studies that have previously been conducted to assess these uncertainties, there is a need for further investigations into the uncertainties of effective parameters (truck loads, material properties, initial flaw conditions, weld profiles, welded joints geometries, etc.), which are related to the fatigue life reliability analysis.

1.2. Objectives and Scope

By using actual truck load data collected from bridge owners in Canada, the present study aims to calibrate some fatigue related bridge code parameters particularly the fatigue truck factor and equivalent number of cycles. In addition, the present work investigates the fatigue life improvement using weld toe grinding for full-scale specimens in fatigue test program. Moreover, this study develops a methodology for the prediction of the remaining fatigue life using reliability-based approaches for welded details in aging steel highway bridges by utilizing the material test results previously investigated at the University of Alberta and probabilistic stress ranges from actual truck data. The principal objectives of the current research work are:

1. To utilize the weigh-in-motion (WIM) databases received from two provinces and one territory in Canada in the calibration of the current fatigue truck factor and equivalent number of cycles, N_d, used in the Canadian Highway Bridge Design Code (CHBDC) (CSA 2006). The equivalent number of cycles could be employed to predict the annual number of cycles due to actual stress ranges for fatigue life reliability prediction of cruciform details. The calibration will be based on dual slope fatigue design (S-N) curves, which is currently applied in the *Limit State Design of Structural Steel* CSA-S16-09 (CSA 2009).

2. To develop a methodology, by which the actual truck data received from the same sources in Canada, that could be used to model probabilistically the stress range histograms (stress range vs number of cycles) for a variety of bridge configurations and lengths (one and multi-span girder bridge) for implementing fatigue life reliability predictions. These stress ranges are transformed into actual number of cycles to represent the loading parameter in the fatigue limit state.

3. To assess weld toe grinding as a method to improve fatigue life of severe welded details "Category E" for full-scale specimens.

4. To establish an assessment method of the fatigue life reliability of cruciform welded detail taking into account the variations in fatigue loading and resistance with a special focus on the variations in truck loads developed from WIM databases, initial weld undercut and fillet weld size. This assessment utilizes previous experimental and literature data of fatigue material properties for initiation and propagation stages. Most of the parameters were considered to be probabilistic while other parameters were deterministic.

1.3. Methodology

In order to achieve and fulfill the research objectives outlined in Section 1.2, the present research implements the following methodology:

For the calibration of fatigue truck, design truck data, actual truck data and a database of influence lines should be defined. The developed fatigue truck calibration procedure is based on equating the fatigue damage that results from the actual traffic and the design truck, using single and dual slope fatigue design curves. Then, the validation of the equivalent number of cycles, N_d , presented in Table 10.5 of CSA-S6-06 (CSA 2006), is based on the predicted fatigue truck factors for single and dual-slope fatigue curves.

In this study, the probabilistic truck loading model, estimated from WIM databases, is employed in the fatigue life reliability prediction. The assessment of the WIM data tolerances to the WIM specification ASTM 1318-09 (ASTM 2009) should be carried out to ensure that the WIM measurements are within the specification limits. Afterwards, the stress range histograms due to actual truck data, employed from the fatigue truck calibration, are fitted by appropriate probabilistic distributions along with defining their probabilistic parameters for each bridge configuration and span.

The research implements an experimental program of three full-scale groove T-joints under constant amplitude cyclic loading to assess weld toe grinding as a method to improve fatigue life of severe welded details “Category E”. Two specimens have their weld toe ground, and the third is considered as "as-welded" specimen. Then, deterministic prediction of fatigue life of tested specimens is developed and validated against the test results. The study employs energy-based approach for fatigue crack initiation life prediction and linear elastic fracture mechanics (LEFM) to estimate the fatigue crack propagation life.

The study develops the probabilistic fatigue life resistance prediction of cruciform welded detail for fatigue category C, which is considered to be a simplified detail for the tested specimens. Both fatigue detail categories C and E are considered to be transversely loaded welds with the fatigue strength of detail C being higher than E. In steel bridges, the transversely loaded weld details are present in many locations such as: transverse stiffeners, cover plates, splices, etc. Finite element analysis is performed for the cruciform detail of Category C to correlate the energy-based method parameters to the initial weld flaw (weld undercut) for eight different fillet weld sizes. Subsequently, the probabilistic prediction of fatigue resistance life is derived for the cruciform detail using fatigue crack initiation and propagation material parameters. Then the study develops the remaining fatigue life reliability analysis using probabilistic stress range histogram and fatigue resistance life of the cruciform detail for a simple span bridge of length 36.0 m to determine the critical welded details that require fatigue life improvement and inspection management.

1.4. Organization of the Thesis

The thesis consists of eight chapters, including the introduction, and seven appendices. The organization of the thesis is summarized in Figure 1.1.

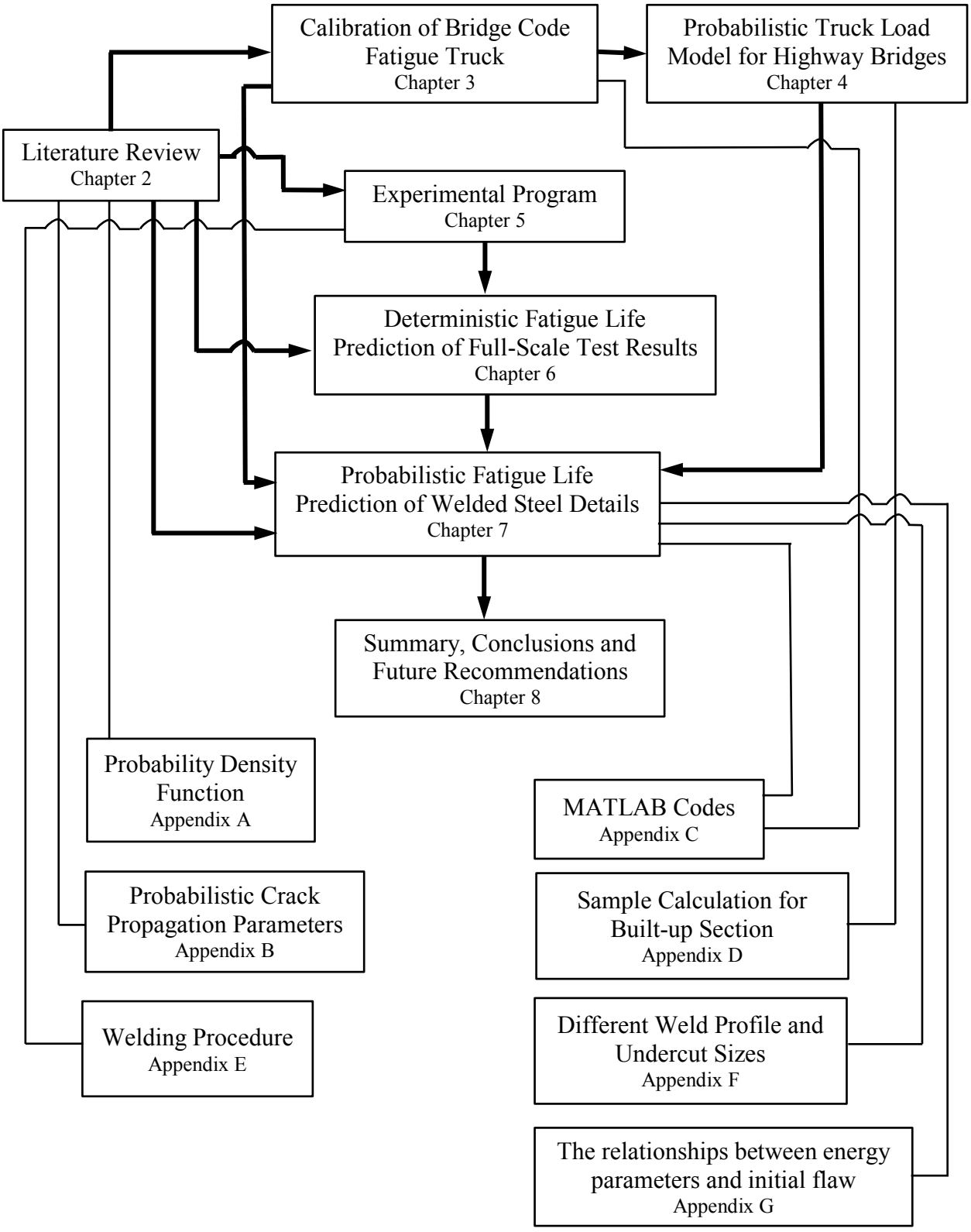

Figure 1.1*Organization of the thesis.*

Chapter 2 presents a specific literature review on uncertainties in fatigue loading, fatigue resistance parameters, fatigue life predictions for crack initiation and crack propagation stages. The review also includes the fatigue repair methods including post-weld treatment, and reliability theory in structural engineering and fatigue applications.

In Chapter 3, the calibration of the fatigue truck factor, reduction factor and equivalent number of cycles due to design truck passage, currently employed in the Canadian Highway Bridge Design Code (CHBDC), are illustrated. The calibration employs the weigh-in-motion WIM data received from the provinces of Quebec and Ontario in addition to the Northwest Territories (NWT) for various sections in one, two and five-span bridges. Rainflow analysis is used to transform the moment histories into moment histograms for calibration purposes.

Chapter 4 illustrates the probabilistic stress ranges due to truck loading by fitting the probabilistic distributions into stress range histograms (predicted from Chapter 3), where the main parameters (e.g. mean, standard deviation, etc.) are defined for various bridge spans, sections and configurations.

The details and results of an experimental program for full-scale specimens are presented in Chapter 5. Full-scale grooves T-joints were tested under constant amplitude cyclic loading to investigate the performance of non-ground (as welded) and ground specimens on the fatigue life of the full-scale specimens.

The study develops in Chapter 6, a deterministic prediction of the full-scale test results based on the literature review presented in Chapter 2. Some information from the experimental program in Chapter 5 was used in this deterministic prediction. Also, the study employs finite element models to obtain local stresses, plastic strain energy densities and strains for no flaw and in presence of initial flaw(s) cases for the prediction of fatigue crack initiation life. Moreover, it investigates different combinations of parameters (initial flaw size, initial flaw shape, short crack effect and residual stress fields) to numerically estimate the fatigue life of the specimens tested in Chapter 5.

Furthermore, Chapter 7 discusses the most appropriate approach to determine probabilistically the remaining fatigue life of cruciform detail from literature. The investigated cruciform detail is transverse weld subject to cyclic stresses, considered to be a simplified detail of the T-joint specimens, tested in Chapter 5. The uncertainties comprise weld profile size, initial undercuts in

addition to the fatigue material parameters for crack initiation and propagation, previously investigated at the University of Alberta. Monte Carlo Simulations (MCS) is conducted to obtain a probabilistic distribution of the fatigue life of cruciform welded detail from literature. It is also used to predict the probability of failure based on applied number of cycles, induced from probabilistic applied stress range histogram, versus the fatigue life resistance for the bridge welded detail for various weld sizes, profiles and undercut conditions.

Finally, Chapter 8 presents the summary, conclusions and recommendations for future work from the present study.

Appendices A to G provide additional information to the body of the thesis. In addition to probabilistic distribution of crack growth material properties, Matlab codes for prediction of the load history, rainflow analysis and probabilistic fatigue life prediction are illustrated. Then, the methodology used for prediction of stress ranges from moment ranges is shown. Moreover, the welding procedure specification applied in the experimental program is outlined. Finally, different weld profiles and undercut conditions for the fatigue reliability analysis are shown in addition to the correlation between energy parameters with various initial flaw sizes.

2. LITERATURE REVIEW

2.1. Introduction

Infrastructure is considered as the main pillar of the development of any country. The expected service life of infrastructure spans many decades. Accordingly, assessments are required to predict their remaining service life to ensure their safety under operation throughout their life. Steel highway bridges are practical examples of these infrastructures. In Canada, many bridges were built in the 1950s, when the traffic demands were lower than the present actual conditions, which are currently regulated by the *Memorandum of Understanding on Vehicle Weights and Dimensions* (MOU) signed by all Canadian provinces, initially in 1988 and amended in 1991 (TAC 1991).

The current status of steel highway bridges faces two major challenges. First, these bridges are almost expended their design life if not approaching the end of it; meanwhile, they are experiencing continuing loading cycles due to the increasing volume of truck traffic and truck weight, which may lead to fatigue fracture. Second, a great portion of these bridges are operating in severe environmental conditions. As a result of these two concerns, it is mandatory to assess the remaining fatigue life of steel highway bridges to ensure their safe service in the future.

Fatigue cracks in steel highway bridges often occur at welded details where stress concentrations are relatively high. The fatigue resistance of welded details varies according to the number of load cycles and the stress range. The stress range is a function of the applied loads and the level of stress concentration at a critical detail, which can be considered by the selection of the proper detail category. For existing steel bridges, fatigue life of critical welded details can be improved by imposing post-weld treatment techniques: weld geometry improvement methods and residual stress method. The latter introduces a compressive stress field in the area where cracks are likely to initiate. The former method reduces the severity of the stress concentrations by improving the weld geometry imperfections. Weld toe grinding is an example of the weld geometry improvement methods, which is considered to be cheap and fast.

One methodology for assessing the remaining fatigue life of steel highway bridges is the development of a reliability-based approach to predict the remaining fatigue life of welded details. However, this is not an easy task to conduct, since there are various uncertainties involved in the loading, fatigue resistance and fatigue life prediction methods. One should

incorporate these uncertainties into the fatigue life assessment by means of suitable probabilistic approaches. Several investigations based on these approaches have been conducted in the past, but there is still a need for further investigations into the uncertainties of effective parameters, which are related to the fatigue life reliability analysis.

This chapter is a review of five aspects of the prediction of fatigue life of steel bridges using reliability-based approaches. First, Section 2.2 discusses the loading uncertainties on aging steel highway bridges. Second, Section 2.3 outlines the fatigue resistance uncertainties in aging steel highway bridges. Following this, Section 2.4 explains the methods used to predict fatigue life for the crack initiation and propagation stages. Afterwards, Section 2.5 addresses the fatigue weld repair using the grinding method. Then, Section 2.6 discusses the reliability concepts and probabilistic analyses. Finally, the problem statement, research objectives and the outline of the thesis are presented in Sections 2.7 and 2.8.

2.2. Loading Uncertainties in Aging Steel Highway Bridges

2.2.1. General

The influential transient loads acting on highway bridges include earthquake loading, blast load and truck loading. The bridge truck loading includes a great extent of uncertainty due to the wide range of variation of truck axle weight, axle spacing and truck position on the bridge.

Residual stresses are another source of loading uncertainties acting on bridge welded details due to its presence during any welding process with variables amplitudes. They are generated during most manufacturing processes involving material deformation, heat treatment, machining or processing operations that transform the shape or change the properties of a material. Residual stresses depend on several factors related to various sources of uncertainties such as fabrication-related aspects (lack of fit, surface preparation, grinding, etc.), welding procedure, joint geometry and material properties. They are also affected by the post-weld treatment methods used to improve the fatigue life of welded details (Wright 1996, Kirkhope *et al.* 1999 and Cheng *et al.* 2003).

2.2.2. Methods for Stress Histories Prediction in Bridges

For any fatigue reliability analysis model, when a truck passes over a bridge, a stress history is generated in a member. Prediction of stress histories in steel bridges requires the assessment of

truck load and truck configuration uncertainties, present in weigh-in-motion (WIM) databases. WIM consists of weighing vehicle axles at normal roadway speeds using sensors embedded into the pavement surface and data acquisition systems equipped with software capable of processing sensor signals into weight and axle spacing. Furthermore, it provides the speed and the length of the passing vehicles. It also attempts to minimize the dynamic effect of the vehicles on the roadways. However, the main challenge is to develop a suitable probabilistic truck load model taking into account the uncertainties encountered in the received WIM data. Thus, there is a need to relate the truck loading uncertainties with the critical welded details in steel highway bridges. Therefore, such uncertainties should be revealed in the form of stress histories due to bending moments and/or shearing forces at locations, where fatigue damages/failures are of high probability. These stress histories are predicted using the influence lines for straining actions at such locations. Examples of these locations are steel girders with stiffeners or cover plates, girder splices, and section discontinuities.

In case of missing truck data for a specific bridge, mounting strain gauges at critical sections is another alternative to predict stress histories at specific locations directly without conducting any structural analysis or using influence lines for simple or continuous bridge girder. Yazdani and Albrecht (1990) mounted strain gauges at critical sections in 40 bridges, where 162 stress range histograms were developed from these strain measurements. Each stress spectrum was transformed into an equivalent stress range, which was then normalized with respect to the design stress range. Similarly, Agerskov and Nielsen (1999) mounted strain gauges to predict the actual stress history of critical details in bridges. They placed two strain gauges on the bottom of one of the trapezoidal longitudinal stiffeners of the deck plate of a steel highway bridge in Denmark. The two strain gauges were monitored for almost one week. A truncation methodology to avoid noise and low non-damaging stress cycles was implemented, so the extremes of the load history were only recorded by the strain gauges.

It is clear that the use of strain gauges procedure to predict load or stress histories is applicable only to specific bridges. This is considered to be the output of strain and stresses from acting bridge loads, while WIM is considered to be the load input for predicting the stress histories using influence lines. Numerical approaches to predict stress histories for any type of bridge configuration and loading should be used. For a welded detail at mid-span of a 10.0 m simply supported bridge, Righiniotis and Chryssanthopoulos (2004) used a numerical approach to

predict the stress ranges histogram from the bending moment, as compared to the work of Yazdani and Albrecht (1990), where strain gauges were mounted on critical sections. The authors used typical commercial vehicle groups and their relative frequency in loaded/unloaded configuration, based on an average mixture of vehicles that is representative of the current highway traffic in the UK (BD 77/98). Influence lines were used to derive the stress history, which was used as input for the rainflow counting method to convert the stress history into a stress spectrum.

The generated stress histories from truck loading are transformed into stress histograms for critical bridge details by using rainflow cycle counting [Matsuishi and Endo (1968), Metropolis (1987), ASTM E1049-85E1 (ASTM 2011)]. The increasing demand of truck loading on aging steel highway bridges causes an increase in traffic flow, number of applied cycles, and stress range magnitudes on critical bridge details. Righiniotis (2004) used the rainflow analysis to predict the stress ranges due to the bending moment for a cover plate location of a highway bridge, with the resulting histogram fitted with a Rayleigh distribution. This distribution was also found to match the stress range spectra from the test results obtained by Fisher *et al.* (1983). They used a Rayleigh fitting histogram during their fatigue experiment on 5.0 m beams under four-point loading conditions.

2.2.3. Calibration of Weigh-in-Motion (WIM) Databases for Truck Loading

2.2.3.1. Various Types of Errors in WIM Databases

Weigh in Motion (WIM) databases are used to provide truck weight information on highways. These databases provide truck weight and size, which can be used to predict the loading history for bridges (Wang *et al.* 2005). However, the output data from WIM stations may include errors from various sources. The development of an accurate prediction of stress history for particular bridge details requires intense investigation of the received WIM data to assess the truck load uncertainties.

The types of errors in WIM data can be categorized into: gross errors, systematic and random errors. The gross errors, representing unrealistic data (Gross Vehicle Weight, truck speed and length, etc.), could be eliminated by applying a screening procedure, which is considered as a data quality control tool for the data used in the prediction. This could not be applied to remove systematic and random errors, which are eliminated by applying statistical procedures.

The systematic error results from the calibration bias in the WIM system[1], which may occur during initial improper calibration or the WIM system falling out of calibration during service (Prozzi and Hong 2007). In Figure 2.1, the −10% bias indicates that the WIM system is undercalibrated, whereas the +10 % bias is an example of overcalibration. In the case of ideal calibration, the bias is zero and only random errors occur. In conclusion, when calibration bias occurs, both random and systematic errors exist.

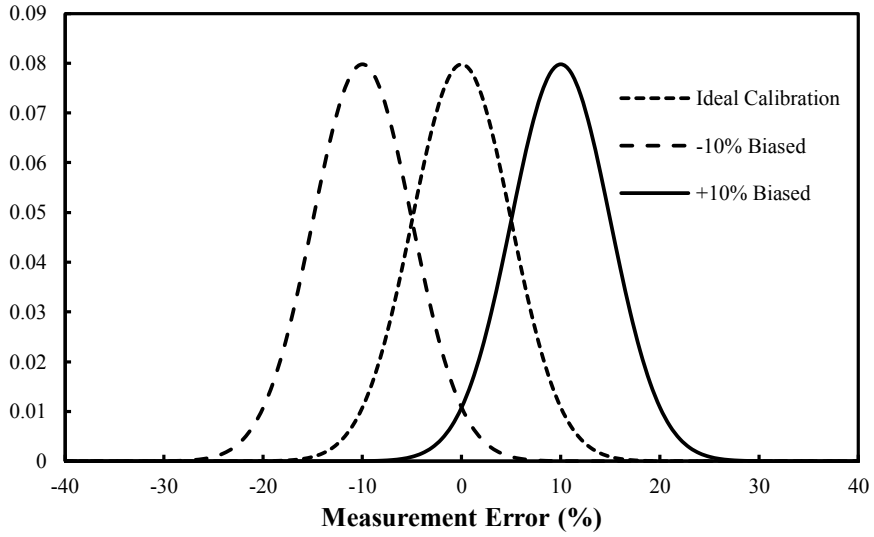

Figure 2.1 *Effect of WIM system biases (Systematic error) on measurement error distribution. (Prozzi and Hong 2007).*

The third type of errors, encountered in the WIM data is the random errors. In general, they are defined as the statistical fluctuations of measurement (in either direction) from the true value, and they are intrinsic to the measurement due to the inability of the device to determine the truth in a precise manner. In absence of systematic errors, these errors could be modeled using normal distribution with zero mean [Davies and Sommerville (1987) and Bergan *et al.* (1997)]. The standard deviation, σ_ε, is a measure indicating the WIM accuracy (Bergan *et al.* 1997). Figure 2.2 shows the distributions of random error induced from weighing gross vehicle weight (GVW) by three typical types of WIM equipment: single load cell (σ_ε = 1.5%), bending strain (σ_ε = 5 %), and piezo (σ_ε = 10 %). The smaller the value of σ_ε, the higher the accuracy of the WIM scale.

[1] Calibration bias in the WIM system is a quantitative term describing the difference between the average of measurements made on the WIM scale due to errors in calibration and its true value.

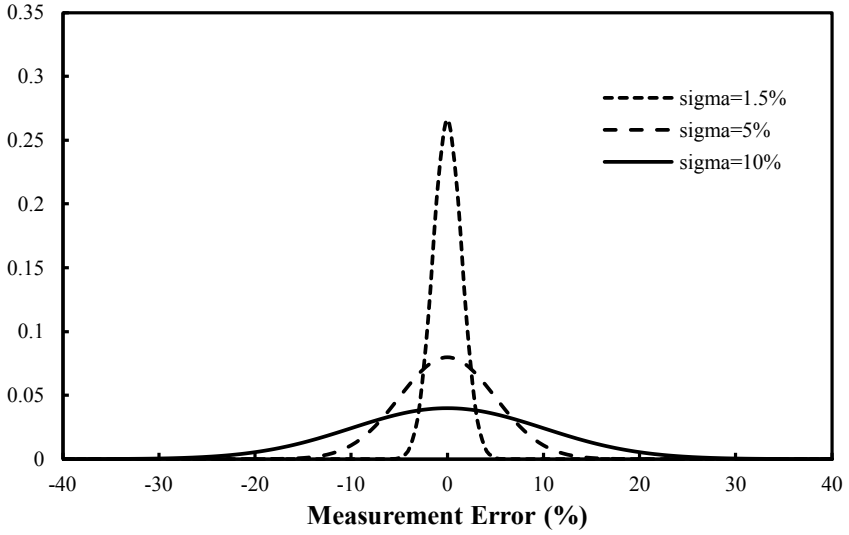

Figure 2.2 *Effect of WIM system accuracy (random error) on measurement error distribution. (Prozzi and Hong 2007).*

2.2.3.2. Use of WIM for Fatigue Truck Calibration in CHBDC

The Canadian Highway Bridge Design Code (CHBDC) CAN/CSA-S6-06 (CSA 2006) employs a fatigue truck factor of 0.52 to calibrate the design truck to the actual highway traffic, which was obtained using WIM data from Ontario and Alberta. This factor accounts for the discrepancy between the fatigue damage induced by the actual truck traffic and the fatigue damage that would be induced by the CL-625 design truck. The factor is based on single-slope fatigue design curves with slope m=3. Although dual-slope (m=3 and 5) S-N curves have been adopted in CAN/CSA-S16-09 (CSA 2009), they have not yet been implemented in the CHBDC. There is a need to assess the value of the current fatigue truck factor for dual-slope S-N curves and weigh-in-motion data obtained from different Canadian sources.

The calibration procedure also requires the determination of the number of stress cycles experienced for each passage of the design truck, N_d. The aim of the calibration of the equivalent stress cycles is to validate the values presented in Table 10.5 of CSA-S6-06 (CSA 2006). These values were based on the current fatigue truck factor of 0.52.

2.2.3.3. Weigh-in-Motion Data Screening in Various Countries

The screening of WIM data is important to remove any gross errors that might be encountered in the collected truck data from WIM stations. Gross errors represent all unrealistic data such as

gross vehicle weights and/or speeds ≤ zero. WIM screening is also utilized to provide boundary values for speed, truck axle weight and spacing to ensure the most effective trucks to form the stress histories at the critical bridge locations. The followings subsections will discuss several data screening approaches to eliminate gross errors in WIM data.

WIM Data Screening in Canada

Very few studies concerning WIM screening are available in Canada, as most bridge owners do not have specified criteria for WIM data screening, or WIM systems subcontractors use their own criteria for screening. Zhi *et al.* (1999) evaluated the WIM data collected from 6 sites in the province of Manitoba between 1996 and 1997. These data included various unrealistic measurements due to improper calibration of the WIM systems. This is induced by equipment shutting down during system maintenance, low battery of WIM sensors and natural disasters such as flooding. As a result of these errors, 99% of the measurements indicate there is no axle number or gross vehicle weight of negative value due to the presence of calibration drift in WIM sensors, Zhi *et al.* (1999) used the following criteria to eliminate any unrealistic records in the WIM data:

- Overall length of the truck ≤ 0;
- Gross vehicle weight (GVW) ≤ 0;
- Number of axles ≤ 1.

WIM Data Screening in United States

The WIM screening criteria in the United States are more sophisticated than the Manitoba data screening. In addition of removal of unphysical data, these criteria also provide constraints for vehicle speed, number of axles, gross vehicle weight (GVW), truck length, steering axle weight limits, individual axle weight limits and axle spacing limits. Abundant research has been done on WIM data in many states. One of these studies was carried out by Pelphrey *et al.* (2008). They developed screening criteria for raw WIM data in Oregon State. In the same year, Sivakumar *et al.* (2008) proposed another attempt to implement another WIM data screening as a part of protocols for collecting and using traffic data for bridge loading.

Table 2.1 illustrates the screening criteria for WIM data in the United States based on the previous criteria limitations using imperial and metric units. The data in the table suggest

screening according to vehicle speed and give a certain range for the speed, as they do not include very slow or very high-speed vehicles. Another important observation is that the minimum number of axles to be considered is 3. Thus motorcycles, passenger cars and pick-up trucks are excluded. Other detailed criteria for ranges of individual axle weight are also provided.

Table 2.1 *WIM screening criteria in USA.*

Criteria	Sivakumar *et al.* (2008)	Pelphrey *et al.* (2008)
Speed less than mph (km/h)	10 (16.1)	10 (16.1)
Speed bigger than mph (km/h)	100 (160.1)	100 (160)
Truck length bigger than ft. (m)	120 (36.57)	200 (70)
Total number of axles less than	3	3
Total number of axles bigger than		13
GVW less than Kips (kN)	12 (53.37)	2 (8.9)
GVW bigger than Kips (kN)		280 (1246)
Individual Axle Weight bigger than Kips (kN)	70 (311.5)	50 (222.5)
Individual Axle Weight less than Kips (kN)	2 (8.9)	2 (8.9)
Steer Axle bigger than Kip (kN)	25 (111.25)	50 (222.5)
Steer Axle less than Kip (kN)	6 (26.7)	
First axle spacing less than ft. (m)	5 (1.52)	5 (1.52)
Any axle spacing less than ft. (m)	3.4 (1.00)	3.14 (1.00)

WIM data screening in Europe and South Africa

O'Brien and Enright (2012) used an extensive database of weigh-in-motion (WIM) data collected at five European sites in recent years. The recorded data were filtered to remove unreliable observations. In South Africa, over 50 weigh-in-motion stations have been installed on major highways. Due to pavement problems that were reflected in the WIM observations; the WIM data were of a very poor quality. For this reason, Ackermann *et al.* (2008) adopted a filtration criteria for WIM data collected from 50 sites across South Africa on major highways which are dependent on vehicle configuration (length, axle weight, axle spacing). Table 2.2 shows the screening criteria for WIM data in Europe and South Africa.

Table 2.2 *WIM screening criteria in Europe and South Africa.*

Criteria	Europe (O'Brien and Enright 2012)	South Africa (Ackerman *et al.* 2008)
Speed less than (km/h)	40	
Speed bigger than (km/h)	120	
Truck length bigger (m)		25
vehicle length less (m)		2.5
Total number of axles less	2	2
Total number of axles bigger		15
Individual Axle Weight bigger (kN)		196.2
Individual Axle Weight less (kN)		9.8
Steer Axle bigger (kN)		98
Steer Axle less (kN)		9.8
First axle spacing less (m)	0.4	2.1
Any axle spacing less (m)	0.4	1.1

2.2.3.4. WIM Measurement Errors Tolerances Specification

WIM scale, installed in specific location on highways, is able to continuously collect and record vehicle information including date and time of passage, lane and direction of travel, vehicle class, speed, wheel and axle weight, and axle spacing. WIM measurement errors, as explained above, result from WIM system instability due to sensor technology, environmental effects, pavement conditions and other factors (Prozzi and Hong 2007), give rise to the concern of its measurement accuracy. Therefore, the review of WIM specifications with focus on accuracy is necessary, due to variations in WIM accuracy levels. The propagation of errors due to WIM measurements is reflected on the estimation of fatigue stress ranges.

The most recent ASTM E1318-09 (ASTM 2009) on highway WIM systems describes four types of WIM systems—Type I, Type II, Type III, and Type IV—to suit the user's need based on different applications ASTM E1318 (ASTM 2009). Types I and II are used in the data collection procedure, while Types III and IV are for the purpose of law enforcement. At present, regarding the ASTM specification for WIM functional performance, the tolerance for 95% probability of conformity in terms of single axle load are ± 20, ± 30, and ± 15 % for Types I, II, and III WIM

systems, respectively. The corresponding values in terms of the axle group load are ± 15, ± 20, and ± 10 %; and ± 10, ± 15, and ± 6 % for the GVW.

2.2.4. Residual Stresses

Residual stresses are another source of loading uncertainties acting on bridge welded details, which generate from the differential plastic deformations of adjacent material region. Welding residual stresses are induced by the consequence of heating and subsequent heat and cool of the base and weld metal throughout the welding process.

There is no external load present to induce residual stresses; accordingly, they should be self-equilibrated in the material. Regarding an elastic-perfectly-plastic material behavior, the magnitude of the residual stresses cannot exceed the yielding stress of the base or weld material.

However, the distribution of the residual stresses across the thickness of the welded joints is very complex, especially if this particular welded detail was subject to repair. To measure the residual stresses in fillet or groove welded details, which are the main focus of the study, the following subsections present a review on the prediction of residual stresses in these details in addition to their probabilistic model.

2.4.4.1. Residual Stresses in Fillet Welds and Groove Welds at T-Joints

Porter-Goff *et al.* (1988) predicted the residual stresses in welded tubular Y-nodes (Y-series) and pipe-on-plate joints (P-series) using the block sectioning methodology. Similar features are shown for the resulting stress field in the material thickness at the toe of the weld: the maximum tensile stresses are within 2 or 3 mm of the surface and sometimes reach the yield strength of the base metal; the surface stresses are slightly less than the maximum stresses; there is a quick decrease in tensile stresses that happened after the maximum stress; compressive stresses occur in the middle portion of the thickness, with a maximum roughly at mid-thickness; tensile stresses (≈ 50 % of the material yield strength) generate at the surface opposite to the weld.

In another study, Cheng and Finnie (1993) employed the crack compliance technique to determine the through-thickness residual stress field near the toe of a weld between a 166 mm thick plate and an attached bracket. Despite the fact that the plate, formed from low-carbon steel, was cladded with a special surface protection agent used in nuclear pressure vessels, Cheng and Finnie (1993) found that the residual stresses showed a pattern similar to what Porter-Goff *et al.*

(1988) found: the induced maximum tensile residual stress was very close to the surface, then decreased rapidly to be compressive in the middle portion of the plate, before producing small tension on the face of the plate opposite to the weld.

Stacey *et al.* (2000) carried out several assessments on T-butt, pipe-to-plate, tubular T- and Y-joint connections. For thick plates (t > 25.0 mm), they found that the residual stresses are tensile, and reach the yield level near the weld toe and are compressive in the central portion. The transverse stresses are usually tensile on the face of the plate opposite to the weld. On the other hand, the thin plates (t < 15.0 mm) demonstrate a more moderate decrease in tensile residual stresses in the direction of the plate center. A conservative assumption of a uniform tensile stress through the thickness could therefore be made.

2.4.4.2. Probabilistic Model of Residual Stresses

Based on the above observations for the residual stresses prediction in fillet and groove welds, there is a need to model them probabilistically. Based on the experimental findings of Porter-Goff (1988), Shetty and Baker (1990) suggested a lognormal distribution (LN) with mean of 300 MPa, and standard deviation of 75 MPa, i.e. LN (300 MPa, 75 MPa), where the residual stresses at the surface is linearly reduced with crack growth. Other values for residual stresses distributions were introduced by Lukic and Cremona (2001), they assumed conservatively a lognormal distribution, LN (355 MPa, 35.5 MPa) for nominal yield strength of 345 MPa since residual stresses close to the surface are near to the yield strength level of the base metal. Moreover, the Joint Committee on Structural Safety JCSS (2001) recommended a lognormal distribution, LN (300 MPa, 60 MPa).

Various studies [Lawrence (1981), Bignonnet *et al.* (1987), Shetty and Baker (1990)] observed that the residual stresses are not essential parameters in crack propagation, but are highly effective during the fatigue initiation stage. In summary, the effect of residual stresses on crack closure will be taken into account in the deterministic prediction for the full-scale specimens in Chapter 6.

2.3. Fatigue Resistance Uncertainties in Welds of Aging Steel Highway Bridges

2.3.1. General

Section 2.2 presented a review on loading uncertainties in the fatigue loading acting on steel highway bridges. Another important parameter affecting the fatigue life of such bridges: fatigue resistance uncertainties. These uncertainties comprise several parameters found in the reviewed literature to be significant to the prediction of fatigue life. In Section 2.3.2, the first of these parameters is the initial weld imperfection, which has been acknowledged by many researchers to be the most important factor in the fatigue resistance (Gurney 1979b and Maddox 1991). Then, the crack propagation material properties are investigated in Section 2.3.3. This review outlines various probabilistic distributions for the fatigue crack growth parameters (C, m and ΔK_{th}). Finally, Section 2.3.4 reviews the variability in fillet weld dimensions (shear leg, tension leg and weld throat).

2.3.2. Initial weld imperfection

2.3.2.1. Definition of Initial Flaw length (a_{init}) and Aspect Ratio $\left(a/c\right)_{init}$

In general, and under fatigue loading, weld flaws and cracks, defined by their initial depth or length, a_{init}, and their aspect ratio, $\left(a/c\right)_{init}$, are considered to be the most detrimental weld discontinuities. For a semi-elliptical surface crack, c is equal to half the crack length and *a* is equal to the crack depth. The term *flaw* is used here in a general way and describes any discontinuity in the weld, such as lack of fusion, weld undercuts, slag inclusions, porosity, or incomplete penetration, without considering whether the discontinuity is acceptable or not from an inspection point of view. A flaw can take different shapes (elliptical or spherical, for example), but is considered here as not having a sharp tip. A crack is defined as a discontinuity with a sharp tip.

2.3.2.2. Non-Destructive Tests for Initial Flaws Detection

Despite the fact that non-destructive methods (e.g. magnetic particle, liquid penetrants, radiography or ultrasound) exist to identify existing cracks, there is a possibility that initial cracks may not be detected due to their small size and/or subsurface location. Therefore, Aoki *et al.* (1986) found that the detection methods assessment of initial crack size and shape is difficult

and might even result in unreliable predictions. This statement is still valid as Shantz (2010) claimed that the true distribution of initial flaw sizes is difficult to accomplish due to inadequate resources and/or the limited capability of non-destructive evaluation (NDE) techniques for reliably detecting small crack sizes.

Definitely, the destructive methods, such as fatigue testing up to failure with subsequent microscopic examination of the crack surface, are the best way to measure initial crack geometry. However, this methodology is not suitable for existing structures and there is a need to predict the size of initial weld discontinuities. Two approaches can be implemented in this instance: adopting the largest flaw size and shape acceptable by applicable standards; or assuming that the crack size corresponds to the smallest crack that can be reliably detected by a specific inspection method.

However, the main drawback of these approaches is that the initial flaw geometry is proposed to be a deterministic upper-bound value, which could lead to unreliable fatigue life prediction. Statistical analysis of data obtained from research investigations can reduce this shortcoming. It is mandatory to associate the agreed initial crack geometry with acceptable defect sizes imposed by design standards and guidelines, as will be discussed in the following section, despite the fact that the acceptable deterministic defect sizes as defined in standards and codes of practice will not be directly used in the present work. This will be followed by an investigation of some literature of research investigations, where initial crack geometries were predicted in linear elastic fracture mechanics (LEFM) models. Appendix A provides the mathematical definitions of probability distributions used in reliability assessments.

For the present work, both complete joint penetration (CJP) welds and fillet welds have been investigated. Cracks are most expected to start from the toe or the root of the weld [Gurney (1979b), Radaj (1990) and Maddox (1991)] for both weld types. Therefore, the following will focus on these locations. Whether the cracks for the specimens tested in the present work actually initiated from these locations will be verified in Chapter 5.

2.3.2.3. Provisions of Welding Codes for Initial Imperfections

USA

The weld inspection in the provisions of the American Specification D1.5 *Bridge Welding Code* (AASHTO/AWS 2008) do not allow weld cracks in any case as indicated in Section 6 of the code. In the same section, AASHTO/AWS D1.5 requires radiographic inspection in addition to visual weld inspection for the complete joint penetration (CJP) groove welds in the butt joint subject to calculated tension or reversal of stress. For cyclically loaded members, the standard does not allow weld undercut beyond 0.25 mm when the weld is transverse to the applied stresses. Magnetic particle testing inspection is required for fillet welds joining primary components of main members. The acceptance criteria for flaws are basically the same as in the case of CJP groove welds.

Canada

The Canadian Standard – *Welded Steel Construction (Metal Arc Welding)* CSA-W59 (2013) covers welding requirements for most applications of welded carbon and low-alloy steel constructions. For welds cyclically loaded in tension, similar procedures and acceptance criteria to AWS D1.1 (AWS 2008) are noted. In addition to the visual inspection of all welds, the Canadian Highway Bridge Design Code (CSA 2006) requires a complete radiographic inspection of groove welds in flange splices under tension or stress reversal to be carried out. This matches the requirements of AASHTO/AWS (2008). For transversely cyclically loaded structures, the weld undercut should not exceed 0.25 mm.

Europe

ISO 5817 *Arc Welded Joints in Steel – Guidance on Quality Levels for Imperfections* was implemented as European Standard EN 25817 in 1992 (EN 1992). EN 25817 does not permit any surface cracks and provides maximum discontinuities dimensions, which is close to the North American Standards. Flaw limitations are given for three quality levels: moderate (D), intermediate (C), and stringent (B). Design considerations such as the type of loading, service conditions (temperature and environment), and consequences of failure should be the basis for any required quality level. An appropriate application is to demand quality B (stringent) based on these criteria for the types of application considered in the present work (welded repairs

subjected to dynamic loading at low operating temperatures). The maximum dimension of single pores is restricted to 3.0 mm and solid inclusions are limited to 2.0 mm for quality B. For quality B, undercut shall not exceed 0.5 mm.

2.3.2.4. Review on Initial Crack Size (a_{init}) and Aspect Ratio $(a/c)_{init}$

Various researches have studied initial sizes for weld discontinuities and the results implemented in probabilistic fatigue life prediction assessments. According to the acceptability criteria of both North American and European standards, these weld discontinuities must not be cracks. However, in the probabilistic fatigue life assessment in literature, they were treated as cracks. The purpose for this hypothesis is that the weld discontinuities are severe enough to induce a significant stress concentration, resulting in practically no initiation life, which is exactly the same if cracks are present. Therefore, the initial weld discontinuity size corresponds to the initial crack size used to describe the crack propagation stage.

According to AASHTO/AWS (2008), undercuts in cyclically loaded connections shall not be more than 0.25 mm. All the welds that were inspected and reported in the literature met even the most stringent standards. This can be attributed to the fact that in an actual weld, code requirements have to be met and often in case of doubt, weld imperfections are rejected rather than accepted. Nevertheless, reported discontinuity sizes in the literature suggest that significant scatter in initial crack size, a_{init}, does exist and must be considered. The size of initial discontinuities reported in the literature ranges from about 0.1 mm to 1.0 mm (See Table 2.3), where the mathematical equations defining the probability density functions (pdf) are presented in Appendix A.

The initial aspect ratio, $(a/c)_{init}$, of cracks also shows a large variability as well (Table 2.4) and often changes during crack propagation. In probabilistic approaches, both a_{init} and $(a/c)_{init}$ are most commonly modeled with lognormal distribution.

In Tables 2.3 and 2.4, the first parameter represents the mean value of the distribution, while the second parameter represents the standard deviation. This is valid for normal, lognormal and Weibull distributions.

Table 2.3 *Summary of distribution from the literature for* a_{init} .

Distribution	1st parameter	2nd parameter	Reference
Exponential (λ)	0.11 mm	---	Bokalrud and Karlsen (1982) Vårdal *et al.* (1999), Lotsberg *et al.* (2000), Moan and Song (2000), Straub and Faber (2004), DNV 30.6 (1992), HSE (1999)
Lognormal(α, β)	1.1 mm 0.13 mm	1.8 mm 0.046 mm	Brückner and Munz (1982) Engesvik and Moan (1983)
Weibull (θ, τ)	0.436	0.507	Brückner and Munz (1982)
Deterministic Deterministic	0.045 0.1	---- ---	Smith and Smith (1982) Agerskov and Nielsen (1999)

Table 2.4 *Summary of distribution from the literature for* $(a/c)_{init}$.

Distribution	1st parameter	2nd parameter	Reference
Normal(α, β)	*0.55 mm*	*0.18 mm*	Brückner and Munz (1982)
LogNormal(α, β)	*0.62 mm*	*0.25 mm*	Shetty and Baker (1990)
	0.01 mm	*0.002 mm*	Righiniotis and Chryssanthopoulos (2003) Lower Bound
	0.5 mm	*0.1 mm*	Righiniotis and Chryssanthopoulos (2003) Upper Bound
	0.5 mm	*0.16 mm*	Walbridge (2005)
Deterministic	0.55	-----	Smith and Smith (1982)

The scatter in initial crack size and aspect ratio in Tables 2.3 and 2.4 could result from the methods, used to predict the weld discontinuity size, which is not reliable in measuring actual

size (Simonen 1995). Other causes are related to the variability in weld process and weld parameter. Finally, the skill of the welder affects the weld quality.

2.3.3. Crack Propagation Material Properties

(LEFM) is an approach to model the stable fatigue crack propagation when the material is behaving in the elastic range. Experiments show that the log in the crack propagation, $\frac{da}{dN}$, is directly proportional to the log of the stress intensity factor range, $\Delta K = K_{\max} - K_{\min}$ (Paris and Erdogan 1963). Equation 2.2 models this relation as follows:

$$\frac{da}{dN} = C.\Delta K^m \tag{2.2}$$

where *C, m* are material constants determined from experiments and *N* is the number of stress cycles during crack propagation. The stress intensity factor, K_i, is a measure to define the stress field at the crack tip, which is a function of several factors: the crack size and shape; the location of the crack relative to a free surface; the crack size relative to the plated size in which the crack is located; and the applied stress magnitude and distribution. In general, the crack propagation life, N_{prop}, can be estimated by integrating equation (2.2) from an initial crack size, a_0, to a final crack size, a_f :

$$N_{prop} = \int_{a_0}^{a_f} \frac{da}{C.\Delta K^m} \tag{2.3}$$

Figure 2.3 illustrates the relationship between ΔK and da/dN on the log-log scale. It could be noticed that no crack growth occurs under constant amplitude fatigue limit for stress range intensity factors below a threshold value, ΔK_{th} (Dowling 1999). This threshold should be incorporated into equation (2.3) for accurate prediction of crack growth. Ohta *et al.* (1986) modeled the transition in Figure 2.3 as:

$$\frac{da}{dN} = C.\left(\Delta K^m - \Delta K_{th}^m\right) \Rightarrow N_{prop} = \int_{a_o}^{a_f} \frac{da}{C.\left(\Delta K^m - \Delta K_{th}^m\right)} \tag{2.4}$$

Gurney (1979a) showed that the threshold stress intensity factor range, ΔK_{th}, depends on various factors, with the most significant being the stress ratio, R.

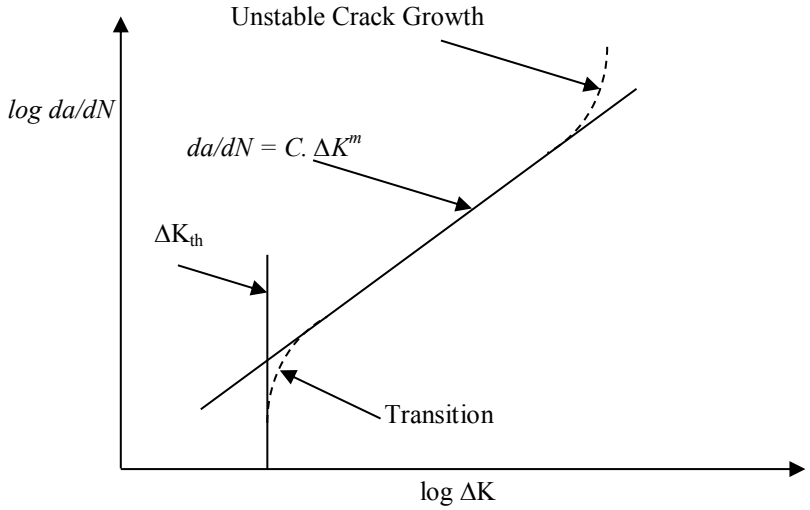

Figure 2.3 *Relationship between* ΔK *and* da/dN *on the log-log scale.*

There are various probabilistic distributions of the crack propagation parameters, C and m. Gurney (1979a) found a strong connection between C and m. Thus, most probabilistic approaches consider m a deterministic value, and C as a random variable, respectively, as the C parameter uncertainty affects the crack propagation rate. Appendix B presents a summary of the probabilistic parameters proposed in two design guides and seven research programs. For the presented research programs, m is assumed to be constant and C is assumed to follow a lognormal distribution, $LN(\alpha,\beta)$, where α and β are the sample mean and standard deviation, respectively.

The threshold stress intensity factor range, ΔK_{th}, influences the crack propagation at low ΔK values according to equation (2.4). The effect of ΔK_{th} is ignored in various probabilistic fracture mechanics models used in the literature. If considered, ΔK_{th} is often assumed to have a deterministic value. Lotsberg *et al.* (2000) used $\Delta K_{th} = 63 MPa\sqrt{mm}$, this was also suggested by BSI (2005) for stress ratios $R \geq 0.5$. Banz and Nussbaumer (2001) used a very similar value of

ΔK_{th}, namely $\Delta K_{th} = 60MPa\sqrt{mm}$. Walbridge (2005) modeled ΔK_{th} using lognormal distribution, LN(100,15). This was based on deterministic predictions carried out by Bremen (1989) and fatigue test results (Shetty and Baker 1990). From the previous values, Josi and Grondin (2010) modeled the same lognormal distribution with lesser values LN(60,6). The mean value of the distribution was also used in BSI (2005). This distribution will be adopted in the probabilistic fatigue life prediction in Chapter 7.

2.3.4. Uncertainties in Transverse Fillet Weld Profile

It is generally accepted that the fillet weld capacity is a function of the direction of the applied load which could be longitudinal or transverse (Higgins and Preece (1969), Clark (1971), Butler and Kulak (1971), Butler *et al.* (1972), Miazaga and Kennedy (1989) and Bowman and Quinn (1994)). The latter represents the fillet weld for cruciform details.

A study done at the University of Alberta by Ng *et al.* (2002) extended the work done by Miazaga and Kennedy (1989) on transverse fillet weld by using the flux core arc welding (FCAW) and filler metal with a toughness requirements for lapped splices and cruciform details. In their research, Ng *et al*. (2002) tested 102 transverse fillet weld specimens for lapped splices and cruciform details using five classifications of filler metal of weld sizes 6.4 mm and 12.7 mm. It was found that there is a great extent of variability in the fillet weld dimensions as well as the angle of the weld. Therefore, it is important to consider the effect of variations in weld shape profile and size in the prediction of remaining fatigue life reliability of welded bridge details. In Chapter 7, the extreme (minimum and maximum) of shear leg, tension leg as well as weld throat sizes, measured by Ng *et al.* (2002), will be taken into account for the fatigue life reliability assessment of cruciform welded details.

2.4. Methods of Predicting Fatigue life in Welded Steel Details

2.4.1. Introduction

In structural steel components, cracks usually occur at locations containing high stress concentrations, high residual tensile stresses and initial flaws, or combinations of these factors. These cracks might be present after fabrication or may be initiated during the life of the structure. They grow in a stable manner under the application of cyclic loading until the crack size becomes large enough to cause unstable crack propagation. Figure 2.3 illustrated the stress

intensity range for the three stages of crack growth: crack initiation stage ($\Delta K \leq \Delta K_{th}$), stable crack propagation stage, and unstable crack propagation stage.

The two commonly used methods for fatigue life prediction are the S-N approach and the fracture mechanics approach. Fatigue design (S-N) curves are adopted in the steel and bridge design codes [CSA-S16-09 (CSA 2009) and CSA-S6-06 (CSA 2006)] to predict the fatigue life of a certain detail based on the applied stress ranges and the degrees of fatigue severity of the investigated joint (Figure 3.1). The main drawback in the S-N approach is that it provides the fatigue life for welding details without a clear distinction between crack initiation and propagation lives. This is not the case in the fracture mechanics approach, which describe the fatigue crack initiation and propagation stages.

2.4.2. Crack Initiation Fatigue Life

2.4.2.1. Introduction

An empirical correlation approach is normally employed to predict fatigue crack initiation life. There are three methods that adopt this methodology: stress-based, strain-based, and energy-based. Although the stress and strain methods have various applications, there is still a need to emphasize the material response of the fatigue damage process, as both the elastic and plastic strain components and their corresponding stress values during fatigue cycles are involved in the explanation fatigue damage for tested material in a precise manner. Josi and Grondin (2010) employed the strain-based approach for predicting the fatigue crack initiation life. They concluded that the method may not be suitable for complicated welded details or load histories. Therefore, the fatigue approach should comprise both components (elastic and plastic strains) to modify damage approaches and to make accurate continuum mechanics basics. As a result, energy-based approaches were introduced to analyze the damage accumulation of notched/welded components (Cui 2002). Lagoda (2008) found that in case of large numbers of cycles, the stress and energy methods are suitable for fatigue prediction, while the strain and energy methods are convenient for small numbers of cycles. Therefore, the energy-based methods seem to be effective in all cases. In this study, the energy-based approach will be used to predict the fatigue crack initiation life. The following sub-section will illustrate the background theory of the energy-based method in addition to the various measures of energy.

2.4.2.2. Energy-Based Approach

Energy approaches are based on the assumption that fatigue damage is directly related to the area under the hysteresis loops created during cyclic loading. The area under the hysteresis loops is related to the plastic deformation taking place during a load cycle, which relates to the 'fatigue damage' sustained during one load cycle.

The energy-based method uses energy as a damage parameter to characterize fatigue, emphasizing the interrelation between stress, strain, and the fatigue damage process. It unifies high and low cycle fatigue, and has the potential to bridge fatigue data obtained in different laboratories using specimens of different geometries and size and tested under different controls [Chan and Miller (1982), Sarihan (1994)].

In general, the total absorbed energy to the point of fatigue failure is supposed to depend on the total number of cycles sustained, and the fatigue damage during each cycle is assumed to relate directly to the area under the hysteresis loops of the stress versus strain curve during cyclic loading (Ellyin 1997). Various measures of energy have been proposed depending on the stress level; namely, the plastic strain energy density per cycle, ΔW^p, the total strain energy density per cycle, ΔW, and the plastic plus tensile elastic strain energy density per cycle, ΔW^t.

The ΔW^p is more suitable when the plastic strains are large, and ΔW is employed for small strain magnitude during high cycle fatigue, the plastic strain energy is small and is difficult to compute accurately. The plastic strain energy density per cycle, ΔW^p, corresponds to the area under a hysteresis loop with a stabilized stress range of $\Delta\sigma$ and plastic strain range of $\Delta\varepsilon^p$. This relationship between plastic strain density energy and plastic strain for Masing-type materials[2] (Ellyin 1997) is given in the following form:

$$\Delta W^p = \frac{1-n'}{1+n'}\Delta\sigma\Delta\varepsilon^p \tag{2.5}$$

Equation (2.5) is based on fatigue test experiments. The relationship between the plastic strain and the total strain is illustrated empirically in the strain-energy approach for fatigue crack initiation prediction in the Smith-Watson-Topper (SWT) model (Smith *et al.* 1970); thus, the

[2] Masing-type materials: the materials which exhibit stable hysteresis loops, where various strain amplitudes are transferred to the same origin i.e. follow Ramberg-Osgood equation.

plastic strain can be determined as a function of material parameters and the fatigue crack initiation life as follows:

$$\frac{\Delta\varepsilon^{p}}{2}=\frac{\sigma_{f}^{'}\varepsilon_{f}^{'}}{\sigma_{\max}}\left(N_{init}\right)^{b+c} \tag{2.6}$$

From equations (2.5) and (2.6), the fatigue crack initiation life (N_{init}) can be expressed in the following form:

$$\Delta W^{p}=\frac{1-n'}{1+n'}\frac{2\sigma_{f}^{'}\varepsilon_{f}^{'}}{\sigma_{\max}}\Delta\sigma\left(N_{init}\right)^{b+c} \tag{2.7}$$

Where

n' = cyclic strain hardening exponent

$\sigma_{f}^{'}$ = fatigue strength coefficient

$\varepsilon_{f}^{'}$ = fatigue ductility coefficient

b = fatigue strength exponent

c = fatigue ductility exponent

$\sigma_{\max}$ = maximum local stress accounting for plasticity.

ΔW^{p} = plastic strain energy density

$\Delta\sigma$ = applied stress range on the welding detail.

The first five parameters (n', $\sigma_{f}^{'}$, $\varepsilon_{f}^{'}$, *b* and *c*) are predicted through fatigue crack initiation tests and dependent on the steel grade used whether base metal or weld metal as shown in Chapter 6.

The total fatigue life, N_{total}, is the summation of crack initiation life, N_{init}, predicted in Eq. (2,7) and crack propagation life, N_{prop}, estimated from Eq. (2.4), and is illustrated as follows:

$$N_{total}=N_{init}+N_{prop} \tag{2.8}$$

2.5. Methods of Fatigue Repair and Strengthening of Welded Details

Once a crack has been detected, various actions can be taken. First, the crack can be monitored over time based on fracture control plans defining inspection intervals. Secondly, the crack can be repaired by adequate means. Lastly, the cracked component can be replaced.

European convention of constructional steelwork ECCS (2005) listed the most important repair and strengthening methods to increase the remaining fatigue life of welded details. These methods are listed below:

- Removal of cracks
- Re-welding
- Post-weld treatments (grinding, shot peening, air hammer peening, Tungsten inert gas TIG dressing, ultrasonic impact treatment UIT)
- Adding plates or fibre reinforced plastic strips (FRP strips)
- Bolted splices
- Shape improvement
- Drilling of stop holes

For steel bridges in service, finding an efficient tool to improve the fatigue resistance of critical weld details is important. Weld toe grinding is considered to be an easy, cheap and fast method. However, this will require further experimental examination; especially for the full-scale specimens to assess the fatigue life improvement of welded details.

Kirkhope *et al.* (1999) reviewed various types of weld toe grinding to improve the weld profile, thus reducing the weld stress concentration. The main ones are burr grinding, disc grinding and water jet eroding. Since the burr grinding will be used in the experimental program in Chapter 5, it is important to review its characteristics and effect on fatigue life improvement.

Weld burr grinding is carried out using a high-speed grinder, which can be a pneumatic, hydraulic or electric grinder, driving rotary burrs at a rotational speed of between 15,000 and 40,000 rpm. There are two types of burr grinding: full profile and weld toe profile. In full profile burr grinding, the complete weld face is machined to remove surface defects and to blend the weld metal with the base plate. Whereas, only the weld toe is machined to remove the defects in weld toe and reduce the weld toe angle, which results in a decrease in the weld toe stress

concentration. It is essential that all defects and undercuts are removed from the weld toe for both procedures. Therefore, material is removed to a depth of at least 0.5 mm below any visible undercut, but should not exceed 2.0 mm or 5% of the plate thickness as recommended by DNV RP-C203 (2010).

The improvement in fatigue strength resulting from toe burr grinding is lower than that obtained by full profile grinding. However, the cost of toe grinding is substantially less (Smith and Hirt 1985).

The burr grinding is considered to be the most effective of all grinding methods. It also had easier accessibility and considered to be the best for improving the fatigue life for fillet welds (Kirkhope *et al.* 1999). However, the unevenness in the fillet weld profile could be difficult to maintain the weld toe grinding, which might reduce the benefit of enhancing the fatigue life. More experimental tests are required to assess the benefits of weld toe grinding on fatigue life improvement for severe welded details as illustrated in Chapter 5.

2.6. Reliability Concepts and Probabilistic Analyses

2.6.1. Introduction

In general, structural failure is normally related to the extreme applied stresses in structural components, though some serviceability measures, such as excessive deflections or cracking, can also be considered as failure (Ang and Cornell 1974). The ultimate limit state is the failure associated with collapse, while the serviceability limit state is related to unsatisfactory performance (Kulak and Grondin 2006). For cyclically loaded structures such as steel bridges and offshore structures, and in addition to the ultimate and serviceability limit states, it is mandatory to check the fatigue limit state.

The basic reliability problem in structural engineering can be defined by two statistical random variables, which are anticipated to be independent: one representing the load effect, S, and the other representing the resistance, R (Melchers 1999). The structure is considered to be in the safe domain if $R > S$. Moreover, the failure surface is defined by $R = S$ or expressed as a limit state function $G(Z)=R-S=0$. Thus, the probability of failure, p_f is defined as:

$$p_f = P\left(G(Z)<0\right) = P\left(R-S<0\right) \tag{2.9}$$

where $P(\bullet)$ denotes the probability of occurrence of event " $\bullet$ "

If the statistical input design variables, z_i, are assumed to be normally distributed, then *R* and *S* are also normally distributed (Weisstein 2003) and the probability of failure, p_f, takes the form shown here (Melchers 1999):

$$p_f = \Phi\left(\frac{-(\mu_R - \mu_S)}{\sqrt{\sigma_R^2 - \sigma_S^2}}\right) = \Phi\left(\frac{-\mu_z}{\sigma_z}\right) = \Phi(-\beta) \tag{2.10}$$

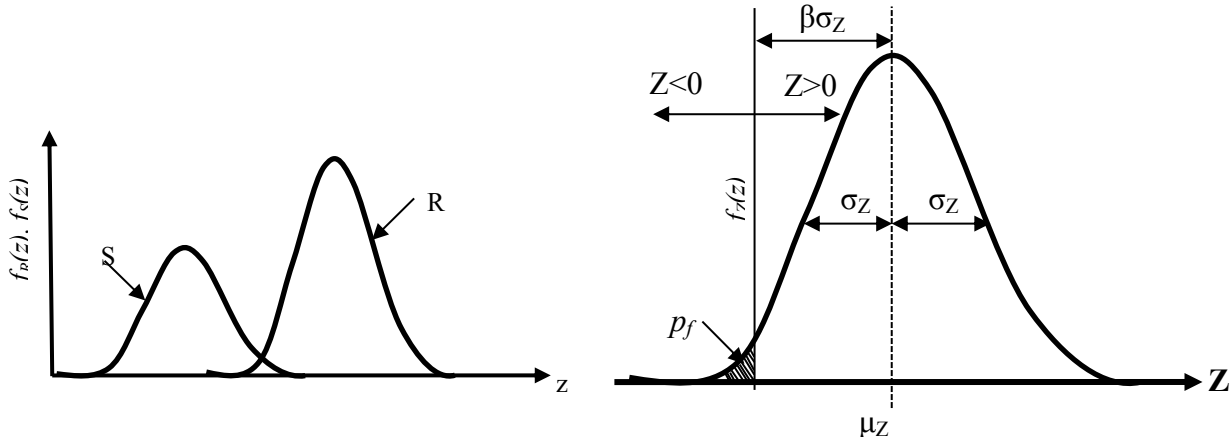

a) In terms of the pdf's of R and S *b) in terms of the pdf of G(Z) = R - S*

Figure 2.4 *The basic reliability problem (Melchers 1999).*

where μ_R and μ_S are the mean values of the resistance and the load effect (solicitation), respectively; also, σ_R and σ_S are the corresponding standard deviations. Figure 2.4a illustrates the reliability problem in terms of the probability density functions (pdf) of *R*, $f_R(z)$, and *S*, $f_S(z)$. Where the two curves overlap, the resistance is smaller than the load effect and the structure is subjected to fail; i.e., the shaded area under the curves is a measure of the probability of failure, p_f. The same information can be presented concerning the limit state function $G(Z) = R - S$, as shown in Figure 2.4b, where the probability of failure, p_f, is defined by the part of the curve to the left of the origin (Z = 0). The distance between the origin and the mean value of G(Z), μ_z, is known as $\beta.\sigma_z$, where σ_z is the standard deviation of G(Z) and β is called the reliability index (Cornell 1969).

Figure 2.4b emphasizes that by moving the origin to the right, the probability of failure, p_f, increases and the safety index, β, decreases. Conversely, to decrease the probability of failure, p_f, the safety index, β, has to increase. This concept is the basis of limit state design.

2.6.2. Monte Carlo Simulation (MCS)

Many researchers [e.g. Ang and Tang (1984), Melchers (1999)] used defined the *Monte Carlo simulation* (MCS) as a method of reliability analysis. This methodology aims to predict the limit state function numerous times, each time with a different set of randomly selected deterministic (i.e. fixed) values for the statistical variables, z_i. The following relationship predicts the probability of failure:

$$P_f = \frac{n\left(G(Z) \le 0\right)}{N_t} \tag{2.11}$$

wherein N_t is the total number of trials, and $n(\mathrm{G}(\mathbf{Z}) \le 0)$ is the number of trials for which the limit state was violated.

To obtain the input samples representing each random variable for checking the limit state function for each trial of the Monte Carlo Simulation, Figure 2.5 illustrates the process used for the random selection or *sampling* of the values for the various basic variables. For each trial, one may select a random number, r_i, ranging from 0 to 1 for each basic variable, X_i. The basic variable, X_i, could represent load or resistance probabilistic distribution. Each selected random number, r_i, is then transformed into a sample input value, x_i, using the following relationship (Melchers 1999):

$$x_i = F_{X_i}^{-1}\left(r_i\right) \tag{2.12}$$

Then, the sample, x_i, is used to check the fatigue limit state. This process of getting the input samples is repeated for all basic variables, defined by probabilistic distributions.

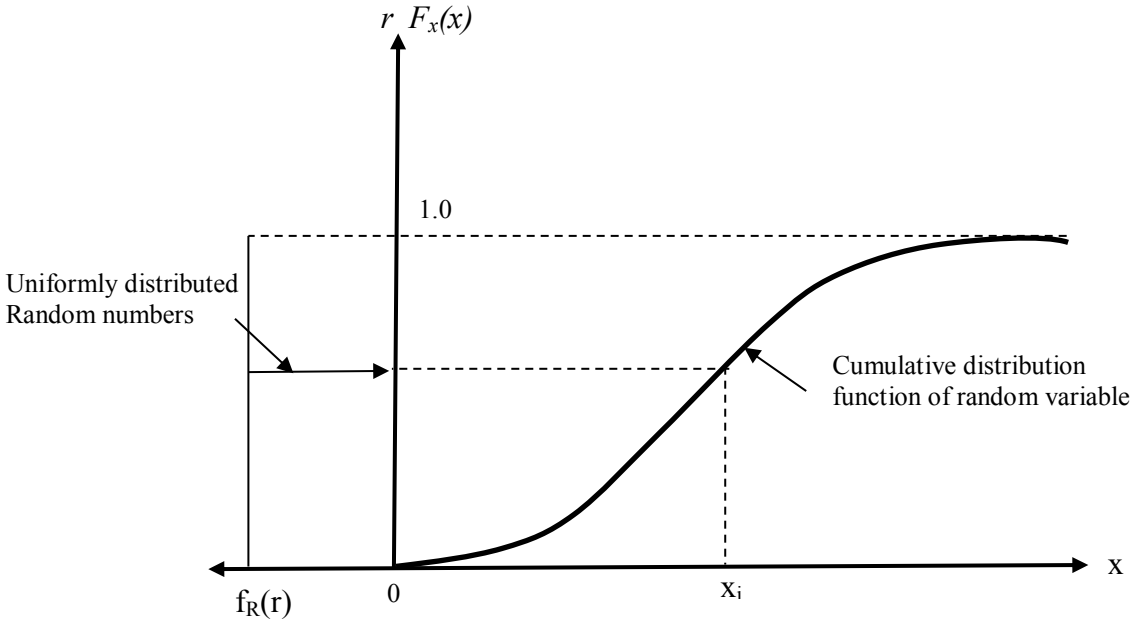

Figure 2.5 *Procedure of random sampling for probabilistic variables in MCS (Melchers 1999).*

The probability of failure, P_f, can be predicted according to Equation 2.11 after a number of trials are carried out in this way. The greater the number of trials performed, the greater the accuracy of the prediction will be achieved. The advantage of the MCS solution method is that the calculation speed is generally not affected by the number of statistical variables involved. However, the major disadvantage of the MCS method is that an extremely large number of trials may be required to attain a satisfactory level of precision. This number is generally considered to depend on the order of magnitude of the probability of failure being sought. In order to reduce the required number of trials, several methods are available such as importance sampling. These methods are commonly referred to as variance reduction techniques. They are discussed in detail in a number of references (e.g. Ang and Tang 1984, Melchers 1999).

In summary, the probabilistic fatigue life prediction of welded details in steel bridges requires the definition of all relevant fatigue loading and resistance parameters. Monte Carlo simulation, as a reliability method, will be implemented to predict the probability of failure and reliability indices of the welded details as illustrated in Chapter 7.

2.7. Problem Statement and Research Objectives

2.7.1. Problem Statement

The literature review emphasized the importance of using WIM to develop actual traffic data. Screening of WIM data must be implemented to ensure the quality for any prediction application. WIM databases collected from two provinces and one territory in Canada could be used to calibrate the fatigue truck factor in Canadian Highway Bridge Design Code (CSA 2006) dual slope S-N curves, currently used in CSA-S16-09 (CSA 2009). WIM data could also be employed to determine the number of stress cycles experienced for each passage of the design truck, N_d, which is compared with the values provided in CSA-S6-06 (CSA 2006). This parameter affects the annual number of cycles for fatigue life reliability prediction.

For fatigue life reliability of steel bridges, the bridge truck loading causing the acting stress range cycles at critical sections in one and multi-span bridge should be modeled using appropriate probabilistic distributions (normal, lognormal, Weibull, etc.) with its defining parameters (mean, standard deviation, etc.). Such truck loading probabilistic models will be employed to predict the remaining fatigue life of welded details and estimate the reliability index with the time to consider the failure consequence and inspection management.

The assessment of weld toe grinding as an easy, cheap and fast method for fatigue life improvement for welded details requires further investigation especially for severe welding details.

The energy-based method is more suitable in the fatigue crack initiation life to overcome the shortcomings in the stress-based and strain-based methods, which may not be appropriate for complicated welded details or load histories.

Based on the previous literature review, initial flaw shape and size, variability in weld size profiles need to be investigated to properly model their uncertainties, by expanding the previous studies to cover new research scope for fatigue life reliability prediction in welded steel bridges.

2.7.2. Research Objectives

Based on the above problem statements, the objectives and their specific aims of this research are outlined in the following:

Objective 1

To utilize the WIM databases received from two provinces and one territory in Canada in the calibration of the current fatigue truck factor and number of cycles, N_d, used in the Canadian Highway Bridge Design Code (CHBDC) (CSA 2006). The calibration will be based on dual slope fatigue design (S-N) curves, which is currently used in the Limit State Design of Steel (CSA 2009). This could be achieved through the following aims:

- Definition of the design truck (CL-625 and CL-800), actual truck data obtained from weigh-in-motion stations including the WIM screening criteria to remove any unrealistic data, as well as considering the most effective trucks, and a database of influence lines for various bridge configurations and span lengths.
- Development of the calibration procedure, based on equating the fatigue damage that results from the actual traffic and the design truck, using single and dual slope fatigue design curves.
- Illustration of the fatigue factor calibration results.
- Validation of the equivalent number of cycles, N_d, presented in Table 10.5 of CSA-S6-06 (CSA 2006) based on the predicted fatigue truck factors.

Objective 2

To develop a methodology, by which the actual truck data received from the same sources in Canada, could be used to model probabilistically the stress range histograms (stress range vs number of cycles) in fatigue life reliability predictions for various bridge configurations (one and multi-span girder bridge) and lengths. The steps below emphasized the methodology to achieve this objective.

- Assess the WIM data tolerances to the WIM specification ASTM E1318 (ASTM 2009).
- Fitting the stress histograms, employed for the fatigue truck calibration, by the appropriate probabilistic distributions and defining their probabilistic parameters for each bridge configuration and span.

Objective 3

To assess weld toe grinding as a method to improve fatigue life of severe welded details "Category E". The methodology adopted to satisfy this objective is described below.

- Fatigue testing of three full-scale groove T-joints under constant amplitude cyclic loading: two specimens have their weld toe ground and the third is considered as-welded specimen.
- Deterministic fatigue life prediction for the fatigue test results using finite element models and linear elastic fracture mechanics.

Objective 4

To estimate the remaining fatigue life and reliability indices for fatigue life reliability prediction for cruciform detail, that is considered to be a simplified detail for the tested specimens. Most of the parameters were considered to be probabilistic while other parameters were deterministic. The following steps are considered the specific aims to achieve such objective.

- Finite element analysis for cruciform detail of Category C to correlate the energy-based method parameters to the initial weld flaw (weld undercut) for eight different fillet weld sizes.
- Probabilistic prediction of fatigue resistance life using Monte Carlo Simulation for the cruciform detail using fatigue crack initiation, propagation material parameters in addition to residual stresses.
- Assessment of the remaining fatigue life reliability, using fatigue limit state, of a cruciform welded detail in a simple span bridge of length 36.0 m taking into account the probabilistic stress range histograms from WIM data and uncertainties of fatigue resistance uncertainties especially weld size profiles and weld undercut size.

2.8. Thesis Outline

By using the WIM databases from three Canadian sources, Chapter 3 explains the procedure and the results of the calibration of the fatigue truck factor, reduction factor and equivalent number of cycles due to design truck passage, employed in the Canadian Highway Bridge Design Code (CHBDC). In Chapter 4, the stress range histograms due to truck loading will be fitted into the appropriate probabilistic distributions for various bridge spans, sections and configurations. These distributions could be used for fatigue life reliability predictions. The small experimental program to assess the effect of weld toe grinding as post-weld treatment for full-scale groove T-joints is shown in Chapter 5. Chapter 6 presents the deterministic fatigue life prediction of the full-scale test results using the energy-based method for prediction of fatigue crack initiation life and linear elastic fracture mechanics for fatigue crack propagation life. Furthermore, Chapter 7 illustrates the reliability-based approach, which takes into account all the probabilistic and

deterministic input variables, to predict the fatigue life prediction for cruciform welded detail "Category C". Moreover, fatigue life reliability using probabilistic stress range histograms and fatigue life resistance is developed. Finally, Chapter 8 presents the research summary, conclusions as well as the recommendations for future work.

3. CALIBRATION OF BRIDGE CODE FATIGUE TRUCK

3.1. Introduction

In this chapter, WIM data is used to calibrate Canadian Highway Bridge Design Code (CHBDC) (CSA 2006) fatigue truck factor, reduction factor, C_L , and the number of design stress cycles, N_d , per truck passage on a bridge. This calibration is influenced by the source and quality of the WIM. Other parameters also affect the calibration such as bridge span length, configuration and fatigue detail category in case of using dual-slope fatigue curves. It was found that there is a need to adopt dual slope fatigue design curves in addition to implementing three different values of fatigue truck factors and number of cycles according to the bridge span length and configuration. Section 3.2 describes the methodology for fatigue truck calibration from the WIM data obtained from two provinces and one territory in Canada for the dual-slope fatigue design curves used in CAN/CSA-S16-09 (CSA 2009). Then, the calibration procedure of the equivalent stress cycles due to passage of design truck, N_d , is illustrated in Section 3.3. Finally, a summary of the calibration results is presented in Section 3.4.

3.2. Fatigue Truck Calibration for Bi-linear Fatigue Curves

3.2.1 General

In general, there are two main factors that affect the fatigue resistance of a fabricated steel structure: the number of load cycles and the stress range. The stress range is a function of the applied loads and the level of stress concentration at a critical detail, which can be considered by the selection of the proper detail category. This approach to account for stress concentration is convenient since only a nominal stress range, which does not include the effect of stress concentration, is used for design. For a given detail category, the relationship between stress range and the fatigue life, expressed as the number of load cycles to failure, takes the form of a linear relationship on a log-log scale, expressed as:

$$\log N = \log M - m \log \Delta\sigma_r \tag{3.1}$$

where N is the number of stress cycles to failure, $\Delta\sigma_r$ is the stress range, and M and m are numerical constants determined from a regression analysis of test data. For design, the fatigue curve usually represents the mean regression line minus two standard deviations. The value of m is generally taken as 3.0 for single slope S-N curves, and 3.0 and 5.0 for dual-slope S-N curves

and the value of M is chosen according to the severity of the analyzed detail (stress concentration). Figure 3.1 shows the fatigue curves adopted in CSA-S16-09 (CSA 2009) for eight different fatigue categories, which reflect the degrees of strength of fatigue resistance. For steel details, fatigue category A has the highest fatigue resistance, while fatigue category E1 has the lowest resistance. The steel details for various categories are shown in Figure 3.1.

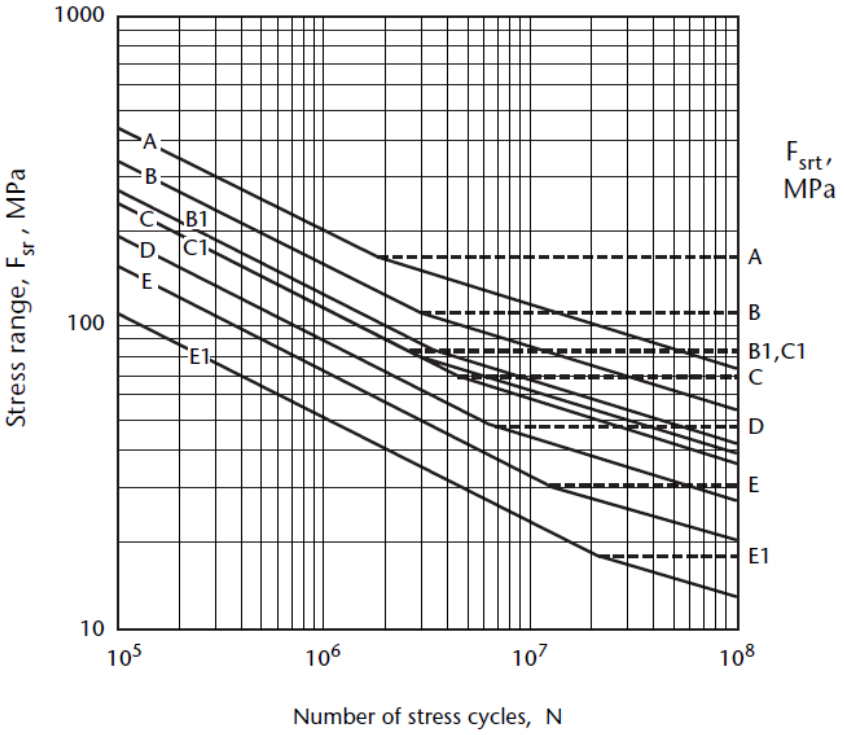

Figure 3.1 *Single and dual slope S-N fatigue design curves CSA-S16-09 (CSA 2009).*

CHBDC uses a five-axle design truck (CL-W) for the ultimate and serviceability limit states (ULS and SLS), to model all potential types of truck configurations on Canadian highways (axle weight, spacing, etc.). In order to achieve this with a single design truck, the CHBDC specifies that any of the truck axles that reduce the force effect shall be neglected. The approach used for the fatigue limit state preserves the same truck configuration as for the ULS and SLS, without removing any of the axles. The fatigue design truck is calibrated using WIM data so that the fatigue truck imparts to the structure the same amount of damage as the actual trucks.

The current value of the fatigue truck factor for steel bridges is 0.52 (CSA 2006). This was derived based on single-slope fatigue curves. On the other hand, the Canadian steel design standard, CSA-S16-09 (CSA 2009) has adopted dual slope S-N fatigue design curves, with a

slope of 3 above the constant amplitude fatigue limit (CAFL) and a slope of 5 below the constant amplitude fatigue limit. The dual slope concept, with a shallower slope below the CAFL is consistent with design for variable amplitude loading.

This section presents the calibration of the fatigue design trucks (CL-625 and CL-800) using dual slope S-N curves. Weigh-in-motion data from two provinces and one territory are used to assess the difference in fatigue truck between different regions and to suggest a suitable truck factor generated from dual-slope S-N curves. Section 3.2.2 describes the information required for the fatigue truck factor calibration, including the design truck configuration, the actual WIM traffic data, the procedure for WIM data screening and the influence lines adopted to predict load histories in critical sections in one and multi-span bridge girders. Then, the calibration procedure is addressed in detail in Section 3.2.3. Finally, the results of the fatigue truck calibration and the discussion are presented in Sections 3.2.4 and 3.2.5, respectively.

3.2.2 Information Required for Calibration of Fatigue Truck Factor

The calibration process for a fatigue truck requires the definition of a design truck, actual truck data obtained from weigh-in-motion stations, and a database of influence lines for various bridge configurations and span lengths.

3.2.2.1 Design Truck

The CL-W truck adopted in CSA-S6-06 (CSA 2006) is based on a set of regulations for interprovincial transportation in the *Memorandum of Understanding on Vehicle Weights and Dimensions* (MOU) signed by all Canadian provinces, initially in 1988 and amended in 1991 (TAC 1991). The MOU gives weight and dimension limits for straight trucks (single unit trucks), tractor/semi-trailer combinations, and trains. These represent minimum values of the maximum loads any province must allow on its principal highways carrying interprovincial traffic.

Regulatory loads vary quite widely across Canada, and several provinces seem to have some particular areas in which loads are allowed to exceed the levels of the MOU. These higher loads may apply only to some vehicles, specific to commodities, roads, or during certain times of the year. The minimum standard is represented by the CL-625 truck (illustrated in Figure 3.2) with a gross vehicle weight (GVW) of 625 kN. The CL-625 truck adopted in CSA-S6-06 (CSA 2006) has a GVW matches well the legal gross vehicle weight from the MOU. In the eight different

truck categories covered in the MOU, the maximum weight for a single truck axle is 9.1 tonnes (89 kN). Therefore, the individual axles of the Cl-625 truck can significantly be heavier than the MOU truck by as much as 40% to 90%.

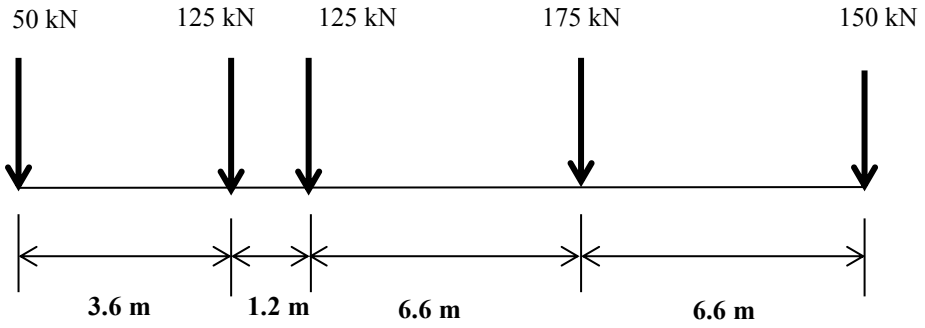

Figure 3.2 *CL-625 truck axles configuration in CSA-S06-06 (CSA 2006).*

Different provinces have adopted different design trucks, depending upon the local situation, by using a different load level such as CL-750 or CL-800, for example. The fatigue truck calibration for Ontario and Quebec WIM databases used the CL-625, while the fatigue truck calibration for Alberta and Northwest Territories (NWT) adopted the CL-800 fatigue truck. The axles spacing for CL-800 is the same as CL-625, but the axle weights are 28% higher than for the CL-625 truck.

3.2.2.2 WIM Traffic Data

The Ontario and Quebec ministries of transportation and the Northwest Territories department of transportation provided to the University of Alberta the weigh-in-motion (WIM) data (axle weights and axle spacing) used in this study. The WIM databases from Alberta were not available to conduct the calibration.

The Ontario truck data included 13365 trucks, collected in 1995. The time period for recording the WIM received from Ontario was not recorded in the database. Two truck data surveys were received from Quebec for two different sites with 100,000 truck data each in 2002: Batiscan site on Highway 40 and Nicolas site on Highway 20. The WIM data from Quebec were collected over a period of 130 days for the Batiscan site and 52 days for the Nicolas site. Lastly, the NWT Department of Transportation provided four sets of WIM truck data for four consecutive years from 2008 to 2011. The sets are: NWT2008 (112151 trucks); NWT2009 (92493 trucks); NWT2010 (95501 trucks); and NWT2011 (25633 trucks). The WIM data from NWT were

collected for twelve months (January to December) for years 2008, 2009 and 2010, while the WIM data for 2011 were collected for three months only (January, February and March) for each year from 2008 to 2011, inclusively.

It should be noted that Ontario and Quebec WIM data were received after being pre-screened for gross errors (GVW $\leq$ 0 and speed $\leq$ 0). However, this was not the case for the Northwest Territories WIM data, which contained a large percentage of unrealistic data that included truck gross vehicle weight or speeds with zero values. This represented a significant percentage of the WIM data received from the NWT. The percentage of unrealistic data (zero GVW and speed) was 15%, 34%, 21% and 11% for the data sets NWT2008, NWT2009, NWT2010, and NWT2011, respectively. Table 3.1 presents the number of trucks received from Ontario, Quebec and the Northwest Territories before implementing the detailed screening criteria for WIM as illustrated in Section 3.2.2.3. The intent of removing the gross errors (GVW $\leq$ 0 and speed $\leq$ 0) from the NWT data is to maintain them in the same ranking with the Ontario and Quebec WIM data.

Table 3.1 *Number of original truck data received versus WIM location.*

WIM Source	**Original Number of Trucks**	**After Removing Gross Errors** GVW $\leq$ 0 and speed $\leq$ 0	**Percentage of Trucks Remaining**
Ontario	13365	13365	100%
Quebec-Batiscan-Highway 40	100000	100000	100%
Quebec-Nicolas-Highway 20	100000	100000	100%
NWT 2008	112151	95518	85%
NWT 2009	92493	60717	66%
NWT 2010	95501	75015	79%
NWT 2011	25633	22798	89%

3.2.2.3 WIM Data Screening

The derivation of a precise and accurate truck loading model for steel highway bridges not only depends on the quantity of data to get a representative data set, but also relies on the quality of WIM data. Once the gross errors were removed from the NWT data only since Ontario and Quebec WIM data are already pre-screened from these errors, as shown in Table 3.1, further screening for all the seven sets of WIM data on several steps is required to remove vehicles from the database that do not satisfy a specific screening criteria for maximum speed, truck length, number of axles, minimum GVW, minimum axle weight and axle spacing limitations as shown in Table 3.2.

Many studies provided several WIM data screening criteria as shown in Table 3.2. The only WIM screening criteria directly applicable to Canada was carried out by Zhi *et al.* (1999) by removing the gross errors (GVW and/or speed is equal to zero) from Manitoba WIM data for pavement design. There were no studies in Canada to suggest a certain screening criteria for the WIM in the assessments of highway bridges compared to other countries. For this reason, this study reviewed various screening procedures used in the United States, Europe and South Africa. However, some trucks in the screened data exceed the weight and length specifications in the memorandum of understanding for trucks in Canada (TAC 1991) especially the special permit trucks. Although these trucks exceed the load limits of the MOU, they are present on the highways and they still cause fatigue damage and they should remain in the database.

Table 3.2 *WIM screening criteria from literature and suggested criteria.*

Criteria	USA (Sivakumar *et al.* 2008)	USA (Pelphrey *et al.* 2008)	Europe (O'Brien and Enright 2012)	South Africa (Ackermann *et al.* 2008)	TAC Limits (1991)	Suggested Criteria
Speed higher than (km/h)	160.1	160	120			160
Truck length larger than (m)	36.58	70		25	25	36
Truck length less than (m)				2.5		
Total number of axles less than	3	3	2	2	3	3
Total number of axles larger than		13		15		14
GVW less than(kN)	53.4	8.9				53.4
GVW larger than (kN)		1245.9			613.1	
Individual axle weight larger than (kN)	311.5	222.5		196.2	89.3	311.5
Individual axle weight less than (tons)	8.9	8.9		9.8		9.8
Steer axle heavier than (kN)	111.2	222.7		98	71	111
Steer axle less than (kN)	26.7	8.9		9.8		
First axle spacing less than (m)	1.52	1.52	0.4	2.1	3	1.5
Any axle spacing less than(m)	1.04	1.04	0.4	1.1		1.0

The suggested criteria in Table 3.2 have been implemented in seven filtration steps as shown in Table 3.3.

- Step 1: Remove trucks with speed > 160 km/h

  WIM data collected from high speed vehicles (> 160 km/h) are generally unreliable due to the limitations of the data collection equipment and need to be removed during the data screening.

- Step 2: Remove trucks with GVW < 53.4 kN

  Light weight trucks do not generally cause fatigue damage on highway bridges. To keep a truck count that reflects the number of trucks that cause fatigue damage, all the light trucks that do not cause fatigue damage should be eliminated from the database. This screening

criterion was particularly important in the NWT data, which had a large proportion of light vehicles.

- Step 3: Remove trucks with lengths > 36.0 m

  This value represents a reasonable length that had been used by Sivakumar *et al.* (2008) and gives allowance for special permit trucks that is beyond the truck length regulation limit, which is set to be 25.0 m (TAC 1991).

- Step 4: Remove trucks with steer axle weight > 111.2 kN

  For the maximum steer axle weight, Sivakumar *et al.* (2008) stated that the average steer axle weight for Class 9 trucks [AASHTO (2007) Truck Classification] is fairly constant for most WIM sites and significant deviation of steer axle weights is a sign of scale operational problems. TAC (1991) sets the limit of maximum steer axle weight to 70 kN. However, since regulations are not followed strictly to accommodate special permit trucks, the maximum steer axle weight in this study was increased to 111 kN.

- Step 5: Remove trucks with a total number of axles < 3

  Passenger vehicles and light weight pick-up trucks are not affecting the fatigue resistance. So it can be removed. According to TAC (1991), the minimum number of truck axles is set to be 3.

- Step 6: Remove trucks with axle weight (except steer axle) < 9.8 kN or > 311.5 kN

  This range is chosen to filter off any axle weight less than 9.8 kN. This value was assumed to satisfy the minimum axle weight to carry the suspension, braking system and any other components. This minimum axle weight value was also used in the screening criteria in the literature [Sivakumar *et al.* (2008), Pelphrey *et al.* (2008) and Ackerman *et al.* (2008)]. TAC (1991) sets a limit for the maximum weight of any axle, except the steering axle, to be 90 kN. The maximum axle weight of 311.5 kN proposed by Sivakumar *et al.* (2008) was found to be reasonable to have as much heavy truck axles as possible. As this data set will have a significant effect on the fatigue behavior of the highway bridges. However, this filter step did not result in a significant reduction of the WIM i.e. roughly 1.2% of the total WIM data.

- Step 7: Remove trucks with any axle spacing (except the first one) < 1.0 m

Axle spacing less than 1.0 m is not physically possible as the tires would overlap. As a result, any recorded data with axle spacing should be filtered out.

The remaining trucks after each screening step for the seven WIM data sets are presented in Table 3.3, where the percentage of the remaining trucks at each step is illustrated to highlight the significance of each filtration step. From Table 3.3, it can be seen that filters 2, 5 and 7 are the only ones that had a significant impact on the data set. It is noted that the vehicle speed and vehicle length were not available in the Ontario WIM data.

It should be noted that the filtering presented in Table 3.3 is cumulative from step 1 to step 7. For example, the filtering at step 4 consists of all the filters from step 1 to step 4 and the difference between the number of trucks at step 3 and step 4 is the number of truck removed from applying the filter at step 4.

Table 3.3 *Number of trucks remaining versus each filtration step for Ontario, Quebec and Northwest Territories WIM data.*

WIM Data Set	Ontario		Quebec-Batiscan (Highway 40)		Quebec-Nicolas (Highway 20)		NWT2008		NWT2009		NWT2010		NWT2011	
	No. of trucks	% residual filtered trucks	No. of Trucks	% residual filtered trucks	No. of Trucks	% residual filtered trucks	No. of Trucks	% residual filtered trucks	No. of Trucks	% residual filtered trucks	No. of Trucks	% residual filtered trucks	No. of Trucks	% residual filtered trucks
No filtration	13385	100	100000	100	100000	100	95518	100	60717	100	75015	100	22798	100
Step 1: Remove Vehicle Speed < 16 kmh and > 160 kmh	13385	100	100000	100	100000	100	94884	99.3	60357	99.4	74701	99.5	22760	99.8
Step 2: Remove GVW < 53.4 kN	13037	97.4	98650	98.7	99218	99.2	47212	49.4	29437	48.5	38244	51.0	12706	55.7
Step 3: Remove trucks with length > 36 meter.	13037	97.4	98406	98.4	98632	98.6	47161	49.4	29336	48.3	38190	50.9	12699	55.7
Step 4: Remove steer axle weight (P1) < 1 tons (9.8 kN) and > 11.34 tons (112 kN)	13000	97.1	98398	98.4	98626	98.6	44091	46.2	26822	44.2	34106	45.5	12513	54.9
Step 5: Remove two axle trucks: S2 ≠ 0	11844	88.5	92119	92.1	90754	90.8	38783	40.6	22633	37.3	29189	38.9	11942	52.4
Step 6: Remove any axle weight < 1.0 ton (9.8 kN) and > 31.75 tons (312 kN)	11719	87.6	91409	91.4	90218	90.2	34159	35.8	20799	34.2	27238	36.3	11336	49.7
Step 7: Remove any axle spacing < 1.0 meter	11700	84.8	90800	90.8	89166	89.2	32366	33.9	11843	19.5	25021	33.3	11205	49.2

Figures 3.3 to 3.9 present histograms of the gross vehicle weight (GVW) for the filtered data (after applying the seven steps illustrated above) compared to the non-filtered data for the seven sets of WIM data. The term non-filtered, which is used in these figures, refers to the WIM data filtered from gross errors (gross vehicle weight and/or speeds ≤ zero) only as illustrated in Table 3.1. In Figures 3.3 to 3.9, the frequency axis is cut-off at 5000 for the purpose of comparison between different WIM data sets.

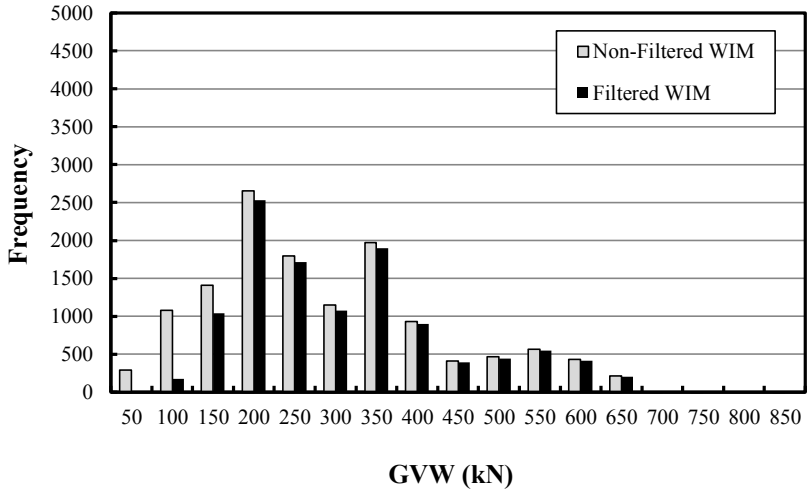

Figure 3.3 *Comparison of filtered and non-filtered GVW histogram for Ontario truck data Survey.*

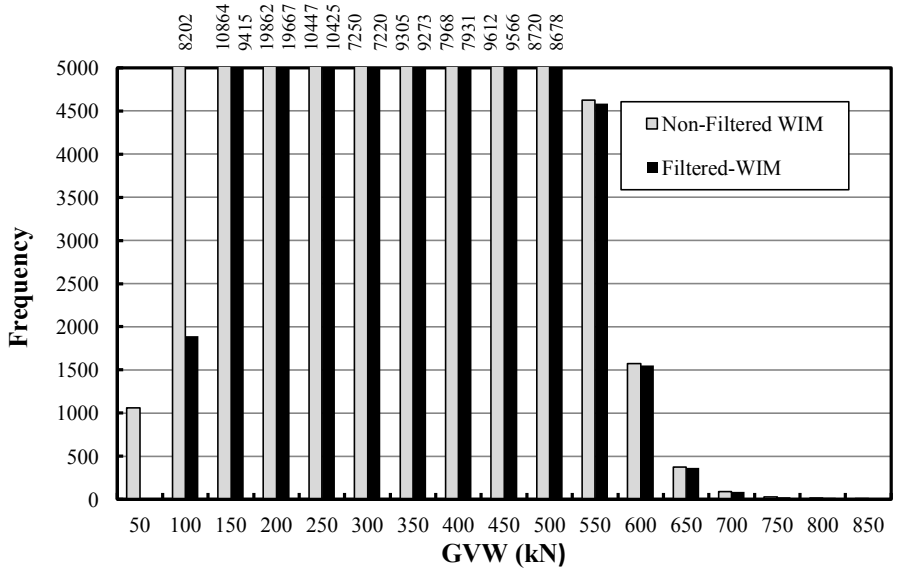

Figure 3.4 *Comparison of filtered and non-filtered GVW histogram for Quebec truck data survey (Batiscan site (Highway 40)).*

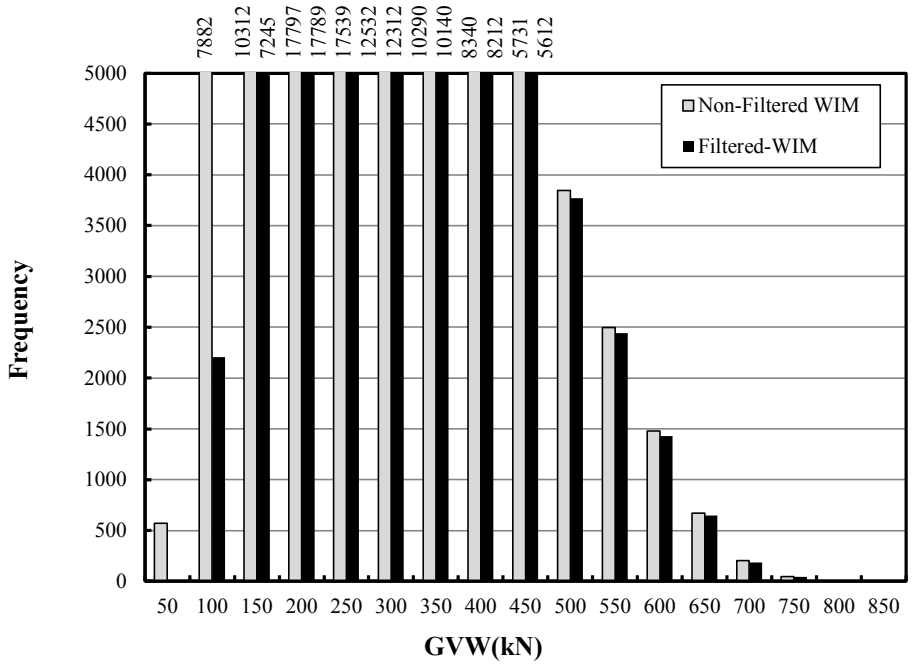

Figure 3.5 *Comparisons of filtered and non-filtered GVW histogram for Quebec truck data survey (Nicolas site (Highway 20)).*

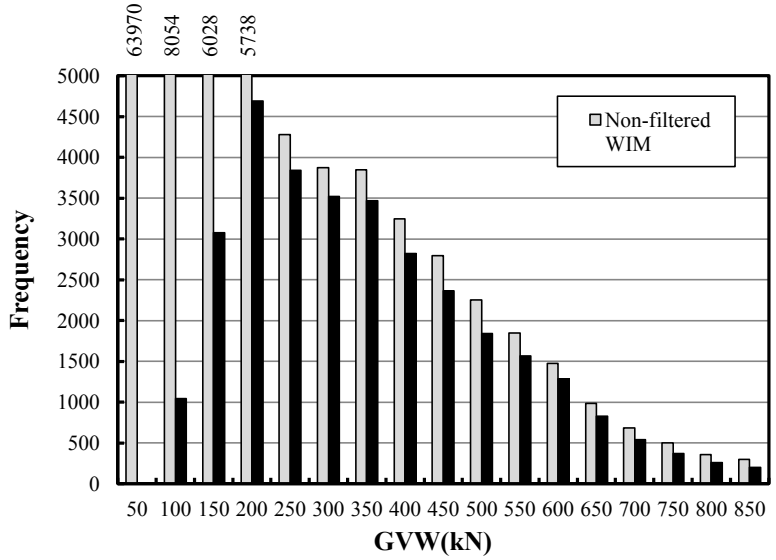

Figure 3.6 *Comparisons of filtered and non-filtered GVW histogram for NWT2008 truck data survey.*

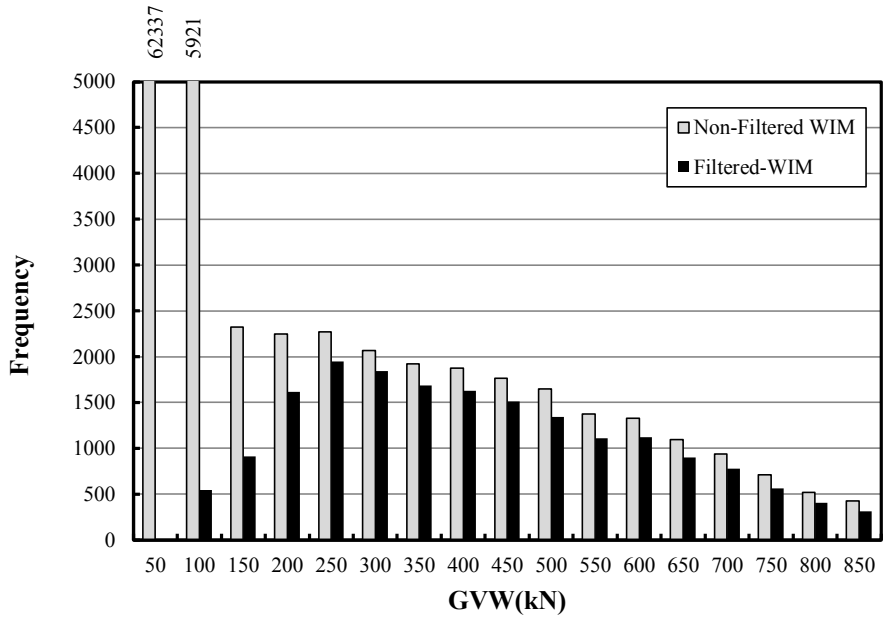

Figure 3.7 *Comparisons of filtered and non-filtered GVW histogram for NWT2009 truck data survey.*

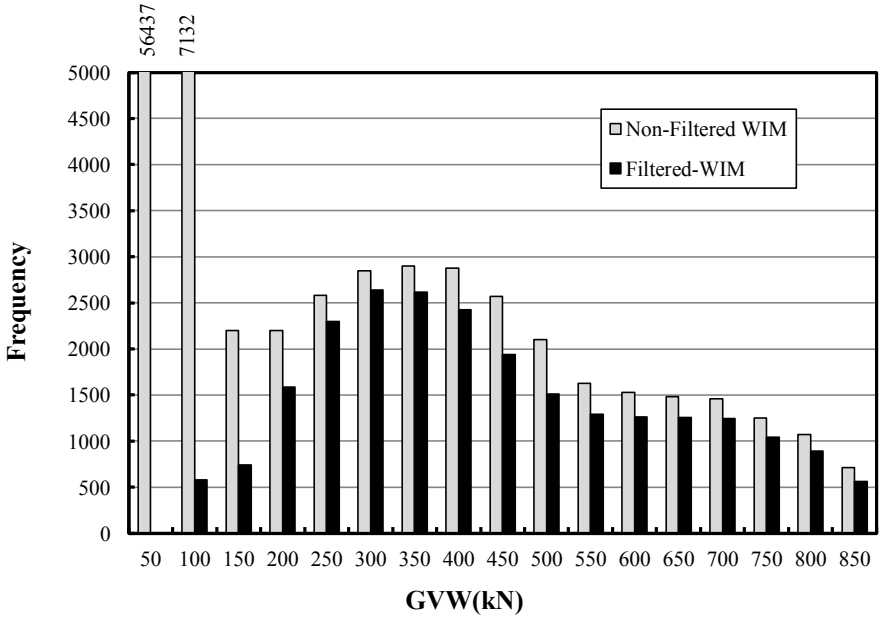

Figure 3.8 *Comparisons of filtered and non-filtered GVW histogram for NWT2010 truck data survey.*

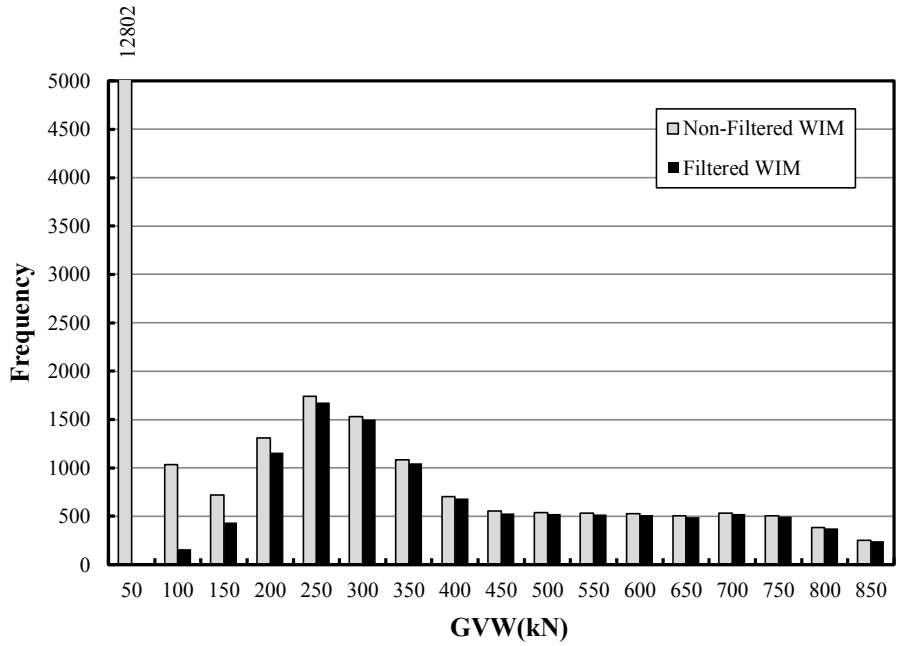

Figure 3.9 *Comparisons of filtered and non-filtered GVW histogram for NWT2011 truck data survey.*

For the Ontario and Quebec WIM data (Figures 3.3 – 3.5), the discrepancies between filtered and non-filtered data are small because the WIM data sets received from the ministries of transportations in Ontario and Quebec were already filtered for gross errors (GVW and speeds ≤ 0). However, further screening, according to the seven steps explained above, removed a maximum of 15.5% of the total WIM data from the population. This was not the case for the Northwest Territories WIM data (Figures 3.6 – 3.9), which revealed that the majority of original WIM data had been eliminated because of its large number of light weight vehicles (GVWs < 53.4 kN).

In order to compare the traffic data between different WIM data sets, Table 3.4 illustrates the weighted average for GVW for non-filtered and filtered WIM data for the seven sets of data. It can be observed that the weighted average truck using Ontario and Quebec ranges from 284 and 302 kN for the non-filtered data. After applying the seven filtration steps, the weight average for GVW increased from 6 – 8 %. For NWT data, the non-filtered weight average GVW emphasizes that most of the traffic on these highways were representing light weight trucks (142.8 kN –

213.6 kN). After applying the filtration procedure, the average weight for GVW increased by 92% to 190%.

Table 3.4 *Comparisons of weighted average GVW for filtered and non-filtered in WIM truck data survey.*

WIM Data Set	Weight Average GVW (kN)	
	Non-Filtered	Filtered
Ontario	288.1	312.3
Quebec-Batiscan	302.2	321.3
Quebec-Nicolas	284.5	301.6
NWT2008	156.5	348.6
NWT2009	142.8	415.5
NWT2010	176.1	439.3
NWT2011	213.6	411.8

3.2.2.4 Influence Lines

Influence lines are used to generate the bending moment histories at critical sections along bridge girders caused by the trucks contained in the databases and the design truck. Three different bridge span configurations will be used for calibration: single span, two-span continuous, and five-span continuous beams. Influence lines for positive moment at midspan for one, two and five-span beams, negative moment at the interior supports for two and five-span beams will be used in this study (Figure 3.10). For the three span continuous bridge, the influence lines for positive moment at midspan and the negative moment at interior support were found to have a similar ordinate values to the positive moment at midspan for five-span and negative moment at interior support for two-span bridges respectively. Therefore, the three span continuous bridge was not considered in this study since their influence lines will be adopted from the two and five-span bridge configurations. Coughlin and Walbridge (2010) found that the shear force histories are not critical. Therefore, the fatigue truck factor in this study was calibrated only for bending moments.

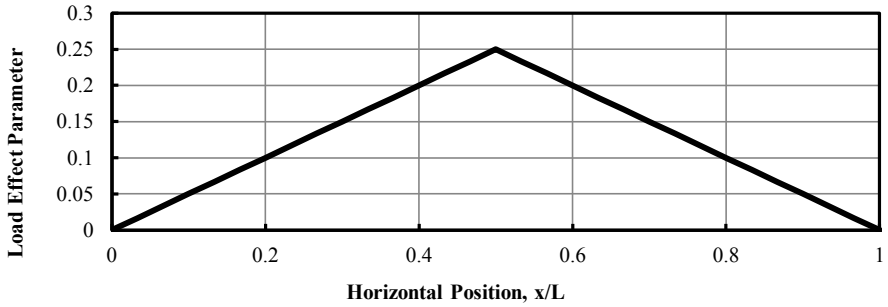

a) One Span

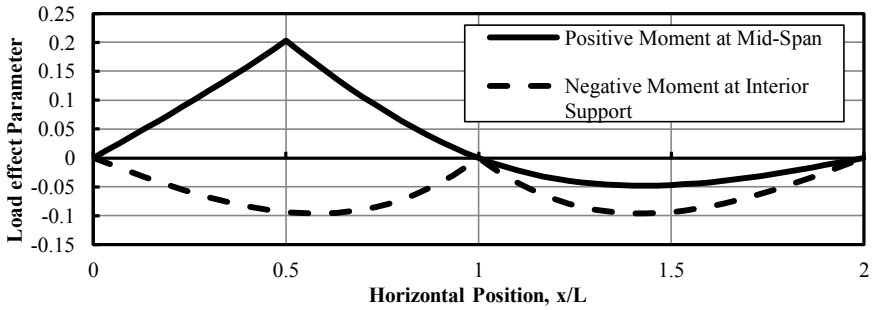

(b) Two Equal Spans

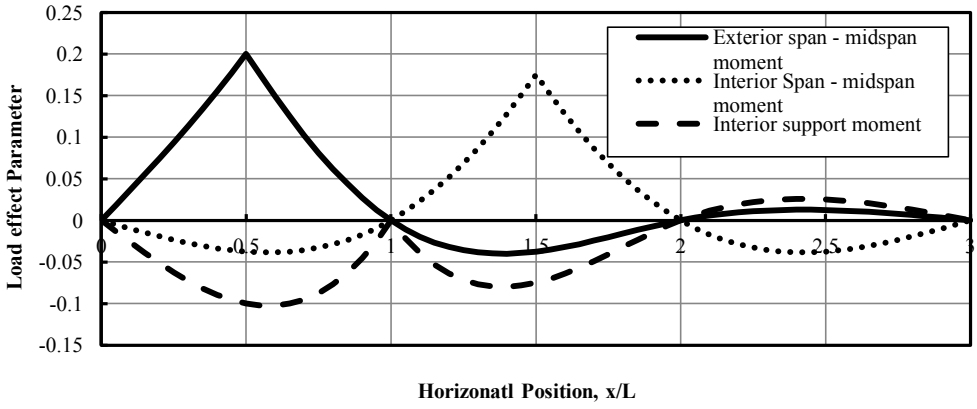

(c) Three Equal Spans

Figure 3.10 *Influence lines for midspan positive moment and negative moment in one, two, three, and five equal span bridge girders.*

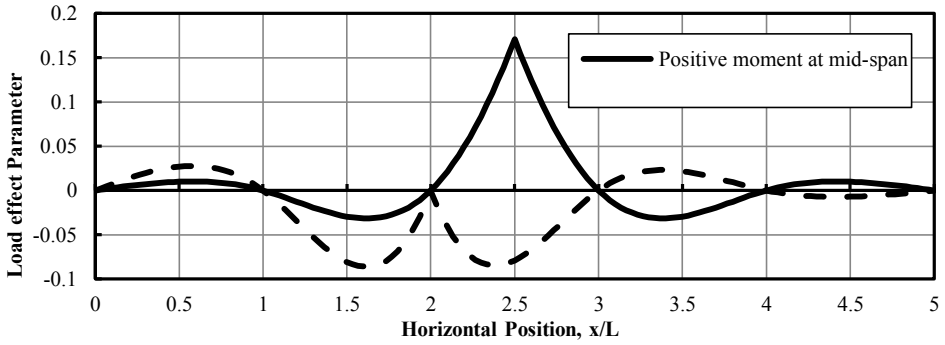

(d) Five Equal Spans

Figure 3.10 *(cont'd)*

3.2.3 Calibration Procedure

Coughlin and Walbridge (2010) developed a fatigue truck calibration procedure using single slope fatigue design curves for aluminum bridges based on WIM data from Ontario. Their fatigue truck factor is estimated using the fatigue life constants, γ, predicted from real and design truck data that will cause a fatigue damage of value of 1.0 by choosing an arbitrary fatigue life constant. Accordingly, the number of cycles due to real and design trucks are adjusted to result a fatigue damage summation of 1.0. The estimated design truck factor, γ_{code}, is based on the maximum stress range induced by the code truck and does not encounter any other smaller stress ranges. The fatigue truck factor is also affected by the dynamic effects due to many factors including pavement roughness. Hong *et al.* (2010) found that the fatigue truck factor is significantly decreased if the pavement roughness is ignored. Their result assumed that the traffic volume used for the design is the actual traffic volume, the bridge deck roughness parameters are suitable and finally that this was for simple span bridge. Since the current research investigates the fatigue truck factor for one, two and five span bridge, and due to lack of data, the dynamic effect was not considered.

In this study, seven sets of WIM data, collected from two provinces and one territory in Canada, will be employed to develop more comprehensive procedure for fatigue truck calibration in steel highway bridges using single and dual-slope fatigue design curves.

Although the developed procedure starts with estimating the load effect histograms due to real and design trucks, which is similar to Coughlin and Walbridge (2010) methodology, the effect of

various fatigue detail categories and bridge span lengths is illustrated to investigate their effect on the fatigue truck prediction for single and dual-slope fatigue curves.

The developed procedure for the fatigue truck calibration, using single and dual slope fatigue design curves, is based on equating the fatigue damage that results from the actual traffic to the damage resulting from the same number of design trucks as the number of actual trucks.

Since the number of trucks in the database is very large, MATLAB was used to establish the load histories for different critical sections. Appendix C illustrates the MATLAB files used to calculate the bending moment histories and to obtain the moment range spectrum. The calculations were conducted for one, two and five-span bridges with spans varying from 2.0 to 70.0 m. For Quebec WIM data, the calculations were conducted from span length of 2.0 m to span length of 52.0 m for the midspan and interior support moments in two and five-span bridge due to numerical problems in predicting the load histories because it contained the highest number of trucks. For each span length / influence line combination, the calibration procedure is as follows:

1. Each influence line is loaded with each truck from the traffic data (one truck at a time) by moving the truck in increments of 1.0 m along the influence line to generate the moment history for all trucks in the database. The step size of 1.0 m was used in the fatigue truck calibration for all span lengths including the small span length of 2.0 m. The fatigue truck calibration results emphasized that the peak fatigue truck values occurred from span lengths of 10.0 to 18.0 m. Therefore, the step size does not affect the calibration results especially for the least span length of 2.0 m.
2. Once the moment history for all of the trucks is generated, the rainflow method (See Appendix C) is used to count the stress/load cycles and provide a moment range spectrum (moment range versus frequency). The bending moment range in each location for every span length is then transformed into stress range by employing appropriate built-up steel sections for the main girders of the bridges. Appendix D illustrates a sample calculation for the design of built-up sections and the prediction of stress ranges from moment ranges. The stress range spectrum is required to derive the probabilistic model for stress ranges as illustrated in Section 4.2.3. However for the fatigue truck calibration, the transformation is not required at this stage since the fatigue truck is computed as a function of the ratio between the damage due the real

(D_{real}) and design truck (D_{code}). Therefore, the section properties are not affecting the results of fatigue truck calibration.

3. To calculate the fatigue damage due to truck load (D), Miner's (Miner 1945) cumulative damage rule is used along with the bending moment histogram. D_{real} is the fatigue damage using bending moment range histogram for real traffic, while D_{code} is the fatigue damage due to the bending moment histogram for design truck multiplied by the total number of actual trucks. In both cases, the fatigue damage was predicted using all fatigue categories for the single slope and the dual slope fatigue design curves. In the dual slope curves, the constant amplitude fatigue limit (CAFL) is taken into account in the fatigue damage calculation.
4. The fatigue truck factor is calculated as the mth root of the ratio of the damage caused by the real trucks, D_{real}, to the damage caused by the same number of design trucks as the total number of trucks in the database, D_{code}. For a single slope fatigue curve with m = 3, this is expressed as:

$$\text{Fatigue truck factor} = \left(\frac{D_{real}}{D_{code}} \right)^{(1/3)} \tag{3.2}$$

   A similar procedure is used for the fatigue factor related to the dual slope fatigue curves, except that the fatigue damage caused by the factored truck is calculated using the dual slope fatigue curves. Since the fatigue damage is not linearly related to the fatigue curve when we are using a dual slope fatigue curve, equation (3.2) cannot be used. Therefore, the calculations are conducted in a spreadsheet and the fatigue damage for the factored truck is calculated in terms of an unknown fatigue truck factor determined iteratively to result in the same amount of damage as the trucks from the database.

The fatigue damage, calculated using Miner Summation for real trucks, D_{real} and design truck, D_{code}, is based on stress ranges not stress amplitudes. The stress amplitude is used in CSA-S6-06 (CSA 2006) as a limitation for design purposes (Clause 10.17.2.3.1 in CSA-S6-06), the fatigue stress range resistance should be bigger than or equal the constant amplitude threshold stress range of each detail, defined in Table 10.4 in CSA-S6-06 (CSA 2006). The aim of calibration is not to determine the fatigue stress range resistance, but to calibrate the fatigue truck factor of

0.52. This was carried out by equating the fatigue damage, using stress ranges from the rainflow analysis, from real and design trucks. Then, calculate the fatigue truck factor that makes these two fatigue damages equal.

3.2.4 Results of Calibration

The results of the truck calibration for different fatigue categories (categories A to E1) reflect different steel details severities for one, two and five-span bridges. For the three-span bridge case, it will be developed from the fatigue truck calibration results of two and five-span bridge. Consequently, the calibration results of positive moment for interior five-span bridge are used as the calibration results for positive moment for interior three-span bridge. Furthermore, the results induced by the negative moment of interior two-span bridge are employed for the negative moment for interior three-span bridge.

Most curves exhibit a peak value in the short span lengths and reach a constant value in span lengths greater than about 30.0 m in most cases. Because of the high sensitivity of the fatigue truck factor between span lengths of 2.0 m and 30.0 m, the recommended fatigue truck factors were estimated for three regions: span length $\leq$ 12.0 m; 12.0 m < span length $\leq$ 30.0 m; and span length > 30.0 m. The span length of 12.0 m is currently used in CSA-S6-06 (CSA 2006) as a boundary span for the values of equivalent stress cycles, which will be validated in Section 3.3.

3.2.4.1 Ontario Truck Data

For the Ontario WIM data, the fatigue truck factors are shown in Figures 3.11 to 3.13. Figure 3.11 illustrates the fatigue truck calibration using the single slope fatigue curves used in CSA-S6-06 (CSA 2006), while Figures 3.12 and 3.13 display the calibration using the dual slope fatigue curves. Figure 3.11 shows the relationship between the fatigue truck factor and span length for the bending moment computed at five critical sections as described above. The values of the truck factor are significantly higher for the midspan bending moment in one and two-span bridges as well as the negative moment at interior support of the two-span bridges than for the midspan bending moment and the negative moment at interior spans in five-span bridges. The peak fatigue truck factor is 0.60 at a span length of 16.0 m. The truck factor is almost constant at 0.56 for span lengths from 28.0 to 70.0 m. The other fatigue truck factor curves shown in Figure 3.11 (the moment at the middle of an interior span and the moment at the first interior support for

the five-span continuous) show similar trends but with lower truck factors than those predicted from the midspan moments for one and two-span bridge.

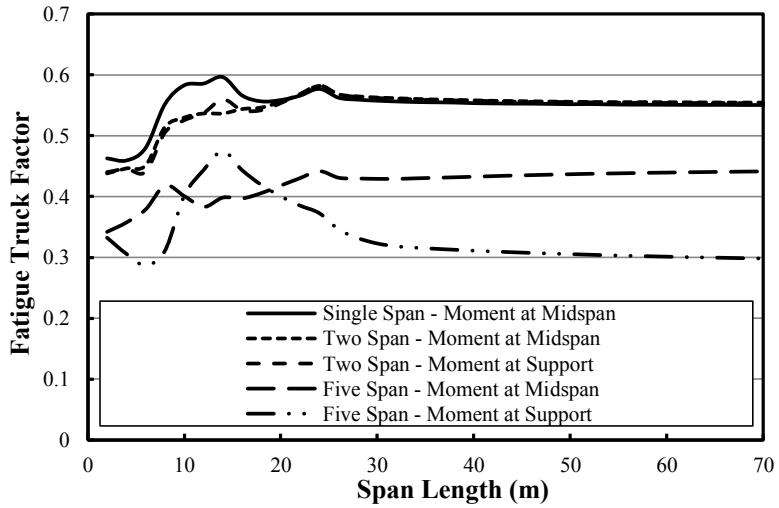

Figure 3.11 *Fatigue truck factor for single slope fatigue curves (Ontario data).*

Figure 3.12 presents the fatigue truck factors for single span and two-span bridges using the dual slope fatigue curves. For the moment at midspan in a single span bridge (Figure 3.12(a)), there is a variation in the value of the fatigue truck factor between 0.46 and 0.58 for spans from 2.0 to 10.0 m due to the differences in fatigue constants in various fatigue categories. Most of the variation in the fatigue truck factor values is observed in the short span range (2.0 to 10.0 m). The peak value for the truck factor is about 0.6 at a span length of 17.0 m. For span longer than 30.0 m, the fatigue truck factor remains nearly constant at a value of about 0.55.

The fatigue truck factor for the midspan and interior support bending moments for two-spans bridge girders (Figures 3.12 (b) and (c)) shows similar variations with a maximum truck factor of 0.57 at a span length of 24.0 m. For span lengths greater than 25.0 m the fatigue truck factor is nearly constant with a value of about 0.56. The figures illustrating the fatigue truck factor versus span length are derived for the eight fatigue categories (A to E1) of CSA-S6-06 (CSA 2006).

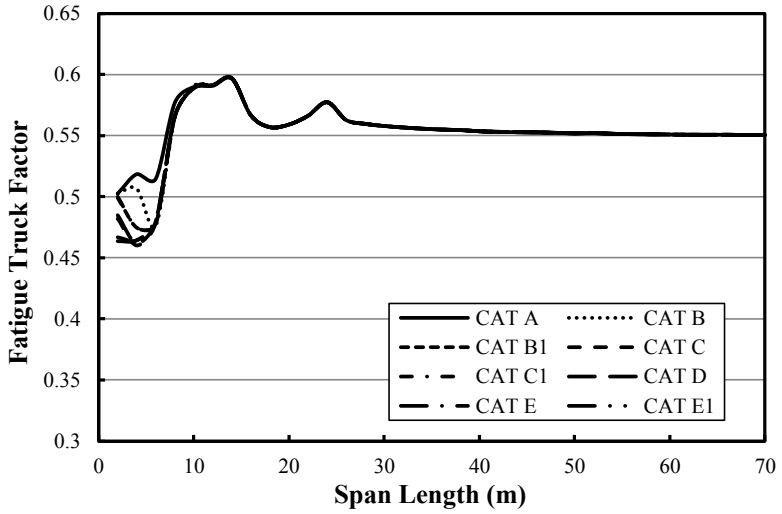

(a) Single span – Moment at midspan

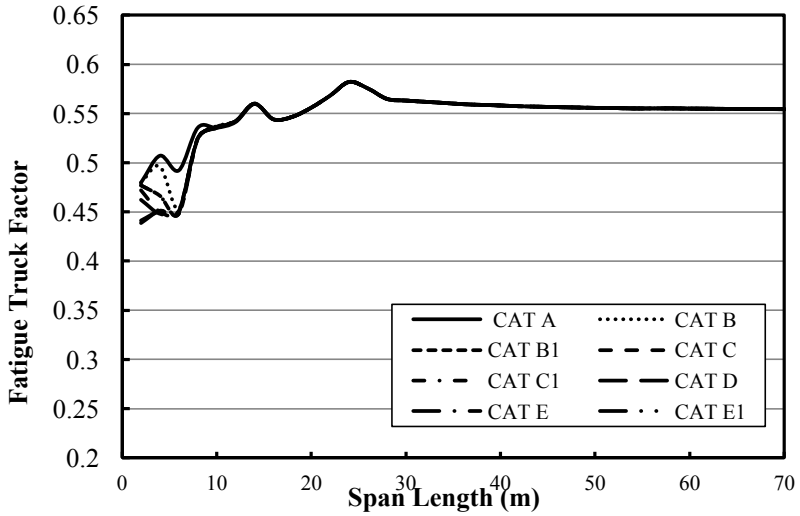

(b) Two-spans- Moment at midspan

Figure 3.12 *Fatigue truck factor for dual slope fatigue curves (Ontario data).*

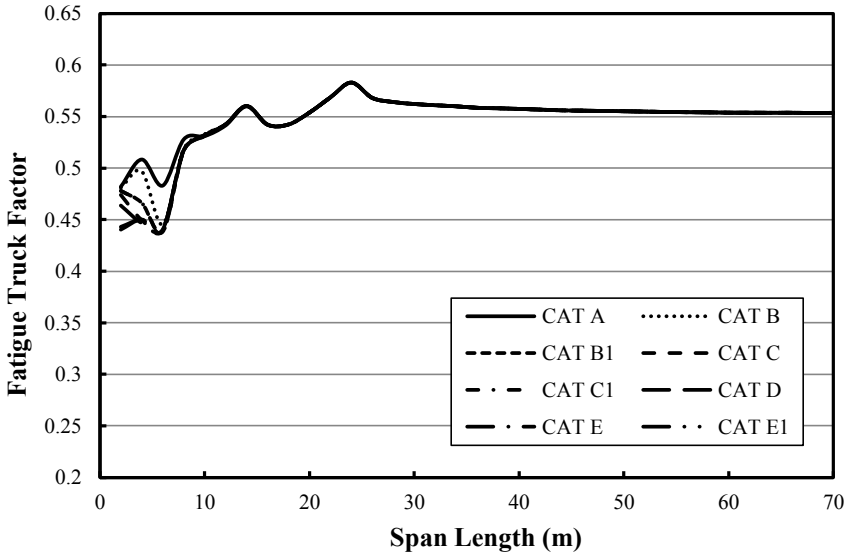

(c) Two-span- Interior support moment

Figure 3.12 *(cont'd)*

Figure 3.13 presents the fatigue truck factor for dual slope fatigue curves for midspan and interior support moments in five-span continuous bridges for different fatigue categories. For the five-span midspan moment case (Figure 3.13(a)), the truck factor starts with a small value ranges from 0.28 to 0.37 at span length of 2.0 m according to the fatigue category. At a span length of 12.0 m, all the curves converge and reach a peak value of 0.44. The truck factor remains almost constant at 0.44 beyond a span length of 25.0 m. The truck factor for the interior support moment (Figure 3.13 (b)) exhibits a different trend, as the truck factor ranges from 0.28 - 0.37 at span length of 2.0 m, then increase rapidly to reach a peak of 0.47 at span length of 18.0 m. A rapid decline occurs from the peak value to a value of 0.30 for spans longer than 30.0 m.

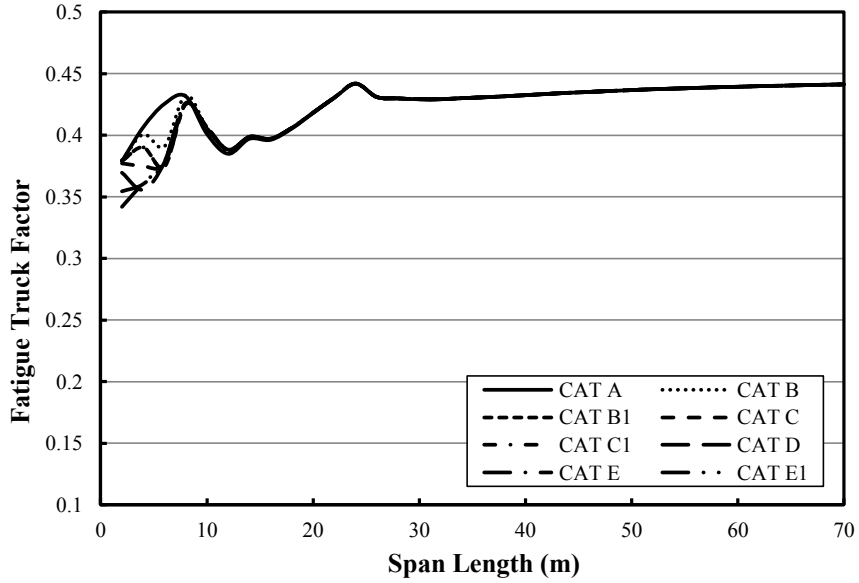

(a) Five-span – Moment at midspan

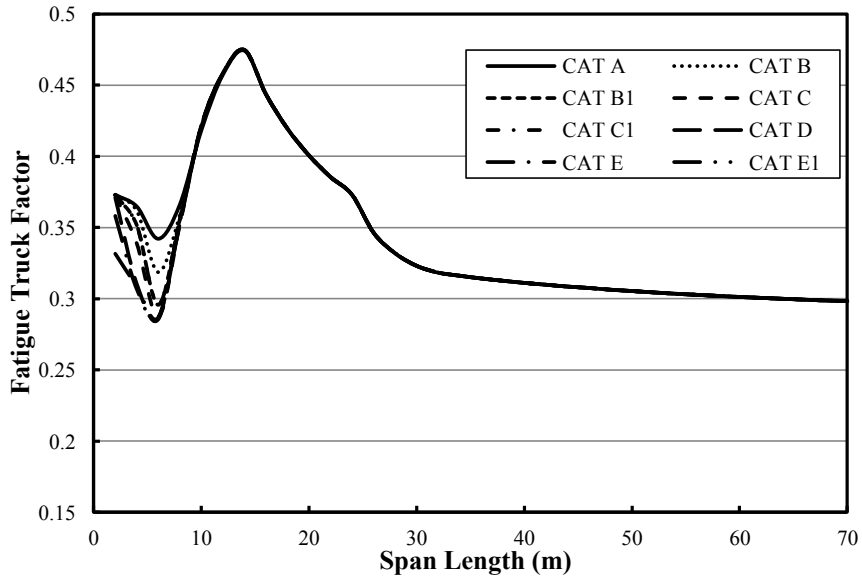

(b) Five-spans – Interior support moment

Figure 3.13 *Fatigue truck factor for dual slope curves and five-span continuous bridge (Ontario data).*

3.2.4.2 Quebec Truck Data (Highway 40, Batiscan Site)

The fatigue truck factor obtained from the WIM truck data collected from Batiscan site on Quebec's Highway 40 is shown in Figures 3.14 to 3.16. Figure 3.14 applies to single slope

fatigue curves while Figures 3.15 and 3.16 are based on the dual slope fatigue curves. Figure 3.14 shows the fatigue truck factor for critical sections in one, two and five-span bridges. The fatigue truck factor is significantly higher than for the other two moment cases (midspan and interior support bending moments for five-span bridge). The peak fatigue truck factor is 0.58 at a span length of 14.0 m. For span lengths from 25.0 m to 70.0 m, the truck factor is almost constant at 0.55. The other fatigue truck factor curves shown in Figure 3.14 (midspan and interior support moments for five-span continuous) demonstrate related developments but with lower values than those predicted one and two-spans.

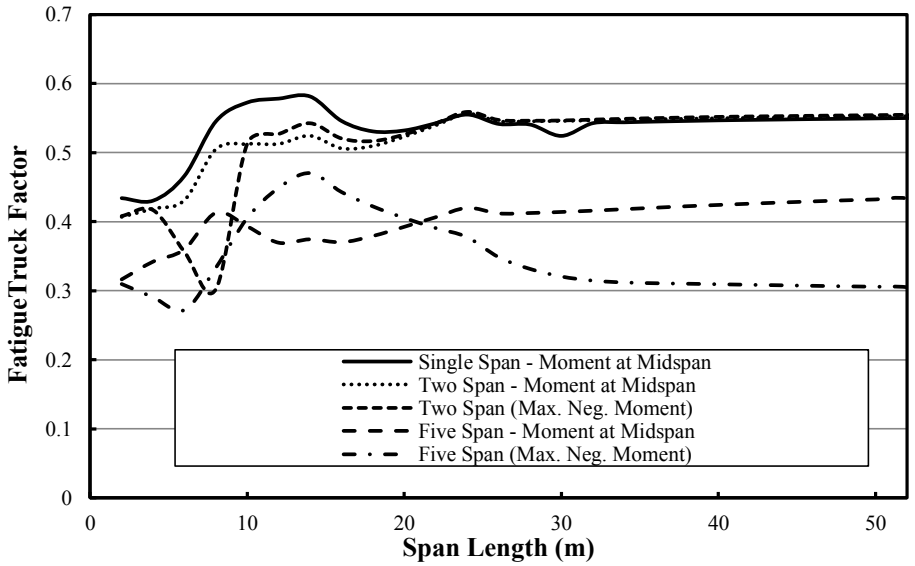

Figure 3.14 *Fatigue truck factor for single slope fatigue curves (Batiscan truck data).*

Figure 3.15 illustrates the fatigue truck factor for dual slope fatigue curves for one and two-span bridges. For the midspan moment in a single span bridge (Figure 3.15(a)), the fatigue truck factor varies between 0.43 and 0.52 for spans up to about 10.0 m. The fatigue truck factor then increases to reach a peak of 0.58 at span length of 15.0 m. The fatigue truck factor decreases slightly reach a value of 0.55 after span length of 30.0 m. Figure 3.15(b) shows the truck factor versus span length for moment in midspan for two-span bridge girder. Similar variations in the truck factor values are observed in spans shorter than 8.0 m for different fatigue categories. However, at a span length of 8.0 m, all the curves converge and reach a maximum value of 0.56 at a span length of 24.0 m. After span length of 25.0 m, the fatigue truck factor is almost constant at 0.55. In Figure 3.15(c), the fatigue truck factor relationship exhibits another pattern especially in the small range spans. The truck factor is about 0.42 for a 2.0 m span and decreases sharply to

0.3 at a span length of about 9.0 m. The maximum truck factor is 0.56 for span between 10.0 m and 30.0m. For spans longer than 30.0 m, the fatigue truck factor is approximately 0.55.

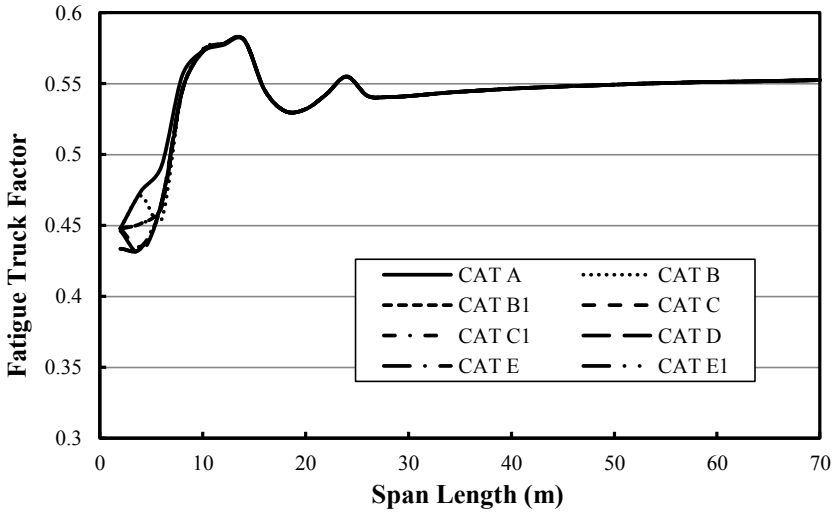

(a) One span – Moment at midspan

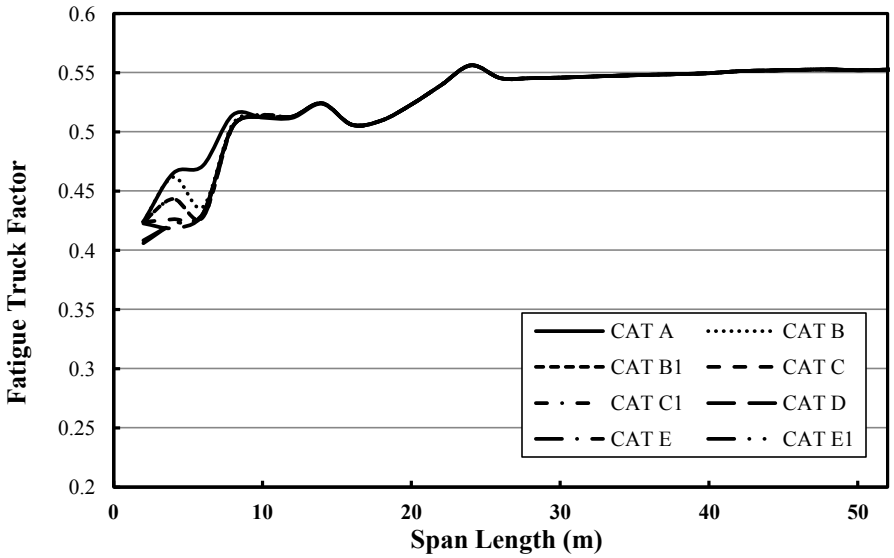

(b) Two-span- Moment at midspan

Figure 3.15 *Fatigue truck factor for dual slope fatigue curves (Batiscan truck data).*

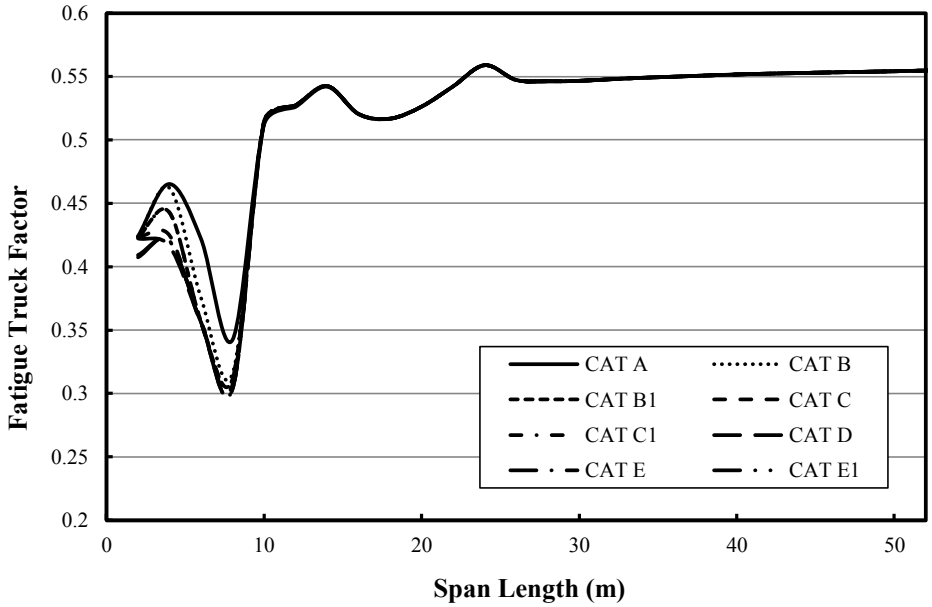

(c) Two-span- Interior support moment

Figure 3.15 *(cont'd).*

Figure 3.16 shows the fatigue truck factor for the dual slope fatigue curves for positive moment for midspan and negative moments at interior support in five-span bridges for different fatigue categories. The truck factor for the five-span midspan moment case (Figure 3.16(a)) is 0.33 at span length of 2.0 m. At a span length of 12.0 m, all the curves merge into the same curve. The maximum truck factor is 0.42 for span ranges less than 30.0 m, while the truck factor is 0.44 for spans larger than about 30.0 m. The truck factor for the interior support moment (Figure 3.16 (b)) displays a different trend. For span lengths of 2.0 m to 9.0 m, the truck factor ranges from 0.27 to 0.35. A rapid increase in truck factor is observed for spans lengths between 10.0 m and 15.0 m the factor increases rapidly and reaches a peak of 0.47 at span length of 15.0 m. For spans longer than 15.0 m there is a rapid decline in truck factor to a value of 0.30 for span lengths beyond 30.0 m.

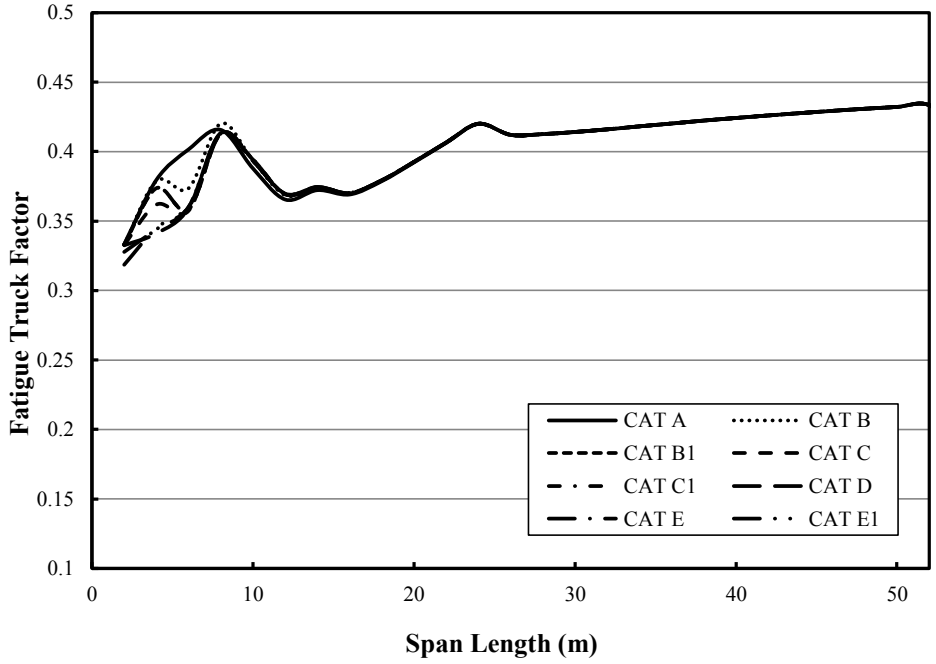

(a) Five-span – Moment at midspan

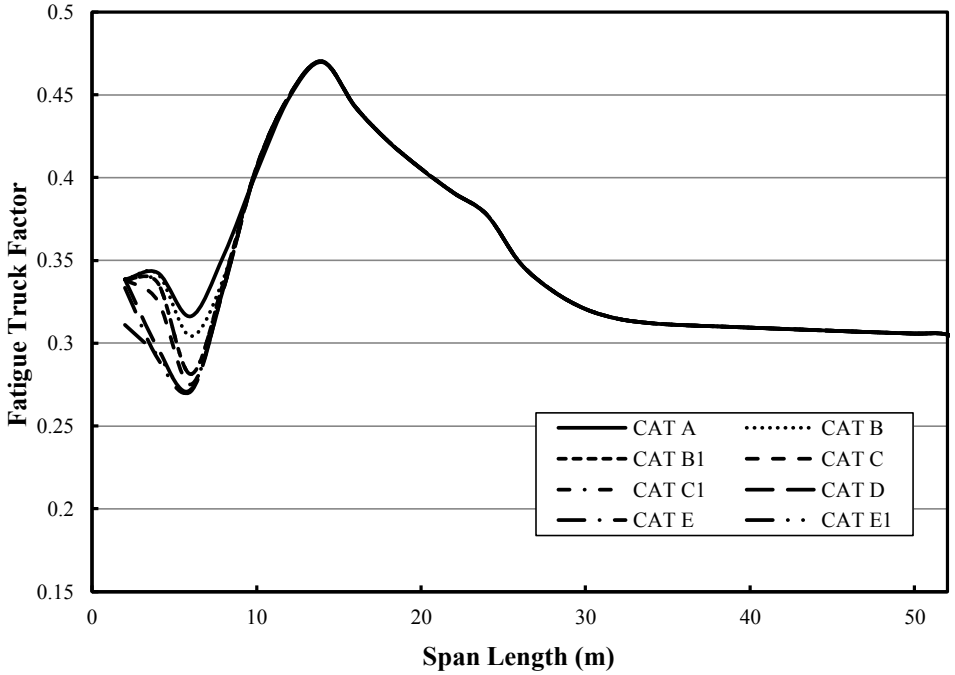

(b) Five-span – Interior support moment

Figure 3.16 *Fatigue truck factor for dual slope fatigue curves and five-span continuous bridge (Batiscan truck data).*

3.2.4.3 Quebec Truck Data (Highway 20, Nicolas Site)

The fatigue truck factor for the truck data survey collected from Nicolas site on Quebec's Highway 20 is shown in Figures 3.17 to 3.19. Figure 3.17 is based on the single slope fatigue curves used in CSA-S6-06 (2006) while Figures 3.18 and 3.19 are based on the dual slope fatigue curves used in CSA-S16-09 (2009). A comparison of the fatigue truck factors for the single slope fatigue curves as shown in Figure 3.17 show significantly higher values for one and two-span bridges than for five-span bridges. The peak fatigue truck factor is 0.57 at a span length of 14.0 m. The fatigue truck factor is almost constant at 0.51 for span lengths longer than 25.0 m. The other fatigue truck factor curves shown in Figure 3.17 (midspan and at support moments for five-spans continuous) have similar trends but with lower values than those predicted in one and two-span.

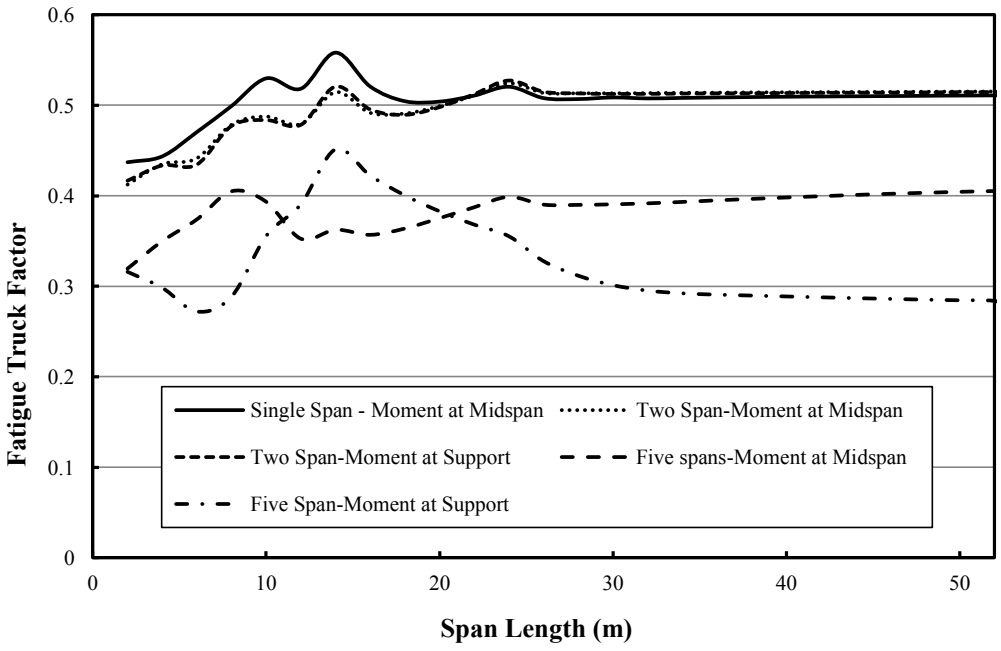

Figure 3.17 *Fatigue truck factor for single slope fatigue curves (Nicolas truck data).*

The fatigue truck factor for dual slope fatigue curves for one, two and five-span bridges is presented in Figures 3.18 and 3.19. In case of midspan moment in a single span bridge (Figure 3.18(a)), the fatigue truck factor fluctuates, at the start-end, between 0.43 and 0.46. This variation vanishes at span length 11.0 m. Then, the truck factor starts to increase to reach a peak of 0.57 at span length 12.0 m. For span lengths bigger than 30.0 m, the fatigue truck factor decreased slightly to sustain an average value of 0.52 beyond span length of 30.0 m. Similar

variations in the truck factor values for the midspan and interior support bending moments for two-span bridges (Figures 3.18(b) and 3.18(c)) are observed in the small length region. The maximum truck factor is 0.52 for span ranges less than 30.0 m. After 30.0 m, a value of 0.53 is found to be the average value.

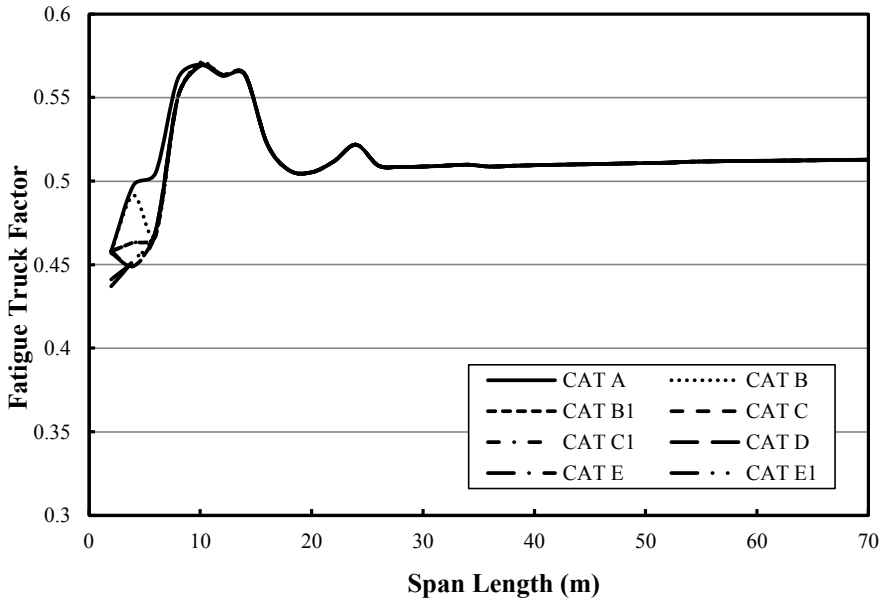

(a) One span – Moment at midspan

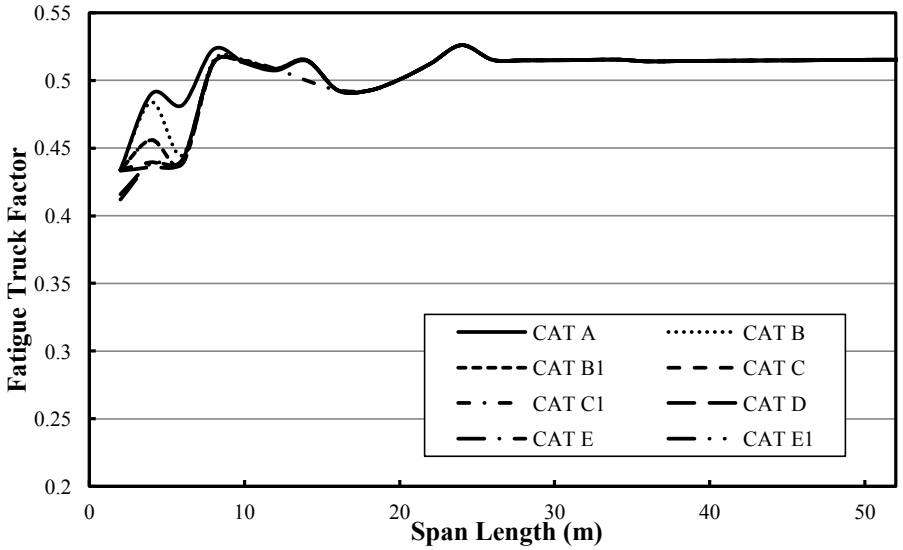

(b) Two-span- Moment at midspan

Figure 3.18 *Fatigue truck factor for dual slope fatigue curves (Nicolas truck data).*

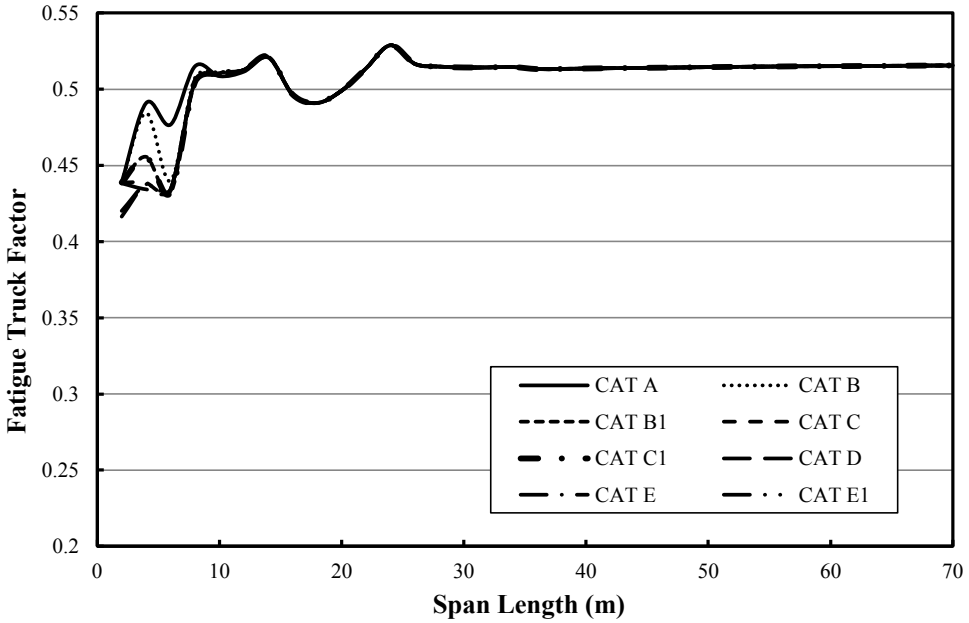

(c) Two-span- Interior support moment

Figure 3.18 *(cont'd).*

Figure 3.19 shows the fatigue truck factor using dual slope fatigue curves for midspan and at interior support moments in five-span bridges for different fatigue categories. At span length of 2.0 m, the truck factor for the five-span midspan moment case (Figure 3.19(a)) starts with an average small value of 0.33. The maximum truck factor is 0.43 for span ranges less than 30.0 m, while the truck factor is 0.40 for spans larger than 30.0 m. The truck factor for the interior support moment (Figure 3.19 (b)) displays a diverse trend, as the truck factor varies from 0.33 to 0.37 at span length of 2.0, then increase rapidly to reach a peak of 0.45 at span length of 16.0 m. Afterwards, the fatigue truck shows a fast decay to reach a value of 0.29 for span lengths beyond 30.0 m.

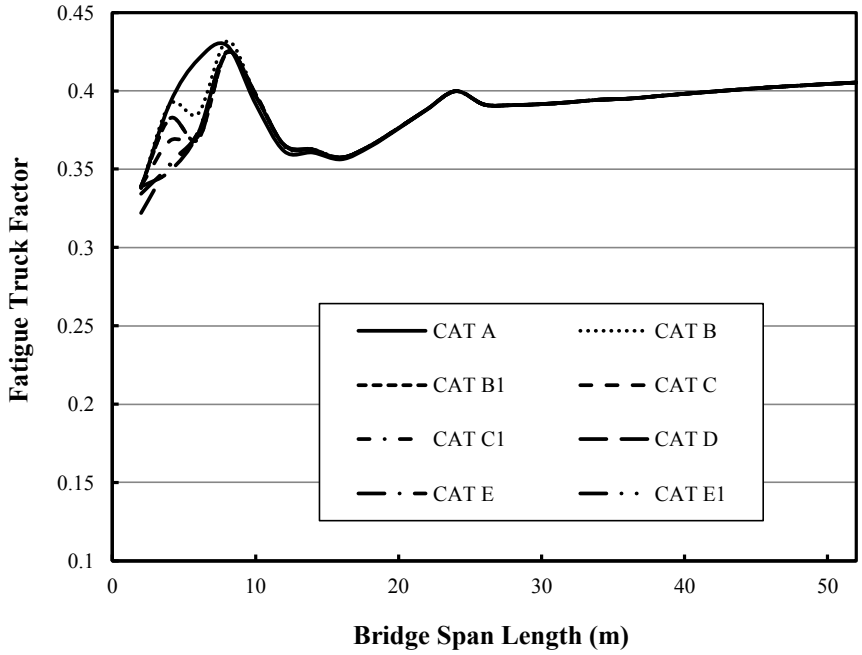

(a) Five-span – Moment at midspan

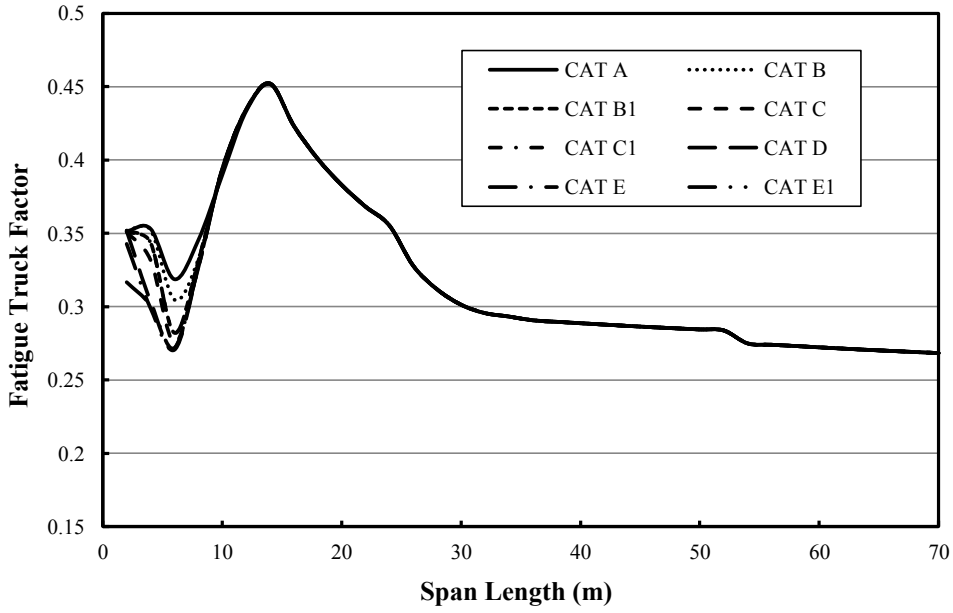

(b) Five-span – Interior support moment

Figure 3.19 *Fatigue truck factor for dual slope fatigue curves and five-span continuous bridge (Nicolas truck data).*

3.2.4.4 NWT2008 Truck Data

The fatigue truck factor for the truck data survey collected from the North West Territories collected in 2008, and designated by NWT2008 are illustrated in Figures 3.20 to 3.21. Fatigue truck factors using single slope fatigue curves are shown in Figure 3.20, while Figures 3.21 and 3.22 are based on the dual slope fatigue curves. From Figure 3.20, it can be observed that the fatigue truck factor for midspan moments in one and two-span bridge is larger than those of the five-span bridge cases for span lengths up to 15.0 m. The peak fatigue truck factor is 0.65 at a span length of 12.0 m. Then, the truck factor for two-span bridge case is almost constant at 0.59 for spans longer than 25.0 m, while the truck factor for moment at midspan in one-span bridge is 0.55. The other fatigue truck factor curves shown in Figure 3.20 (midspan and interior support moments for five-span continuous) show similar trends with slightly less values.

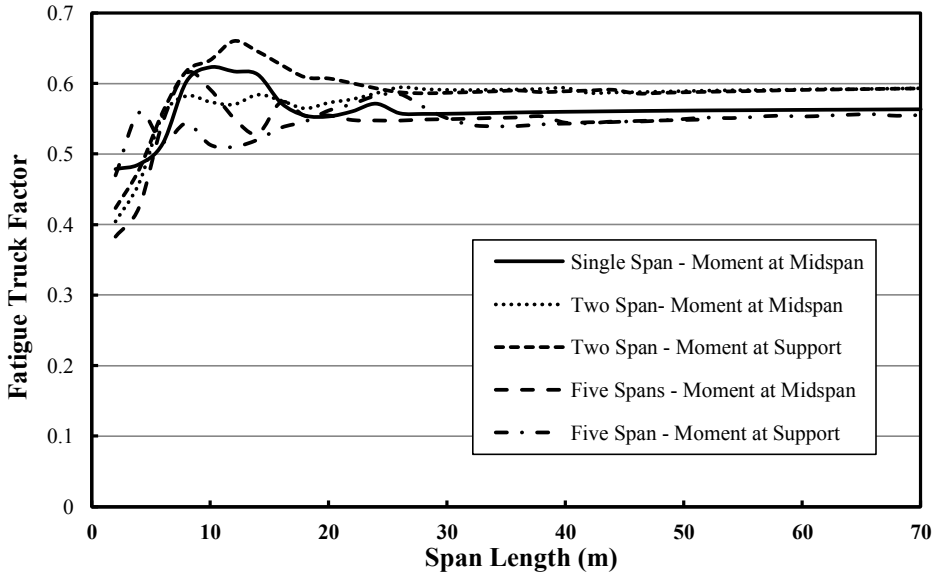

Figure 3.20 *Fatigue truck factor for single slope fatigue curves (NWT2008 data).*

The fatigue truck factor for dual slope fatigue curves for one and two-span bridges are shown in Figure 3.21. For the midspan moment in single span bridges (Figure 3.21(a)), the fatigue truck factor varies between 0.57 and 0.61 at span length of 2.0 m. This variation disappears at span length 8.0 m, where all the curves merge together. The maximum fatigue factor is 0.63 for span lengths less than 30.0 m, while a constant value of 0.56 is generated for span lengths bigger than 30.0 m. Figure 3.21(b) shows the truck factor versus span length for midspan moment for two-span bridge girder. Similar variations in the truck factor values are observed in the beginning due

to the effect of various fatigue categories. However, at span length of 8.0 m, all the curves coincide and reach a maximum value of 0.60. After span length of 25.0 m, the fatigue truck factor is almost constant of 0.59. In Figure (3.21(c)), the fatigue truck factor relationship exhibits another pattern especially in the small range spans. The truck factor starts roughly at value of 0.51. Then, the factor decreased sharply to be 0.22, the maximum truck factor is 0.66 for span ranges less than 30.0m. For larger spans (bigger than 30.0 m), a value of 0.58 is found to be the average value.

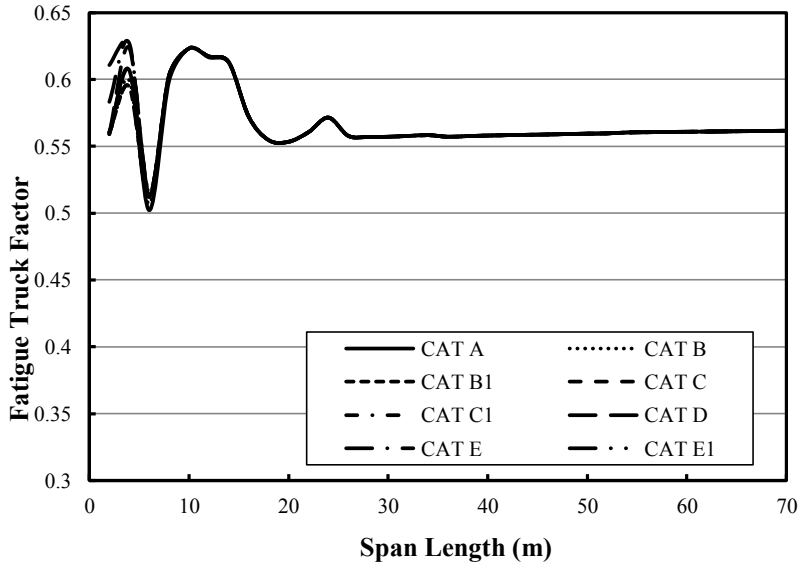

(a) One span –Moment at midspan

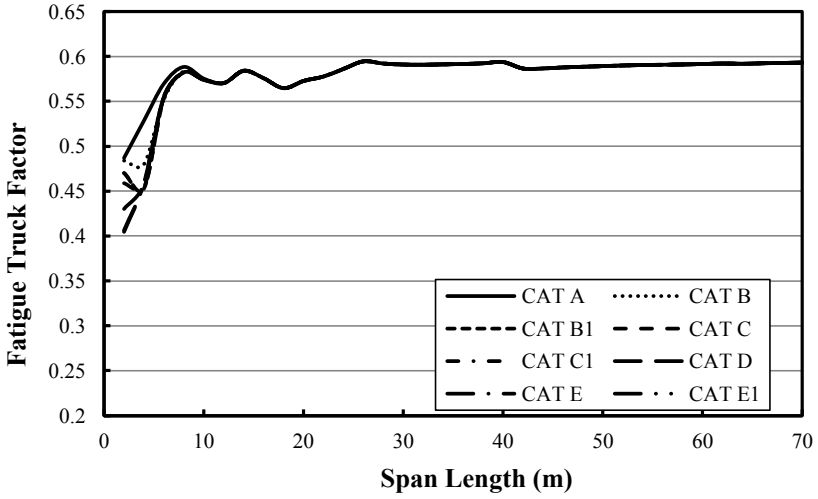

(b) Two-span- Moment at midspan

Figure 3.21 *Fatigue truck factor for dual slope fatigue curves (NWT 2008 truck data).*

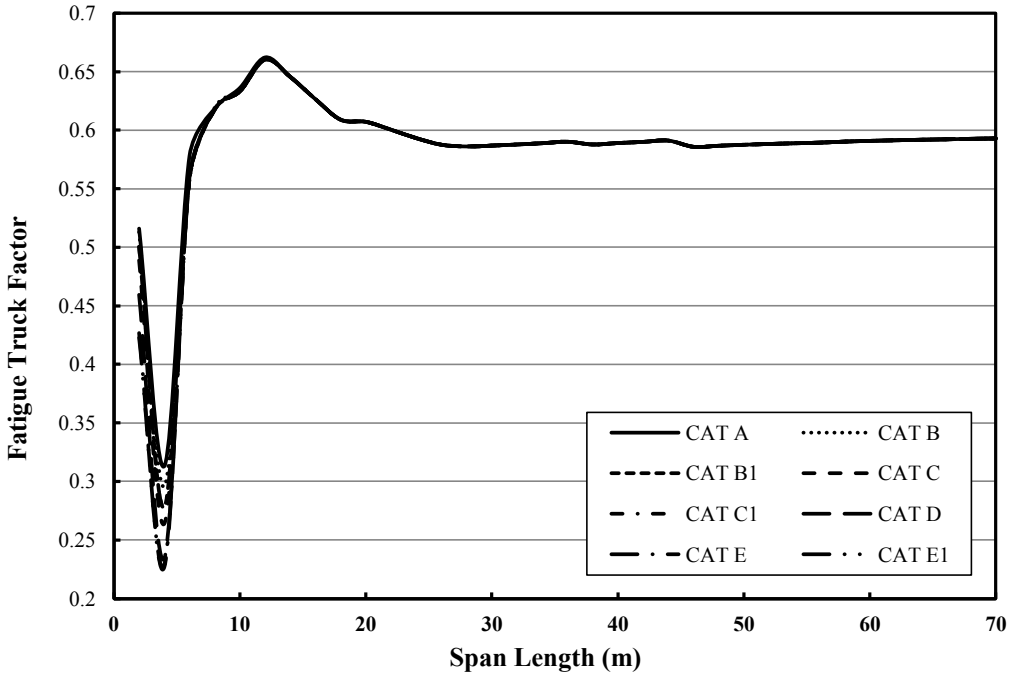

(c) Two-span- Interior support moment

Figure 3.21 *(cont'd)*

Figure 3.22 shows the fatigue truck factor for dual slope fatigue curves for midspan and interior support bending moments in five-span girder. In Figure 3.22(a), the truck factor for the five-span midspan moment case starts with a range between 0.38 and 0.47. The maximum truck factor is 0.61 for span ranges less than 30.0 m, while the truck factor is 0.55 for spans larger than 30.0 m. The truck factor for the interior support moment (Figure 3.22(b)) shows a similar trend, as the truck factor started at a range of 0.46 - 0.52, then increase rapidly to reach a peak of 0.66 at a span length of 6.0 m. for spans longer than 30.0 m, the fatigue truck is almost constant at a value of 0.55.

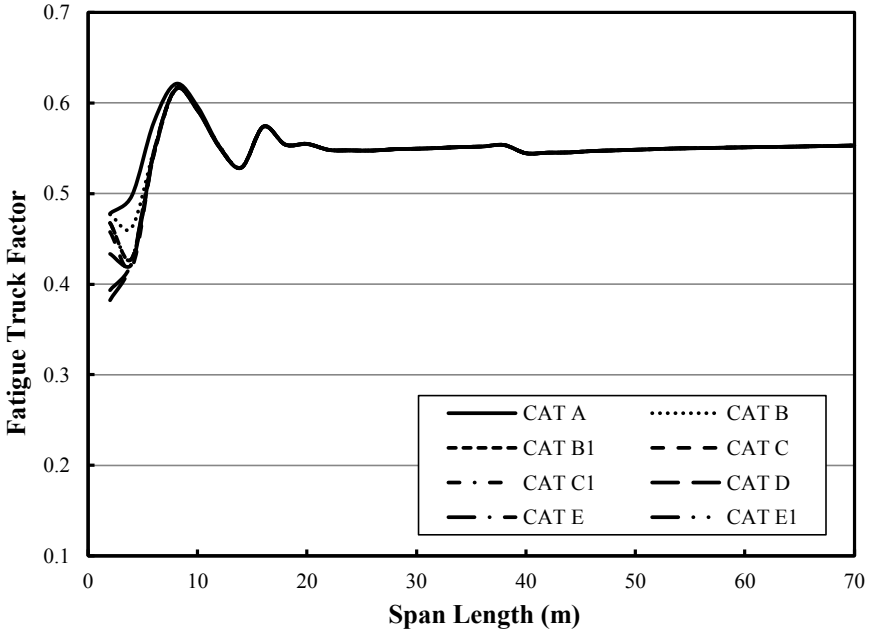

(a) Five-span – Moment at midspan

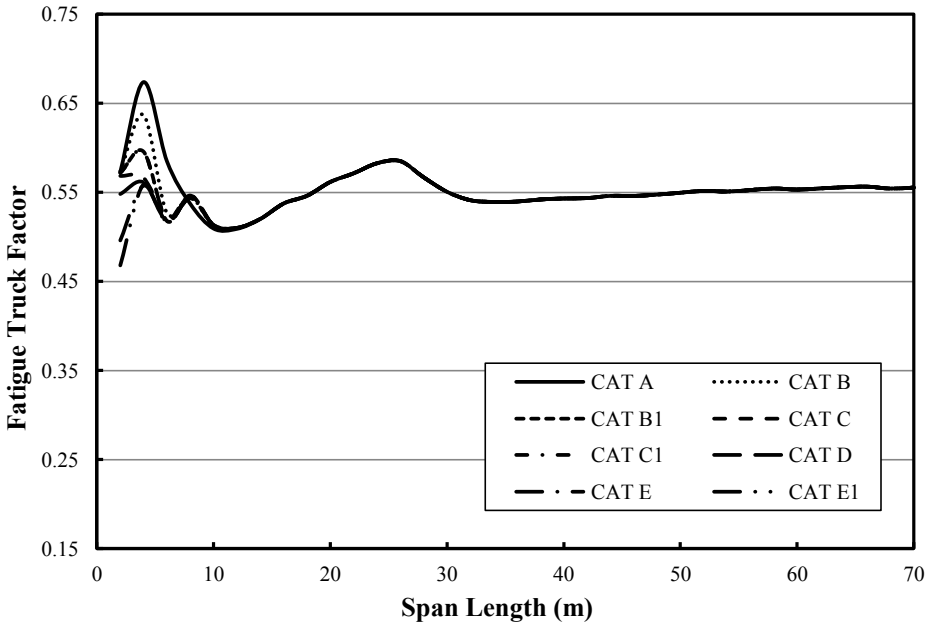

(b) Five-span – Interior support moment

Figure 3.22 *Fatigue truck factor for five-span continuous bridge and dual slope fatigue curves (NWT 2008 truck data).*

3.2.4.5 NWT2009 Truck Data

Figures 3.23 to 3.25 demonstrate the fatigue truck factor for the truck data survey collected from North West Territories collected in 2009 (NWT2009). Figure 3.23 shows the fatigue truck factors based on single slope fatigue curves, used in CSA-S6-06 (CSA 2006), while Figures 3.24 and 3.25 are based on the dual slope fatigue curves used in CSA-S16-09 (CSA 2009). In Figure 3.23, the values of the truck factor are higher for the midspan and interior support bending moment in two-span bridges than for the midspan bending moment in one span and five span bridge in addition to negative moment at interior span in five-span bridges. The peak fatigue truck factor is 0.85 at a span length of 16.0 m for interior support moment of two-span bridge. Then, the truck factor is almost constant at 0.80 for span lengths from 20.0 to 70.0 m for the midspan and interior support bending moments of the two-span bridge. For the midspan moment for one-span, the fatigue truck factor curve shown in Figure 3.23 shows similar trends but with lower truck factors than those predicted from the midspan moments for two and five-span bridge.

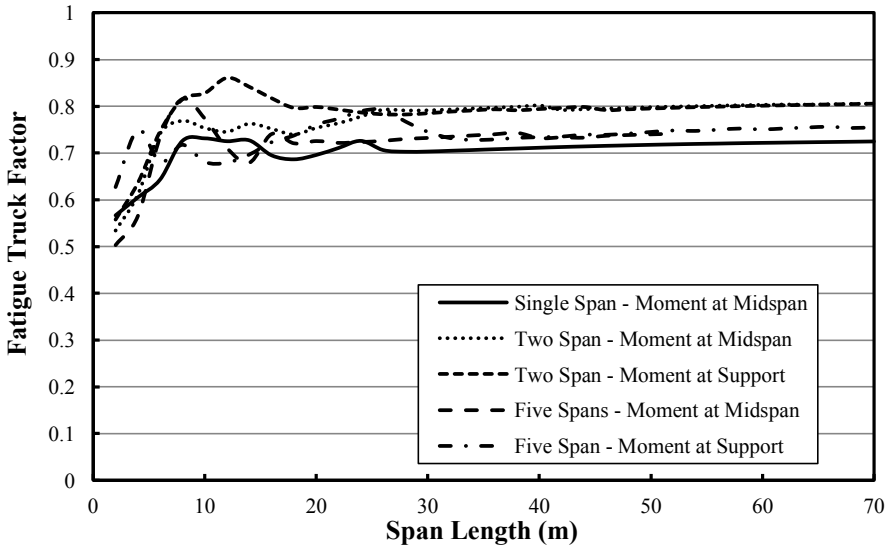

Figure 3.23 *Fatigue truck factor for single slope fatigue curves (NWT2009 data).*

Figure 3.24 shows the fatigue truck factor using dual slope fatigue curves for one and two-span Bridge for NWT2009 truck data. In case of the moment at midspan in one-span Bridge (Figure 3.24(a)), the fatigue truck factor changes, at the start-end, between 0.56 and 0.61. This variation vanishes at span length 8.0 m. The maximum fatigue factor is 0.73 for span lengths less than 30.0 m, while a constant value of 0.71 is generated for span lengths bigger than 30.0 m. Figure

3.24(b) shows the truck factor versus span length for midspan bending moment for two-span bridge girder. At span length of 6.0 m, all the curves coincide and reach a maximum value of 0.80. After span length of 25.0 m, the fatigue truck factor is almost constant of 0.80. In Figure (3.24(c)), the fatigue truck factor relationship demonstrate similar trend. The truck factor starts roughly at value of 0.55. Then, it increased to reach the value of 0.84 for span ranges less than 30.0 m. For larger spans (bigger than 30.0 m), a value of 0.80 is considered to be the average value.

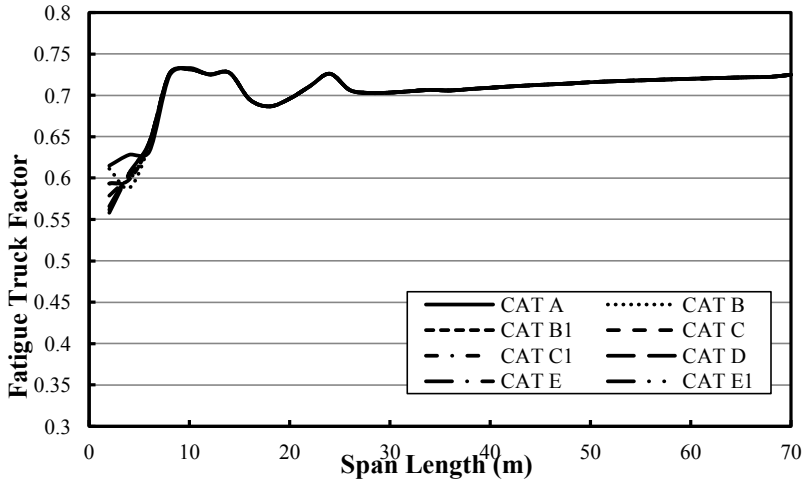

(a) One span – Moment at midspan

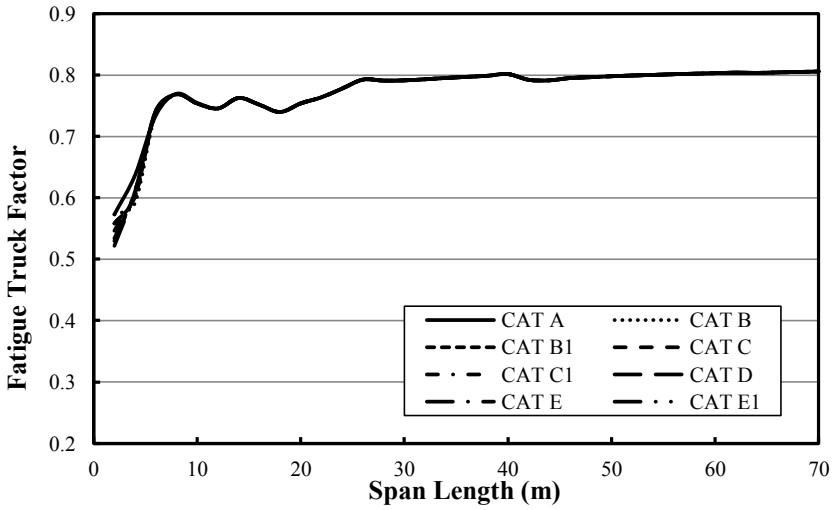

(b) Two-span- Moment at midspan

Figure 3.24 *Fatigue truck factor for dual slope fatigue curves (NWT 2009 truck data).*

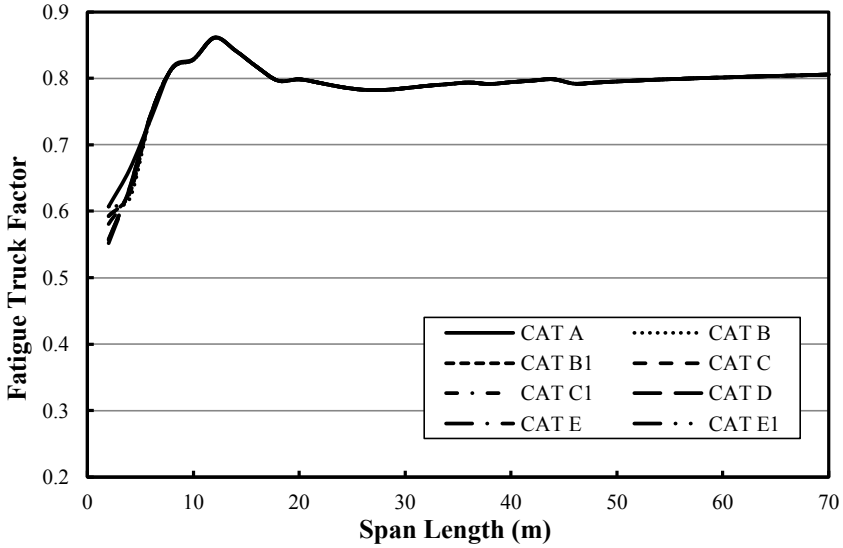

(c) Two-span- Interior support moment

Figure 3.24 *(cont'd).*

The fatigue truck factor using NWT2009 truck data and dual slope fatigue curves for midspan and interior support bending moment in five-span bridges are illustrated in Figure 3.25. In Figure 3.25(a), the truck factor for the midspan positive moment case starts with a range between 0.51 and 0.55. The maximum truck factor is 0.81 for span ranges less than 30.0 m, while the truck factor is 0.73 for spans larger than 30.0 m. The truck factor for the interior support negative bending (Figure 3.25(b)) shows a similar trend, as the truck factor started at a range of 0.62 - 0.68, then increase rapidly to reach a peak of 0.80 at span length of 6.0 m. For spans longer than 30.0 m, the fatigue truck factor is almost constant at a value of 0.75.

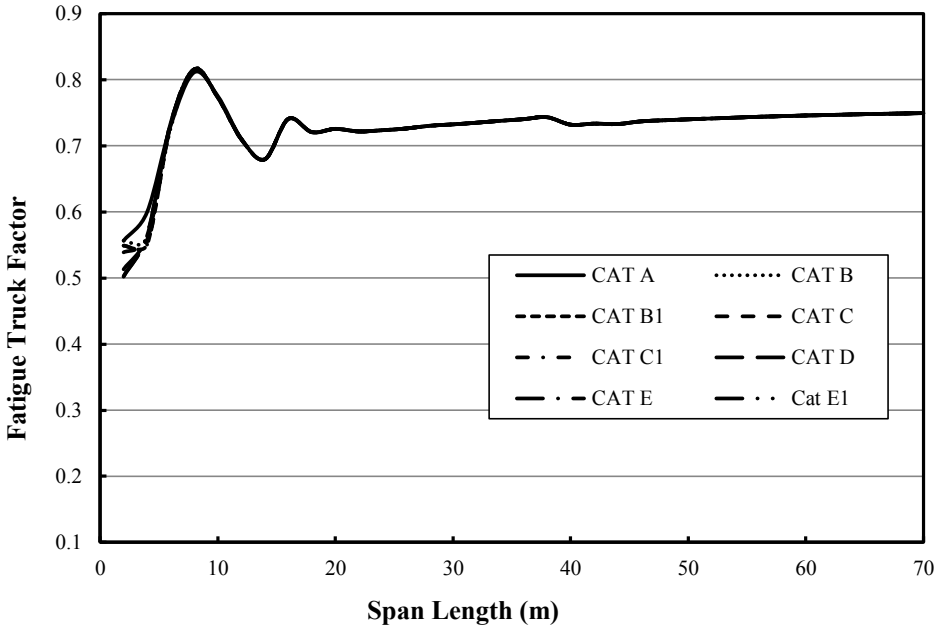

(a) Five-span - Moment at midspan

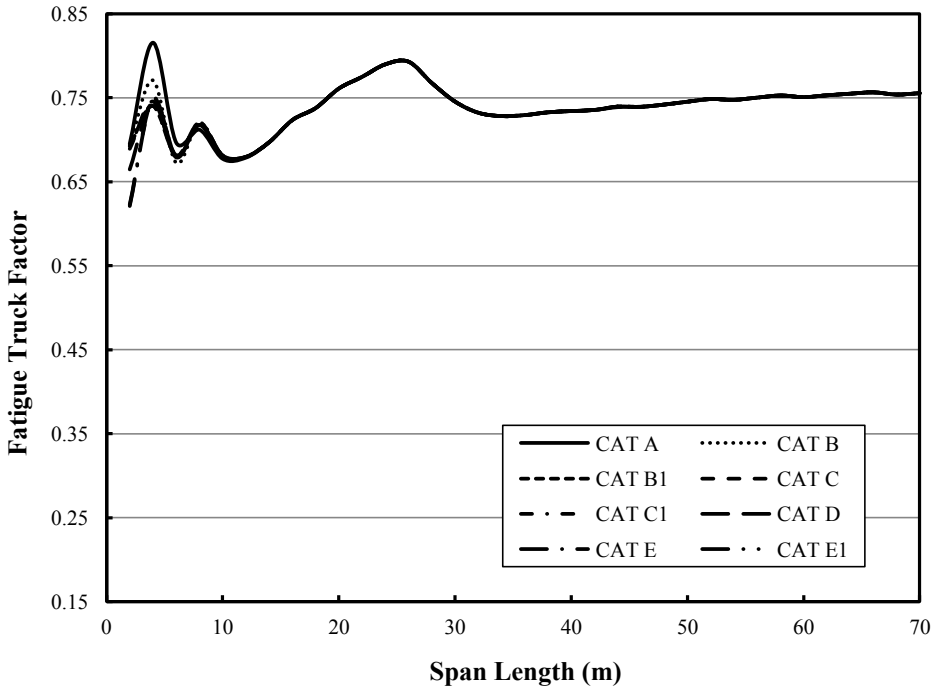

(b) Five-span - Interior support moment

Figure 3.25 *Fatigue truck factor for five-span continuous bridge and dual slope fatigue curves (NWT 2009 truck data).*

3.2.4.6 NWT2010 Truck Data

The fatigue truck factor for the truck data survey collected from North West Territories collected in 2010 (NWT2010) is shown in Figures 3.26 to 3.28. Fatigue truck factors based on single slope fatigue curves, adopted in CSA-S6-06 (CSA 2006), are shown in Figure 3.26 while Figures 3.27 and 3.28 are based on the dual slope fatigue curves used in CSA-S16-09 (CSA 2009). In Figure 3.26, maximum fatigue truck factor is 0.75 at a span length of 12.0 m for interior support moment for two-span Bridge. Then, the truck factor is almost constant at 0.72 at large span lengths (greater than 25.0 m) for midspan and interior support moments of two-span bridge. The other fatigue truck factor curves shown in Figure 3.26 (midspan and interior support moments for one and five-span continuous beams) show similar trends with a peak fatigue truck value of 0.72 at a span length of 10.0, and constant value of 0.68 for span lengths 20.0 m to 70.0m.

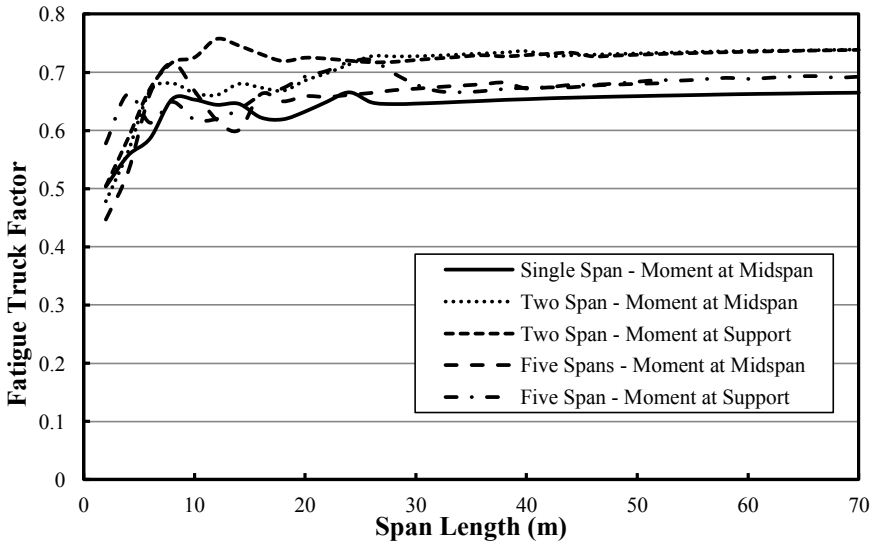

Figure 3.26 *Fatigue truck factor for single slope fatigue curves (NWT2010 data).*

The fatigue truck factor using dual slope fatigue curves for one, two and five-span bridge for NWT2010 truck data is shown in Figures 3.27 and 3.28. In Figure 3.27(a), the fatigue truck factor for the moment at midspan in one-span girder initiates at a variable range between 0.64 and 0.70. This variation disappears at span lengths longer than 10.0 m. The maximum fatigue factor is 0.70 for span lengths less than 30.0 m, while a constant value of 0.66 is generated for span lengths bigger than 30.0 m. Figure 3.27(b) shows the truck factor versus span length for midspan moment for two-span bridge girder. At span length of 10.0 m, all the curves coincide and reach a maximum value of 0.73. This was the same value that was dominant after span

length of 25.0 m. In Figure (3.27(c), the fatigue truck factor relationship shows similar trend. The truck factor ranges at span length of 2.0 m from 0.50 to 0.55. Then, it increased to reach the value of 0.75 for span ranges less than 30.0m. A value of 0.73 is found to be the average value for spans longer than 30.0 m.

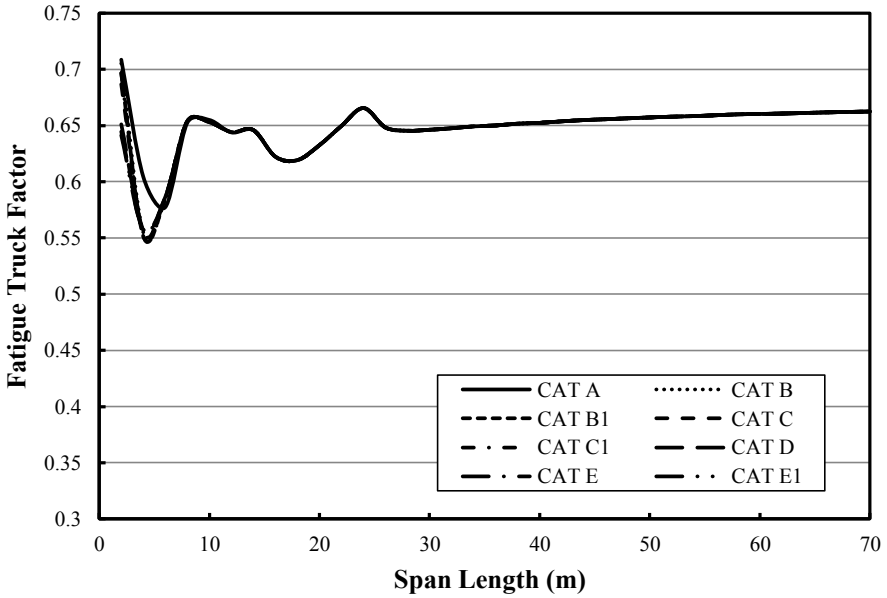

(a) One span- Moment at midspan

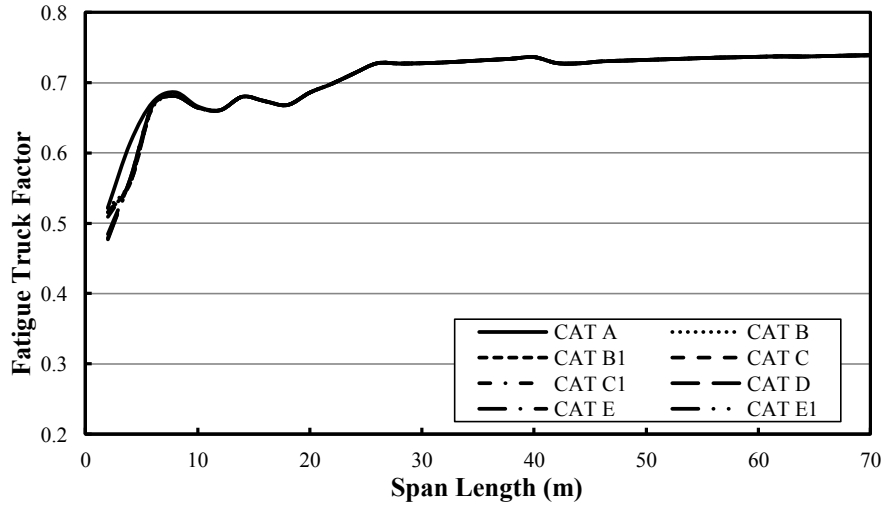

(b) Two-span- Moment at midspan

Figure 3.27 *Fatigue truck factor for dual slope fatigue curves (NWT 2010 truck data).*

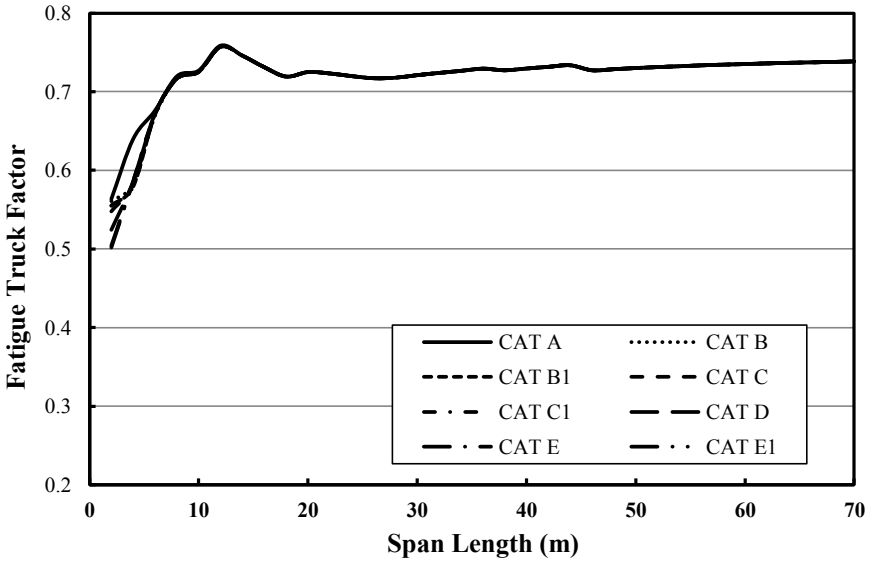

(c) Two-span- Interior support moment

Figure 3.27 *(cont'd).*

Figure 3.28 shows the variation of the fatigue truck factor as a function of span length using NWT2009 truck data and dual slope fatigue curves for midspan and interior support moments in five-span bridges. In Figure 3.28(a), the truck factor for the midspan moment for five-span case starts with a range between 0.45 and 0.49. The maximum truck factor is 0.71 for spans shorter than 30.0 m, while the truck factor is 0.69 for spans longer than 30.0 m. The truck factor for the interior support (Figure 3.28(b)) shows similar trend with different values for fatigue truck factor. At the span length of 2.0 m, the fatigue truck factor fluctuates from 0.60 to 0.70, then increase rapidly to reach a peak of 0.76 at span length of 6.0 m. After span length 30.0 m, the fatigue truck shows is almost constant at a value of 0.67.

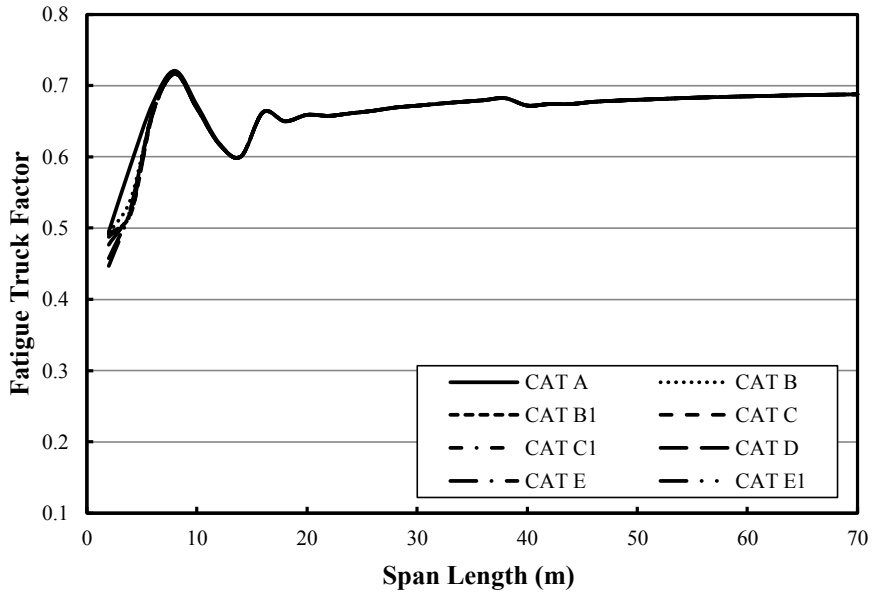

(a) Five-span – Moment at midspan moment

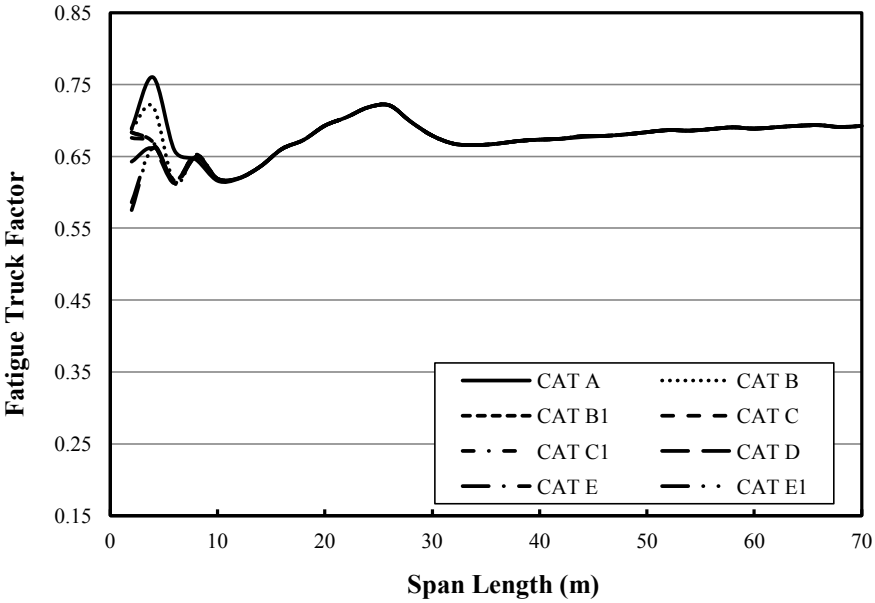

(b) Five-span – Interior support moment

Figure 3.28 *Fatigue truck factor for five-span continuous bridge and dual slope fatigue curves (NWT 2010 truck data).*

3.2.4.7 NWT2011 Truck Data

The fatigue truck factor using the truck data survey collected from North West Territories collected in 2011 (NWT2011) is illustrated in Figures 3.29 to 3.31. Figure 3.29 employs the

single slope fatigue curves, used in CSA-S6-06 (CSA 2006), to generate the fatigue truck factors while Figures 3.30 and 3.31 are based on the dual slope fatigue curves used in CSA-S16-09 (CSA 2009). In Figure 3.29, the maximum fatigue truck factor is 0.65 at a span length of 12.0 m for moment at interior support for two-span Bridge. Then, the truck factor is almost constant at 0.68 at large span lengths (greater than 25.0 m) for midspan and interior support moments for two-span bridge. The other fatigue truck factor of midspan and interior support moments for one and five-span continuous, shown in Figure 3.29, illustrates similar trends with slightly less values.

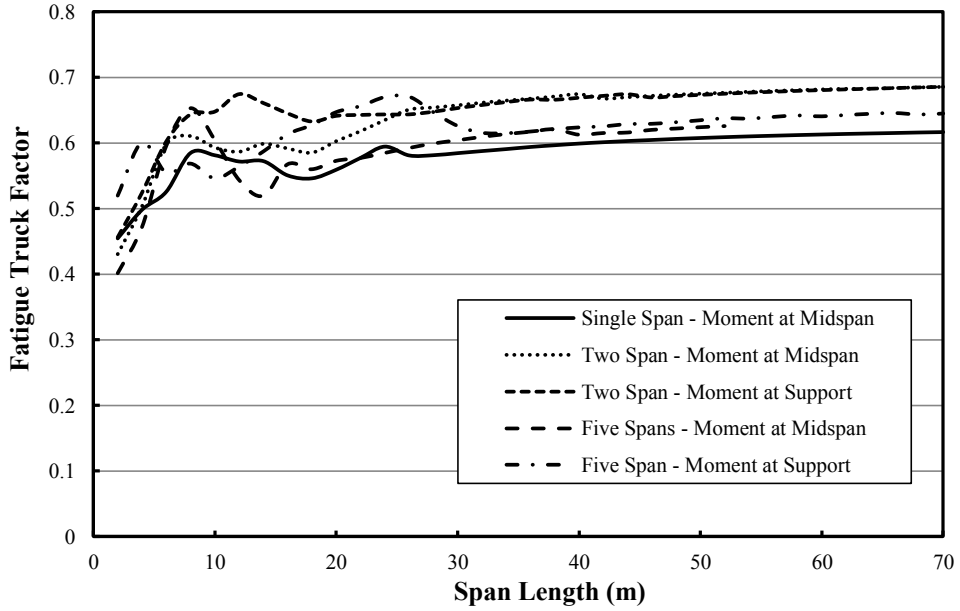

Figure 3.29 *Fatigue truck factor for single slope fatigue curves (NWT2011 data).*

The fatigue truck factor using dual slope fatigue curves for one, two and five-span Bridge for NWT2010 truck data is shown in Figures 3.30 and 3.31. In Figure 3.30(a), the fatigue truck factor for the moment at midspan in one-span girder starts at a variable range between 0.58 and 0.63. At span length 8.0 m, this fluctuation vanishes. For span lengths less than 30.0 m, the maximum fatigue factor is 0.72, while a constant value of 0.61 is generated for span lengths bigger than 30.0 m. Figure 3.30(b) shows the truck factor versus span length for midspan moment for two-span bridge girder. The fatigue factor ranges from 0.43 to 0.46 at the start end. At span length of 12.0 m, all the curves coincide and reach a maximum value of 0.65. After span length of 30.0 m, the dominant value is 0.68. In Figure (3.30(c)), the fatigue truck factor relationship demonstrate similar trend. The truck factor ranges from 0.45 to 0.5 at span length of

2.0 m. Then, it increased to reach the value of 0.67 for span ranges less than 30.0 m. For larger spans (bigger than 30.0 m), a value of 0.68 is found to be the average value.

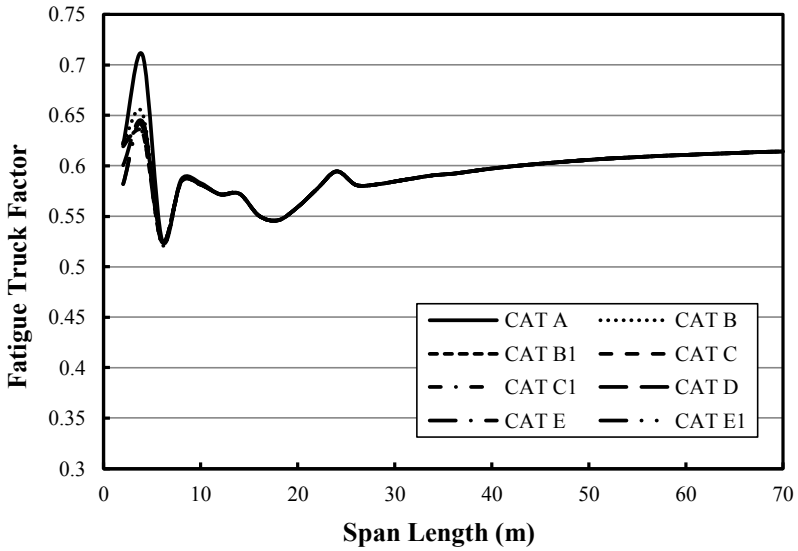

(a) One span – Moment at midspan

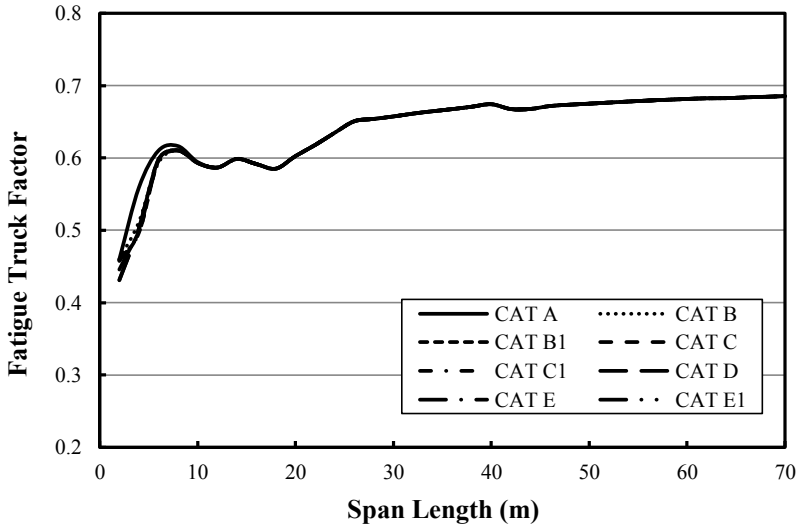

(b) Two-span- Moment at midspan

Figure 3.30 *Fatigue truck factor for dual slope fatigue curves (NWT 2011 truck data).*

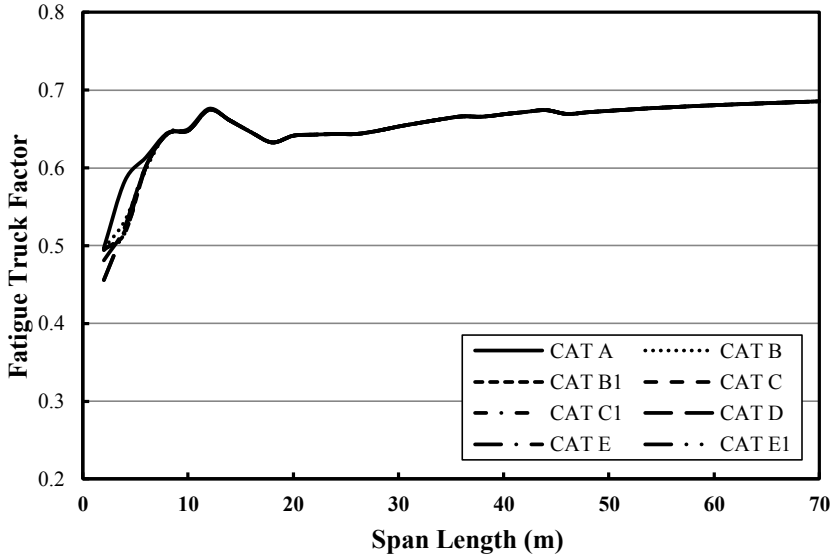

(c) Two-span – Interior support moment

Figure 3.30 *(cont'd).*

The fatigue truck factors obtained from the NWT2011 truck data and dual slope fatigue curves are presented in Figure 3.31 for the midspan and interior support moment for interior span in five-span bridges. In Figure 3.31(a), the truck factor for the five-span midspan moment case starts with a range between 0.41 and 0.43. The maximum truck factor is 0.65 for span ranges less than 30.0 m, while the truck factor is 0.62 for spans larger than 30.0 m. The truck factor for the interior support moment (Figure 3.31(b)) shows a similar trend with different values for fatigue truck factor. It starts a range of 0.52 - 0.63, then increase rapidly to reach a peak of 0.66 at span length of 6.0 m. After span length 30.0 m, the fatigue truck shows is almost constant at a value of 0.64.

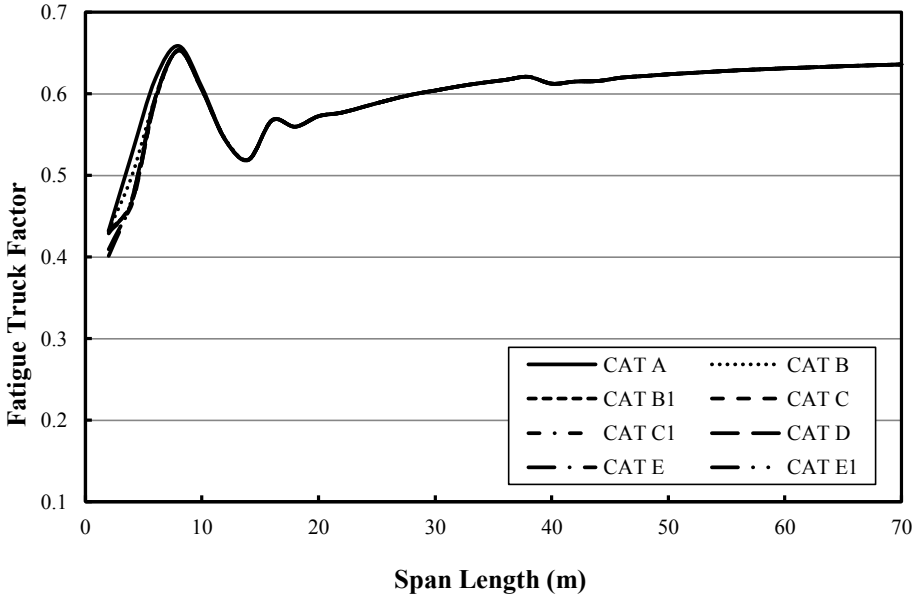

(a) Five-Span – Moment at midspan

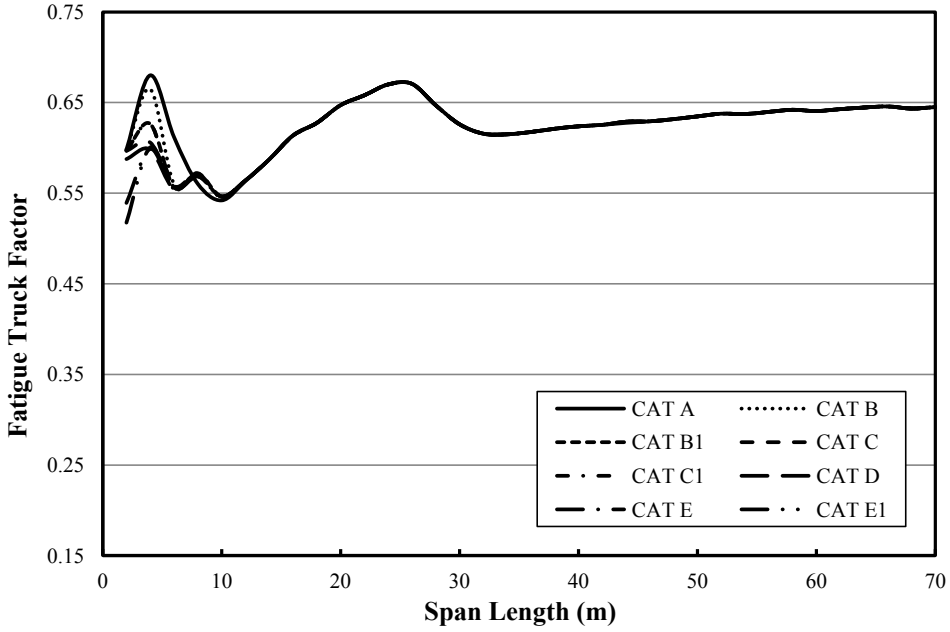

(b) Five-Span – Interior support moment

Figure 3.31 *Fatigue truck factor for five-span continuous bridge and dual slope fatigue curves (NWT 2011 truck data).*

3.2.5 Discussion of Results

In general, the calibration procedure, carried out by Coughlin and Walbridge (2010), evaluated the fatigue truck factor based on one source of WIM only and did not consider other WIM sources to verify their results. Moreover, their study did not consider the influence of bridge span length as well as dual-slope fatigue design curves on the fatigue truck factor values. Furthermore, Coughlin and Walbridge (2010) did not take into account the effect of different fatigue detail categories (see Figure 3.1), which was found to be highly affecting the fatigue truck predictions especially in the dual-slope fatigue design curves as illustrated above.

Based on the above mentioned short falls, there was a need to develop more inclusive fatigue truck calibration procedure, which employs wider range of truck data collected from various sources of WIM data. This will lead to more reliable fatigue truck calibration, which results by comparing fatigue truck values using different independent WIM sources. The fatigue truck calibration incorporated the dual-slope fatigue design curves, which is expected to be adopted in the next versions of the Canadian Highway Bridge Design Code CSA-S6-06 (CSA 2006). It also takes into account the variations of fatigue truck factors with respect to bridge span length and configuration. This could lead to present various fatigue truck factors for various span lengths instead of the current code value of 0.52 regardless the span length and configuration.

In this study, and by making use of seven sets of WIM data collected from two provinces and one territory in Canada, a more comprehensive procedure was developed for fatigue truck calibration in steel highway bridges using single and dual-slope fatigue design curves. Weigh-in-motion data from seven different sources were used to assess the difference in fatigue truck between different regions and to assess the difference in fatigue truck calibration for single slope S-N curves in comparison with dual slope fatigue curves. To take into account the effect of bridge span length and configuration, the developed fatigue truck procedure in this research recommends new values for fatigue truck factor for different bridge span ranges ($L \leq 12.0$ m, $12.0 \text{ m} \leq L \leq 30.0$ m, and $L > 30.0$ m) instead of the current value of 0.52 which does not take into account the span length effect and dual slope curves.

In the fatigue truck calibration, step size of 1.0 m was employed to predict the load history for various bridge span lengths. This step could have an effect on the accuracy of the developed load histories using influence lines especially for the short bridge spans (2.0 m to 6.0 m). However,

this effect decreases as the span length increases. The fatigue calibration results illustrated in Section 3.2.4 emphasized that 90% of the peak fatigue factor for small span ranges ≤ 12.0 m is located between span 10.0 m to 12.0 m. Although, the small bridge spans from 2.0 m to 6.0 m using step size of 1.0 results in less values in most cases, further investigations are required to increase the fatigue truck calibration accuracy for such spans.

The results of fatigue truck calibration for single and dual slope fatigue design curves were presented in the previous sections. The calibration procedure has shown that the fatigue truck factor obtained for dual slope fatigue design curves is affected by the variation in fatigue detail category especially the short span range, where the effect of the constant amplitude fatigue limit (CAFL) is present and some of the stress ranges are located in the region of slope 5. For spans longer than 10.0 m to 20.0 m, all the fatigue categories converge to yield the same fatigue truck factor. This is due to that the stress ranges are large enough to be located in the slope of 3.0 of the fatigue design curve. The current fatigue truck factor in CHBDC is 0.52, which was based on single slope fatigue design curve. Initially, it was decided to retain the value of fatigue truck factor to be 0.52 and adjust the number of load cycles per passage according to the span length. In bridge span lengths less than 12.0, there is a great variability in truck factors values. Then, this variability decreases from span lengths 12.0 m to 30.0 m. After 30.0 m, the fatigue truck factor is almost constant in most cases. From the values predicted for the truck factor using single and dual slope fatigue curves, there is a need to propose fatigue truck factors for three different span ranges ($L \leq 12.0$ m, $12.0 \text{ m} \leq L \leq 30.0$ m, and $L > 30.0$ m). In the current bridge code, CSA-S6-06 (CSA 2006), the span ranges, $L \leq 12.0$ m and $L > 12.0$ m are used for defining the equivalent number of cycles as explained later in Section 3.3.

For the three-span bridge, the fatigue truck factor for the exterior midspan moment will be the same as the midspan moment of the two-span bridge. Furthermore, the fatigue truck factor for interior support moment of three-span bridge will match the results of the interior support moment of the two-span bridge. Finally, the calibration results of interior midspan moment for five-span bridge could be used as the calibration results for positive moment for interior three-span bridge.

Table 3.5 presents a summary of the suggested fatigue truck factors at midspan moment of one-span, midspan and interior support moments for exterior and interior multi-span girders (two,

three, four and five-span) using Ontario, Quebec and NWT WIM databases. Based on the results in Section 3.2.4, the maximum values for fatigue truck factors for the three span ranges ($L \leq 12.0$ m, $12.0 \text{ m} \leq L \leq 30.0$ m, and $L > 30.0$ m) are illustrated in Table 3.5.

Table 3.5 *Fatigue truck factors using single and dual slope fatigue design.*

WIM Set	***Moment History Case***	***Fatigue Truck Factor for Single Slope***			***Fatigue Truck Factor for Dual Slope***		
		L ≤ 12 m	**12 m < L ≤ 30 m**	**L > 30 m**	**L ≤ 12 m**	**12 m < L ≤ 30 m**	**L > 30 m**
Ontario	*One-span - Moment at midspan.*	*0.58*	*0.6*	*0.55*	*0.58*	*0.6*	*0.55*
	Exterior span - Moment at midspan	*0.54*	*0.56*	*0.55*	*0.53*	*0.57*	*0.55*
	Exterior span - Moment at interior support	*0.53*	*0.54*	*0.55*	*0.54*	*0.57*	*0.55*
	Interior span - Moment at midspan	*0.42*	*0.44*	*0.43*	*0.43*	*0.44*	*0.44*
	Interior span - Moment at interior Support	*0.42*	*0.47*	*0.32*	*0.45*	*0.47*	*0.32*
Quebec – Batiscan – Hw 40	*One-span - Moment at midspan.*	*0.57*	*0.58*	*0.55*	*0.57*	*0.58*	*0.55*
	Exterior span - Moment at midspan	*0.51*	*0.55*	*0.55*	*0.52*	*0.56*	*0.55*
	Exterior span - Moment at interior support	*0.52*	*0.54*	*0.54*	*0.51*	*0.56*	*0.55*
	Interior span - Moment at midspan	*0.42*	*0.41*	*0.43*	*0.41*	*0.42*	*0.44*
	Interior span - Moment at interior Support	*0.43*	*0.47*	*0.32*	*0.38*	*0.47*	*0.32*
Quebec – Nicolas – Hw 20	*One-span - Moment at midspan.*	*0.52*	*0.55*	*0.51*	*0.57*	*0.56*	*0.51*
	Exterior span - Moment at midspan	*0.49*	*0.52*	*0.51*	*0.52*	*0.53*	*0.52*
	Exterior span - Moment at interior support	*0.49*	*0.52*	*0.51*	*0.51*	*0.53*	*0.52*
	Interior span - Moment at midspan	*0.41*	*0.40*	*0.40*	*0.43*	*0.40*	*0.41*
	Interior span - Moment at interior Support	*0.37*	*0.44*	*0.30*	*0.37*	*0.45*	*0.29*
NWT2008	*One-span - Moment at midspan.*	*0.62*	*0.61*	*0.56*	*0.63*	*0.62*	*0.56*
	Exterior span - Moment at midspan	*0.58*	*0.59*	*0.58*	*0.58*	*0.59*	*0.59*
	Exterior span - Moment at interior support	*0.62*	*0.65*	*0.59*	*0.63*	*0.66*	*0.59*
	Interior span - Moment at midspan	*0.6*	*0.55*	*0.54*	*0.62*	*0.58*	*0.55*
	Interior span - Moment at interior Support	*0.53*	*0.59*	*0.55*	*0.66*	*0.57*	*0.55*
NWT2009	*One-span - Moment at midspan.*	*0.72*	*0.71*	*0.71*	*0.73*	*0.72*	*0.71*
	Exterior span - Moment at midspan	*0.76*	*0.78*	*0.8*	*0.76*	*0.78*	*0.8*
	Exterior span - Moment at interior support	*0.81*	*0.83*	*0.79*	*0.84*	*0.85*	*0.8*
	Interior span - Moment at midspan	*0.82*	*0.74*	*0.72*	*0.81*	*0.73*	*0.75*
	Interior span - Moment at interior Support	*0.73*	*0.79*	*0.72*	*0.82*	*0.8*	*0.75*
NWT2010	*One-span - Moment at midspan.*	*0.65*	*0.66*	*0.65*	*0.71*	*0.67*	*0.66*
	Exterior span - Moment at midspan	*0.68*	*0.71*	*0.73*	*0.68*	*0.72*	*0.73*
	Exterior span - Moment at interior support	*0.75*	*0.73*	*0.73*	*0.75*	*0.72*	*0.73*
	Interior span - Moment at midspan	*0.72*	*0.76*	*0.68*	*0.72*	*0.68*	*0.68*
	Interior span - Moment at interior Support	*0.65*	*0.72*	*0.69*	*0.76*	*0.73*	*0.67*
NWT2011	*One-span - Moment at midspan.*	*0.58*	*0.59*	*0.6*	*0.71*	*0.59*	*0.61*
	Exterior span - Moment at midspan	*0.61*	*0.65*	*0.68*	*0.62*	*0.65*	*0.68*
	Exterior span - Moment at interior support	*0.67*	*0.65*	*0.68*	*0.67*	*0.65*	*0.68*
	Interior span - Moment at midspan	*0.61*	*0.6*	*0.61*	*0.65*	*0.6*	*0.63*
	Interior span - Moment at interior Support	*0.6*	*0.67*	*0.63*	*0.67*	*0.67*	*0.64*

In general, the fatigue truck factor predicted using NWT data is higher than those computed using Ontario and Quebec data. This is due to the larger fatigue damage induced from NWT actual truck, which was reflected in larger weighted average for GVW compared to Ontario and

Quebec. However, since a big majority of the NWT population was filtered due to errors and light weight vehicles, a relatively heavy weight truck, compared to Ontario and Quebec induced higher fatigue truck factors. The CL-800 design truck was used to calibrate the NWT WIM data, while the CL-625 design truck was employed to calibrate Ontario and Quebec WIM data.

Suggested values for various critical sections could be summarized from Table 3.5. Table 3.6 shows the average value of the predicted fatigue truck factors for Quebec-Batiscan and Quebec-Nicolas tabulated in Table 3.5 for critical sections in one, exterior and interior span bridge. Then, Table 3.7 illustrates the recommended fatigue truck factor based on the average values of Ontario and Quebec (Table 3.6). Lastly, Table 3.8 presents the values of the fatigue truck factor based on the average of the four sets of NWT data in Table 3.5 for the same sections.

Table 3.6 *Fatigue truck factor for different bridge span configuration using Quebec data.*

Moment History Case	***Fatigue Truck Factor for Single Slope***			***Fatigue Truck Factor for Dual Slope***		
	L ≤ 12 m	12 m < L ≤ 30 m	L > 30 m	L ≤ 12 m	12 m < L ≤ 30 m	L > 30 m
One-span - Moment at midspan.	0.55	0.57	0.53	0.57	0.57	0.53
Exterior span - Moment at midspan	0.50	0.54	0.53	0.52	0.55	0.54
Exterior span - Moment at interior support	0.51	0.53	0.53	0.51	0.55	0.54
Interior span - Moment at midspan	0.42	0.41	0.42	0.42	0.41	0.43
Interior span - Moment at interior Support	0.40	0.46	0.31	0.38	0.46	0.31

Table 3.7 *Fatigue truck factor for different bridge span configuration using Ontario and Quebec data.*

Moment History Case	***Fatigue Truck Factor for Single Slope***			***Fatigue Truck Factor for Dual Slope***		
	L ≤ 12 m	12 m < L ≤ 30 m	L > 30 m	L ≤ 12 m	12 m < L ≤ 30 m	L > 30 m
One-span - Moment at midspan.	0.56	0.58	0.54	0.57	0.58	0.54
Exterior span - Moment at midspan	0.51	0.54	0.54	0.52	0.55	0.54
Exterior span - Moment at interior support	0.51	0.53	0.53	0.52	0.55	0.54
Interior span - Moment at midspan	0.42	0.42	0.42	0.42	0.42	0.43
Interior span - Moment at interior Support	0.41	0.46	0.31	0.40	0.46	0.31

Table 3.8 *Fatigue truck factor for different bridge span configurations using NWT data.*

Moment History Case	***Fatigue Truck Factor for Single Slope***			***Fatigue Truck Factor for Dual Slope***		
	L ≤ 12 m	12 m < L ≤ 30 m	L > 30 m	L ≤ 12 m	12 m < L ≤ 30 m	L > 30 m
One-span - Moment at midspan.	0.64	0.64	0.63	0.70	0.65	0.64
Exterior span - Moment at midspan	0.66	0.68	0.70	0.66	0.69	0.70
Exterior span - Moment at interior support	0.71	0.72	0.70	0.72	0.72	0.70
Interior span - Moment at midspan	0.69	0.66	0.64	0.70	0.65	0.65
Interior span - Moment at interior Support	0.63	0.69	0.65	0.73	0.69	0.65

The previous Tables 3.7 and 3.8 showed new values for fatigue truck factors instead of the current value in S6-06 (CSA 2006), which is 0.52. The modification for the fatigue truck factor could also lead to a change in the current reduction factor, C_L, that is defined in Clause 17.20.2.2 in CSA-S6-06 (CSA 2006). The new factor for each span range and moment history could be defined as follows:

$$C_L = \frac{\text{Fatigue Truck Factor (NWT)}}{\text{Fatigue Truck Factor (Ontario and Quebec)}} \tag{3.3}$$

Where the fatigue truck factor (NWT) is obtained from Table 3.8 and the fatigue truck factor (Ontario and Quebec) is shown in Table 3.7. Table 3.9 illustrates the values of the C_L factor based on equation 3.3.

Table 3.9 C_L *factor for different bridge span configurations using NWT data.*

Moment History Case	C_L ***Factor for Single Slope***			C_L ***Factor for Dual Slope***		
	L ≤ 12 m	12 m < L ≤ 30 m	L > 30 m	L ≤ 12 m	12 m < L ≤ 30 m	L > 30 m
One-span - Moment at midspan.	1.15	1.11	1.17	1.21	1.12	1.18
Exterior span - Moment at midspan	1.28	1.26	1.30	1.26	1.24	1.30
Exterior span - Moment at interior support	1.39	1.34	1.31	1.39	1.30	1.30
Interior span - Moment at midspan	1.65	1.59	1.52	1.65	1.54	1.52
Interior span - Moment at interior Support	1.54	1.51	2.07	1.82	1.49	2.10

3.3. Calibration of Number of Cycles per Truck Passage

3.3.1 Introduction

The current number of design stress cycles for each passage of the design truck (The number of stress cycles induced when a design truck passes over a certain bridge span), N_d, is given in Table 10.5 of CSA-S6-06 (CSA 2006), which is presented in Table 3.10.

Table 3.10 *Values of* N_d *(CSA 2006).*

Longitudinal members	**Span Length, L, ≥ 12 m**	**Span Length, L, < 12 m**
Simple-span girders	1.0	2.0
Continuous girders		
Near interior support (within 0.1L on either side)	1.5	2.0
All other locations	1.0	2.0
Cantilever girders	5.0	5.0
Trusses	1.0	1.0
Transverse members	**Spacing ≥ 6.0 m**	**Spacing < 6.0 m**
All cases	1.0	2.0

The values in Table 3.10 were based on single slope fatigue design curve in addition to the current fatigue truck factor, used in CSA-S6-06 (CSA 2006), which is 0.52. From section 3.2, new values for fatigue truck factors are developed for three span ranges using single and dual slope fatigue design curves. Therefore, this section uses the moment range spectra obtained from the passage of the fatigue design truck (CL-625) for Quebec and Ontario for the critical sections explained in Section 3.2 for the same bridge configurations (single, two equal spans, and five equal spans). The NWT truck data comprises a high percentage of passenger trucks and generated a relatively high truck factors as shown in Table 3.8 compared to Ontario and Quebec fatigue truck factors. Therefore, the recommended fatigue truck factors for NWT, illustrated in Table 3.8, will not be used in the derivation of equivalent number of cycles. Section 3.3.2 outlines the procedure used to calibrate the equivalent stress cycle for each passage of the design truck. Then, the results of the calibration using Ontario, Quebec and NWT WIM data are presented in Section 3.3.3. Lastly, the discussion on the results is illustrated in Section 3.3.4.

3.3.2 Calibration Procedure

The aim of the calibration of the equivalent stress cycles is to validate the values presented in Table 10.5 of CSA-S6-06 (CSA 2006). These values were based on the predicted fatigue truck factors presented in Table 3.7, where different fatigue truck factors were proposed for three bridge span lengths using single and dual slope fatigue design curves. Therefore, the developed calibration procedure employs new fatigue truck factors for three different span ranges, compared to the two span ranges in Table 10.5. It also extends the scope of evaluating the equivalent stress using dual slope fatigue design curve, which is currently used in CSA-S16-09 (CSA 2009) and not implemented in CSA-S6-06 (CSA 2006).

In the developed calibration procedure, the moment range spectra for real and design trucks will be used in the equivalent cycle calibration. For the prediction of equivalent stress cycles due to truck passage using single-slope fatigue design curves, it was found that the type of detail category (e.g. A, B, C, etc…) has no effect on the predicted values. In case of dual-slope fatigue design curves, the predictions showed a very small percentage (less than 1%) in the predicted equivalent stress cycles for different fatigue categories. This difference does not have any effect on the final result of equivalent stress cycles employing dual-slope fatigue design curves. In this section, fatigue category A will be used for the prediction purpose of equivalent stress cycle due to truck passage. The calculations were conducted for single, two and five-span bridges that range from 2.0 to 70.0 m. The calibration procedure is developed as follows:

1. Assume any fatigue truck factor (FTF) from Table 3.7.
2. Multiply the assumed fatigue truck factor from step 1 by the maximum stress range induced from the rainflow analysis of the load history due to the standard truck, $\Delta\sigma_{\max,des}$.
3. The total number of cycles to failure based on the fatigue design curve N_c, is estimated based on $\Delta\sigma_{\max,des}$ multiplied by the fatigue truck factor (FTF)as follows:

   For single slope fatigue design curves, $N_c = \gamma \times \left(\Delta\sigma_{max,des} \times FTF\right)^{-3}$ (3.4)

   For dual slope fatigue design curves;

$$N_c = \gamma' \times \left(\Delta\sigma_{max,des} \times FTF\right)^{-5} \quad \text{for } \Delta\sigma_{max,des} \times FTF < \text{CAFL}$$

$$N_c = \gamma \times \left(\Delta\sigma_{max,des} \times FTF\right)^{-3} \quad \text{for } \Delta\sigma_{max,des} \times TF > \text{CAFL} \tag{3.5}$$

Where γ, γ' and CAFL are fatigue constants and constant amplitude fatigue limit for the fatigue category under investigation used in CSA-S16-09 (CSA 2009). In this section, fatigue category A will be used for the prediction purpose of equivalent stress cycle due to truck passage.

4. If the total number of actual trucks is designated by T_N, and the total cycles to failure using single or dual slope fatigue design curve is designated by N_c, Equation 3.6 estimates the equivalent stress cycles for each passage of the design truck, N_d, based on the previous parameters and the cumulative damage caused by the trucks from the WIM database. D_{real}, calculated in Section 3.2.3, using Miner's (Miner 1945) cumulative damage rule as follows:

$$N_d = \frac{N_c \times D_{real}}{T_N} \tag{3.6}$$

5. Repeat the above steps for all the fatigue truck values in different moment sections.

3.3.3 Results of Equivalent Number of Cycles Calibration

The results of the equivalent stress cycles using the WIM data from Ontario, Quebec are derived using the design truck CL-625. The predicted equivalent cycles are based on the fatigue truck factors for Ontario and Quebec WIM data using single and dual slope S-N curves. Table 3.11 summarises the number of cycles for single slope fatigue curves, while Table 3.12 shows the number of cycles derived using dual slope fatigue curves. The number of equivalent load cycles was derived for three span ranges, namely, span lengths larger than or equal 30.0 m, span lengths between 12.0 m and 30.0 m, and spans shorter than 12.0 m. The recommended number of cycles is considered to be the maximum value of Ontario and Quebec, since their results are close and they are using the same fatigue truck CL-625.

To validate the number of equivalent stress cycle values in CSA-S6-06 (CSA 2006) and compare it with the predicted values in Table 3.11, it was found that the current code values of equivalent stress cycles are conservative for the span ranges less than 12.0 m. For span lengths longer than 12.0 m, the code equivalent numbers of cycles are less than the predicted values for Ontario and Quebec data.

Table 3.11 *Number of cycles for design trucks using Ontario and Quebec data for CL-625 for single-slope fatigue design curves.*

WIM Data	***Moment History Case***	***Equivalent number of cycles for Single Slope***			**CSA-S06-06(CSA 2006)**	
		L < 12 m	**12 m ≤ L ≤ 30 m**	**L > 30 m**	**Span Length, L < 12 m**	**Span Length, L ≥ 12 m**
Ontario	*One-span - Moment at midspan.*	1.3	1.1	1.1	2.0	1.0
	Exterior span - Moment at midspan	1.4	1.3	1.1	2.0	1.0
	Exterior span - Moment at interior support	1.4	1.3	1.2	2.0	1.0
	Interior span - Moment at midspan	1.4	1.2	1.2	2.0	1.5
	Interior span - Moment at interior Support	1.3	1.1	1.1	2.0	1.0
Quebec-Batiscan	*One-span - Moment at midspan.*	1.1	1.0	1.1	2.0	1.0
	Exterior span - Moment at midspan	1.2	1.1	1.1	2.0	1.0
	Exterior span - Moment at interior support	1.2	1.2	1.2	2.0	1.0
	Interior span - Moment at midspan	1.2	1.0	1.1	2.0	1.5
	Interior span - Moment at interior Support	1.3	1.1	1.1	2.0	1.0
Quebec-Nicolas	*One-span - Moment at midspan.*	1.1	0.9	0.9	2.0	1.0
	Exterior span - Moment at midspan	1.3	0.9	0.9	2.0	1.0
	Exterior span - Moment at interior support	1.3	1.0	0.9	2.0	1.0
	Interior span - Moment at midspan	1.3	0.9	0.9	2.0	1.5
	Interior span - Moment at interior Support	0.9	0.9	0.9	2.0	1.0

Table 3.12 *Number of cycles for design trucks using Ontario and Quebec data for CL-625 for dual-slope fatigue design curves.*

WIM Data	***Moment History Case***	***Equivalent number of cycles for Dual Slope***		
		L < 12 m	**12 m ≤ L ≤ 30 m**	**L > 30 m**
Ontario	*One-span - Moment at midspan.*	1.2	1.1	1.1
	Exterior span - Moment at midspan	1.5	1.2	1.1
	Exterior span - Moment at interior support	1.5	1.2	1.1
	Interior span - Moment at midspan	1.6	1.2	1.1
	Interior span - Moment at interior Support	1.5	1.1	1.1
Quebec-Batiscan	*One-span - Moment at midspan.*	1.0	1.0	1.1
	Exterior span - Moment at midspan	1.1	1.0	1.1
	Exterior span - Moment at interior support	1.0	1.1	1.1
	Interior span - Moment at midspan	1.2	1.0	1.0
	Interior span - Moment at interior Support	1.4	1.1	1.1
Quebec-Nicolas	*One-span - Moment at midspan.*	1.1	0.9	0.8
	Exterior span - Moment at midspan	1.3	0.9	0.9
	Exterior span - Moment at interior support	1.3	0.9	0.9
	Interior span - Moment at midspan	1.5	0.9	0.8
	Interior span - Moment at interior Support	1.3	1.0	0.9

3.3.4 Discussion of Equivalent Number of Cycles Calibration

The number of cycles for design trucks was derived for different values of fatigue truck factors recommended for Ontario and Quebec (Table 3.7). The current equivalent stress cycles in CSA-S6-06 (CSA 2006) is based on two ranges of bridge span lengths: span length < 12.0 m and span

length ≥ 12.0 m. This was based on one value for fatigue truck factor for all span lengths. As shown in Section 3.2, there was a need to define three different values of fatigue truck factors for different span lengths. As a result, it is recommended to specify three different values of equivalent stress cycles due to truck passage for the three span ranges: span range < 12.0 m; 30.0 m ≥ span range ≥ 12.0 m; and span range > 30.0 m instead of the currently two span ranges. Tables 3.11 and 3.12 illustrated that the predicted equivalent stress cycles decreases as the fatigue truck factor increase.

In Table 3.11, it was noticed that the values of equivalent stress cycles, predicted using single-slope fatigue design curves, for Ontario and Quebec are generally less than the current value used in CSA-S6-06 (CSA 2006) for span lengths < 12.0 m. In single span case, the predicted equivalent number of cycles for Ontario is 35% less than the code value, while this percentage increased to 45% for Quebec-Batiscan and Quebec-Nicolas. These percentages increased in the multi-span cases for both exterior and interior spans. For exterior span lengths, the value predicted for span length < 12.0 m is less than code by 30 % for Ontario, while the difference increased to 40% for Quebec-Batiscan. Similar observations are noticed in interior spans. In general, the current used values in CSA-S6-06 (CSA 2006) are conservatives for bridge spans < 12.0 m.

For the other span lengths (30.0 m ≥ span range ≥ 12.0 m; and span range > 30.0 m) in Table 3.11, the evaluated equivalent number of cycles for Ontario and Quebec-Batiscan WIM data was generally slightly higher than the current code values. Exterior spans for Ontario and Quebec-Batiscan showed an increase of 10% - 25% in equivalent stress cycles when compared to the code values. This was not the same observation for the interior spans, where the percentage dropped to 10%. On the other hand, the predicted values in case of Quebec-Nicolas are less than the current code values by 10% - 40%.

Table 3.12 illustrated the equivalent number of cycles using dual slope fatigue design curves, which are not yet implemented in CSA-S6-06 (CSA 2006). For span ranges less than 12.0 m, the predicted value for equivalent number of cycles in single span using Ontario was slightly higher than Quebec data by 16%. This finding was also valid for other span ranges with a difference of 9% - 18%. For exterior spans, the predicted values for Ontario are higher than Quebec by 13% - 33% for spans less than 12.0 m. For bigger span ranges, the maximum difference decreased to

25%. In interior span case, the predicted number of cycles in Ontario was bigger than Quebec for the three span ranges with similar percentages as in exterior case.

Based on the above discussion and results in Tables 3.11 and 3.12, the maximum values generated from Ontario, Quebec-Batiscan and Quebec-Nicolas will be employed in Table 3.13 to propose values for the equivalent number of cycles due to design truck. A summary of the suggested equivalent number of cycles using single and dual-slope fatigue design curves for: midspan one-span moment; midspan and interior support moment for exterior span; and midspan and interior support moment for interior span is presented in Table 3.13.

Table 3.13 *Recommended equivalent number of cycles due to the passage of design truck for different bridge span configuration using Ontario and Quebec data.*

Moment History Case	***Equivalent number of cycles for Single Slope***			**CAN/CSA-S06-06**		***Equivalent number of cycles for Dual Slope***		
	L < 12 m	**12 m ≤ L ≤ 30 m**	**L > 30 m**	**L < 12 m**	**L ≥ 12 m**	**L < 12 m**	**12 m ≤ L ≤ 30 m**	**L > 30 m**
One-span - Moment at midspan.	1.3	1.1	1.1	2.0	1.0	1.2	1.1	1.1
Exterior span - Moment at midspan	1.4	1.3	1.1	2.0	1.0	1.5	1.2	1.1
Exterior span - Moment at interior support	1.4	1.3	1.2	2.0	1.0	1.5	1.2	1.1
Interior span - Moment at midspan	1.4	1.2	1.2	2.0	1.5	1.6	1.2	1.1
Interior span - Moment at interior Support	1.3	1.1	1.1	2.0	1.0	1.5	1.1	1.1

3.4. Summary and Conclusions

The procedures of the calibration of fatigue truck factor and equivalent cycles due to the passage of design truck were discussed in Section 3.2. The collected WIM data from two provinces and one territory in Canada was implemented in the calibration of the fatigue truck factor and the number of equivalent stress cycles due to the passage of design truck. For calibration purposes, gross errors in WIM data were removed initially from the WIM data. This means that any unphysical data record (Gross vehicle weight ≤ 0, speed ≤ 0) was removed. Then, a suggested filtration criteria was developed based on several researches in the United States, Europe and

South Africa. It provided specific boundaries to filter the input WIM data for GVW, axle weights, axle spacing, truck speed and truck length. Load histories for critical locations in one, two and five-span bridge with spans range from 2.0 m to 70.0 m were developed. The rainflow cycle counting method was used to transform the bending moment loading histories into bending moment range spectra. These histograms employed both single and dual slope fatigue design curves to predict the fatigue truck factors for each case. While the current fatigue truck factor in CSA-S6 (2006) is 0.52.

Two factors were found to affect the fatigue truck factor: the span length for both single and dual slope fatigue curves; the fatigue detail category influences truck factor for short spans and dual slope curves only. In bridge span lengths less than 12.0, there is a great variability in truck factors values. Then, this variability decreases from span lengths 12.0 m to 30.0 m. After 30.0 m, the fatigue truck factor is almost constant in most cases. Accordingly, three fatigue truck factors for three different span ranges ($L \leq 12.0$ m, $12.0 \text{ m} \leq L \leq 30.0$ m, and $L > 30.0$ m) is required to accommodate the variability in fatigue truck factor with respect to span lengths for single and dual slope fatigue design curves. The latter is currently used in the limit state steel design code CSA-S16-09 (CSA 2009), and not yet adopted in the CSA-S6-06 (CSA 2006). Furthermore, the evaluated fatigue truck factors using Ontario and Quebec were found to have similar fatigue truck predictions, when compared to the predicted results using NWT WIM data. Finally, the fatigue truck calibration was done for NWT WIM data, which employed CL-800 as design truck. Section 3.2 proposed values for the reduction factor, C_L for the same span lengths ranges illustrated above.

Furthermore, equivalent stress cycles due to the passage of design trucks were calibrated using the same WIM data in Section 3.3. The current values for equivalent stress cycles due to design truck passage ranges from 1.0 to 5.0 depending on the simple or continuous spans, and whether the member is longitudinal or transverse. The current code values are developed using single-slope fatigue design curve and fatigue truck factor for two bridge span lengths with 12.0 m to be the boundary. After the emphasis of using three fatigue truck factors for three different spans in Section 3.2, it is more convenient to employ the same concept for the equivalent stress cycles calibration. The proposed values of the equivalent stress ranges were based on the recommended fatigue truck factors, developed in Section 3.2 for single and dual slope fatigue design curves.

For the predictions using the single-slope fatigue design curve, the current code values were found to be conservative for the span lengths < 12.0 m.

In conclusion, the calibration of fatigue truck factor and number of cycles is highly affected by the WIM source and quality. The results of fatigue truck factor using Ontario and Quebec WIM induced very close results although they are considered different sources. This is due to the high quality of the data received from these stations, which was reflected on the data filtration steps in 3.2.2.3. Moreover, the calibration of fatigue truck factor and equivalent number of stress cycles using the dual-slope fatigue design curve illustrated the need to propose these values in next revisions of the current bridge code CSA-S6-06 (CSA 2006).

4. PROBABILISTIC TRUCK LOAD MODEL FOR HIGHWAY BRIDGES

4.1. Introduction

For the reliability-based approach developed in the present research, the loading and resistance parameters should be modeled using appropriate probabilistic models. Therefore, each parameter should be defined by its type of probabilistic distribution (e.g. normal, lognormal, Weibull, etc.) and the probabilistic parameters defining this distribution.

This chapter focuses on the development of probabilistic truck load model, based on the predicted load histories using WIM from Ontario and Quebec, predicted in Chapter 3. First, the procedure to develop the truck loading, collected from WIM databases, into probabilistic stress range models for steel highway bridges is outlined in section 4.2. Then, a summary of the bridge loading models is presented in Section 4.3. These models will be used as input parameters for the probabilistic prediction of remaining fatigue life for cruciform weld detail illustrated in Chapter 7.

4.2. Probabilistic Truck Loading Procedure

4.2.1 Introduction

Weigh-in-motion (WIM) databases are used to develop the probabilistic truck loading model required for fatigue life reliability analysis in steel highway bridges. The following sections will outline the assessment of the truck loading uncertainties in their probabilistic forms i.e. statistical distribution type and parameters. First, the uncertainties in WIM data will be assessed according to ASTM E1318 (2009) in Section 4.2.2. Then, the probabilistic models for the truck loading for various critical sections in one, two and five-span bridges will be presented in Section 4.2.3.

4.2.2 Uncertainties in WIM data

In this section, ASTM E1318 – *Standard Specification for Highway Weigh-In-motion (WIM) Systems with User Requirements and Test Methods* (ASTM 2009) – is employed for the statistical analysis of the error measurements encountered in the received WIM data. ASTM E1318 (2009) comprises acceptable accuracy specifications for four different types of WIM systems and the essential properties that each type based on the vehicle speed, various features that each type should provide and also the application of WIM system such as weight-enforcement or pavement design purposes. As for this study, WIM systems are assumed to be of

Type I[3]. The error E in the WIM weight measurements could be evaluated as follows (ASTM E1318 2009):

$$E = 100 \times \frac{W_{WIM} - W_{Static}}{W_{Static}} \tag{4.1}$$

Where:

E = WIM weight error (%)

W_{WIM} = Weight recorded by the WIM system (kg)

W_{Static} = Weight recorded by the static scale (kg)

The errors for the following weight parameters are calculated for each WIM sensor axles:

- Single Steering axle load;
- Tandem Drive axle load;
- Tandem Load axle load; and
- Gross Vehicle Weight.

The acceptable limits are provided in the ASTM E1318 (2009) for different WIM types. For each type of WIM systems (I to IV), the acceptable ranges for different parameters are provided in Table 4.1. For Type I, which is the focus of this study, tolerances of ± 20 %, ± 15 %, and ± 10 % at 95% confidence are used for axle load, axle-group load, and gross vehicle weight, respectively.

Table 4.1 *Acceptable Tolerances for the WIM systems (ASTM E1318 2009).*

Function	Tolerance for 95% Compliance				
	Type I	Type II	Type III	Type IV	
				Value ≥ lb (kg)	± lb (kg)
Wheel load	± 25 %		± 20 %	5000 (2300)	300 (100)
Axle load	± 20 %	± 30 %	± 15 %	12 000 (5400)	500 (200)
Axle-Group Load	± 15 %	± 20 %	± 10 %	25 000 (11 300)	1200 (500)
Gross-Vehicle Weight	± 10 %	± 15 %	± 6 %	60 000 (27 200)	2500 (1100)
Speed	± 1 mph (2 km/h)				
Axle-spacing and wheelbase	± 0.5 ft (0.15 m)				

[3] This type of WIM system is designed for installation in one or more lanes at a traffic data-collection site i.e. WIM station and are capable to accommodate highway vehicles moving at speed, which ranges from 16 to 130 km/hr (ASTM E1318 2009).

In a recent study at the University of Alberta, Farkhideh (2012) evaluated the WIM systems in the province of Alberta. In that study, the department of transportation in Alberta ran a full repeatability and full environmental reproducibility verification test program on the investigated WIM systems in seven sites. Every month, a Federal Highway Association (FHWA) Class 9 truck passed 10 times over each of the 20 WIM sensors in Alberta. FHWA Class 9 truck is a five-axle single trailer truck which is one of the dominant truck types in the Province of Alberta. This truck is equivalent to Category 1 in MOU in Canada (TAC 1991).

The WIM data in this study, which contains the truck classification as part of the data extracted via the WIM systems, are Quebec and NWT only. Since NWT are comprised of light weight trucks, they will not be included in the probabilistic distribution of WIM parameters as their traffic trends is characterized by light vehicle weights, which will not be reflected on the fatigue life. Moreover, Ontario WIM databases did not encounter the truck classes. As a result, the errors in the WIM measurements are implemented for the two sites of Quebec (Batiscan and Nicolas) for Class 9 trucks only, and are compared to the static weights of the typical Class 9 truck provided in Farkhideh (2012).

In this study, four WIM parameters were considered: steering weight axle, tandem drive axle weight, tandem load axle weight and GVW. The WIM systems were considered of Type I of the ASTM standard (from truck speed 16 km/hr to 130 km/hr). Farkhideh (2012) emphasized that class 9 truck is the most dominant truck on highways in Alberta. For Quebec-Batiscan and Quebec-Nicolas WIM data, class 9 comprises around 33 % and 48 % respectively. Table 4.2 illustrates the number of errors in the four WIM parameters for Quebec-Batiscan WIM data calculated using Eq. (4.1). The values in the table are shown in Figure 4.1.

Table 4.2 *Number of errors and error percentages in WIM class 9 truck data (Quebec Batiscan WIM).*

	Steer axle		Tandem drive		Tandem load		GVW	
Bin Size Error (%)	**Frequency**	**Error (%)**	**Frequency**	**Error (%)**	**Frequency**	**Error (%)**	**Frequency**	**Error (%)**
Less than - 80.0	0	0.00	30	0.10	516	1.79	10	0.03
-80.0 to -50.0	380	1.32	12825	44.39	15310	52.99	11973	41.44
-50.0 to -20.0	7786	26.95	11479	39.73	7251	25.10	10851	37.56
-20.0 to -15.0	3899	13.50	1905	6.59	1593	5.51	2107	7.29
-15.0 to -10.0	4384	15.17	1254	4.34	1561	5.40	1904	6.59
-10.0 to 0.0	7449	25.78	1061	3.67	1770	6.13	1638	5.67
0.0 to 10.0	3620	12.53	247	0.85	619	2.14	311	1.08
10.0 to 15.0	670	2.32	44	0.15	108	0.37	50	0.17
15.0 to 20.0	329	1.14	20	0.07	64	0.22	23	0.08
20.0 to 50.0	354	1.23	23	0.08	89	0.31	22	0.08
50.0 to 80.0	18	0.06	1	0.00	8	0.03	0	0.00
More than 80.0	1	0.00	1	0.00	1	0.00	1	0.00
Total number of errors	28890		28890.00		28890.00		28890.00	
Number of negative errors	23898	82.72	28554.00	98.84	28001.00	96.92	28483.00	98.59
Number of positive errors	4991	17.28	335.00	1.16	888.00	3.07	406.00	1.41

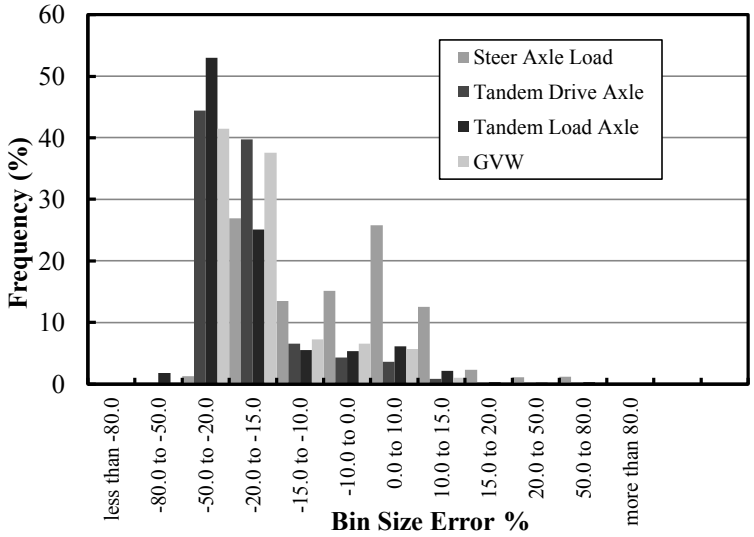

Figure 4.1 *Histograms for errors in WIM class 9 truck data (Quebec Batiscan WIM).*

Regarding the Quebec-Nicolas WIM data, Table 4.3 illustrates the number of errors in the four WIM parameters. These values are plotted in the histograms in Figure 4.2.

Table 4.3 *Number of errors and error percentages in WIM class 9 truck data (Quebec Nicolas WIM).*

	Steer axle		Tandem drive		Tandem load		GVW	
Bin Size Error (%)	**Frequency**	**Error (%)**	**Frequency**	**Error (%)**	**Frequency**	**Error (%)**	**Frequency**	**Error (%)**
Less than - 80.0	0	0.00	46	0.11	427	1.01	21	0.05
-80.0 to -50.0	1386	3.27	11576	27.34	16946	40.02	9680	22.86
-50.0 to -20.0	7101	16.77	18441	43.55	14264	33.69	20078	47.42
-20.0 to -15.0	3780	8.93	2637	6.23	2060	4.87	2664	6.29
-15.0 to -10.0	4593	10.85	2411	5.69	1863	4.40	2458	5.81
-10.0 to 0.0	10232	24.17	3873	9.15	3164	7.47	3915	9.25
0.0 to 10.0	8193	19.35	2269	5.36	2027	4.79	2356	5.56
10.0 to 15.0	2778	6.56	529	1.25	604	1.43	601	1.42
15.0 to 20.0	1962	4.63	319	0.75	416	0.98	319	0.75
20.0 to 50.0	2298	5.43	238	0.56	554	1.31	248	0.59
50.0 to 80.0	19	0.04	3	0.01	17	0.04	2	0.00
More than 80.0	0	0.00	0	0.00	0	0.00	0	0.00
Total number of errors	42342		42342		42342		42342	
Number of negative errors	27092	63.98	38984	92.07	38724	91.46	38816	91.67
Number of positive errors	15250	36.02	3358	7.93	3618	8.54	3526	8.33

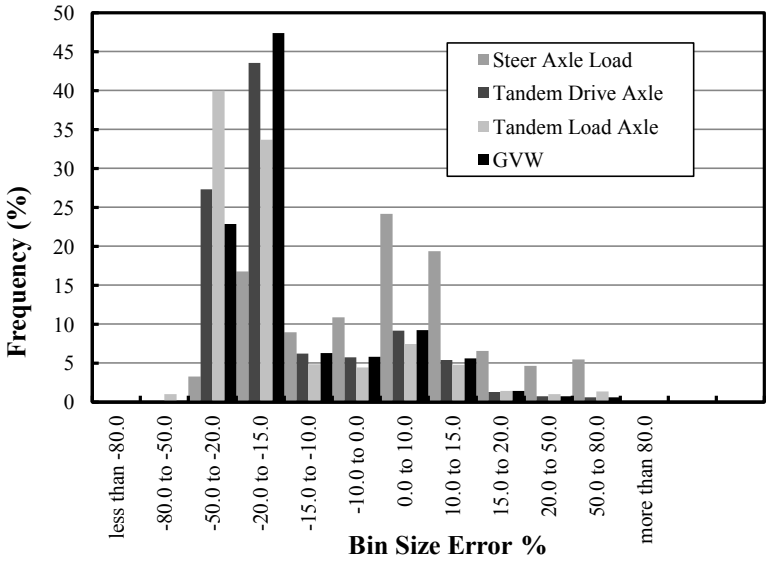

Figure 4.2 *Histograms for errors in WIM class 9 truck data (Quebec Nicolas WIM).*

The results showed that the numbers of negative errors are considered to be the majority (more than 90% of the total errors) for Batiscan WIM data (Figure 4.1). A similar trend could be observed in WIM Nicolas data as illustrated in Figure 4.2. ASTM E1318 (2009) stated that the lower values (negative values) are not usually a concern for WIM enforcement. This means that they may still be included in the WIM input data as their effect will be counted towards the fatigue cycles. Due to the lack of information about the static validation of truck classes' weights (other than class 9) in Quebec data, the same procedure could not be applied on the rest of the truck classes in Quebec WIM data.

For truck load modeling, WIM data could be used despite the measurement errors in the WIM data class 9 trucks according to the ASTM E1318 (2009) specification; most of these errors are in the negative side i.e. conservative sides. Trucks classes, other than class 9, could not be verified due to the lack of information. Ontario WIM truck data could not be verified as well since it did not include truck classifications.

4.2.3 Truck Loading

One method to predict the truck loading for fatigue life evaluation is the weigh-in-motion (WIM) databases. The procedure used to screen the WIM data for Ontario, Quebec and NWT was explained in section 3.2. WIM data from Ontario and Quebec only are adopted to develop the probabilistic distribution of applied stress ranges, while NWT data will not be used as they comprised a large percentage of light weight trucks that won't affect the fatigue strength.

Bending moment range histograms, developed in Section 3.2.4, for midspan and interior support locations in one, two and five-span bridges with span lengths, which ranges from 6.0 m to 60.0 m are employed. Then, the loading histories, represented by the bending moment range at each section (midspan and interior support of one, two and five-span bridge) for every span length, is then transformed into stress range by employing appropriate built-up steel sections for the main girders of the bridges. Appendix D illustrates a sample calculation for the design of built-up section and the prediction of stress ranges from moment ranges.

Several researches introduced the methods of transforming the stress range histograms into statistical distributions for bridge loading. Righiniotis (2004) used a Rayleigh distribution to fit the frequency diagram, which then forms the input for the fatigue reliability analysis. Other probabilistic distributions such as lognormal (Snyder *et al.* 1985) are employed to fit the stress

histograms developed from WIM sites. In this study, stress range histograms are fitted into appropriate probabilistic distributions, using a curve fit software, depending on the source of WIM data and the span length. Ontario and Quebec WIM data were used in the development of probabilistic fit of the stress range histograms. The software provides the best fit of the stress range histograms using one of the probabilistic distributions (normal, lognormal, Weibull, etc.). It also employs all the possible probabilistic distributions and sets them in order of their proximity to fit the stress range histograms with their parameters (mean, standard deviation, etc.).

In the following sub-sections, the results of the fitting of probabilistic distributions to various stress ranges are illustrated.

4.2.3.1 One span – Midspan Moment

The stress range histograms for the midspan moment of one-span bridge are fitted into the appropriate probabilistic distribution using Easy Fit software. As an example of the fitted stress histograms, Figures 4.3 to 4.5 illustrate the probabilistic distribution fit for the corresponding stress range histograms using Ontario WIM data for three span ranges 12.0 m, 24.0 m and 48.0 m to model three different bridge lengths.

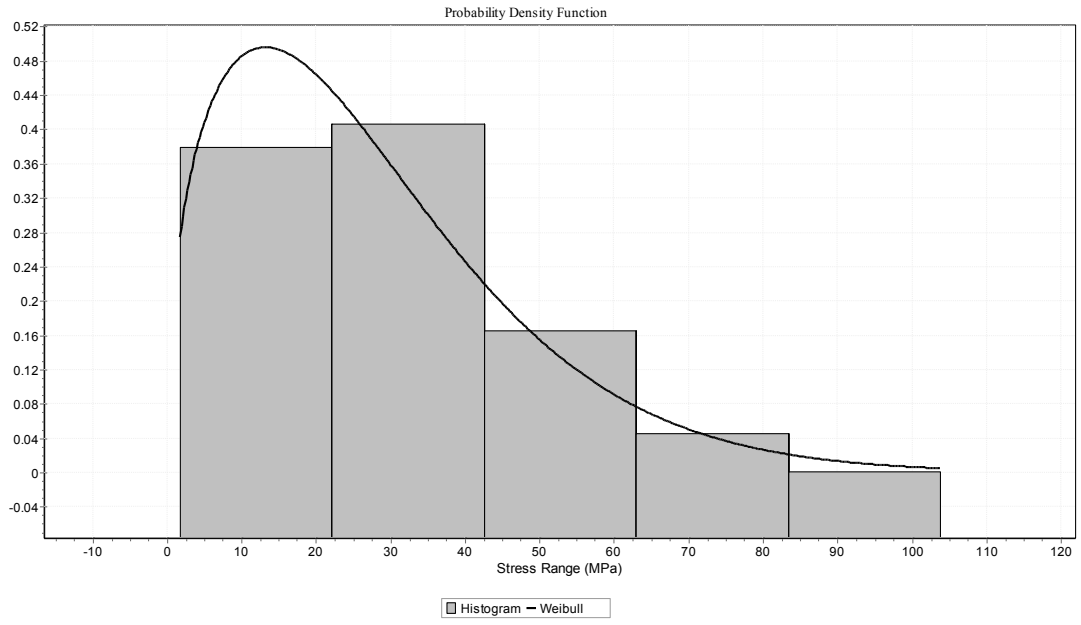

Figure 4.3 *Weibull Distribution for 12.0 m using Ontario WIM data.*

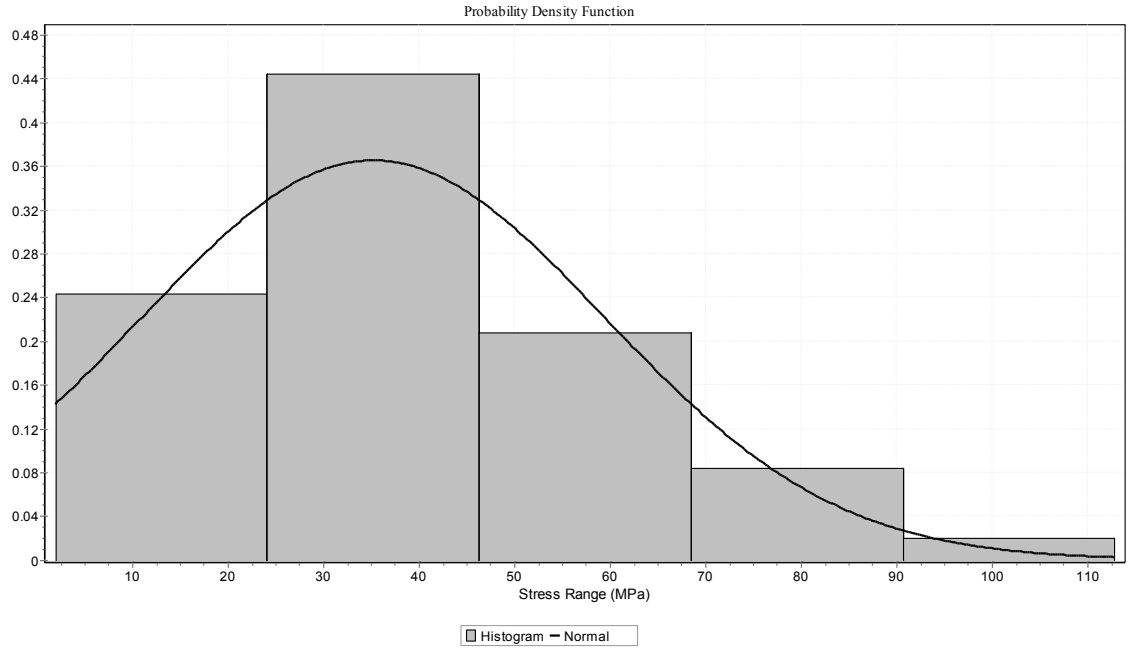

Figure 4.4 *Normal Distribution for 24.0 m using Ontario WIM data.*

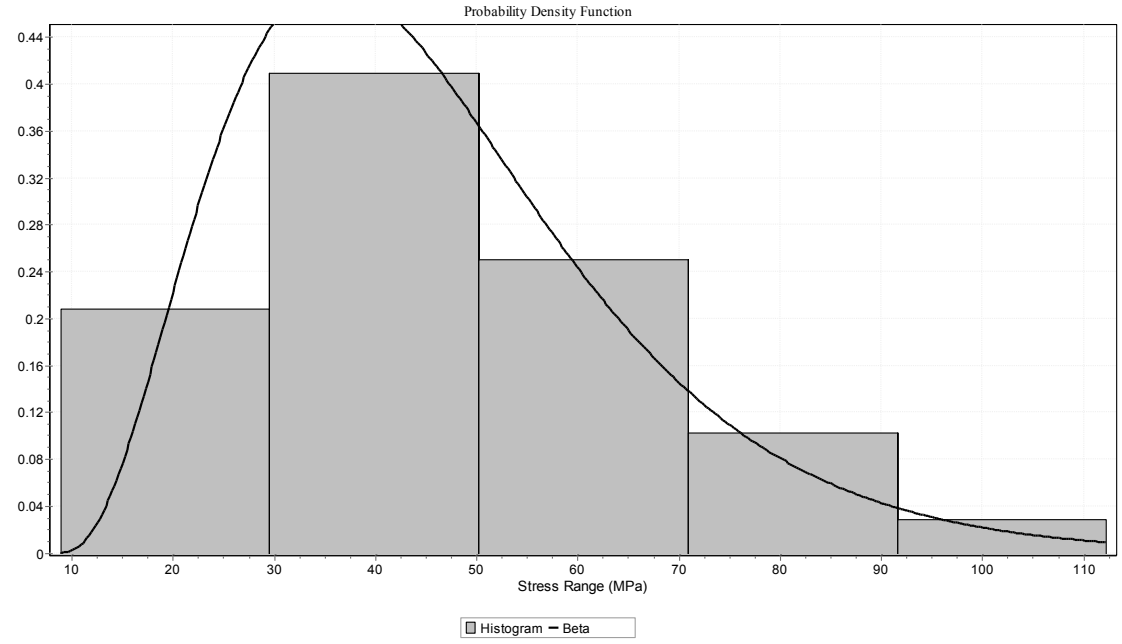

Figure 4.5 *Beta Distribution for 48.0 m span using Ontario WIM data.*

In Table 4.4, all the probabilistic stress range distribution and associated parameters for midspan moment of one span bridge using Ontario, Quebec-Batiscan and Quebec-Nicolas WIM data are illustrated. The probabilistic distributions in Table 4.4 are found to be the most suitable statistical distributions to model the stress range histograms in their specific span lengths. It can be noticed

that Weibull probabilistic distribution is dominant for span ranges from 6.0 m to 18.0 m. From span lengths that ranges from 24.0 m to 42.0 m, the normal and lognormal distributions were found to be more suitable, while the beta statistical distribution is dominant in the large span lengths (from 48.0 m to 60.0 m).

Table 4.4 *Probabilistic stress range distributions and associated parameters for midspan moment of one span bridges (Ontario and Quebec WIM data).*

WIM Data	Span (m)	Distribution	1st parameter	2nd parameter	3rd parameter	4th parameter
Ontario	6.00	Weibull (θ, τ)	33.45	1.59		
	12.00	Weibull (θ, τ)	30.37	1.44		
	18.00	Weibull (θ, τ)	11.9	0.92		
	24.00	Normal (α, β)	35.2	24.2		
	30.00	Normal (α, β)	45.5	23.77		
	36.00	Normal (α, β)	43.81	25.32		
	42.00	Normal (α, β)	41.7	24.5		
	48.00	Beta(α, β, a, b)	3.69	4.83E+06	8.72	4.85E+07
	54.00	Beta(α, β, a, b)	4.45	5.36E+06	5.52	4.82E+07
	60.00	Beta(α, β, a, b)	4.24	6.53E+06	3.91	6.39E+07
Quebec - Batiscan	6.00	Weibull (θ, τ)	29.78	1.66		
	12.00	Weibull (θ, τ)	28.1	1.64		
	18.00	Weibull (θ, τ)	12.8	1.09		
	24.00	Normal (μ, σ)	25.8	19.03		
	30.00	Normal (μ, σ)	35.85	17.79		
	36.00	Lognormal (α, β)	3.74	0.37		
	42.00	Lognormal (α, β)	3.75	0.355		
	48.00	Beta(α, β, a, b)	1.81	6.72	18.9	1.41E+02
	54.00	Beta(α, β, a, b)	1.71	5.69	18.66	127.95
	60.00	Beta(α, β, a, b)	1.63	5.01	19.15	123.71
Quebec - Nicolas	6.00	Weibull (θ, τ)	33.9	1.65		
	12.00	Weibull (θ, τ)	31.3	1.60		
	18.00	Weibull (θ, τ)	12.47	0.97		
	24.00	Normal (μ, σ)	31.5	22.43		
	30.00	Normal (μ, σ)	35.85	17.96		
	36.00	Lognormal (α, β)	3.75	0.38		
	42.00	Lognormal (α, β)	3.77	0.38		
	48.00	Beta(α, β, a, b)	2.1	9.93	8.33	9.43E+01
	54.00	Beta(α, β, a, b)	2.02	8.55	18.28	190.39
	60.00	Beta(α, β, a, b)	1.96	7.71	16.97	166.85

4.2.3.2 Two-span – Moment at midspan

For the midspan moment in the two-span bridges, the same procedure, implemented in section 4.2.3.1, is employed to fit the stress range histograms into their corresponding probabilistic distribution using Easy Fit software. Two probabilistic distributions were found to fit accurately the stress ranges histograms for Ontario and Quebec WIM data: Weibull and normal distribution. Weibull distribution for span ranges 6.0 m to 18.0 m; and normal distribution for span ranges bigger than or equal 24.0 m. For Ontario, Quebec-Batiscan and Quebec-Nicolas, it can be noticed that the Weibull distribution parameters have similar values for span lengths 6.0 m, 12.0 m and 18.0 m. Then, the normal distribution became dominant, where the mean value increases as the span length increases. For the Quebec-Nicolas data, the mean values of normal distribution curves are higher than those in Ontario and Quebec-Batiscan by a range of 7 % - 17 %.

Table 4.5 *Probabilistic stress range distributions and associated parameters for midspan moment of two span bridges (Ontario and Quebec WIM data).*

	Ontario			Quebec - Batiscan			Quebec - Nicolas		
Span (m)	**Dist.**	**1st parameter**	**2nd parameter**	**Dist.**	**1st parameter**	**2nd parameter**	**Dist.**	**1st parameter**	**2nd parameter**
6.00	Weibull (θ, τ)	29.66	1.42	Weibull (θ, τ)	27.28	1.54	Weibull (θ, τ)	31.44	1.60
12.00	Weibull (θ, τ)	21.99	1.078	Weibull (θ, τ)	20.92	1.18	Weibull (θ, τ)	23.69	1.19
18.00	Weibull (θ, τ)	17.66	0.76	Weibull (θ, τ)	19.06	0.7	Weibull (θ, τ)	22.48	0.77
24.00	Normal (μ, σ)	30.1	25.62	Normal (μ, σ)	29.57	24.59	Normal (μ, σ)	15.98	17.2
30.00	Normal (μ, σ)	41.01	26.57	Normal (μ, σ)	36.91	25.14	Normal (μ, σ)	44.83	29.45
36.00	Normal (μ, σ)	43.98	23.85	Normal (μ, σ)	46.05	26.57	Normal (μ, σ)	55.42	30.97
42.00	Normal (μ, σ)	45.99	23.51	Normal (μ, σ)	46.66	24.88	Normal (μ, σ)	55.8	29.07
48.00	Normal (μ, σ)	46.57	23.1	Normal (μ, σ)	46.22	23.44	Normal (μ, σ)	55.03	27.45
54.00	Normal (μ, σ)	46.49	22.59	Normal (μ, σ)	51.32	25.12	Normal (μ, σ)	60.9	29.5
60.00	Normal (μ, σ)	43.6	20.93						

4.2.3.3 Two-span – Moment at interior support

In a similar trend to the midspan moment of two-span bridges, the probabilistic stress range distribution for moment at interior support for the same bridge configuration displayed that Weibull and normal distributions are the most fitting curves for the predicted stress histograms. Weibull distribution was fit for span length 6.0 m to 36.0 m, while the normal distribution was fit

for span lengths bigger than or equal 42.0 m. The parameters defining the probabilistic distributions were almost equal for all the span ranges. This was observed for both distributions; Weibull and normal. Table 4.6 displays the probabilistic stress range distributions of moment at support for various span lengths using Ontario and Quebec WIM data.

Table 4.6 *Probabilistic stress range distributions and associated parameters for interior support moment of two-span bridges (Ontario and Quebec WIM data).*

	Ontario			Quebec - Batiscan			Quebec - Nicolas		
Span (m)	**Dist.**	**1st parameter**	**2nd parameter**	**Dist.**	**1st parameter**	**2nd parameter**	**Dist.**	**1st parameter**	**2nd parameter**
6.00	Weibull (θ, τ)	11.82	1.05	Weibull (θ, τ)	10.4	1	Weibull (θ, τ)	12.51	1.04
12.00	Weibull (θ, τ)	10.22	0.84	Weibull (θ, τ)	9.4	0.89	Weibull (θ, τ)	10.465	0.86
18.00	Weibull (θ, τ)	9.48	0.71	Weibull (θ, τ)	10.77	0.73	Weibull (θ, τ)	11.77	0.711
24.00	Weibull (θ, τ)	11.29	0.77	Weibull (θ, τ)	11.69	0.75	Weibull (θ, τ)	14.236	0.75
30.00	Weibull (θ, τ)	18.78	0.73	Weibull (θ, τ)	14.13	0.87	Weibull (θ, τ)	16.42	0.88
36.00	Weibull (θ, τ)	16.79	0.91	Weibull (θ, τ)	21.47	0.93	Weibull (θ, τ)	25.39	0.93
42.00	Normal (μ, σ)	22.07	20.76	Normal (μ, σ)	22.6	24.83	Normal (μ, σ)	29.02	26.74
48.00	Normal (μ, σ)	26.33	22.8	Normal (μ, σ)	25.3	21.42	Normal (μ, σ)	29.25	25.35
54.00	Normal (μ, σ)	24.82	19.95	Normal (μ, σ)	26.36	20.88	Normal (μ, σ)	30.28	24.73
60.00	Normal (μ, σ)	26.09	19.8						

4.2.3.4 Five-span – Moment at midspan

The Weibull probabilistic distribution is found to match all the span lengths for Ontario, Quebec-Batiscan and Quebec-Nicolas WIM data. Table 4.7 illustrates the probabilistic stress range distributions and associated parameters for midspan moment of five-span bridges.

Table 4.7 *Probabilistic stress range distributions and associated parameters for midspan moment of five-span bridges (Ontario and Quebec WIM data).*

	Ontario			Quebec - Batiscan			Quebec - Nicolas		
Span (m)	**Dist.**	**1st parameter**	**2nd parameter**	**Dist.**	**1st parameter**	**2nd parameter**	**Dist.**	**1st parameter**	**2nd parameter**
6.00	Weibull (θ, τ)	11.06	0.81	Weibull (θ, τ)	5.01	0.83	Weibull (θ, τ)	11.42	0.81
12.00	Weibull (θ, τ)	7.48	0.77	Weibull (θ, τ)	6.7	0.75	Weibull (θ, τ)	7.54	0.76
18.00	Weibull (θ, τ)	6.92	0.76	Weibull (θ, τ)	5.67	0.77	Weibull (θ, τ)	6.46	0.76
24.00	Weibull (θ, τ)	6.93	0.762	Weibull (θ, τ)	6.88	0.75	Weibull (θ, τ)	7.62	0.74
30.00	Weibull (θ, τ)	7.94	0.72	Weibull (θ, τ)	5.68	0.73	Weibull (θ, τ)	6.37	0.73
36.00	Weibull (θ, τ)	9.42	0.72	Weibull (θ, τ)	6.63	0.72	Weibull (θ, τ)	7.63	0.72
42.00	Weibull (θ, τ)	10.08	0.72	Weibull (θ, τ)	7.18	0.72	Weibull (θ, τ)	8.45	0.73
48.00	Weibull (θ, τ)	10.8	0.72	Weibull (θ, τ)	6.83	0.72	Weibull (θ, τ)	8.07	0.73
54.00	Weibull (θ, τ)	11.33	0.72	Weibull (θ, τ)	7.26	0.72	Weibull (θ, τ)	5.95	0.744
60.00	Weibull (θ, τ)	10.55	0.72						

4.2.3.5 Five-span – Moment at interior support

The probabilistic distributions for moment at support of five-span bridge were the same as the midspan moment for the same bridge configuration with slightly higher parameters around 10%. Therefore, the Weibull probabilistic distribution is found to fit well the developed stress range histograms. The probabilistic stress range distributions and associated parameters for moment at support for five-span bridges is shown in Table 4.8.

Table 4.8 *Probabilistic stress range distributions and associated parameters for moment at support of five-span bridges (Ontario and Quebec WIM data).*

	Ontario			Quebec - Batiscan			Quebec - Nicolas		
Span (m)	**Dist.**	**1st parameter**	**2nd parameter**	**Dist.**	**1st parameter**	**2nd parameter**	**Dist.**	**1st parameter**	**2nd parameter**
6.00	Weibull (θ, τ)	9.12	0.93	Weibull (θ, τ)	7.65	0.89	Weibull (θ, τ)	8.72	0.901
12.00	Weibull (θ, τ)	7.54	0.77	Weibull (θ, τ)	6.87	0.81	Weibull (θ, τ)	7.68	0.79
18.00	Weibull (θ, τ)	8.99	0.72	Weibull (θ, τ)	7.72	0.73	Weibull (θ, τ)	8.8	0.72
24.00	Weibull (θ, τ)	5.97	0.79	Weibull (θ, τ)	10.09	0.79	Weibull (θ, τ)	11.55	0.78
30.00	Weibull (θ, τ)	12.42	0.87	Weibull (θ, τ)	10.52	0.87	Weibull (θ, τ)	12.14	0.88
36.00	Weibull (θ, τ)	15.54	0.91	Weibull (θ, τ)	12.93	0.93	Weibull (θ, τ)	15.22	0.94
42.00	Weibull (θ, τ)	19.5	0.94	Weibull (θ, τ)	16.23	0.97	Weibull (θ, τ)	19.06	0.97
48.00	Weibull (θ, τ)	23.02	0.97	Weibull (θ, τ)	19.09	0.99	Weibull (θ, τ)	22.27	0.99
54.00	Weibull (θ, τ)	21.71	1.01	Weibull (θ, τ)	17.7	1.02	Weibull (θ, τ)	16.64	1
60.00	Weibull (θ, τ)	22.95	1.05						

4.3. Summary and Conclusions

The probabilistic truck loading model for fatigue life prediction is illustrated in Section 4.2, where the detailed methodology to develop probabilistic stress range from WIM databases is explained. It was found that the errors in WIM measurements according to ASTM E1318 (2009) do not have any effect on the WIM databases since they are in the negative side. The WIM error assessment was carried out for Class 9 trucks due to the lack of information for the rest of the truck classes. The loading model assumes one truck model on the bridge since the information about the exact arrival times of the trucks to consider the correlation of two following trucks was missing. Only the WIM from Ontario and Quebec were included in the load history prediction as the NWT WIM data comprised a lot of light weight vehicles which will be have no effect on the fatigue life. The bending moment ranges, predicted in Section 3.2, for one, two and five-span bridges for spans that range from 6.0 m to 60.0 m are employed to develop the stress range histograms by assuming appropriate girder sections as explained in Appendix D. The stress range histograms are fitted into suitable probabilistic distributions for various span lengths. For Ontario and Quebec WIM data, section 4.2.3 also provided the probabilistic distributions for all span

length ranges in the five sections, where the stress histograms are developed for one, two and five-span bridge.

In Chapter 7, the fatigue reliability analysis will be carried out using actual number of cycles using Quebec (Batiscan) and Quebec (Nicolas) probabilistic stress range distributions. As this WIM data included the total monitoring time to be 130 and 52 days respectively. Although the probabilistic stress histograms are predicted for Ontario, the monitoring period information was missing in the received WIM data. Therefore, the probabilistic stress distributions for Quebec only were encountered in the fatigue life reliability predictions as explained later in Chapter 7.

5. EXPERIMENTAL PROGRAM

5.1. Introduction

Chapter 2 outlined various methods that have been applied to fatigue repair and strengthening to increase the remaining fatigue life of welded details. Post-weld treatment is one of these methods, the main purpose of which is to improve the fatigue life of critical steel welded details. Well-known examples of such treatments include peening and weld toe grinding. The investigation of the effectiveness of these techniques requires fatigue testing on treated welded details to compare the fatigue resistance with that of as welded details. To improve the fatigue resistance of critical weld details of steel bridges in-service using post-weld treatment, weld toe grinding is considered to be an easy, cheap and fast method, when compared to other methods such as peening, which requires skilled operators in addition to its high cost. Therefore, weld toe grinding needs further experimental examination, especially for the full-scale specimens to assess the fatigue life improvement of welded details.

Full-scale specimens of welded details representing critical fatigue details (fatigue category E) were tested in this research program, where post-weld treatment in the form of weld toe grinding is imposed to the welds to assess its performance on the fatigue life of the welded detail. In the experimental program, three specimens were tested under constant amplitude stress range: two specimens have their weld toe ground and the third is considered as-welded specimen. The fatigue life predictions resulting from the fatigue test are estimated by a deterministic fatigue life prediction approach using finite element models and linear elastic fracture mechanics, presented in Chapter 6.

The set-up of the full-scale test and the geometrical characteristics of the test specimens, employed in the test program are explained in details in Section 5.2. Then, the information for the test specimens' preparation, including fabrication, welding, grinding, installation and instrumentation are provided in Section 5.3. Following that, the test program matrix, which illustrates the sequence of the full-scale specimens tested under cyclic loading, is outlined in Section 5.4. Afterwards, the procedure of the experimental program and the test results are outlined in section 5.5 and 5.6 respectively. Section 5.7 presents the observations of the fractured surfaces of the three tested specimens. Finally, Section 5.8 provides a summary and discussion of the test results.

5.2. Description of Full-scale Test Set-Up

5.2.1. General

A small test program was designed to investigate the benefit of weld toe grinding on the fatigue resistance of a fatigue category E detail for full-scale specimens. To model this severe fatigue category, the steel welded detail under investigation connects a wide flange beam connected to an end plate. Three test specimens were used in the experimental program, namely, one specimen tested in the as-welded condition and two specimens treated by weld toe grinding.

5.2.2. Test Specimens Geometry

In this test program, the test specimens are formed from two steel cross-sections assembled together. The wide flange beam of W310x86 with an average height of 310 mm is shown in Figure 5.1.

Figure 5.1 *The half beam W310x86 used in the full-scale test specimens.*

The end plate moment connection should have a special detail to allow the all-around groove weld to pass across the beam web to ensure complete attachment between the half beam and the end plates. As a result, weld access holes should be cut out from the beam web to achieve that purpose. Figure 5.2 shows the beam flange and web weld preparation details and the weld access holes to allow groove welding between the beam and the end plate. The Canadian Welding Code CSA-W59 (2013) provides the necessary dimensions for such holes.

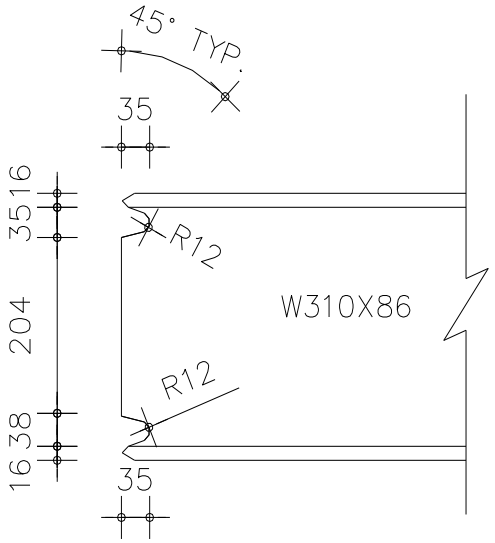

Figure 5.2 *Weld access holes dimension at the welding side of the wide flange beams.*

The end plate used in the test specimens is 570 mm high and 254 mm wide, which equals the width of the beam flange. Moreover, the end plate thickness is 45 mm. The two end plates are connected together back to back using 8 high-strength bolts of grade A-325 of 1-1/4 inch (31.75 mm) diameter and 150 mm length. The detailed dimensions of the end plate, in addition to the edge and pitch distances of the bolt holes, are shown in Figure 5.3.

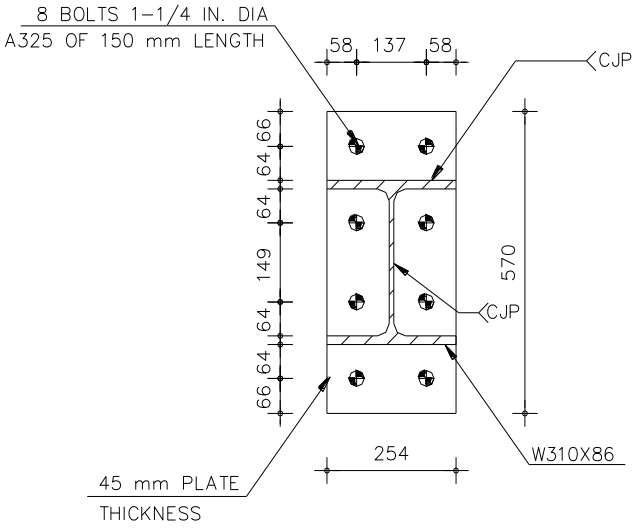

Figure 5.3 *End plate dimensions and bolt hole locations.*

5.2.3. Fatigue Test Setup

The Structures Morrison Lab at the University of Alberta employs a Pegasus system to apply cyclic loading under constant amplitude stress range on the welded details of fatigue category E, where high cycle fatigue is applied to the specimens. The test set-up consists of two half beams connected to two end plates in the middle, where the upper loading jack of the Pegasus system will apply cyclic loading to the two upper sides of the end plates. The end plates are adjusted to be exactly in the middle of the beam. Consequently, the upper jack of the fatigue machine will apply cyclic loadings to the middle of the beam.

Each half beam is attached to the end plate using all-around groove welds, which is the focus of the investigation. Figure 5.4 shows a schematic elevation of the set-up and a section of the beam with the end plate. The total length of the specimens (two half beams and end plates) is 3000 mm. The two half beams with their two bolted end plates rest on two supports, which are spaced at 2500 mm, with edge distance of 250 mm equally at each side. One support is a roller while the other is a hinge with a knife-edge. The upper jack of the machine will act exactly in the line of symmetry of the test set-up.

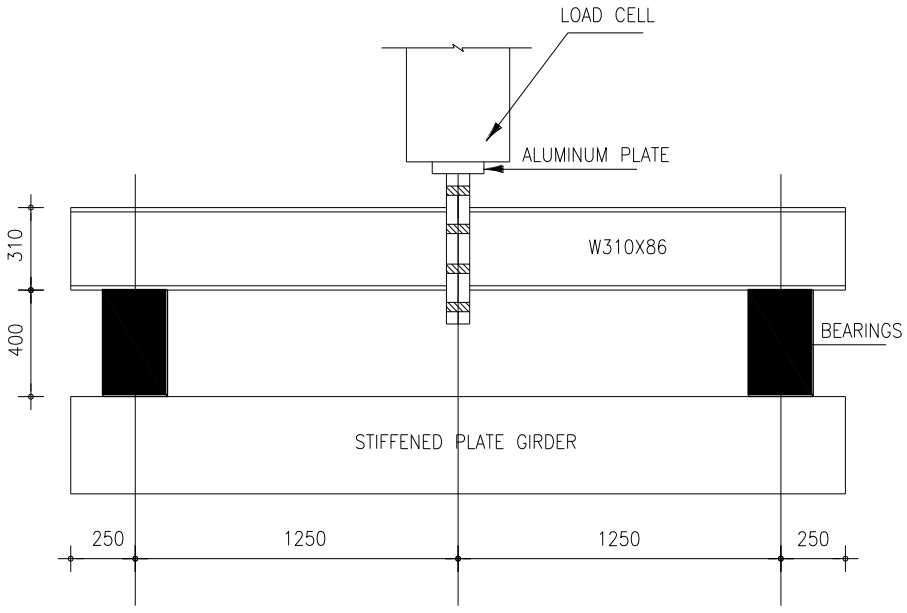

Figure 5.4 *Schematic elevation for the test set-up of the full-scale tests (dimensions in mm).*

The test set-up simulates a simple beam model, where the maximum positive bending moment is located at in mid-span of the beam. As a result of this configuration, the bottom flanges of the W310x86 beams and the groove weld connecting the end plate are subjected to tensile stresses in the beam mid-span vicinity.

The beam was loaded using a single hydraulic actuator with a maximum dynamic capacity of approximately 500 kN. Each of the supports consists of a cylindrical roller bearing sandwiched between two hardened steel plates with concave surfaces. This allows for a symmetrical response in the test, allowing free rotation and enough translation in the longitudinal direction to avoid any introduction of unwanted stresses in the beam and splice plate.

Overall lateral movement of the beam is restrained by roller bracings at the ends of the beam, which allows for free vertical movement of the beam. The actuator provides sufficient stiffness to prevent any longitudinal movement of the load point and thus acts as an overall longitudinal translation restraint. Rotation of the load points is free, using a concave reaction plate on a convex bearing. The supports rest on a large stiffened plate girder with a convenient height for installation and inspection of the reaction beam and the splice plates. Figure 5.5 displays an overall elevation view of the test set-up.

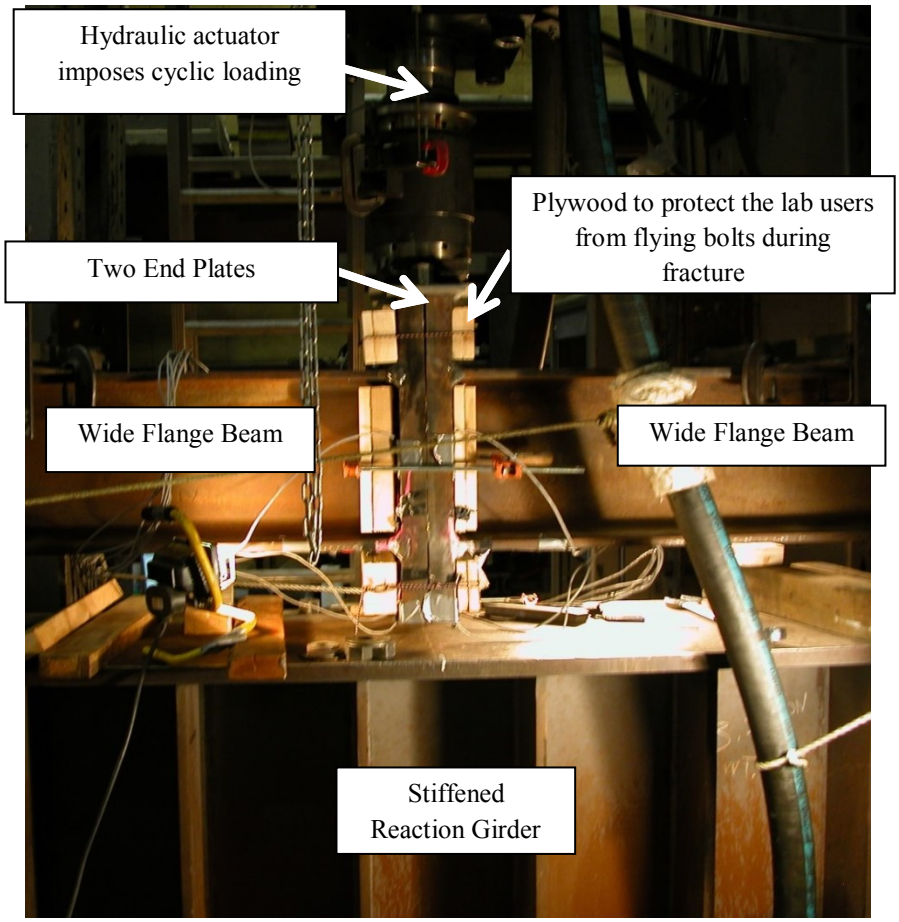

Figure 5.5 *Elevation view of full-scale set-up looking west.*

5.3. Preparation of Test Specimens

5.3.1. Introduction

This section outlines the steps taken to prepare the specimens for the full-scale fatigue test. Section 5.3.2 explains the fabrication and welding of beam and end plates. Then, the weld toe grinding procedure is illustrated in Section 5.3.3. Afterwards, Section 5.3.4 shows the installation between the beams and the end plates to form the test assemblies. Finally, Section 5.3.5 outlines the instrumentation of the test specimens.

5.3.2. Fabrication and Welding of the Beam and End Plates

The beams and plates were fabricated by a local steel supplier. Tolerances according to CSA S16-06 (CSA 2006) were prescribed and met. The potential beam flange and end plate surfaces, where the strain gauges would be mounted, were sandblasted and surface ground to allow a

smooth surface for strain gauges. Steel grade 350W was used for the fabrication of beams and end plates.

No fatigue crack was present in the test specimens prior to the fatigue test, welding and grinding were executed in the Structures Morrison Lab. Figure 5.6 shows the welding for the three investigated details, N-N-2 (Figure 5.6a), G-N-2 (Figure 5.6b) and G-N-3 (Figure 5.6c), before any grinding processes took place.

(a) Welding of end plate and beam for N-N-2

(b) Welding of end plate and beam for G-N-2

Figure 5.6 *The specimens after the weld between the wide flange beam and end plate.*

(c) Welding of end plate and beam for G-N-3

Figure 5.6 *(cont'd).*

In the three test assemblies, end plates are welded to the half beams with a groove weld, as indicated above. This was accomplished using the flux core arc welding (FCAW) process with a seamless wire [Drahtzug Stein Megafil® 713R, E491T1 according to AWS 5.20 (2005)] as the filler material. Appendix E provides more information about the welding procedure.

The welds were ground flush and the surface was shiny after grinding, which helped with visual crack detection, requiring only the assistance of a strong light. A magnifying glass was used for the as-welded and treated specimens. No surface defects were detected in any of the welds.

Despite not performing ultrasonic inspections on the welds which might include some weld defects, these welds were tested for fatigue. The rationale is these welds contain defects such as inclusions that could also be present in field applications. So it is beneficial to assess the fatigue resistance of these weld repairs in full-scale specimens.

5.3.3. Test Program Matrix

The procedure of executing the test program is to assemble two specimens using the high-strength bolts to form one test setup. Each specimen could be formed of either ground or non-ground specimens. The test program matrix consists of three test setups as illustrated below.

The first test setup consisted of the two specimens with designations of G-N-2 (ground) and N-N-2 (non-ground) in the bottom side of the beam (tension side). It was expected that the beam and plate comprising the N-N-2 as tension would fail first, and at that point the first experiment was done.

In the second test setup, the failed specimen N-N-2 from the first test was replaced with another ground specimen containing the tension side designated G-N-3. Therefore, test setup 2 consisted of G-N-2 and G-N-3 in the tension side. The fatigue test showed that G-N-2 failed first while G-N-3 did not fail. In this case, the number of cycles exerted on G-N-2 was the summation of cycles imposed in test setups 1 and 2 until it failed.

For the third test setup, the failed G-N-2 specimen from test setup 2 was replaced with G-N-1. Therefore, the test setup comprised the two ground specimens G-N-3 and G-N-1. In this case, the specimen G-N-3 failed. Table 5.1 provides a summary of the test setups illustrated above.

Table 5.1 *Experimental program matrix.*

Test Setup No.	Specimen	Tension Side	Specimen	Tension Side
1	1	G-N-2	2	N-N-2
2	1	G-N-2	3	G-N-3
3	3	G-N-3	4	G-N-1

The test setup for various specimens in the fatigue Pegasus system is shown in Figures 5.7 to 5.8. Figure 5.7 demonstrates test setup No. 1, which comprises specimens N-N-2 and G-N-2. Then, Figure 5.8 shows the setup No. 2, which includes specimens G-N-2 and G-N-3 after removing the failed specimen N-N-2. Finally, Figure 5.9 displays test setup No. 3 that consists of specimens G-N-3 and G-N-1 after removing the failed specimen G-N-3.

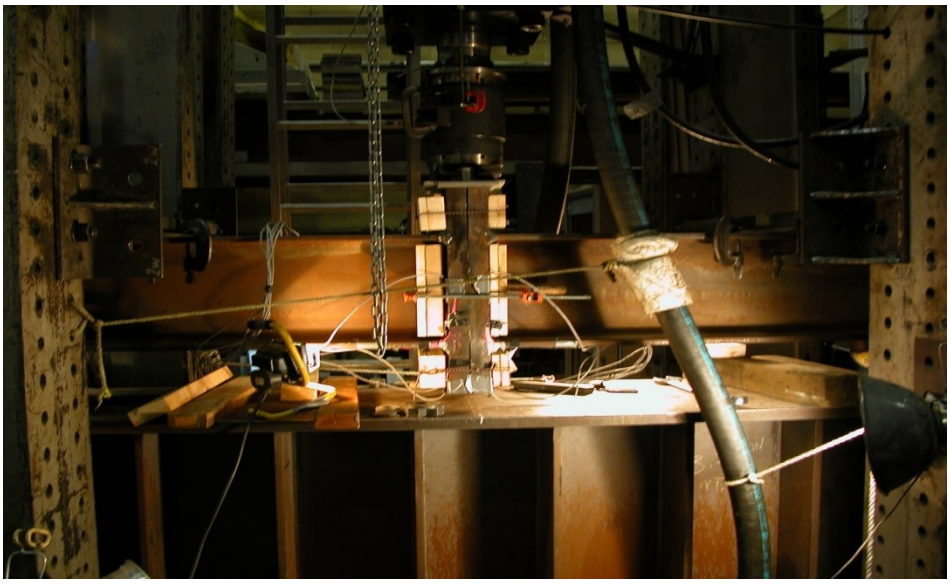

Figure 5.7 *Test setup no. 1 [G-N-2(right) - N-N-2(left)] looking east.*

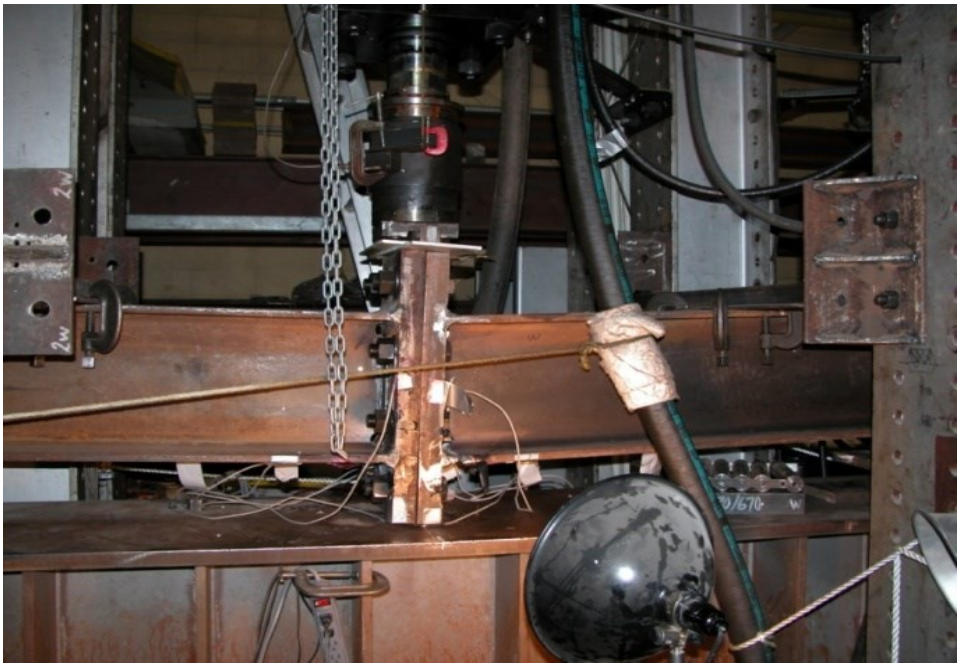

Figure 5.8 *Test setup no. 2 [(G-N-2(left) - G-N-3(right)] looking east.*

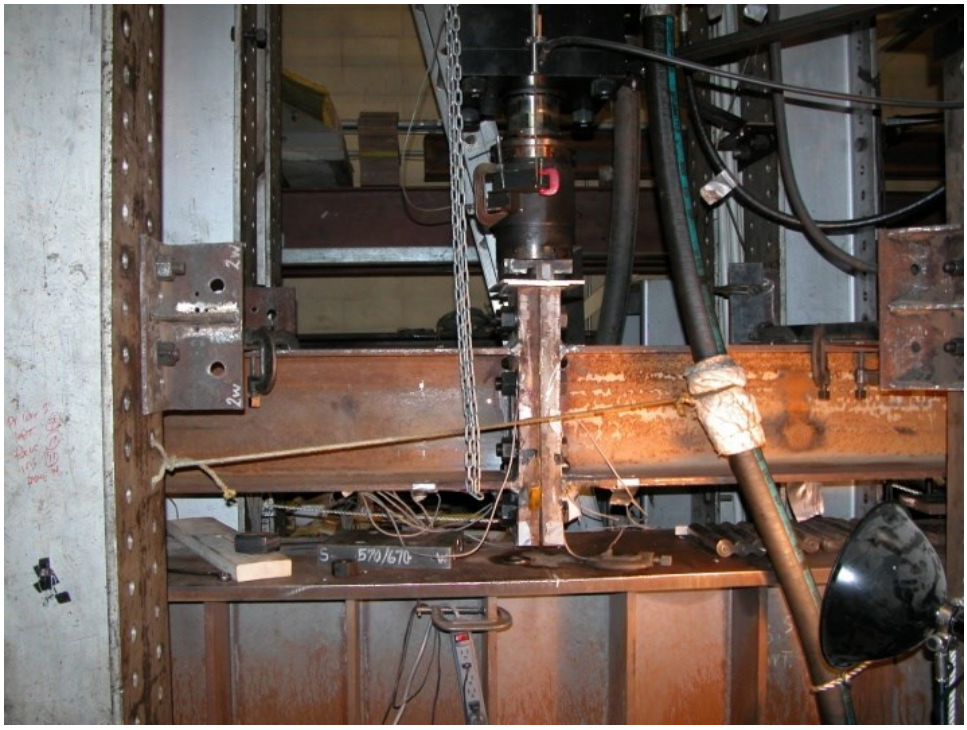

Figure 5.9 *Test setup no. 3 [G-N-2(left) - G-N-1(right)] looking east.*

5.3.4. Weld Toe Grinding Procedure

In this experimental program, the procedure outlined in DNV-RP-C203 (DNV 2010) for weld toe grinding was implemented. It should be noted that only the external welds located below the lower flange and the end plate were subject to grinding, not the internal welds, since this section contains the highest tensile stresses due to the bending moment acting along the beam.

Figure 5.10 is a schematic sketch that illustrates the weld grinding procedure. For best practices, the depth of grinding of weld toes should not be less than 0.5 mm below the bottom of any visible undercut, as displayed in the figure.

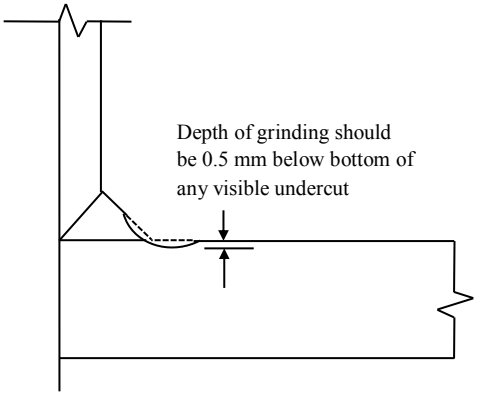

Figure 5.10 *Weld toe grinding (DNV 2010).*

The weld toe grinding in the test specimens was executed using a high-speed electric burr grinder, driving rotary burrs at a rotational speed of between 15,000 and 40,000 rpm. In general, DNV-RP-C203 (2010) recommends grinding of weld toes with a rotary ball-shaped burr with typical diameter of 12 mm, as shown in Figure 5.11.

Figure 5.11 *Weld toe grinding burr 12 mm diameter.*

5.3.5. Installation of End Plates with Beams

To allow a convenient installation of the end plates and the beams, each beam that would be welded to the end plate was rested on two supports on the structures lab floor. Then the eight high-strength bolts were snug tightened. After the snug tightening procedure was completed, each bolt in the connection was additionally pre-tensioned by the applicable amount of turns defined by Table 8 in CSA-S16-09 (CSA 2009). In this case, the bolt diameter is 1.25 inch (31.75 mm) and the bolt length is 150 mm; therefore, the ratio between the length and diameter is 150/31.75 = 4.72, which is between 4 and 8. As a result, one half turn is needed to pre-tension the bolts. Figure 5.12 illustrates a sample of the test set-up assembly after the installation of beams and the end plates using the bolts on the lab floor.

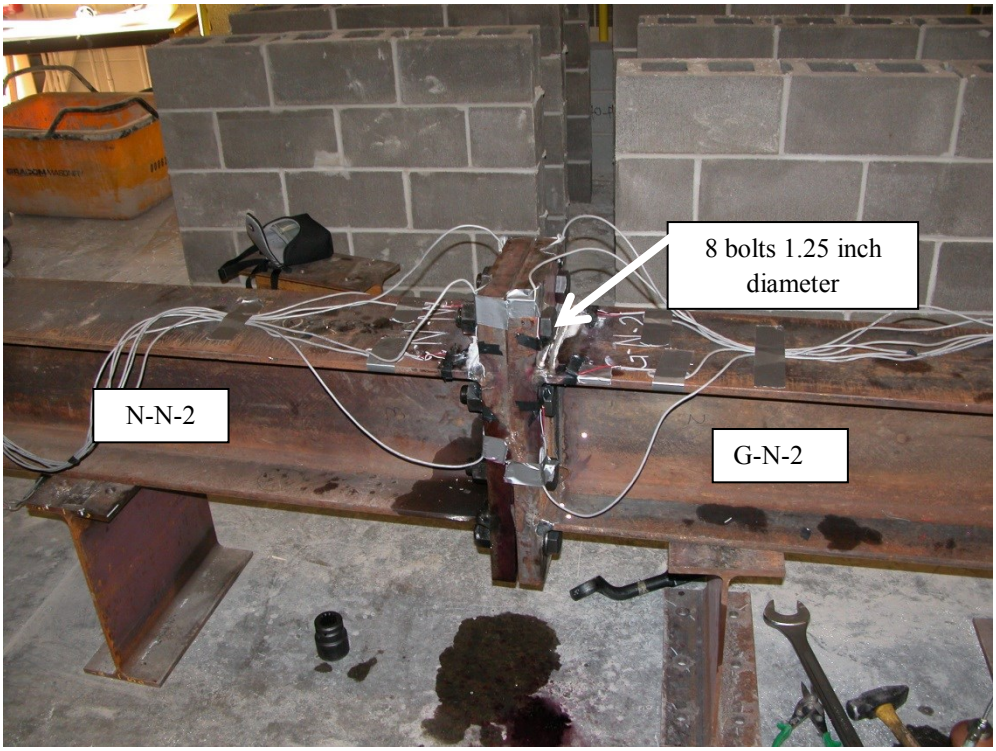

Figure 5.12 *Test set-up assembly.*

5.3.6. Instrumentation of Test Specimens

Six strain gauges are mounted on each test specimen, which are labelled with the same annotation as the specimen groups (e.g. G-N-1, or N-N-3), with the addition of an extra label to identify them easily. Four strain gauges (P1 to P4) are mounted vertically on the end plate above and below the tension flange (Figure 5.13) to measure the vertical strains in the plate due to cyclic loading, and two strain gauges (F1 and F2) are mounted horizontally on the beam tensile flange (Figure 5.14) to measure the strains due to tensile stresses.

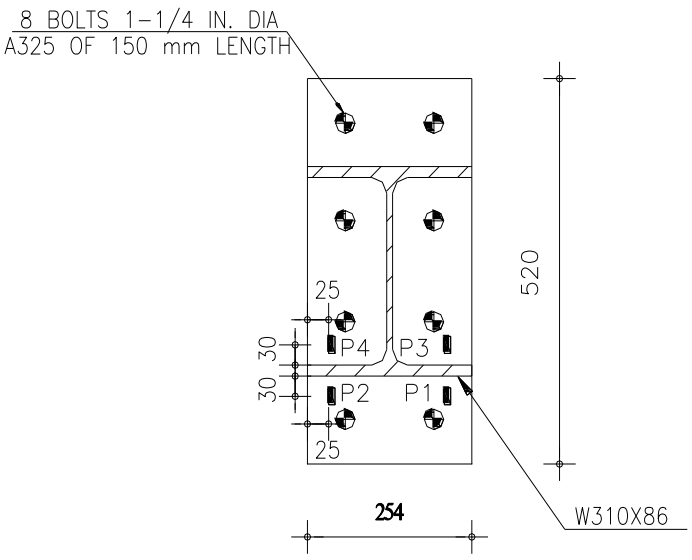

Figure 5.13 *Location of vertical strain gauges on end plates.*

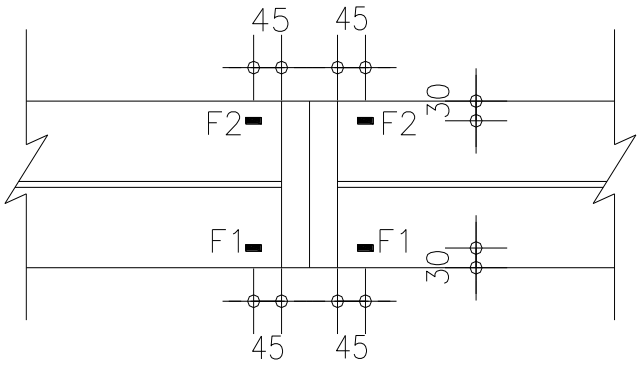

Figure 5.14 *Location of horizontal strain gauges on beams.*

The following sections display the location of instrumentations on the test specimens.

5.3.6.1 Test Setup 1: G-N-2 - N-N-2

For test setup No. 1 (G-N-2 - N-N-2), the instrumentation used to install strain gauges at the end plates and the flanges are shown in Figures 5.15 to 5.17. Figure 5.15 displays the instrumentation on the entire beam, while Figures 5.16 and 5.17 illustrate the instrumentation of specimens G-N-2 and N-N-2, respectively.

Figure 5.15 *Instrumentations for specimen N-N-2 - G-N-2.*

Figure 5.16 *Instrumentation for specimen G-N-2.*

Figure 5.17 *Instrumentation for specimen N-N-2.*

5.3.6.2 Test Setup 2: G-N-2 - G-N-3

Figure 5.18 shows the strain gauge locations for test set-up No. 2 (G-N-2 - G-N-3), while Figures 5.19 and 5.20 demonstrate the strain gauges on specimens G-N-2 and G-N-3, respectively.

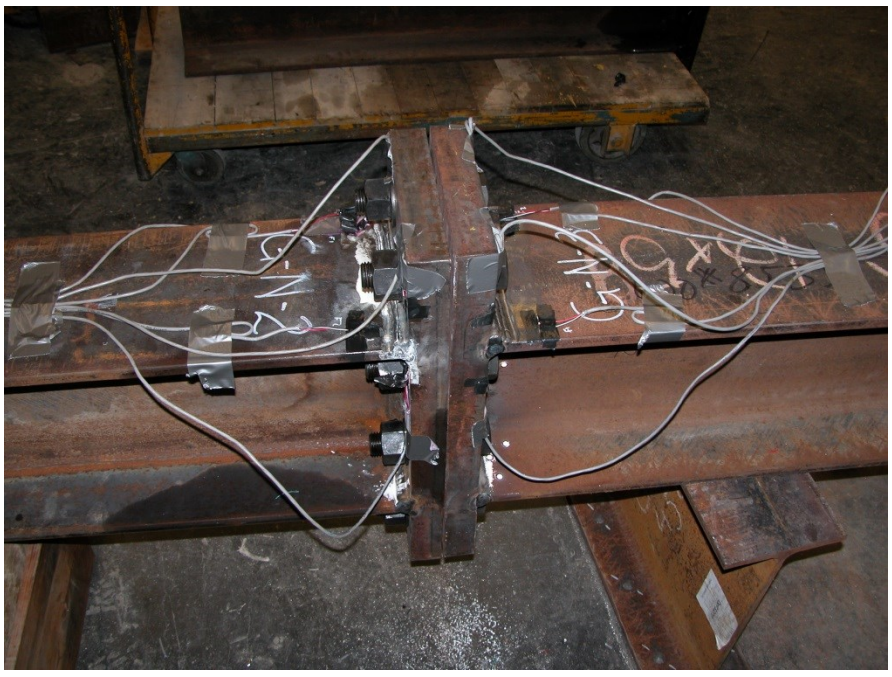

Figure 5.18 *Instrumentation for specimen G-N-2 - G-N-3.*

Figure 5.19 *Instrumentation for specimen G-N-2.*

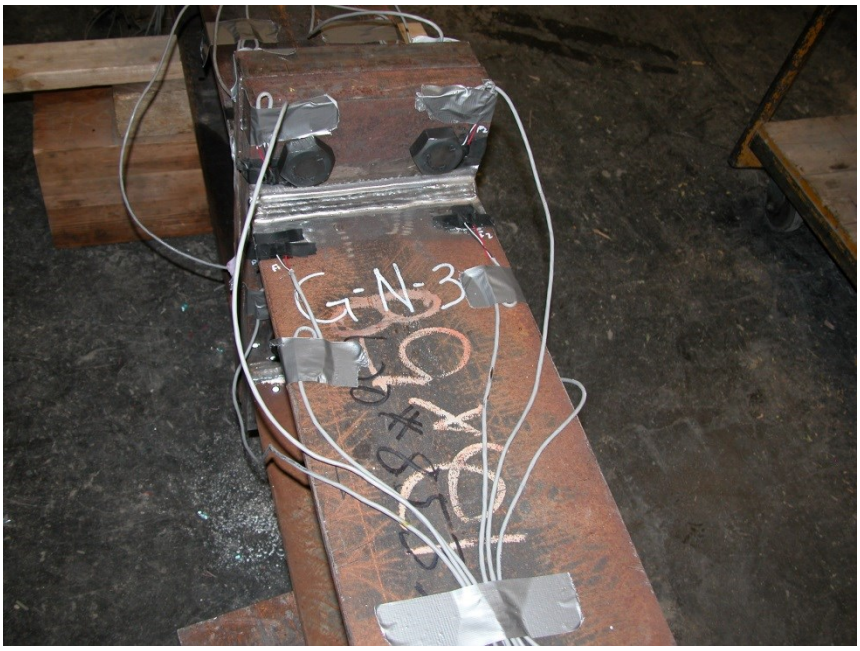

Figure 5.20 *Instrumentation for specimen G-N-3.*

5.3.6.3 Test Setup 3: G-N-3 - G-N-1

Lastly, test setup No. 3 (G-N-3 - G-N-1) is the third and final fatigue test setup, and the specimen G-N-2 was replaced by G-N-1 at the Pegasus system location using an over-head crane. Figures 5.21, 5.22 and 5.23 illustrate the instrumentation for the entire beam of G-N-2 - G-N-3, in addition to the instrumentation for G-N-3 and G-N-1, respectively.

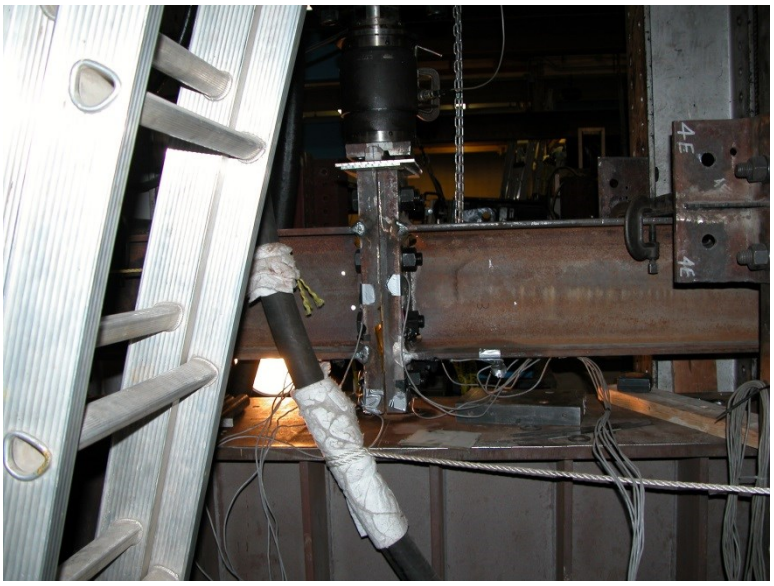

Figure 5.21 *Instrumentation for specimens G-N-1 (left) and G-N-3 (right).*

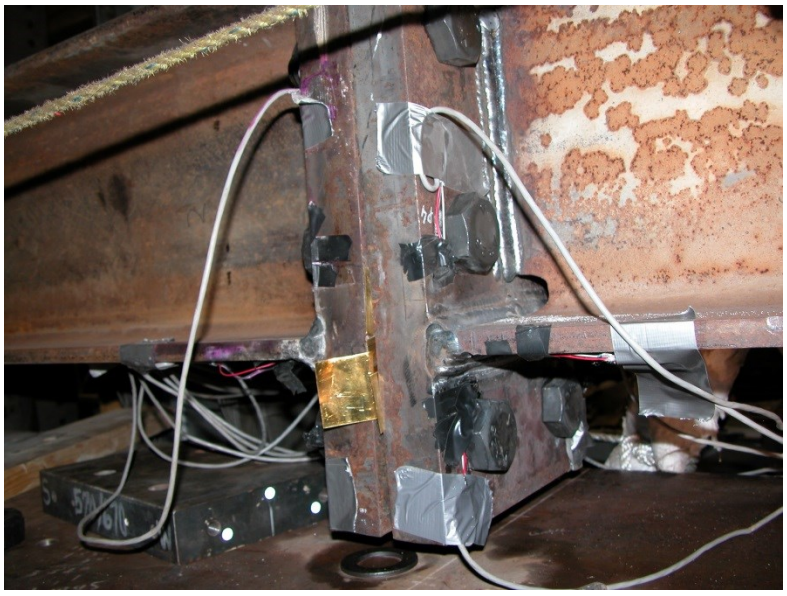

Figure 5.22 *Instrumentation for specimen G-N-3 (left).*

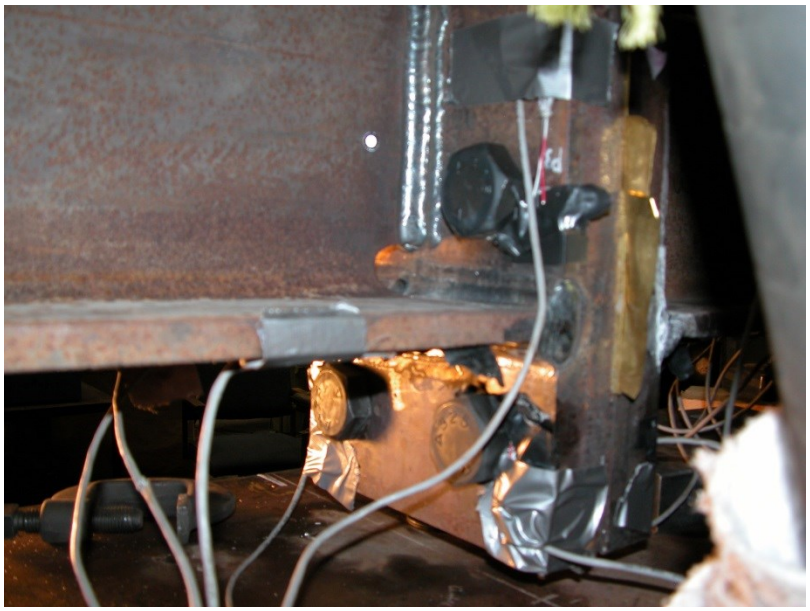

Figure 5.23 *Instrumentation for specimen G-N-1.*

5.4. Experimental Program Procedure

5.4.1. Fatigue Test Control and Data Acquisition

Static, cyclic loads and strokes were controlled by electrical servo valves on the actuators. One controller (Kelsey Instruments K7500 Servocontroller), one per actuator, generated the desired output. This guaranteed that the cyclic loading of the actuator was developed. The cyclic loads followed a sine wave function, with a frequency of a range 3.5 - 4.0 Hz for all tests.

The strains in the beam and end plate were measured with electrical resistance strain gauges. The corresponding stresses were calculated using the measured modulus of elasticity from the tension coupon tests for the plate (~210,000 MPa), and a reasonable average modulus of elasticity of 205,000 MPa for the beam (Galambos and Ravindra 1978).

During fatigue testing, the loads and strokes were continuously monitored by the Kelsey controller and the peaks displayed. The strains were also continuously acquired through the LabVIEW program. The sampling frequency for both the Kelsey controller and the LabVIEW program was 100 Hz.

To protect the specimens and testing machine from unexpected events, lower and upper bound limits on loads and displacements were set. The test was stopped automatically when any one of these limits was exceeded.

5.4.2. Cracks Inspection

The welds were ground flush for the two ground specimens G-N-2 and G-N-3 and the surface was shiny after grinding, which helped with visual crack detection, requiring only the assistance of a strong light. A magnifying glass was used to inspect the as-welded and treated specimens. Furthermore, dye penetrants were used to investigate any growing crack during the test.

Inspection intervals were set according to the expected fatigue life, increasing the inspection frequency when approaching the predicted end of any test. Visual inspection was scheduled twice a day until the first detection, and then more frequently depending on crack propagation.

5.4.3. Failure Criterion

For practical reasons, the failure criterion was taken as a crack size at which it became a through -thickness crack i.e. when the crack is visible on both surfaces of the flange. The test was continued until the crack was through the thickness and long enough to expose the fracture surface.

5.4.4. Post Test Examination

After completion of any test, the two end plates were separated by unscrewing the eight high slip critical bolts. A manageable area from each beam and end plate around the crack was cut out, without touching the crack tips. The crack was then opened by successively cutting with a band saw from sound material towards the crack tips until the two halves on each side of the crack were separated. All cracks were inspected visually with the naked eye. The fractured surfaces examination is discussed in Section 5.7.

5.5. Test Results

Table 5.2 provides the results of the full-scale tests prepared with welding and with or without weld toe grinding procedures. This includes the maximum load, minimum load, stress range, stress ratio and frequency applied to each specimen in the fatigue test. Observations of some crack propagation rates confirmed that once a crack reached both flange faces, the crack growth rate becomes very high, being close to unstable. This underlines the suitability of the chosen failure criterion.

Table 5.2 *Results of full-scale tests.*

Specimen Designation	Wire	Treatment	Pmax [kN]	Pmin [kN]	Δσ [MPa]	R [-]	Frequency (Hz)	No of Cycles
N-N-2	Megafil	Non-treated	254	160	50	0.63	3.5	10,000,000
	Megafil	Non-treated	300	90	114	0.3	4.0	4,640,509
G-N-2	Megafil	Ground	254	160	50	0.63	3.5	10,000,000
	Megafil	Ground	300	90	114	0.3	4.0	7,421,211
G-N-3	Megafil	Ground	300	90	100	0.30	3.5	1,382,124

In Table 5.2, the number of cycles reached 10 million without any signs of fatigue crack for N-N-2 and G-N-2. This occurred under the effect of a stress range of 50 MPa. This results in an almost infinite fatigue life; that is, the stress range is below the constant amplitude fatigue limit (CAFL) of the fatigue design curves. In order to fracture the whole specimens, causing them to fail, the stress range was increased to 114 MPa after expending the first 10 million cycles.

5.6. Examination of Fractured Surfaces

For better investigation of the fractured surfaces of the tested specimens, the regions surrounding the fractured surfaces were cut from the specimen with a pneumatic saw. As a result of this cut-out, two sides of the fractured surfaces were generated: one surface at the side of the flange and the endplate one, denoted as side 1; and the other surface at the side of the flange only, denoted as side 2.

Visual inspection is carried out to investigate the fractured surfaces of the test specimens N-N-2, G-N-2 and G-N-3. Such inspection emphasized that once the crack reached the face of the weld toe, the crack propagation rate increased significantly as evidenced by the rougher crack surface appearance. Moreover, the fractured surfaces occurred at the beam flanges, not the end plates, and they are located outside the weld toes and roots for the ground surface, while it is at the weld toe for the as-weld specimen. In the following subsections, detailed discussion about the fractured surfaces, initial crack sites, etc. is introduced.

5.6.1. Fractured Surface for G-N-2

The G-N-2 specimen was one of the specimens that had been post-weld treated using weld toe grinding. The fractured surface of G-N-2 is considered to be brittle failure, mostly flat and its

plane is normal to the direction of principal stresses. The examined fractured surface showed that there is a slight change in the surface near the middle of the specimen, where the fatigue crack initiated. The fractured surface was located outside the weld toe in the flange of the wide flange. Figure 5.24 illustrates the fractured surface of side 1, where the potential crack initiation site could be visualized, while Figure 5.25 shows the fractured surface of side 2 of the specimen.

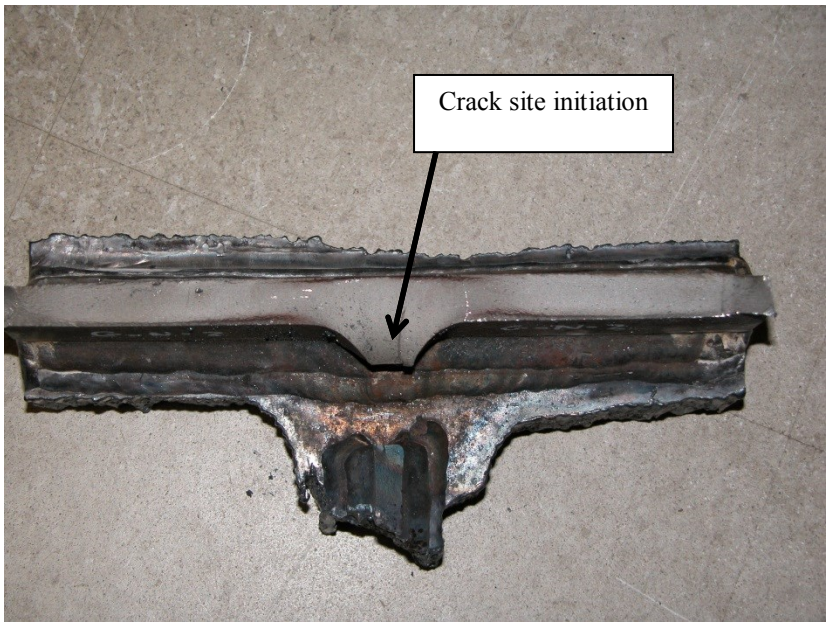

Figure 5.24 *Fractured surface of side 1 of specimen G-N-2.*

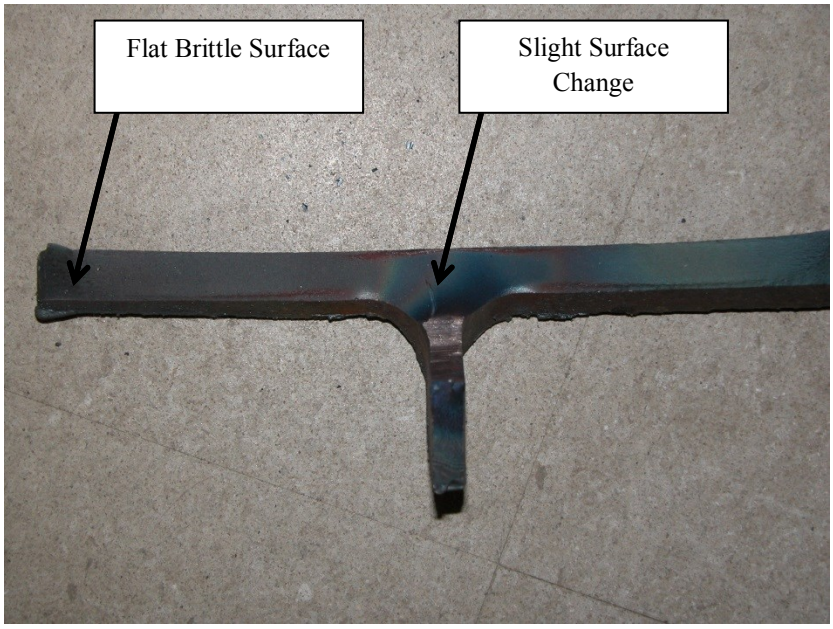

Figure 5.25 *Fractured surface of side 2 of specimen G-N-2.*

Both sides of the fractured surface of specimen G-N-2 illustrated that this is a brittle facture with little deformation (strain) and a flat surface that is normal to the direction of cyclic loading.

Although the steel is considered to be ductile material, the service temperature and the state of stresses can alter the ductility in some cases. The steel ductility is decreased when the ambient temperature is low and/or the shearing stress is restricted by biaxial or triaxial stresses, as at stress concentrations of a member with sharp changes in the cross-sectional areas.

5.6.2. Fractured Surface for N-N-2

The N-N-2 specimen is the only specimen that had not been treated by grinding, and was tested in the as-weld condition. For this specimen, N-N-2, the fractured surface was located at the weld toe at the beam flange side. In this specimen, the crack initiation site was located in the middle at the weld toe. The fractured surface of N-N-2 emphasized that the fractured surface comprised several notches at locations where the fractured surface changed. This rough surface, visualized with the naked eye, is illustrated in the right hand side in Figure 5.26. In the same figure, the flat surface for brittle fracture behaviour is dominant at the left hand side.

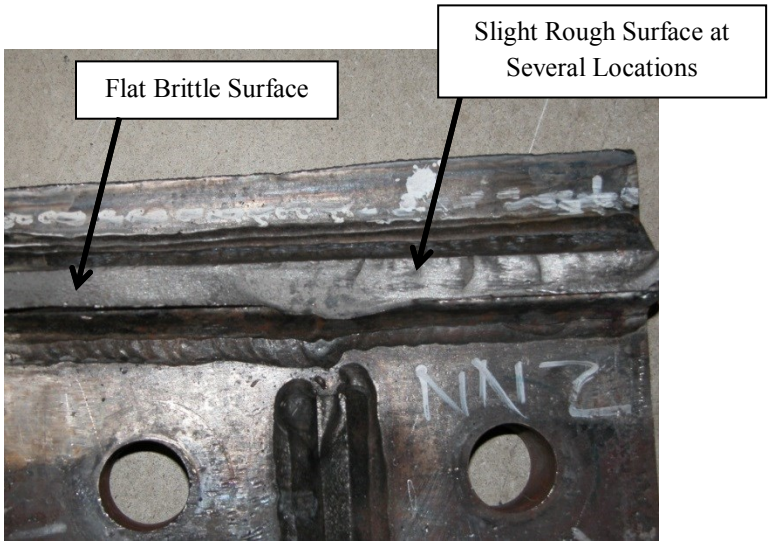

Figure 5.26 *Fractured surface of side 1 of specimen N-N-2.*

On side 2 of the fractured surface of specimen N-N-2, Figures 5.27 shows the notches on the fractured surface of side 2, which assists in the fatigue crack propagation till fracture.

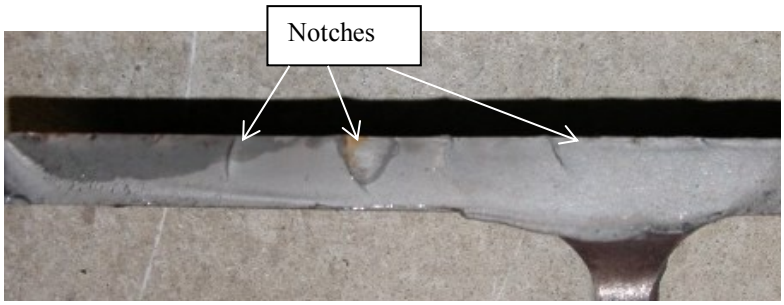

Figure 5.27 *Clear edge notches in the fractured surface for side 2 of specimen N-N-2.*

5.6.3. Fractured Surface for G-N-3

For the G-N-3 specimen, where weld toe grinding was introduced as a method of post-weld treatment, it is observed that the fatigue life of this ground detail is smaller than the other fractured specimens. The fractured surface of this specimen was just outside of the weld toe and was characterized by its inclined surface. This indicates that the mode of failure is a mix of ductile and brittle fracture. Figure 5.28 shows the fractured surface of side 1, where ductile fracture surfaces in the right hand edge show large deformation (strain) and shearing characteristics, which are inclined to the direction of cyclic loading. Fatigue crack in this specimen also started in the middle of the flange and propagates outwards through the flange width.

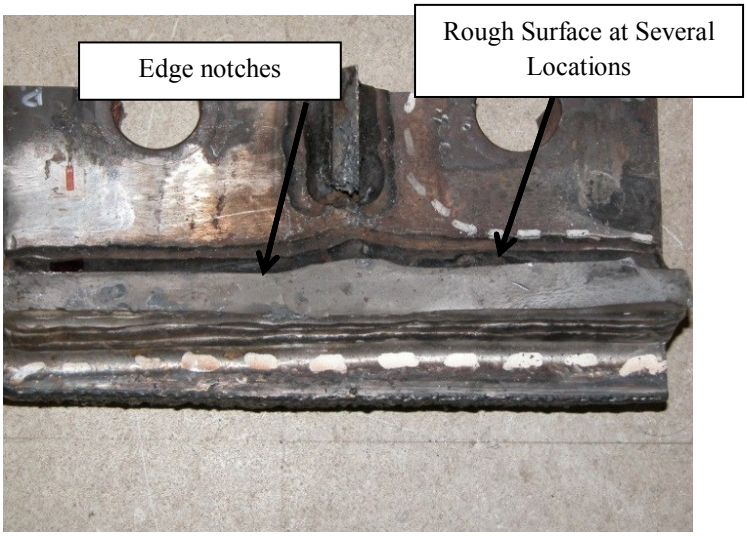

Figure 5.28 *Fractured surface of side 1 of specimen G-N-3.*

Figure 5.29 illustrates the fractured surface in side 2. Few notches could be seen near the middle of the beam flange, where the crack initiated.

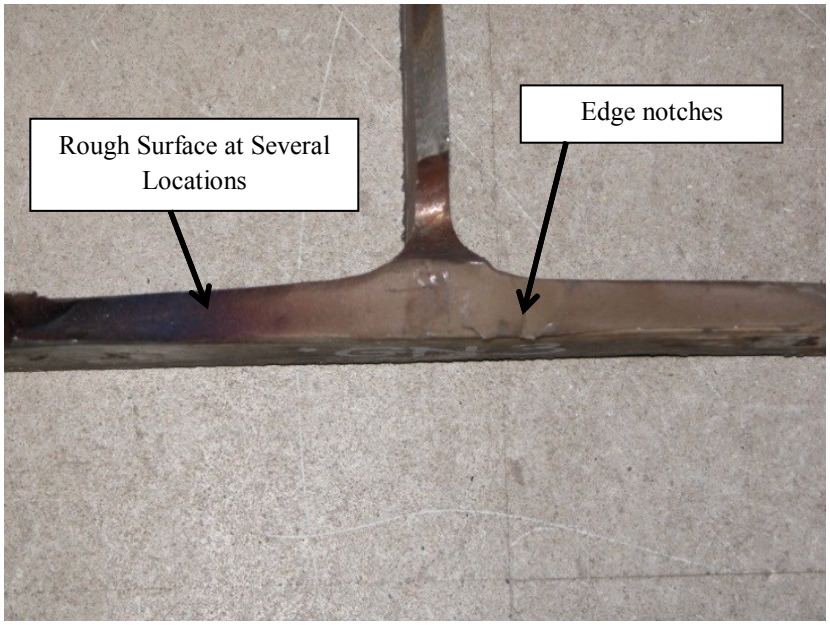

Figure 5.29 *Fractured surface of side 2 of specimen G-N-3.*

5.7. Discussions

This chapter provides the details of the experimental program used to assess the effect of weld-toe grinding on the fatigue life improvement of severe fatigue category (E) for full-scale specimens. Section 5.2 began with an overview of the full-scale test setup, which includes a description of test specimen geometry and test setup. The fabrication, welding, grinding of test specimens, the installation of test assembly and the test procedure is further explained in detail in Section 5.3.

The test results in Section 5.5 indicated that the first test round of specimens G-N-2 and N-N-2 was under a constant amplitude stress range of 50 MPA. As a result of this relatively low stress range, the number of fatigue cycles therefore reached 10 million cycles without noticing any crack initiation in the weld vicinity of the test specimens. For this particular incident, the stress range was increased in the second round to be in a range of 100 - 114 MPa for the test specimens.

This increase in the constant applied stress range leads to the fatigue failure of test specimens. In test set-up 1, the non-ground N-N-2 specimen failed first and was replaced with the ground G-N-

3 specimen. Afterward, the test specimen G-N-2 failed. Finally, the ground specimen G-N-1 replaced G-N-2.

The fatigue test results illustrated that the fatigue life of G-N-2 was more than that of N-N-2. This fatigue life improvement using weld-toe grinding results from the benefit of reduction of the stress concentration at weld toes. This is carried out by producing a favourable weld shape and by removing harmful defects and undercuts at the weld toe. These actions lead to an increase of the fatigue crack initiation life, which is reflected in the longer fatigue life of G-N-2 as compared to the as-weld (non-ground) specimen, N-N-2. The fatigue life of the ground specimen, G-N-2, is improved by 60%, compared to the as-welded specimen, N-N-2. This increase is in accordance with the range stated by Smith and Hirt (1985), which predicted the fatigue strength improvement due to burr grinding at 2 x 10^6 cycles between 50 and 200% depending on the type of joint. Mohr *et al.* (1995) conducted statistical analysis on some improvement techniques as applied to welded specimens with transverse attachment plates, and found that the improvement on fatigue life produced by grinding was a factor of approximately 2.2.

Fatigue life improvement for various types of post-weld treatment methods other than grinding is dependent on the techniques used. The remelting method of the weld toe region using a TIG or plasma torch generally induces significant fatigue strength improvements due to the production of a smooth transition between the plate and the weld metal. The increase in fatigue strength in air at 2x10^6 cycles as compared with as-welded joints is approximately 100%. However, this fatigue life improvement does not increase with increasing material tensile strength unlike the case of grinding. Moreover, the seawater corrosive environment could have an adverse effect on the fatigue life improvement using TIG technique. Mohr *et al.* (1995) obtained a factor of 2.2 from a statistical analysis of many tests for fatigue life improvement for weld toes treated by TIG dressing.

In case of the peening methods (hammer, shot and ultrasonic impact), the fatigue life improvement results from inducing favourable compressive residual stresses to replace the tensile residual stresses produced by the welding process at the weld region. Accordingly, the fatigue crack initiation life of the welded components is substantially increased due to these compressive stresses fatigue life. The improvement in fatigue strength obtained by peening treatments are among the highest reported and are typically of the order of 50-200% for hammer

peening, 30% for shot peening and 50-200% for ultrasonic impact peening (Kirkhope *et al.* 1999). In some conditions, the enhancement is so large that the weld is no longer critical and failure initiates in the base plate away from the weld (Josi and Grondin 2010) or in other cases for fillet welds the point of eventual failure moves from the weld toe to the weld root.

Comprising two post-weld treatments has a significant effect on the fatigue life improvement techniques. In general, these combinations should only take into account the weld geometry improvement method with a residual stress method (e.g., toe grinding and hammer peening, but not toe-grinding and TIG dressing) (Kirkhope *et al.* 1999). Although, this approach may lead to an expensive solution, it can be applied in cases where costs are of minor importance such as repair of a damaged structure or in other cases where extensive redesign of the structure to meet fatigue requirements is to be avoided.

Among the various post-weld treatment methods, weld toe grinding is considered to be cost effective. Weld toe grinding requires a burr grinding tool, which is considered to be relatively cheap compared to other tools used in post-weld treatments especially peening methods. It is also an easy method that does not require any further tests or checks as in peening and remelting methods. It does not need highly skilled and trained personnel like peening methods. Moreover, it has easier accessibility, when compared to disc grinding and water-jet eroding. It is also considered the best solution for fillet welds subjected to transverse loading (Kirkhope *et al.* 1999).

Although, the test specimen, G-N-3, was post-weld treated using weld toe grinding, the predicted fatigue life of G-N-3 did not improve due to such treatment. In fact, the fatigue life for specimen, G-N-3, was found to be less than those of either G-N-2 or N-N-2. Many reasons could cause this result such as the unevenness in the fillet weld profile. Kirkhope *et al.* (1999) illustrated that there could be initial weld defects and undercuts, which were not removed from the weld toe by the burr grinding. From the investigation of fractured surface, shown in Section 5.6.3, it was found that there are several notches at the weld toe that might lead to the development of many crack initiation sites. As indicated in Chapter 2, the unevenness in the fillet weld profile could be difficult to maintain the weld toe grinding, which might reduce the benefit of enhancing the fatigue life. The trend of getting this adverse effect of fatigue life improvement also occurs in

other post-weld treatment methods. More experimental investigations on the improvement of fatigue life using weld toe grinding are required.

The limitation of the improvements obtained by TIG and plasma dressing are due to the uncertainty about the initiation site of the fatigue crack, caution should be used when considering applying TIG dressing improvement techniques to the longitudinally loaded joints and other weld details. Moreover, checks should be made to ensure that fatigue failure will not first occur at the weld root or some other site in the weld detail (Kirkhope *et al.* 1999). TIG dressing is sensitive to weld contaminants, much more so than other weld improvement methods. As a result, the weld and adjacent plate should be thoroughly de-slagged and wire brushed to remove all traces of mill scale, rust, oil and paint. Kirkhope *et al.* (1999) emphasized the limitations of fatigue life improvement regarding the hammer peening treatment, where excessive peening induce cracks, while the corrosion effect could reduce the effect of shot peening as its effect is applied for a very small thickness.

6. DETERMINISTIC FATIGUE LIFE PREDICTION OF FULL-SCALE TEST RESULTS

6.1. **Introduction**

This chapter illustrates the deterministic fatigue life methodology required to predict the fatigue life of full-scale tested specimens, as investigated in Chapter 5. For such prediction to take place, this study employed an energy-based method for fatigue crack initiation and linear elastic fracture mechanics (LEFM) for fatigue crack propagation, based on the information presented in the literature review in Chapter 2. Section 6.2 presents the methodology used to predict the fatigue life in fatigue crack initiation and propagation stages knowing the input parameters. The section also illustrates the finite element analysis employed to assess the stress and strain energy distributions resulting from the applied force, exerted by the Pegasus fatigue system in the structures lab, and residual stresses at the critical locations for predicting the crack initiation life using energy-based method. Section 6.3 introduces the results of the finite element analysis and deterministic fatigue life prediction. Finally, a discussion on the analytical fatigue life predictions and comparison between the analytical and test results is presented in section 6.4.

6.2. **Methodology**

Two limiting shapes were defined in the deterministic fatigue life prediction cases: 1) a spherical or/and elliptical flaw, resulting in the least severe condition for a weld discontinuity; and 2) a perfect weld with no discontinuity, simulating the best case scenario. The fractured surfaces were located in the base metal (outside the weld toe) for the ground specimens, G-N-2 and G-N-3, while the crack initiated at the weld toe in the non-ground specimen, N-N-2. Therefore, the study assumed initial spherical and elliptical weld flaws for the non-ground specimen, N-N-2. The other ground specimens were modeled without weld flaws, since their fractured surface was outside the weld toe.

Fatigue material characteristics for crack initiation and propagation had been investigated in previous researches and were used herein. This study adopted finite element analysis to estimate the energy parameters (plastic strain density and maximum stresses) for cases 1 and 2 in the initiation stage. For that purpose, global finite element models representing the three test specimens were employed to determine maximum stresses at the weld flaw locations, where crack initiation is likely to start. No cracks were modeled in the finite element analysis. Then,

local models were used to refine the mesh to predict the energy parameters more accurately for different initial flaw cases. The generated plastic strain energy densities and maximum stresses under the constant amplitude stress range, along with the fatigue initiation properties, lead to the prediction of the crack initiation life, N_{init}, by solving equation (2.7). The study implemented linear elastic fracture mechanics (LEFM) approach to estimate the fatigue crack propagation life. Four different approaches were used in the crack propagation stage (including or neglecting ΔK_{th}, including or neglecting crack closure, i.e., residual stresses) (Josi and Grondin 2010). For each approach, and taking into account the crack propagation material properties, the applied loading, the residual stresses and the initial and final crack sizes, a_0 and a_f, the crack propagation life, N_{prop}, is computed using equation (2.4). Finally, the crack initiation and propagation lives were added to determine the total fatigue life, N_{total}. Figure 6.1 illustrates the procedure of deterministic prediction of the fatigue life of full-scale test specimens.

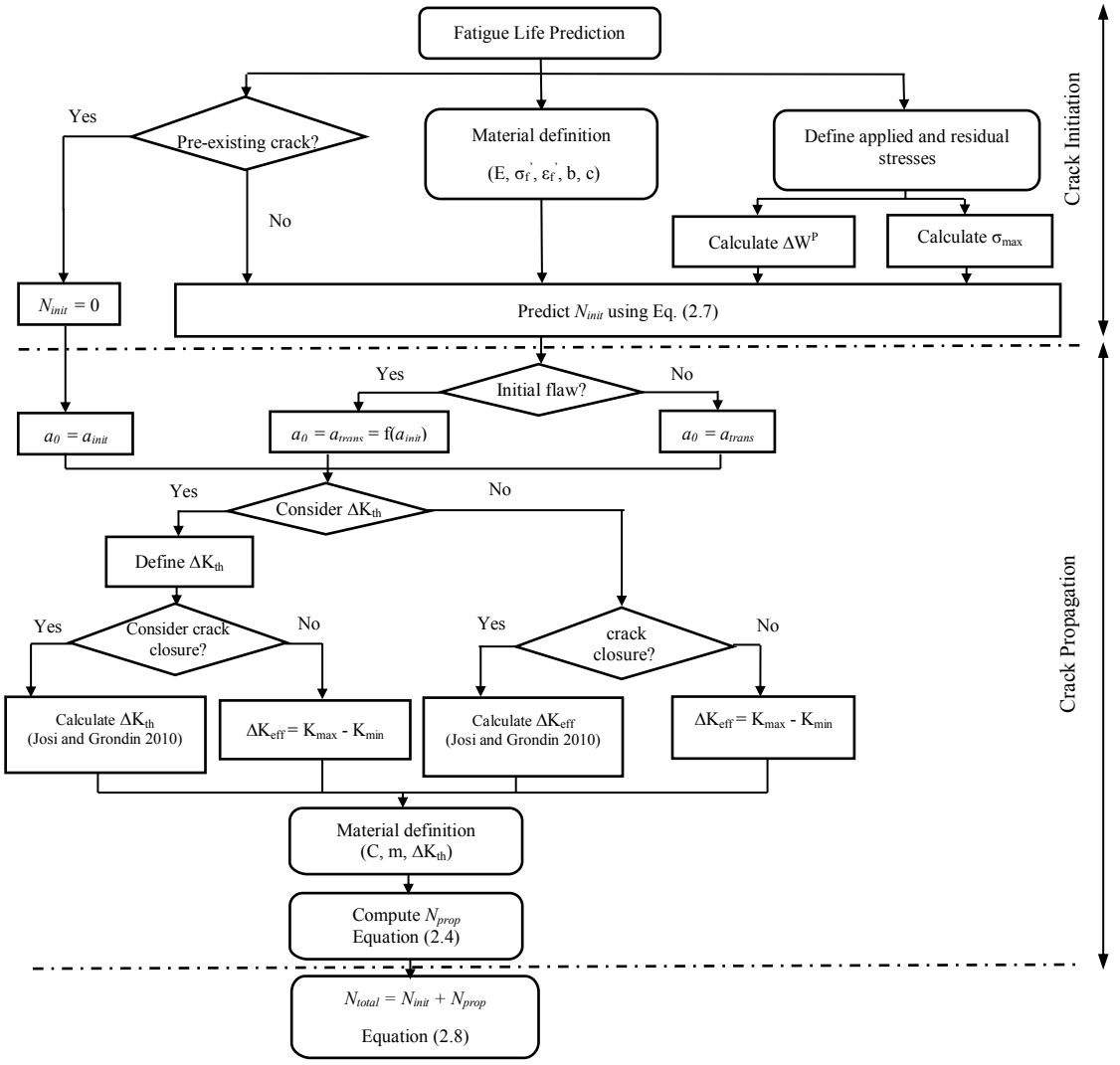

Figure 6.1 *The flow chart for deterministic prediction of fatigue life.*

6.2.1 Fatigue Crack Initiation Prediction

Input Material Parameters

The material properties for the fatigue test specimens in this research were exactly the same material properties as used by Josi and Grondin (2010). Table 6.1 illustrates the material properties in fatigue crack initiation.

Table 6.1 *Material properties for fatigue crack initiation in base and weld metals (Josi and Grondin 2010).*

Material Properties	Weld Metal	Base Metal
E (MPa)	207,000	213,000
σ'_f (MPa)	630	532
ε'_f	0.34	0.0715
n'	0.037	0.15
b	-0.059	-0.07
c	-0.63	-0.4

Finite Element Analyses

To model the weld profiles of the test specimens in a precise manner in the finite element analyses, the study used a three dimensional (3D) scanner (Figure 6.2) to scan the weld surface for all the specimens resulting in weld profiles for various weld conditions (as-welded and ground). The three-dimensional scanning process directs red laser beams to the weld surface using small reflection points (Figure 6.2) sticking to the metal surface in order to set the coordinates for every scanned portion.

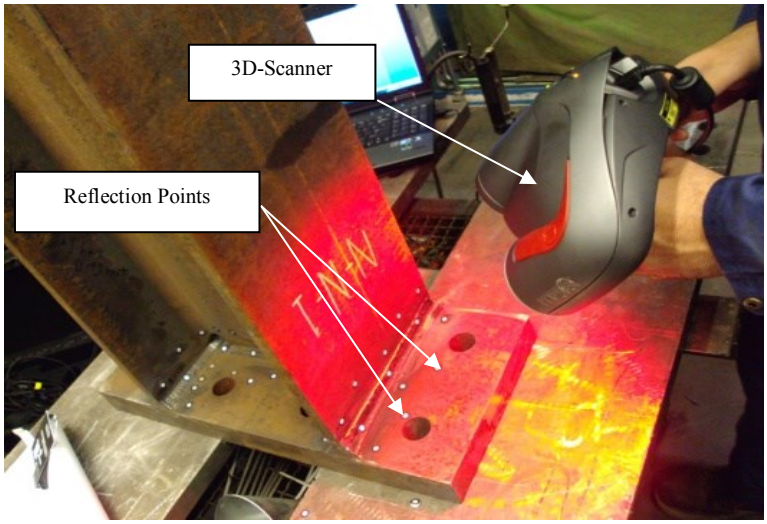

Figure 6.2 *The 3D scanner and reflection points used to model the weld surfaces.*

The generated weld surfaces for the three test setups, used in the experimental program in Chapter 5, were developed using Geomagics Studio software. Figure 6.3 illustrates the generated surface for the weld surface using the 3D scanner for specimen G-N-2.

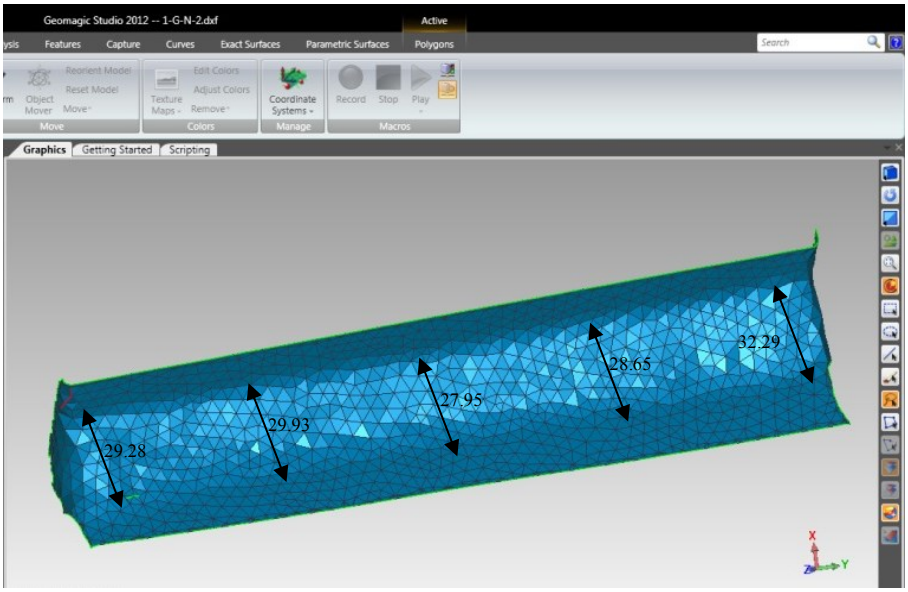

Figure 6.3 *The resultant surface weld profile for test setup G-N-2.*

A reasonable approximation for the weld model for the test specimens, based on measuring the weld widths of the scanned surfaces of the weld roots at five different locations along the weld profile length, was assumed (Figure 6.3). These were consequently modeled as triangular welds in the finite element model. Figure 6.4 outlines the designation of the weld legs dimensions connecting between the end plate and the wide flange beam. Table 6.6 provides the average values of the shear and tension weld dimensions, measured from the scanned actual weld surfaces.

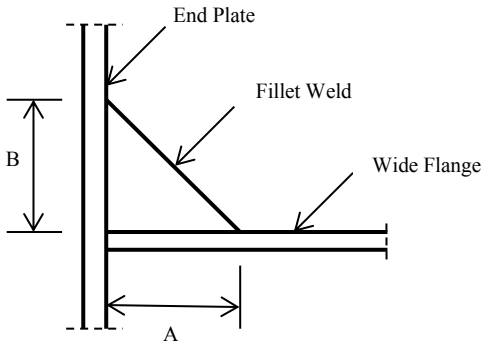

Figure 6.4 *Schematic sketch for the dimensions of the proposed fillet weld geometry.*

Table 6.2 *Approximate fillet weld sizes.*

Specimen No	Weld Designation	Shear Leg A (mm)	Tension Leg B (mm)
1	G-N-2	15	15
	N-N	13.56	18
2	N-N-2	20	18.5
	N-N	15	21.3
3	G-N-3	13	20
	G-N	14.6	25

The finite element analysis of all test specimens was executed using ABAQUS. Only one half of each test setup (one half beam and one end plate) was required to be modeled in the global finite element analysis because of the main plane of symmetry that was assumed: at the center of the specimen in the longitudinal direction (negative z – direction).

Two types of 3D solid elements were used in the global finite element model. The first type is the 8-node solid (C3D8), which was used to model the coarse mesh of the beam and the plates. The second type is the 10-node solid (C3D10), which was employed to model the weld profiles as well as the fine mesh of the beam attached to the weld, and also to model the transition zone in the beam between the coarse and fine meshes. The element size was chosen to be 5.0 mm for the weld profiles. The wide flange beam mesh sizes started with 10.0 mm at the end zone (near the end plate), followed by a transition zone from a fine mesh of size 10.0 mm to a coarse mesh of 20.0 mm. Finally, the last part of the beam mesh was of size 20.0 mm. Figure 6.5 illustrates a general 3D view of the global finite element model with the types of meshes used in the analysis. The coarse mesh at the beam extends from the beam edge for 1205.0 mm length. Then, a transition zone is developed for 185.0 mm to refine the mesh from an element size of 20.0 mm to a 10.0 mm size. Finally, the last portion of the beam is modeled with a fine mesh with element size of 10.0 mm. The element type for the end plate and the coarse mesh of the beam is C3D8, while C3D10 element type was used for transition zone, welds and the fine mesh of the beam (near the end plate).

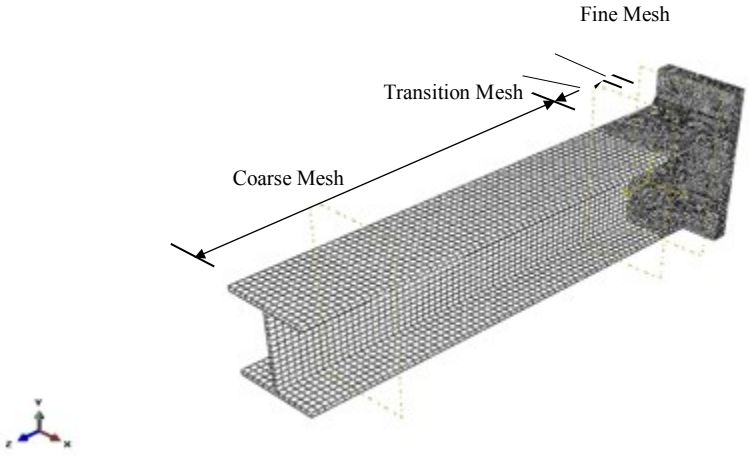

Figure 6.5 *Global finite element model with various types of mesh size for the three specimens.*

Table 6.3 illustrates the exact number of elements used for the three test specimens, whether these elements were used in the coarse mesh, transition, and fine mesh zone of the beam in addition to the weld.

Table 6.3 *Number of elements used in the global finite element model.*

Specimen	No of hexahedral element C3D8 elements	No of quadratic C3D10 elements
G-N-2—N-N	10720	26631
G-N-3—G-N	10680	27459
N-N-2—N-N	10735	25099

Due to the symmetry around the x-y plane, only half the load is modeled as cyclic pressure over the end plate. This pressure, used in the global finite element model, was based on the maximum and minimum values of the forces induced by the load cell in the structures lab along with the load frequency (see Table 5.2). The boundary conditions of all the three global models (G-N-2, N-N-2 and G-N-3) are pinned at the supports.

The dimensions and boundary conditions of specimen G-N-2 - N-N are displayed in Figure 6.6. The flange thicknesses used in the finite element model were 15.7 mm for G-N-2 side (lower flange) and 15.18 mm for N-N side (upper flange). The input values are the average value from the flange width measurements done in the lab before the fatigue test. Moreover, the average web thickness for the beam is 9.9 mm.

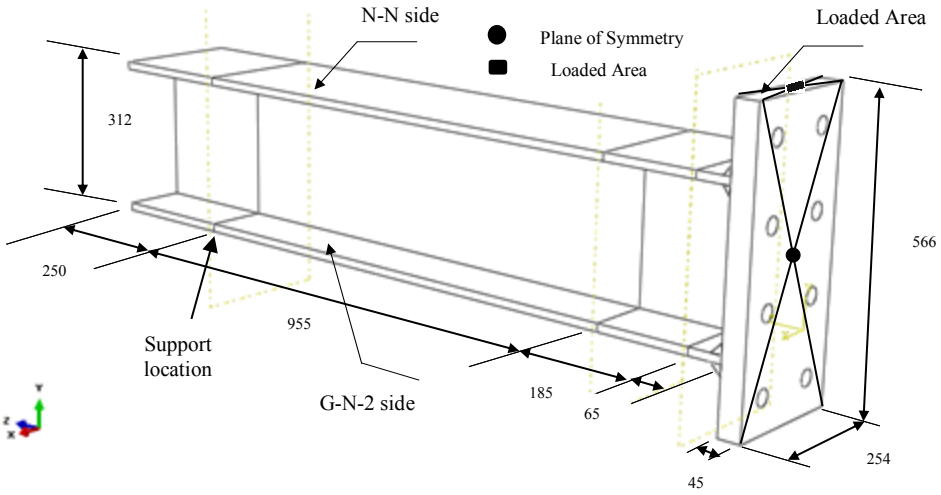

Figure 6.6 *Dimensions and boundary conditions of the global finite element model for G-N-2 - N-N.*

Figure 6.7 provides the main dimensions and boundary conditions of specimen G-N-3 - G-N, where the flange thicknesses of the beam, employed in the finite element model, were 15.2 mm and 16.2 mm for the lower flange (G-N-3) and upper flange (G-N) respectively. The average web thickness of the beam is 9.2 mm.

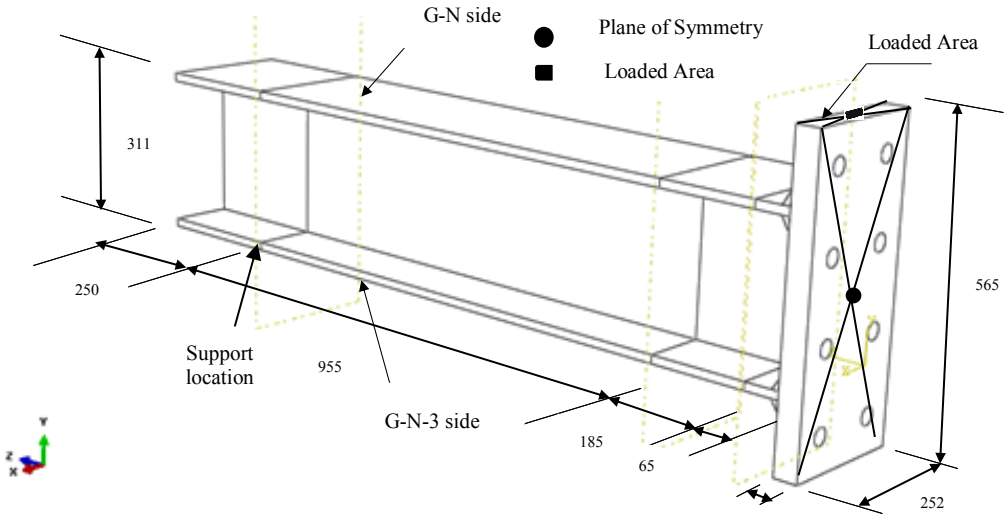

Figure 6.7 *Dimensions and boundary conditions of the global finite element model for G-N-3 - G-N.*

Figure 6.8 shows the dimensions and boundary conditions of specimen N-N-2 - N-N. The average beam flange widths were 15.84 mm and 15.27 mm for N-N-2 and N-N sides, respectively. The average web thickness is 9.95 mm.

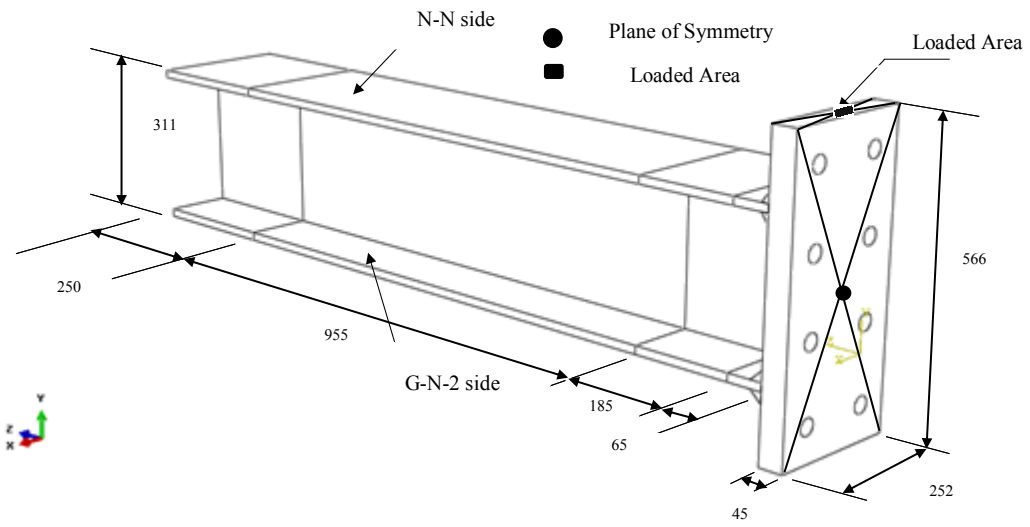

Figure 6.8 *Dimensions and boundary conditions of the global finite element model for N-N-2 - N-N.*

The above figures did not include the dimensions of the welds connecting the beams with the end plate for the three specimens, which were illustrated previously in the fillet weld model.

In the global finite element models (Figures 6.6 to 6.8), a refined mesh was generated at locations of fractured surfaces, determined from the fatigue tests. Fine meshing allows a close insight of the local stresses and strain energy densities in order to predict the fatigue initiation life. This is considered to be the greatest accuracy achieved as the complications induced by geometrical imperfections, in addition to residual stresses that keep changing many times during the welding, grinding, and machining processes, make the exact computations of stresses and energy density strains in the test specimens impossible.

As a result, an independent local model, where the applied loads are based on the global analysis, was preferred to consider the complexity of the model, aiming for more preciseness of the analysis. However, this could not be achieved as the sub-model needs significantly more computational capabilities.

The locations of maximum stresses from the global finite element models were identified. These locations were in front of the weld toes from the wide-flange side representing the regions of the local model, which in most cases is comprised from part of the lower beam flange and the weld attaching it to the end plate. No imperfections had been introduced to the sub-model except the

weld flaws. Figure 6.9 illustrates the local sub-models with respect to the global model for the three specimens. Figure 6.10 shows the local sub-model finite element for no flaw case and the surface weld flaw sizes cases (0.1 and 1.0 mm).

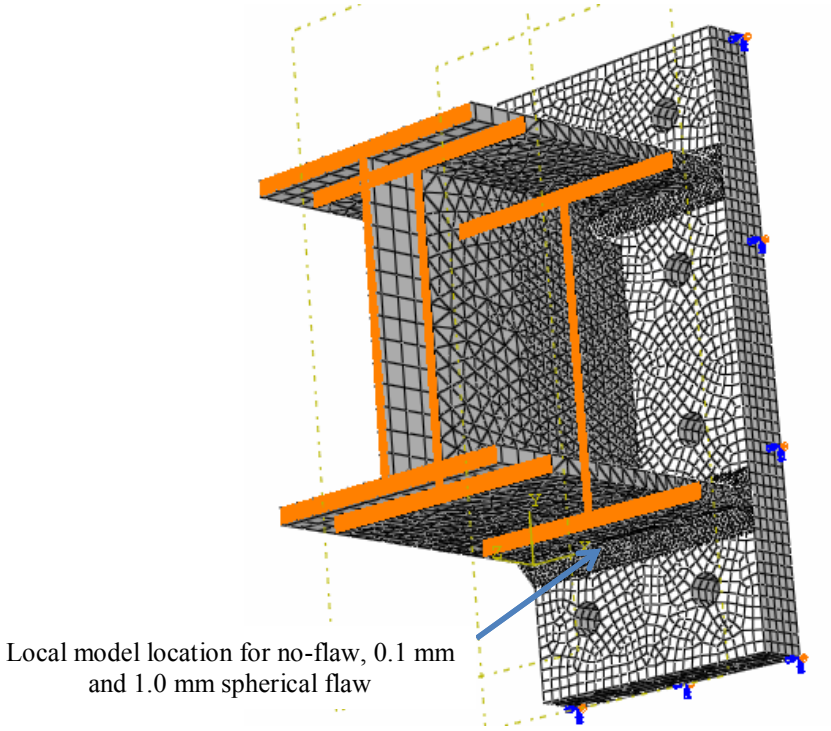

Figure 6.9 *Location of local models in the global model.*

The local model applied stresses were inherited from the global model analysis results. The location of weld flaws in specimen N-N-2 was suggested to be exactly at the mid-length of the weld and the tension flange. The sub-model analysis allowed more reduction in the model size by employing smaller portion of the weld and tension flange, which is symmetric about z-plane at mid-thickness. Figure 6.10 illustrates the boundary conditions (symmetry and load areas) of the local finite element models for the three test specimens G-N-2, G-N-3 and N-N-2, which are the same for the global model with an additional plane of symmetry, as previously mentioned. Due to the small size of the sub-model, the stress gradient from the global model has no significant effect on the stresses and energy density strains at the critical location.

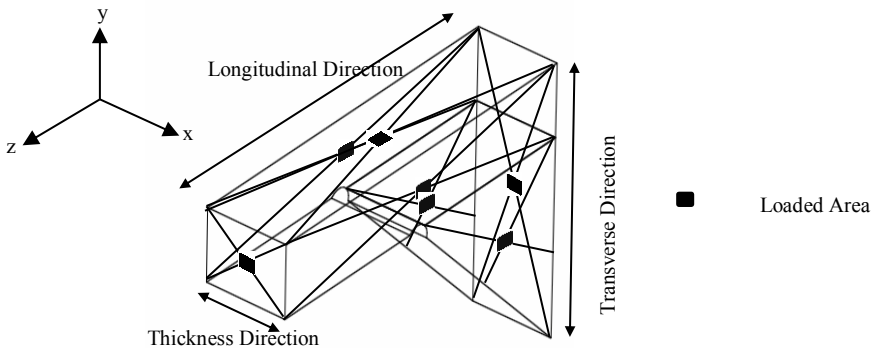

(a) Specimen G-N-2

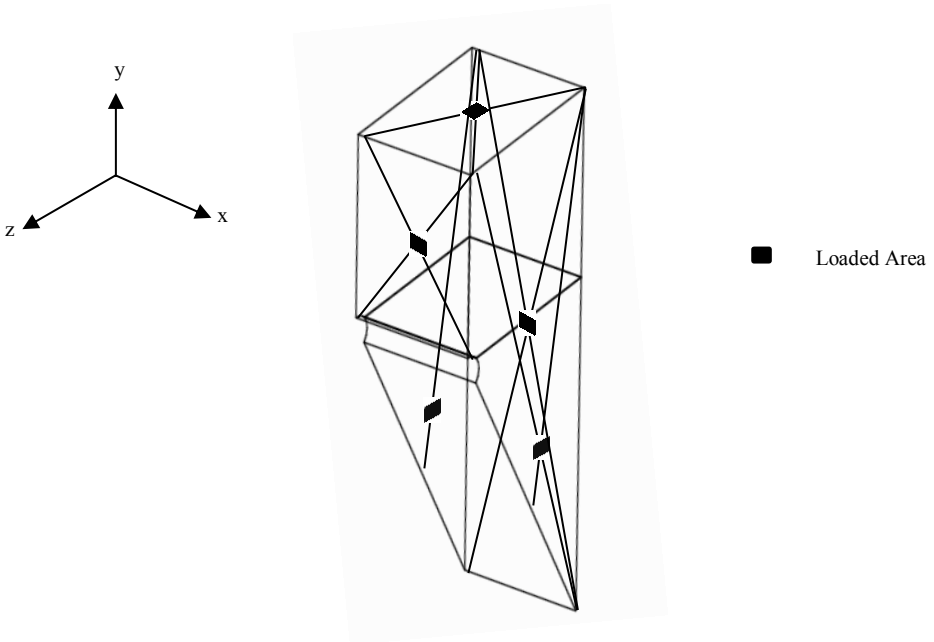

(b) Specimen G-N-3

Figure 6.10 *Schematic representation of the symmetry boundary conditions and the loaded areas of the local finite element models.*

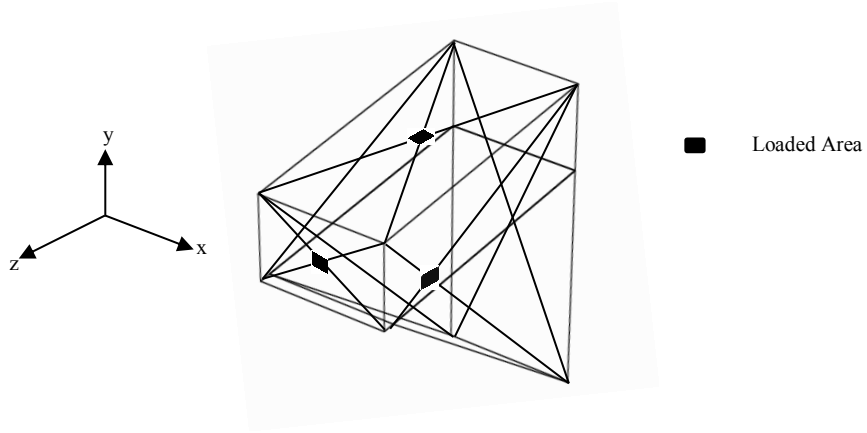

1) No Flaw

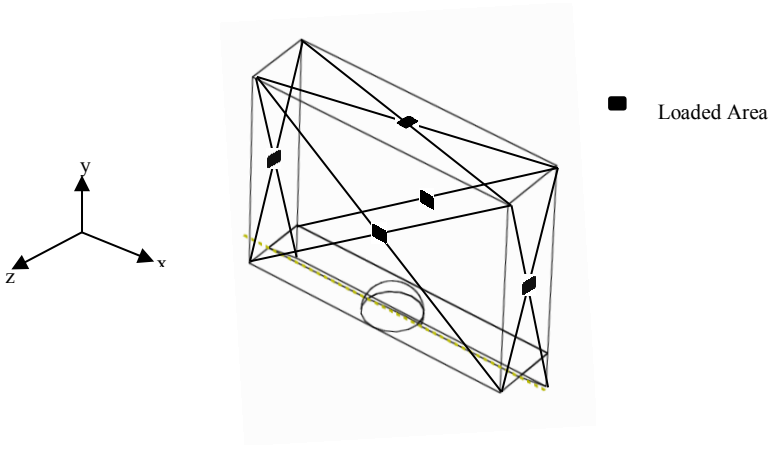

2) 1.0 mm Flaw

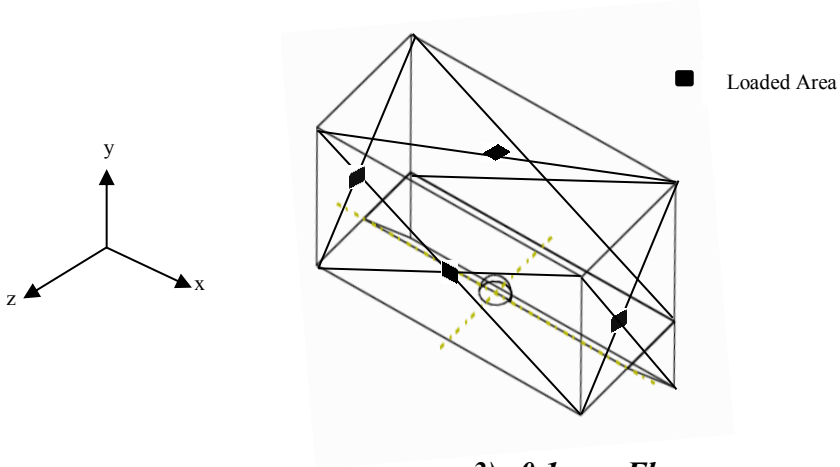

3) 0.1 mm Flaw

(c) Specimen N-N-2

Figure 6.10 *(cont'd).*

For surface flaws considered in this research, the center of the spherical or elliptical flaws was in the center from the z-plane of symmetry.

The transfer from the global model to the local model does skip the process of mesh transition, despite the fact that the aim of the local model is to obtain more mesh refining. The transition from coarse to fine mesh that surrounds the weld flaw was defined in ABAQUS. Table 6.4 shows sub model sizes, mesh size and number of nodes and elements for each specimen.

Table 6.4 *Mesh size and number of elements used in the sub-models.*

Specimen	***Flaw***	***Model Size B x T x L [mm]***	***Mesh Size [mm]***	***Number of***	
				Nodes	***Elements***
G-N-2	***No Flaw***	*28 x 10 x 41*	*1.0*	*56815*	*38112*
G-N-3	***No Flaw***	*42.5 x 10 x 15*	*1.0*	*47094*	*31623*
N-N-2	***No Flaw***	*28.4 x 10 x 22.5*	*1.0*	*36062*	*23932*
	1 mm surface	*9.33 x 10 x 2.5*	*0.22*	*150668*	*105110*
	0.1 mm surface	*1.47 x 2 x 1*	*0.05*	*136070*	*93463*

The same inelastic material was employed as for the global model. Poisson's ratio for steel, υ = 0.3, was specified for all the local models.

The tested specimens were exposed to two types of stresses: external stresses from the testing machine, and embedded residual stresses within the material itself. These two stresses were superimposed to form the resultant stresses acting on the components. The residual stress field was imposed as surface pressures on the negative x-plane in the local finite element models.

Since the only post-weld treatment was weld toe grinding, only the tensile residual stresses were applied to the local models. The residual stresses are characterized as being in a state of self-equilibrium within the global model. Thus, they were applied as external tensile force in the same direction as the stresses induced by the testing machine. Josi and Grondin (2010) investigated the effect of three different residual stress distributions, and found that the exact stress residual gradient is not critical to determine local stresses and strains in the finite element local model. Thus, an assumption of uniform distribution of residual stresses seems to be

conservative as the local model has very small dimensions, where the residual gradient will have no effect.

The first load step of the analysis consists of applying the residual stresses[4]. The stresses from the externally applied load are then imposed in the second time step, using the results from the analysis of the global finite element model.

6.2.2 Fatigue Crack Propagation Prediction

For case 1 (initial flaw), it was suggested that the transitional crack size[5], a_{trans}, is equal to the initial flaw size (Josi and Grondin 2010) for crack propagation. Although the crack at the beginning of crack propagation must be at least the initial flaw size, this approach led to slightly conservative fatigue life predictions, as long as small crack behavior is not present. Josi and Grondin (2010) adopted this simplified definition for a_{trans}. Thus, the initial crack size, a_0, in the crack propagation model is always supposed to be equal to the initial flaw size, a_{init}. For perfect welds (case 2), the transitional crack size, a_{trans}, is assumed to be 0.1 mm. This value is chosen based on previous researches.

The Paris equation (2.4) could not be applied to small cracks; thus, a reasonable simplification in this case is to neglect ΔK_{th} completely. Furthermore, neglecting ΔK_{th} implicitly accounts for the presence of a technical crack size after initiation that is somewhat larger than assumed above ($a_0 = a_{init}$). However, this approach resulted in overly pessimistic predictions. Therefore, either approaches either accounting for or neglecting ΔK_{th}, were taken into account in the deterministic models. The stress intensity factors, K_i, were determined using the correction factors, β, defined in Anderson (2005).

The effect of residual stresses is believed to be much more substantial during the crack initiation stage than in the crack propagation stage (Lawrence 1981). Consequently, the residual stresses could be neglected in the crack propagation equation (2.4) as a simple assumption. However, due to the existing tensile residual stresses, this assumption may lead to overly optimistic fatigue life

[4] Due to the relatively short dimension of the models in the x-direction, the desired residual stresses at the critical location (flaw on positive x-plane) could be obtained by introducing these desired stresses on the negative z-plane (i.e., practically no redistribution of the stresses occurred from the negative to the positive x-plane).

[5] Transitional crack size, a_{init} is defined as the distance from the notch root, where both the initiation and propagation growth rate are equal (Socie *et al.* 1979).

predictions. As a result, two models, one taking into account the crack closure effect and one neglecting crack closure, were studied here.

Final crack size, a_f, is usually governed by either brittle fracture or yielding of the remaining cross-section. As all the fatigue tests were executed at room temperature, it is likely that the steel was tough enough to allow the propagation of a crack over most of the lower flange of the beam, where the fracture surface occurs. The transition from a corner or surface crack to a through-thickness crack increases the level of complexity of the crack growth problem. In order to avoid this transition, the surface crack size, where they reach the corners, should not exceed the following values:

2c = 15.806 mm $\Rightarrow a_f$ = 0.5c = 3.95 mm for G-N-2

2c = 15.843 mm $\Rightarrow a_f$ = 0.5c = 3.96 mm for N-N-2

2c = 15.213 mm $\Rightarrow a_f$ = 0.5c = 3.80 mm for G-N-3

where 2c = bottom flange thickness

The final crack size values used in this research are considered as the failure criteria despite the fact that they do not exactly correspond to the failure criteria adopted during the tests (completing severing of the cross-section). However, these values are appropriate considering the rather small residual fatigue life remaining at that stage.

The fatigue crack growth parameters in Eq. (2.4) are adopted from the work of Josi and Grondin (2010) and are defined as follows:

C = 3.5 x 10^{-13} (mm/cycle).$\left(MPa\sqrt{mm}\right)^{-3}$ (weld metal)

C = 2.75 x 10^{-13} (mm/cycle).$\left(MPa\sqrt{mm}\right)^{-3}$ (base metal)

ΔK_{th} = 60 MPa $\sqrt{mm}$ (with and without crack closure)

m = 3.0

6.3. Results

6.3.1 Finite Element Results for Global Models

The governing longitudinal stresses in the global finite element models indicated the maximum stress concentration at the weld flaws and base metal, as illustrated in the fractured surfaces. The maximum stress concentrations were generally located in the mid-length of the bottom flange of the beam close to the weld connecting the beam to the end plate. Table 6.5 illustrates the maximum stress location and value for the three specimens.

Table 6.5 *Maximum stresses at mid-length and weld toes for the three specimens.*

Specimen	Maximum Stress (MPa)	Location
N-N-2	160	Lower weld toe in the tension flange
G-N-2	272	Lower side of the tension flange close to the weld vicinity
G-N-3	220	Lower side of the tension flange close to the weld vicinity

6.3.2 Finite Element Results for Local Models

Each local model was analysed with two different residual stress distributions, σ_{res}: 1) tensile stress of 100 MPa at the surface (intersection of positive x-plane and negative z-plane), corresponding to an expected upper bound residual stress field for the ground specimens; 2) no residual stress field, corresponding to an expected lower bound residual stress field for the non-treated specimens.

In the following sub-sections, the crack initiation parameters using energy-based method ($\sigma_{\max}$ and ΔW^p) were predicted from local finite element models for a non-ground specimen (N-N-2) and ground specimens (G-N-2 and G-N-3). First, no initial flaws were considered for all the specimens. Then, 0.1 mm and 1.0 mm spherical flaws were assumed at the crack initiation sites at the weld metal for N-N-2. Furthermore, elliptical flaws with minor axes of 0.1 mm and 1.0

mm were introduced to the non-ground specimen (N-N-2) only to compare the predicted crack initiation life to the values obtained from spherical flaws.

6.3.2.1 Models without a Flaw

The governing maximum longitudinal stresses, $\sigma_{\max}$, in addition to the plastic strain energies, ΔW^p, predicted from the local finite element models without a flaw are illustrated in Table 6.6. The stresses and energies were generated at location of the most highly stresses for two cases: no residual stress and 100 MPa residual stresses.

Table 6.6 *Governing maximum stresses, $\sigma_{\max}$, and strain energy densities, ΔW^p, for local models without flaws.*

Test Setup	σ_{res}	σ_{max}	ΔW^p
G-N-2	*100 MPa*	*150 MPa*	*0.072*
	0 MPa	*134 MPa*	*0.071*
G-N-3	*100 MPa*	*260 MPa*	*0.043*
	0 MPa	*235 MPa*	*0.043*
N-N-2	*100 MPa*	*205 MPa*	*0.044*
	0 MPa	*203 MPa*	*0.044*

6.3.2.2 Models with 0.1 mm Spherical Flaw

Table 6.7 presents the governing maximum longitudinal stresses, $\sigma_{\max}$, in addition to the plastic strain energies, ΔW^p, for each of the models with a 0.1 mm spherical surface flaw. The stresses and energies were obtained as an average of all the outputs of the nodes delimiting the flaw on the positive x-plane.

Table 6.7 *Governing maximum stresses, $\sigma_{\max}$, and strain energy densities, ΔW^p, for local model with 0.1 mm spherical surface flaw.*

Test Setup	σ_{res}	σ_{max}	ΔW^p
N-N-2	*100 MPa*	*243 MPa*	*0.18*
	0 MPa	*240 MPa*	*0.19*

6.3.2.3 Models with 1.0 mm Spherical Flaw

The governing maximum longitudinal stresses, $\sigma_{\max}$, in addition to the plastic strain energies, ΔW^p, for each of the models with a 1.0 mm spherical surface flaw are shown in Table 6.8. The stresses and energies were obtained as an average of all the outputs of the nodes delimiting the flaw on the positive x-plane.

Table 6.8 *Governing maximum stresses, $\sigma_{\max}$, and strain energy densities, ΔW^p, for local model with 1.0 mm spherical surface flaw.*

Test Setup	σ_{res}	σ_{max}	ΔW^p
N-N-2	*100 MPa*	*317 MPa*	*0.13*
	0 MPa	*300 MPa*	*0.13*

6.3.2.4 Models with 0.1 mm Elliptical Flaw

Table 6.9 illustrates the governing maximum longitudinal stresses, $\sigma_{\max}$, in addition to the plastic strain energies, ΔW^p, for specimen N-N-2 with a 0.1 mm elliptical surface flaw. The stresses and energies were obtained as an average of all the outputs of the nodes delimiting the flaw on the positive x-plane.

Table 6.9 *Governing maximum stresses, $\sigma_{\max}$, and strain energy densities, ΔW^p, for local model with 0.1 mm elliptical surface flaw.*

Test Setup	σ_{res}	σ_{max}	ΔW^p
N-N-2	*100 MPa*	*233 MPa*	*0.32*
	0 MPa	*159 MPa*	*0.32*

6.3.2.5 Models with 1.0 mm Elliptical Flaw

The governing maximum longitudinal stresses, $\sigma_{\max}$, in addition to the plastic strain energies, ΔW^p, for specimen N-N-2 with a 1.0 mm elliptical flaw are illustrated in Table 6.10. The stresses and energies were obtained as an average of all the outputs of the nodes delimiting the flaw on the positive x-plane.

Table 6.10 *Governing maximum stresses, $\sigma_{\max}$, and strain energy densities, ΔW^p, for local model with 1.0 mm elliptical surface flaw.*

Test Setup	σ_{res}	σ_{max}	ΔW^p
N-N-2	*100 MPa*	*205 MPa*	*0.21*
	0 MPa	*166 MPa*	*0.21*

6.3.3 Deterministic Fatigue Life Predictions

The fatigue life of the tested full-scale specimens was determined by adopting the methodologies emphasized in Sections 6.2.1 and 6.2.2 in addition to the finite element results of the local models developed in Section 6.3.2. First, the case of a welded joint with no flaw was investigated for all the non-ground and ground specimens. Then, the spherical and elliptical weld flaws were introduced to the non-ground specimens.

For all the crack propagation predictions that include crack closure, a simplified assumption of constant tensile residual stress field of 100 MPa through the thickness or no residual stresses are presumed. Although the constant tensile residual stress does not follow the self-equilibrium fact of the residual stresses, it was selected as a conservative approach as the residual stresses is anticipated to relax with crack growth (Josi and Grondin 2010).

Josi and Grondin (2010) showed a sample calculation incorporating crack closure and the threshold stress intensity factor range, ΔK_{th}, for a specimen with a 0.1 mm surface flaw (residual stress of +100 MPa surface). This study followed the same procedure for fatigue crack propagation prediction.

The total fatigue life predicted in this chapter relied on several parameters regarding the initial weld flaw conditions, long or short cracks, and presence or lack of residual stresses. The first parameter affects the crack initiation life, while the latter contribute to the fatigue propagation life. Table 6.11 illustrates the total fatigue life for short and long crack effects in addition to the presence or lack of residual stresses. The symbol *S* in the table refers to short crack i.e. no ΔK_{th} is considered, while symbol *L* refers to long crack behaviour, where ΔK_{th} is taken into account for crack propagation.

Table 6.11*Total fatigue life predicted from deterministic approaches.*

Sample	Initial Condition	Crack Initiation	Crack Propagation - No ΔKth (S)	Crack Propagation - ΔKth (L)	Total Predicted Fatigue Life - No ΔKth	Total Predicted Fatigue Life - With ΔKth	Total No. of Cycles predicted from Test Results
G-N-2	No initial flaw (Crack initiation) a_{init} = 0.1 mm (Crack propagation) - No Residual stress (N00NR)	788,920	4,450,827	3,817,033	5,239,747	4,605,953	7,421,211
	No initial flaw (Crack initiation) a_{init} = 0.1 mm (Crack propagation) - Residual stress (NOOR)	602,397	2,141,431	2,391,567	2,743,828	2,993,964	
	No initial flaw (Crack initiation) a_{init} = 1.0 mm (Crack propagation) - No Residual stress (N00NR)	788,920	1,008,234	1,046,664	1,797,154	1,835,584	
	No initial flaw (Crack initiation) a_{init} = 1.0 mm (Crack propagation) - Residual stress (N00R)	602,397	399,762	405,629	1,002,159	1,008,026	
G-N-3	No initial flaw (Crack initiation) a_{init} = 0.1 mm (Crack propagation) - No Residual stress (N00NR)	693,978	736,866	826,772	1,430,844	1,520,750	1,382,124
	No initial flaw (Crack initiation) a_{init} = 0.1 mm (Crack propagation) - Residual stress (NOOR)	663,577	378,982	400,132	1,042,559	1,063,709	
	No initial flaw (Crack initiation) a_{init} = 1.0 mm (Crack propagation) - No Residual stress (N00NR)	693,978	138,995	139,685	832,973	833,663	
	No initial flaw (Crack initiation) a_{init} = 1.0 mm (Crack propagation) - Residual stress (N00R)	663,577	71,635	71,814	735,212	735,391	
N-N-2	0.1 mm Sph. Flaw - No Residual stress (FS01NR)	42,093	2,908,335	8,154,580	2,950,428	8,196,673	4,640,509
	0.1 mm Sph. Flaw - Residual stress (FS01R)	32,878	1,156,941	1,421,653	1,189,819	1,454,531	
	1.0 mm Sph. Flaw - No Residual stress (FS10NR)	44,579	261,251	263,739	305,830	308,318	
	1.0 mm Sph. Flaw - Residual stress (FS10R)	44,579	104,855	105,256	149,434	149,835	
	0.1 mm Ellp. Flaw - No Residual stress (FE01NR)	29,198	2,542,353	2,449,442	2,571,551	2,478,640	
	0.1 mm Ellp. Flaw - Residual stress (FE01R)	13,114	988,289	1,167,571	1,001,403	1,180,685	
	1.0 mm Ellp. Flaw - No Residual stress (FE10NR)	67,151	530,694	541,054	597,845	608,205	
	1.0 mm Ellp. Flaw - Residual stress (FE10R)	42,923	175,791	176,908	218,714	219,831	

6.4. Discussion

The results illustrate 48 predictions of both fatigue crack initiation and propagation lives for the three tested specimens, whether non-ground (N-N-2) or ground (G-N-2 and G-N-3). Finite element analysis results from a global model of the entire specimen were employed to define the applied stresses (from the test load) in local finite element models. Afterwards, the governing maximum stresses and strain energy densities, employed to predict the fatigue crack initiation life, were generated from finite element analyses. Linear elastic fracture mechanics (LEFM) was implemented to estimate the fatigue crack propagation predictions.

Fatigue life predictions for the ground specimens, G-N-2 and G-N-3, are based on no initial flaw conditions, while spherical and elliptical flaw are considered in the non-ground specimen, N-N-2. This resulted in relatively large fatigue crack initiation life for specimens G-N-2 and G-N-3 compared to the as-weld specimen, N-N-2.

Based on various deterministic fatigue life prediction shown in Table 6.11, the minimum and maximum fatigue lives of the ground specimen G-N-2 were one million cycles (N00R – short crack effect with residual stresses) and 5.24 million cycles (N00NR – short crack effect with no residual stresses) cycles. This was for initial crack size of 1.0 mm and 0.1 mm respectively for the fatigue crack propagation. The specimen failed in the actual tests after 7.42 million cycles. Therefore, the deterministic prediction under-estimated the actual fatigue test result of G-N-2. For the other ground specimen (G-N-3), the minimum and maximum predicted fatigue life were 0.73 million cycles (N00R – short crack effect with residual stresses), considering 1.0 mm initial crack size, and 1.52 million cycles (N00NR – long crack effect without residual stresses) based on 0.1 mm crack initial size. Thus, the fatigue life from the fatigue test, that was 1.38 million cycles, was slightly close to the upper bound.

For the non-ground specimen (N-N-2), two initial weld flaw shapes (spherical and elliptical) were introduced at the weld toe with the two extreme flaw size values of 0.1 and 1.0 mm. The minimum and maximum fatigue lives adopting initial spherical flaws were 0.15 million (FS10R – short crack effect with residual stresses) and 8.19 million cycles (FS01NR – long crack effect without residual stresses). The minimum and maximum fatigue lives using initial elliptical flaws were 0.21 million (FE10R - short crack effect with residual stresses) and 2.57 million cycles (FE01NR – short crack effect without residual stresses). The fatigue life obtained from the

fatigue test for the non-ground specimen (N-N-2) was 4.64 million cycles, which lies in the extreme boundaries of the spherical flaw prediction, not the elliptical one. From Table 6.11, it can be deduced that the predicted fatigue lives using initial elliptical flaws for the non-ground specimens underestimated the actual fatigue life.

It can be noticed that the fatigue life predictions for one of the ground specimens (G-N-2) in the fatigue test are higher than the predicted values using the numerical deterministic approach. The difference between the predicted and test results could result due to many reasons. The numerical models for the weld profiles are not exactly the same as the actual weld profiles. The residual stress distribution in the test specimens could be different from the assumed residual stress distribution used in the finite element analysis.

The analytical results showed that an initial spherical flaw size of 0.1 mm with no residual stresses leads to the most accurate prediction of fatigue resistance of the tested specimens. The predicted fatigue lives for the ground specimen, G-N-2 was found to be underestimated, while the predicted fatigue life for ground specimen, G-N-3 and non-ground specimen, N-N-2 were in the boundary of the test result. Crack initiation life was found to be smaller than the propagation life for the specimens without an initial discontinuity or with an initial flaw. Therefore, its contribution towards the total fatigue life prediction should not be missed especially for cases of the no flaw condition, where fractured occur in the base metal not at the weld toe.

7. PROBABILISTIC FATIGUE LIFE PREDICITON OF WELDED STEEL DETAILS

7.1. Introduction

In this chapter, a reliability-based approach is developed to predict the fatigue life of a cruciform welded detail. This cruciform detail is from literature and represents an actual bridge joint and is recognized to be of fatigue category *C*. It is also considered to be a simplified connection between the wide flange beam and the end plate, employed in the full-scale test specimens in Chapter 5. All input parameters, subject to variability, should have a specific probabilistic distribution with its defining parameters (e.g. mean and standard deviation) to be known in advance in order to carry out the reliability analysis.

Section 7.2 emphasizes the methodology developed to predict the fatigue crack initiation and propagation lives for the cruciform detail using the relevant probabilistic inputs. By using fatigue limit state, the study also illustrates the developed procedure to estimate the remaining fatigue life and reliability indices of various weld profiles for the same welded detail.

Then, section 7.3 presents the results of probabilistic fatigue life resistance predictions of the cruciform detail in their probabilistic distributions, and Monte Carlo Simulation. Moreover, the developed fatigue life reliability, based on the fatigue life resistance and the applied cyclic loading due to truck data from Quebec WIM data, predicted in Chapter 4, is established. The discussions on the results are illustrated in section 7.4.

7.2. Methodology

7.2.1 Probabilistic Fatigue Life Prediction for Cruciform Detail

Figure 7.1 illustrates the flow chart for the procedure developed here for the probabilistic fatigue life prediction of the cruciform welded detail. The procedure consists of first defining the initial flaw, the material properties, the applied loading, and the residual stresses. Then the maximum stress, σ_{max}, and the plastic strain energy density, ΔW^p, are determined considering the weld sizes, initial flaws (weld undercuts), the applied loading, and the residual stresses using finite element analysis. Equation (2.7) estimates the crack initiation life, N_{init}, using the maximum stresses and plastic strain energies obtained from a finite element analysis and the fatigue initiation properties. The transitional size, a_{trans}, which is a function of the initial flaw size, is used

as the initial crack size, a_0, in the crack propagation. The crack propagation life, N_{prop}, is determined from equation (2.4), which takes into account the material properties, the applied loading, the residual stresses and the initial and final crack sizes, a_0 and a_f. It also includes ΔK_{th} and crack closure. Finally, the crack initiation and propagation lives are added to obtain the total fatigue life, N_{total}.

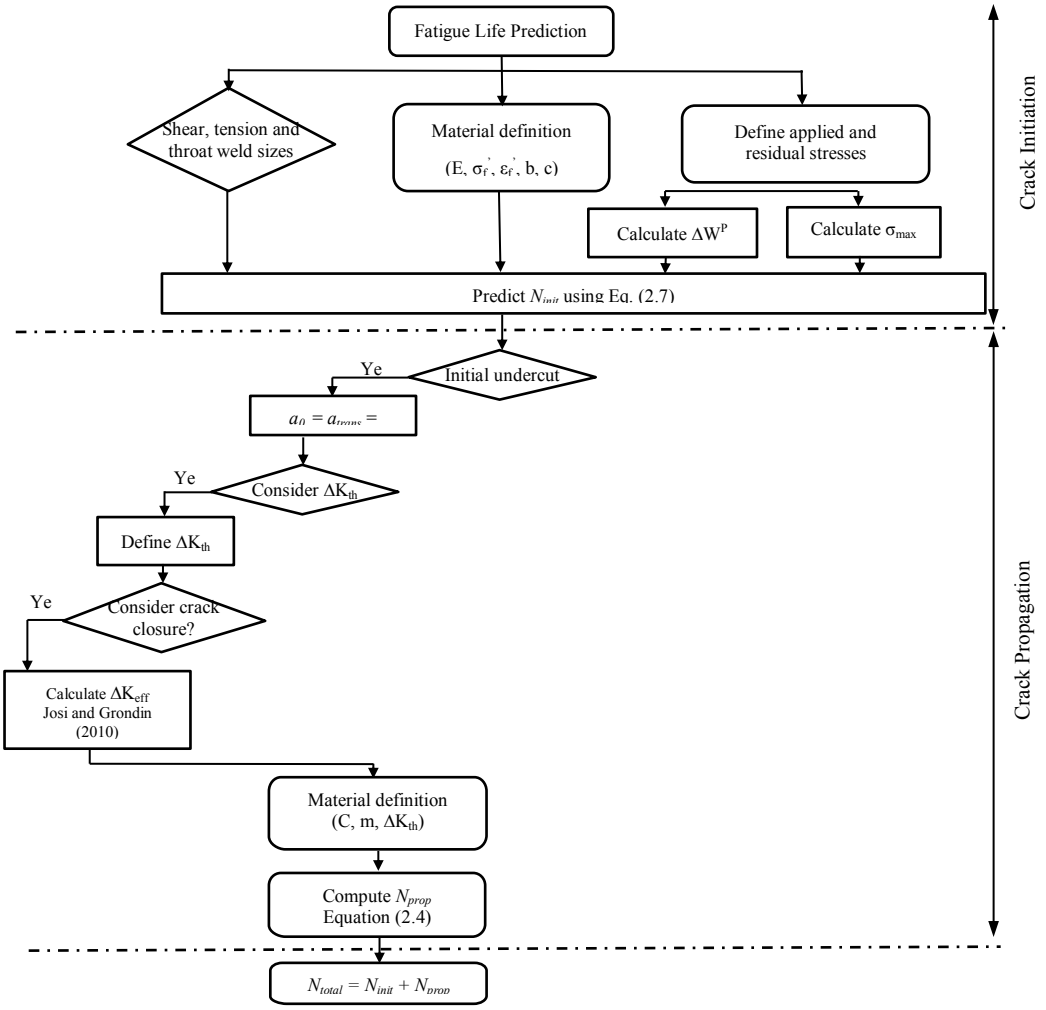

Figure 7.1 *Flow chart of probabilistic approach for fatigue life resistance.*

In the following subsections, the geometrical configuration of the weld detail under investigation, the variations in the fillet weld measurements and the approaches for fatigue crack initiation and propagation predictions are illustrated.

7.2.1.1 Geometrical configuration of the weld detail and weld size variations

In order to implement the probabilistic fatigue life prediction of actual steel highway bridge, a cruciform detail from literature that represents the stiffener connections in steel girders is used. The welded detail in Engesvik and Moan (1983) is adopted in the probabilistic prediction for fatigue life. The dimensions of the main plate are 450 x 100 x 32 mm to which two 100 x 50 x 32 mm transverse plates were attached with fillet welds. In its geometrical form and according to the direction of loading with respect to the weld (transverse loading), this weld detail is recognized to be fatigue category *C*. Figure 7.2 illustrates the dimensions of the cruciform welded detail.

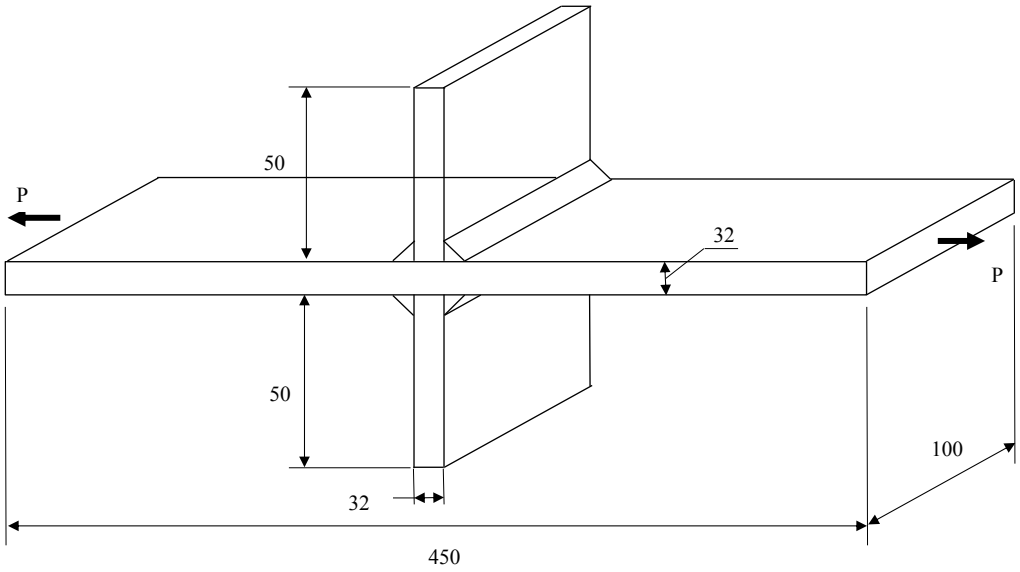

Figure 7.2 *Cruciform welded detail (Engesvik and Moan 1983).*

In this probabilistic prediction, and in order to take into account the variability in the fillet weld sizes connecting the main plate to the stiffener, this study used the measured fillet weld sizes by Ng *et al.* (2002). The authors measured 63 fillet weld sizes of 6.4 mm and 45 fillet weld size of 12.7 mm. The measurements included shear leg size (S), tension leg size (T) and weld throat size (R). The input models for the extreme shear, tension and root weld sizes, employed in the probabilistic fatigue life prediction, are presented below. Figure 7.3 illustrates a schematic layout for various weld sizes and their designations used in this chapter.

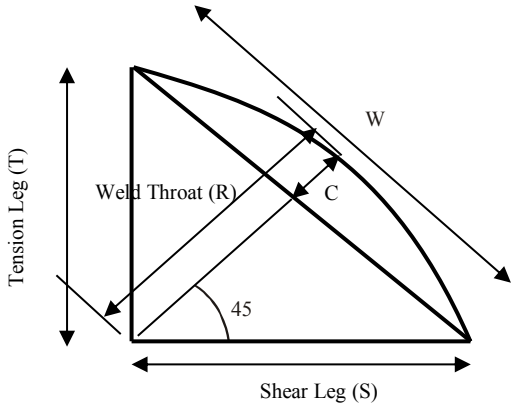

Figure 7.3 *Schematic layout for various weld sizes and their designations.*

Due to the large population of fillet weld sizes, the study only considered the extreme cases i.e. minimum and maximum sizes in the analysis to limit the number of finite element models. As a result, eight different weld size combinations were developed as illustrated in Table 7.1.

Table 7.1 *The fillet weld cases number and their designation.*

Case Number	Shear Leg (S)	Tension Leg (T)	Weld Throat (R)
1	Min S	Min T	Min R
2	Min S	Max T	Min R
3	Max S	Min T	Min R
4	Max S	Max T	Min R
5	Min S	Min T	Max R
6	Min S	Max T	Max R
7	Max S	Min T	Max R
8	Max S	Max T	Max R

Based on the previous cases for weld sizes for shear leg, tension leg and weld throat, Table 7.2 displays the fillet weld sizes for the various eight cases analyzed in the finite element model for the 6.4 mm nominal welds.

Table 7.2 *Shear leg, tension leg, and weld throat sizes in mm for 6.4 mm nominal weld size.*

Case Number	Shear Leg (S) in mm	Tension Leg (T) in mm	Weld Throat (R) in mm	Weld Width (W) in mm	Curvature (C) in mm
1	5.1	4.2	3.9	6.6	0.64
2	5.1	7.8	3.9	9.32	-0.46
3	9.8	4.2	3.9	10.66	-0.26
4	9.8	7.8	3.9	12.53	-2.42
5	5.1	4.2	6.3	6.6	3.04
6	5.1	7.8	6.3	9.32	1.94
7	9.8	4.2	6.3	10.66	2.14
8	9.8	7.8	6.3	12.53	0.16

In Table 7.2, it can be noticed that the value of the curvature is sometimes negative in addition to the positive values. The negative values indicate that the fillet weld profile is concave while the positive values indicate the weld convexity.

The other parameter, considered in the finite element model, is the initial weld undercut. According to the Canadian Welding Code (CSA-W59 2013), the weld undercut size cannot exceed 0.25 mm for transversely loaded weld details. To correlate between the plastic strain density energy, maximum stress and initial undercut, various finite element combinations were required. Therefore, the research considered three weld under-cut sizes: no undercut, 0.1 mm undercut, and 0.25 mm undercut.

7.2.1.2 Fatigue Crack Initiation Prediction

Input Parameters

The fatigue initiation parameters used in equation (2.7) for the base and weld metals are presented in Table 7.3. The fatigue strength coefficient, σ_f', and the fatigue ductility coefficient, ε_f', were modelled with lognormal distributions, while the fatigue exponents, b and c, were assumed to be deterministic.

Table 7.3 *Fatigue initiation parameters for the base and weld metals (Josi and Grondin 2010).*

Metal	σ_f' [MPa]	b [-]	ε_f'	c [-]
Base	LN(532,18)	*Det(-0.07)*	*LN(0.0715,0.013)*	*Det(-0.4)*
Weld	*LN(630,30)*	*Det(-0.059)*	*LN(0.34,0.07)*	*Det(-0.63)*

Finite Element Analysis of Cruciform Detail

A two-dimensional finite element model of a plane strain strip was used to analyze the typical cruciform specimen. Since the test specimens were doubly symmetric, only one quarter of the specimen was modelled. The quadrilateral linear plain strain continuum element CPE4R was used for the plates, while the triangular plain strain continuum element CPE3 was used for the fillet weld regions. A model of approximately 46.0 mm long in both directions was found to be adequate to represent the whole specimen. A typical sample of the finite element model for a strip of unit width with nominal fillet weld sizes of 6.4 mm is shown in Figure 7.4. The potential crack plane is represented by Section A-A.

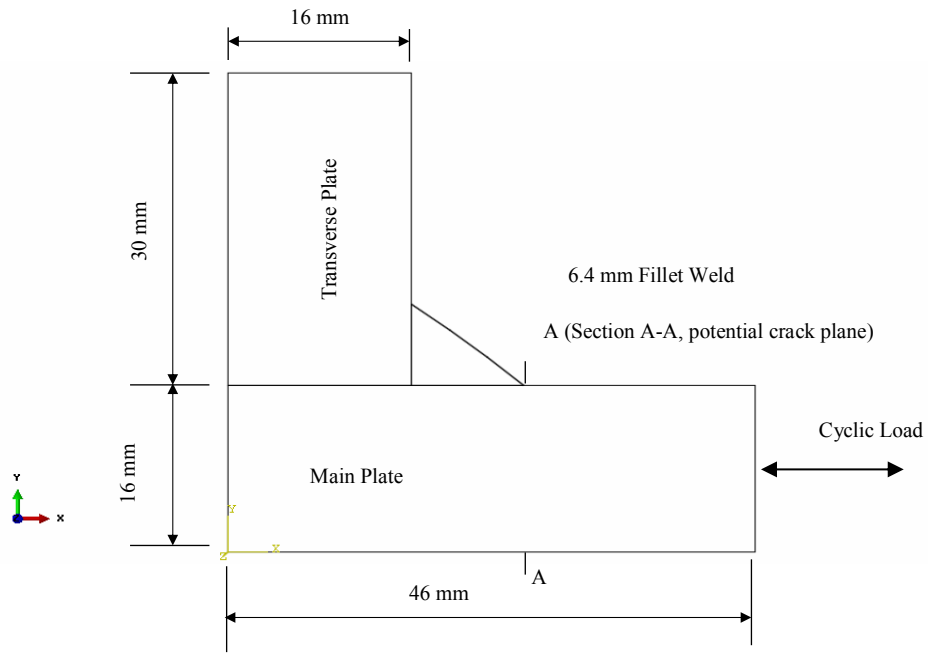

Figure 7.4 *Finite element model for cruciform welded detail using nominal fillet weld 6.4 mm.*

The load steps in the finite element analyses were: cyclic loading and maximum cyclic stresses. The cyclic loading model with defined peak maximum, minimum stresses and frequency was employed to predict the plastic strain energy density exhausted in stress cycles, while the maximum stresses of the cyclic load case was used to predict the maximum stresses at the crack initiation sites near the weld flaw vicinity. The stress ranges for the cyclic loading were 25 MPa, 50 MPa and 75 MPa while the maximum stresses were 82.5 MPa, 115 MPa and 147.5 MPa. These stress ranges cover minimum, maximum and mean values of the stress ranges, which were developed due to the truck loads on bridge details from WIM data as illustrated in Chapter 4. The base metal and the welds were modelled as having the same material properties used in Chapter 6. Table 7.4 illustrates the various finite element models which will used in the probabilistic fatigue crack initiation prediction of the cruciform detail.

Table 7.4 *Finite element models for fillet weld of nominal sizes 6.4 mm.*

Case Number	*Under Cut (UC) Sizes in mm*			*Stress Ranges [MPa]*			*Maximum Loading Stress [MPa]*		
	No UC	*0.1 mm*	*0.25 mm*	*25*	*50*	*75*	*82.5*	*115*	*147.5*
1	X			X	X	X			
1	X						X	X	X
1		X		X	X	X			
1		X					X	X	X
1			X	X	X	X			
1			X				X	X	X
2	X			X	X	X			
2	X						X	X	X
2		X		X	X	X			
2		X					X	X	X
2			X	X	X	X			
2			X				X	X	X
3	X			X	X	X			
3	X						X	X	X
3		X		X	X	X			
3		X					X	X	X
3			X	X	X	X			
3			X				X	X	X
4	X			X	X	X			
4	X						X	X	X
4		X		X	X	X			
4		X					X	X	X
4			X	X	X	X			
4			X				X	X	X
5	X			X	X	X			
5	X						X	X	X
5		X		X	X	X			
5		X					X	X	X
5			X	X	X	X			
5			X				X	X	X
6	X			X	X	X			
6	X						X	X	X
6		X		X	X	X			
6		X					X	X	X
6			X	X	X	X			
6			X				X	X	X
7	X			X	X	X			
7	X						X	X	X
7		X		X	X	X			
7		X					X	X	X
7			X	X	X	X			
7			X				X	X	X
8	X			X	X	X			
8	X						X	X	X
8		X		X	X	X			
8		X					X	X	X
8			X	X	X	X			
8			X				X	X	X

Appendix F shows in detail the different profiles of weld sizes and under-cut conditions, employed in the finite element analysis for the 6.4 mm nominal weld size.

7.2.1.3 Fatigue Crack Propagation Prediction

Equation (2.4) was used for fatigue crack propagation life prediction. Regarding the crack propagation properties for the weld, previous tests on fatigue crack propagation parameters were

conducted at the University of Alberta in different researches [Chen *et al*. (2005), Yin *et al*.(2006), Josi and Grondin (2010)]. For probabilistic fatigue life prediction, the study utilized appropriate material properties from Chapter 2. Consequently, the probabilistic distributions for these parameters are assumed as follows:

- m = 3.0
- C : LN(2.7 X 10^{-13}, 1.4 X 10^{-13})
- ΔK_{th} : LN(60,6)

It was found that for a surface crack, an initial crack size $a_0 = 0.10$ mm yields a stress intensity factor range of $\Delta K = K_{\max} - K_{\min}$ = 193 MPa $\sqrt{mm}$ (Josi and Grondin 2010). This stress intensity range was close to the stress intensity factor range of 190 MPa $\sqrt{mm}$, predicted by Chen *et al.* (2005). The initial crack size of 0.10 mm is also consistent with the investigated crack sizes by Radaj and Sonsino (1998). Based on the above observations, the initial crack size, a_0, was taken as 0.1 mm, using the same probabilistic distributions. The results of the deterministic prediction in Chapter 6 illustrated that the 0.1 mm flaw size provided the most reliable fatigue life prediction for the non-ground specimens. A lognormal distribution for a_0 with LN(0.1,0.02) was considered in this study. The aspect ratio a/c was also assumed to remain constant in the crack propagation stage. The lognormal distribution, LN(0.5,0.16), adopted by Walbridge (2005) was employed in the current study.

For the fatigue crack propagation stage, the final crack size for the cruciform weld detail was taken as half of the main plate thickness, a_f = 16.0 mm. For ease of implementation of the crack propagation model into a probabilistic approach, it is desirable to keep the stress intensity factor calculations for an elliptical surface crack throughout the entire propagation life (Josi and Grondin 2010). However, this approach underestimated the crack growth once the crack has reached the corners, which is ¼ of the plate thickness i.e. 8.0 mm. Consequently, the final crack size used in the probabilistic model had to be smaller than the specimen thickness (32.0 mm) but larger than 8.0 mm. A lognormal distribution for a_f with LN(16, 0.01) was therefore assumed.

According to the findings presented in Chapter 6, the residual stresses for the as-weld specimens should be close to 0. The finite element models with σ_{res} = 100 MPa developed a relatively

shorter fatigue life, when compared to the fatigue life predicted from fatigue tests. The model with no residual stresses induced fatigue life that matches the observed fatigue life in the fatigue tests. Based on the previous findings, no residual stresses were assumed during the probabilistic prediction of fatigue life, i.e., Det(0). Similar assumption was introduced by Josi and Grondin (2010).

Due to the inherent uncertainties in finite element modeling, the maximum and minimum applied stresses are subjected to some variability. This study proposed a lognormal distribution for maximum and minimum applied stress at the weld flaw vicinity, $\sigma_{max,app}$, $\sigma_{min,app}$ respectively. A deterministic value was assumed for the coefficient, *A,* used in the stress gradient correction factor, β_G calculations for both the maximum and minimum stresses (Josi and Grondin 2010). Using the same concept, the maximum applied stresses at locations, where the crack starts propagating was estimated from the finite element analysis for different initial undercut sizes. This was represented in the form of lognormal distribution with a specified mean and standard deviation.

7.2.2 Fatigue Life Reliability Analysis

The probabilistic fatigue life of the cruciform welded detail, explained in Section 7.2.1, is considered to be the fatigue resistance life (N_r) of the cruciform welded detail. In order to estimate the probability of failure within structural reliability concept, a limit state function should be defined as well the probabilistic distribution for the applied number of cycles due to cyclic loading (N_a). The limit state function used in this study for fatigue reliability analysis is defined as follows:

$$G(x) = N_r - N_a = 0 \tag{7.1}$$

Where N_r = Number of cycles for fatigue resistance (Number of cycles to failure)

N_a = Number of cycles for fatigue loading (Number of applied cycles)

If $G(x) \le 0 \Rightarrow$ Failure Domain

$G(x) > 0 \Rightarrow$ Safe Domain (7.2)

The stress range histograms for Ontario, Quebec (Batiscan) and Quebec (Nicolas) were illustrated in Chapter 4 in the form of probabilistic distribution, mean and standard deviation. To convert this probabilistic distribution into actual applied number of cycles representing the truck traffic, Kwon and Frangopol (2010) developed a methodology to predict the applied number of cycles using probability density functions based on equivalent stress range. The stress histories in their study were collected through field measurements using strain gauges. They estimated the average daily truck traffic (ADTT) by dividing the number of total applied cycles by the total WIM monitoring time, considering a stress cycle per truck passage. As mentioned in Chapter 3, Quebec WIM data included the total monitoring time, required for prediction of the actual number of cycles, to be 130 and 52 days for Quebec (Batiscan) and Quebec (Nicolas) respectively. Although the probabilistic stress histograms are predicted for Ontario, it was difficult to estimate the total number of cycles and ADTT since the monitoring period information was missing in the received WIM data. Therefore, the probabilistic stress distributions for Quebec only were encountered in the fatigue life reliability predictions.

In a similar approach to predict the cumulative number of applied cycles from stress range distributions (Kwon and Frangopol 2010), this study estimated the total number of cycles using the mean value of the probabilistic distribution under consideration and the lower bound intercept for the S-N curve of the fatigue detail category. The mean stress range is a more conservative assumption than equivalent stress range since there are uncertainties in the design of steel girder cross sections. Figure 7.5 illustrates the procedure to predict the number of applied cycles during a certain monitoring period based on the mean value of the stress range for any particular span for bridge detail of fatigue category *C*.

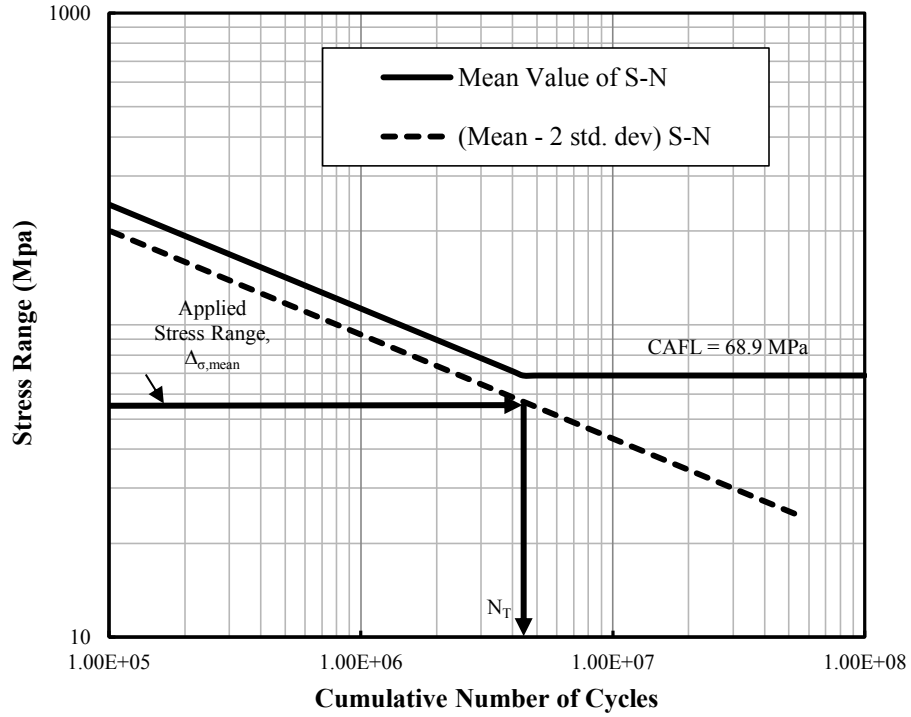

Figure 7.5 *Procedure for prediction of applied number of cycles for fatigue Category-C.*

The S-N curves in CSA-S6-06 (CSA 2006) represent the lower 95 percent confidence limit of the test data. Thus, the intercept of the S-N curves are shifted towards coordinate system origin. For prediction of number of cycles due to truck loading, further reduction of one standard deviation from the current S-N curve of fatigue Category C (Figure 7.5) is assumed. Based on the probabilistic stress-range distributions, predicted earlier in Chapter 4, the mean value of stress range was calculated, and the corresponding total number of cycles, N_T , was estimated as shown in Figure 7.5 which is modeled by the following relationship:

$$LogN_T = (b - 3\sigma) - m \times LogS_{r,mean} \tag{7.3}$$

The total number of cycles, N_T , is divided by the total monitoring time to estimate average daily truck traffic, ADTT (cycles per day), considering a stress cycle per truck passage. Kwon and Frangopol (2010) estimated the annual accumulated number of stress cycles, *N*, based on ADTT and traffic increase rate per year in the following relation:

$$N = 365.ADTT.N_D \frac{(1+\alpha)^y - 1}{ln(1+\alpha)} \tag{7.4}$$

Where α = annual increase of traffic growth

y = number of years

N_D = equivalent number of cycles due to truck passage

7.3. Results

7.3.1. Finite Element Results

Tables 7.5 and 7.6 illustrate the results of plastic strain energy density and maximum stresses for various undercut condition in eight different weld size cases for 6.4 mm weld size.

Table 7.5 *Plastic strain energy densities versus various stress ranges for extreme weld sizes for 6.4 mm fillet welds.*

Under-Cut (UC) Condition	Stress Range	Case 1	Case 2	Case 3	Case 4	Case 5	Case 6	Case 7	Case 8
		MinS-MinT-MinR	MinS-MaxT-MinR	MaxS-MinT-MinR	MaxS-MaxT-MinR	MinS-MinT-MaxR	MinS-MaxT-MaxR	MaxS-MinT-MaxR	MaxS-MaxT-MaxR
NoUC	25 Mpa	2.67142E-05	1.86889E-05	0	0	2.08232E-05	2.88013E-05	3.19761E-05	0
	50 Mpa	3.20596E-05	3.48604E-05	0	0	5.16516E-05	0.000068155	3.49972E-05	4.18545E-05
	75 Mpa	5.70725E-05	5.54198E-05	0	0	0.000095177	9.52571E-05	6.12027E-05	4.86246E-05
0.1UC	25 Mpa	0.000156556	0.000185973	6.20814E-05	0	5.62962E-05	5.21189E-05	0.000216124	0.000224188
	50 Mpa	0.000317744	0.000362968	0.000122879	0.000165711	0.000105442	0.000137433	0.000331084	0.000364196
	75 Mpa	0.000513015	0.000362968	0.000229083	0.000225644	0.000210863	0.000254449	0.000494296	0.000549078
0.25UC	25 Mpa	7.58653E-05	8.20534E-05	0	0	3.79725E-05	6.63455E-05	0.000142347	0.000074544
	50 Mpa	0.000121513	0.00013825	4.38083E-05	0.000101609	7.10684E-05	0.000134062	0.000245153	0.000162099
	75 Mpa	0.000162987	0.000194273	4.11575E-05	0.000237284	9.94002E-05	0.00019105	0.000339782	0.000260912

Table 7.6 *Maximum stresses in MPa versus various stress ranges for extreme weld sizes for 6.4 mm fillet welds.*

Under-Cut (UC) Condition	Maximum Stress	Case 1	Case 2	Case 3	Case 4	Case 5	Case 6	Case 7	Case 8
		MinS-MinT-MinR	MinS-MaxT-MinR	MaxS-MinT-MinR	MaxS-MaxT-MinR	MinS-MinT-MaxR	MinS-MaxT-MaxR	MaxS-MinT-MaxR	MaxS-MaxT-MaxR
NoUC	82.5 Mpa	294.9	277.8	169.1	122.9	314.6	330.0	308.7	267.2
	115 Mpa	356.8	336.2	234.7	171.1	376.8	381.1	360.6	325.9
	147.5 Mpa	399.8	379.8	272.8	218.4	418.4	422.2	403.0	370.7
0.1UC	82.5 Mpa	453.3	476.3	383.2	254.7	462.3	466.6	397.9	469.9
	115 Mpa	522.7	548.1	466.6	337.2	541.6	533.4	459.5	556.2
	147.5 Mpa	578.4	605.9	531.8	392.8	603.0	598.2	521.1	623.7
0.25UC	82.5 Mpa	404.4	448.7	346.7	287.5	404.9	416.9	414.0	435.2
	115 Mpa	479.0	515.4	418.0	371.4	480.5	474.9	474.0	502.0
	147.5 Mpa	533.3	564.3	471.3	428.2	534.8	526.7	525.1	552.8

In the reliability-based approach to predict the fatigue life of the cruciform detail, it was required to correlate the plastic strain energy density, ΔW^p, and the maximum stresses, σ_{max}, with the initial undercut size, which will act as the initial crack size in the fatigue life prediction. The initial crack size is previously defined in its probabilistic form. Therefore, probabilistic simulations for ΔW^p and σ_{max} will be derived from each simulation of the initial crack size.

The following relationships between ΔW^p, σ_{max} and a_{init} for case 1 weld size for 6.4 mm weld can be defined based on linear interpolation of the finite element results illustrated in Tables 7.5 and 7.6 respectively.

Stress Range 25 MPa

$$\begin{aligned}
&\Delta W^p = 1.5x10^{-4} - 0.0005(a_{init} - 0.1) && \text{for } a_{init} > 0.1 \text{ mm} \\
&\Delta W^p = 3.0x10^{-5} + 0.0013a_{init} && \text{for } a_{init} \le 0.1 \text{ mm} \\
&\sigma_{max} = 453.33 - 326.36(a_{init} - 0.1) && \text{for } a_{init} > 0.1 \text{ mm} \\
&\sigma_{max} = 294.87 + 1584.6a_{init} && \text{for } a_{init} \le 0.1 \text{ mm}
\end{aligned} \tag{7.5}$$

Stress Range 50 MPa

$$\begin{aligned}
&\Delta W^p = 0.00027 - 0.0013(a_{init} - 0.1) && \text{for } a_{init} > 0.1 \text{ mm} \\
&\Delta W^p = 0.00003 + 0.0029a_{init} && \text{for } a_{init} \le 0.1 \text{ mm} \\
&\sigma_{max} = 522.693 - 290.97(a_{init} - 0.1) && \text{for } a_{init} > 0.1 \text{ mm} \\
&\sigma_{max} = 356.76 + 1659.3a_{init} && \text{for } a_{init} \le 0.1 \text{ mm}
\end{aligned} \tag{7.6}$$

Stress Range 75 MPa

$$\begin{aligned}
&\Delta W^p = 0.00047 - 0.0023(a_{init} - 0.1) && \text{for } a_{init} > 0.1 \text{ mm} \\
&\Delta W^p = 0.00006 + 0.0046a_{init} && \text{for } a_{init} \le 0.1 \text{ mm} \\
&\sigma_{max} = 578.44 - 301.21(a_{init} - 0.1) && \text{for } a_{init} > 0.1 \text{ mm} \\
&\sigma_{max} = 399.85 + 1785.9a_{init} && \text{for } a_{init} \le 0.1 \text{ mm}
\end{aligned} \tag{7.7}$$

The relationships between ΔW^p, σ_{max} and a_{init} for other cases of weld size 6.4 mm are illustrated in details in Appendix G. In Table 7.7, the mean and standard deviation of the lognormal distributions for the eight fillet weld size cases used for 6.4 fillet weld, used to model the applied maximum and minimum stresses at the crack sites during propagation, are illustrated. The values of maximum and minimum stresses were computed for three different stress ranges, 25 MPa, 50 MPa and 75 MPa.

Table 7.7 *Probabilistic maximum and minimum stresses used for fatigue crack propagation for 6.4 mm fillet welds.*

Case Number	Stress Range (MPa)	Probabilistic Distribution for maximum stress, $\sigma_{max,app}$	Probabilistic Distribution for minimum stress, $\sigma_{min,app}$
1	25	LN(375,26)	LN(196,24)
	50	LN(435,27)	LN(123,25)
	75	LN(488,29)	LN(146,25)
2	25	LN(376,33)	LN(106,16)
	50	LN(442,35)	LN(147,19)
	75	LN(492,37)	LN(166,17)
3	25	LN(276,35)	LN(75,4)
	50	LN(350,38)	LN(104,3)
	75	LN(401,43)	LN(135,5)
4	25	LN(204,27)	LN(102,4)
	50	LN(271,33)	LN(118,6)
	75	LN(323,35)	LN(137,8)
5	25	LN(388,24)	LN(105,23)
	50	LN(458,27)	LN(134,22)
	75	LN(510,30)	LN(165,22)
6	25	LN(398,22)	LN(98,22)
	50	LN(457,25)	LN(127,21)
	75	LN(510,29)	LN(158,21)
7	25	LN(360,17)	LN(60,2)
	50	LN(417,19)	LN(92,26)
	75	LN(464,20)	LN(126,6)
8	25	LN(368,33)	LN(88,6)
	50	LN(440,38)	LN(114,6)
	75	LN(496,42)	LN(141,7)

7.3.2. Probabilistic Fatigue Resistance Life Predictions

The fatigue life of the welding detail models is predicted using Monte Carlo Simulation (MCS). The fatigue model suggested in Section 7.2.1 and the probabilistic distributions defined in Sections 7.2.1.1, 7.2.1.3 and 7.3.1 were used for the MCS. For each model, a total of 100,000

simulations were executed for each weld size case. In general, stable results could be achieved after 50,000 simulations. The subroutines required to run the simulation were written in Matlab®. The results for the crack initiation life, N_{init}, the crack propagation life, N_{prop}, and the total life, N_{total}, were saved in ascii-files, which were exported into Microsoft® Excel to predict the mean and standard deviation for each set.

Tables 7.8 illustrates the simulation results for the various cases (cases 1 to 8) extreme fillet weld sizes under the mean stress range of 50 MPa for fillet weld 6.4 mm. The mean and standard deviation in both tables are for lognormal distribution of the predicted probabilistic fatigue life. The results showed that there are no run-out results had been noticed in the fatigue life predictions.

Table 7.8 *MCS results for number of cycles to failure (N_R) in the 6.4 mm fillet weld (100,000 simulations).*

Weld profile	Mean of N_{total} [cycles]	Standard Deviation of N_{total} [cycles]	Mean of Ninit [cycles]	Number of Run-Outs	Average N_{init}/N_{total}
Case 1	3,383,626	4,383,220	140994.9524	0	4.17%
Case 2	6,966,511	4,377,273	134257.1057	0	1.93%
Case 3	5,170,307	4,655,183	176406.6936	0	3.41%
Case 4	4,038,776	3,497,133	275352.9503	0	6.82%
Case 5	6,608,029	4,560,982	134345.8523	0	2.03%
Case 6	5,846,009	4,733,766	136834.0872	0	2.34%
Case 7	916,953	2,075,390	163176.7136	0	17.80%
Case 8	3,139,856	4,299,379	132969.8994	0	4.23%

7.3.3. Probability of Failures and Reliability Indices

For fatigue category *C*, which represents the cruciform welded details, the following parameters were used (Kwon and Frangopol 2010):

Fatigue detail coefficient, $A = 1.44 \times 10^{12}$ (MPa^3)

Intercept, mean value E(logA) = 10.0

Intercept, lower bound E(logA) – 3 x σ(LogA) = 9.25

Constant amplitude fatigue limit, CAFL = 68.9 MPa

From Table 4.4, the probabilistic stress range prediction for maximum moment- one span length of 36.0 m using Quebec-Batiscan. The lognormal of mean is 3.74; therefore the mean is 42.1 MPa. This span is chosen arbitrarily to model an average bridge span length. Moreover, its mean stress range value is close to the mean stress of 50 MPa employed in the finite element analysis. By implementing Eq. (7.3), the total number of cycles during the monitoring period for one span length of 36.0 m is predicted as:

$$Log N_T = (10 - 3 \times 0.25) - 3 \times Log\, 42.1$$

$$N_T = 23831 \text{ cycles}$$

The average daily truck traffic $ADTT = \frac{N_T}{Time} = \frac{23831}{130} = 184$ cycles/day

where Time = is the total monitoring time for Quebec-Batiscan WIM prediction

To predict the annual accumulated cycles per year, Equation 7.4 can be applied, assuming the annual traffic increase, α, is zero as there is no specific data about the traffic increase for the highways, where the WIM data were collected in Quebec.

N = 184 cycles / day x 365 days = 67160 cycles / year

In the fatigue life reliability, the coefficient of variation of the fatigue loading applied cycles (N_a) is assumed to be the same as the COV of the applied stress range.

The reliability analysis using Monte Carlo Simulation is carried out based on the fatigue limit state function illustrated in equation (7.1) to predict the probability of failure of the cruciform detail. Table 7.9 illustrates the probability of failures for various cases of weld profile dimensions using Quebec-Batiscan – maximum moment of one span of 36.0 m.

Table 7.9 *Probability of Failure for 6.4 mm weld size.*

Weld profile	Case 1	Case 2	Case 3	Case 4	Case 5	Case 6	Case 7	Case 8
Year	P_f	P_f	P_f	P_f	P_f	P_f	P_f	P_f
1	0.00026	0	0	0	0	0	0.10108	0.00057
5	0.03333	0	0.00086	0.00169	0.00001	0.00015	0.46819	0.04845
10	0.12835	0.0001	0.01216	0.02217	0.0005	0.00368	0.66939	0.1612
15	0.23352	0.00117	0.04156	0.07101	0.00364	0.01742	0.7695	0.27653
20	0.33108	0.00518	0.08698	0.13739	0.0129	0.04285	0.82908	0.37722
25	0.41679	0.01491	0.14183	0.21298	0.03037	0.08096	0.86804	0.46105

The fatigue reliability analyses could also represented by the relationship between the reliability indices versus the time. Figure 7.6 shows the fatigue reliability for the 6.4 mm nominal weld size.

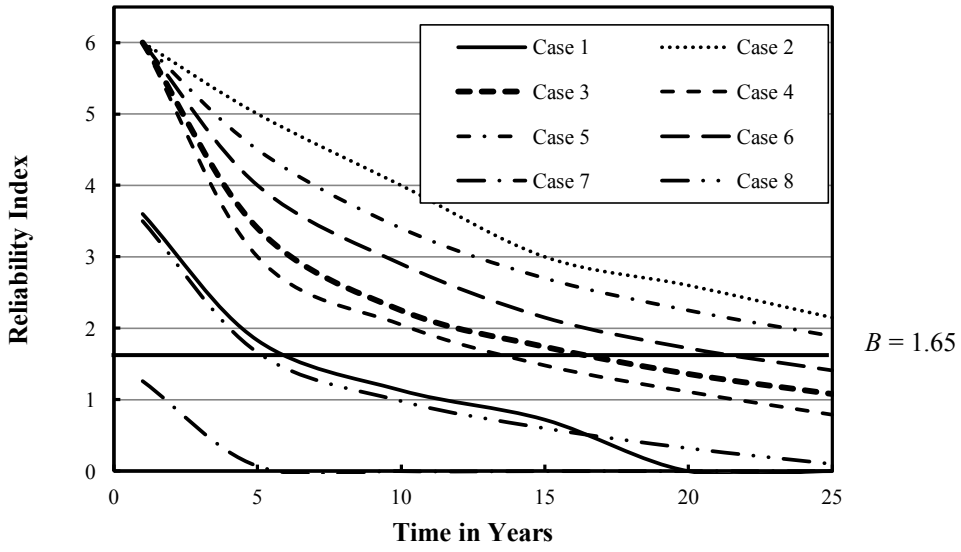

Figure 7.6 *Reliability indices versus time for 6.4 mm weld size.*

7.4. Discussion

7.4.1. Finite Element Results

In Table 7.5, the results of the plastic strain energy density and maximum stresses for the 6.4 mm weld size were shown for eight weld size cases as illustrated in Section 7.2.1.1. For each weld size case, the plastic strain energy density and the maximum stresses were predicted for three initial weld undercut size conditions: a) no undercut; b) 0.1 mm undercut; and c) 0.25 mm under cut. The plastic strain energy density increases as the stress range increases in all the weld size

cases; this was observed in all the results, and this observation matches with the findings of Ellyin (1997). The plastic strain energy density is highly dependent on the weld size profile, its value increases in the triangular fillet weld as well as convex weld profiles (e.g. case 1, 5, 6, 7 and 8). However, in cases 2, 3 and 4, where the weld profiles are concave, the plastic strain energy density decreases. Consequently, these observations are reflected in the predicted crack initiation lives, where concave weld profiles induced larger crack initiation lives, when compared to convex or triangular weld sizes under the same applied stress ranges. The plastic strain energy densities are also affected by the initial under cut. Table 7.5 emphasized that for any weld size case, the no-under cut condition induces the smallest value of plastic strain energy density. On the contrary, the highest values of plastic strain energy densities are induced when the initial undercut size is 0.1 mm, which acts as a sharp tip. In the 0.25 mm initial undercut, the values of the plastic strain energy densities are normally between the two extreme values (no undercut and 0.1 mm undercuts).

Table 7.6 introduced the results of maximum stresses at the crack initiation sites for the 6.4 mm nominal weld size, which are located at the weld toe intersection with the main plate for the same eight weld size, due to the maximum peak stresses in the applied stress ranges. In a similar behaviour to the plastic strain energy density, the maximum stresses at crack initiation sites are a function of the initial undercut size and the weld size profiles. The convex weld profiles, illustrated in cases 1, 5, 6, and 7, prompted higher stresses at crack initiation sites than the concave weld profiles in cases 2, 3 and 4. The results of maximum stresses in the triangular weld profile (case 8) were close to the results to the concave weld profile in case 2. Although the maximum stresses in this particular case were similar for cases 2 and 8, the values of plastic strain energy densities in case 8 are higher than those in case 2, which in turns, reflected in smaller crack initiation life for the triangular weld size than the concave weld size as shown in Section 7.3.2. Furthermore, the initial under-cut size played a role in determining the severity of the maximum stresses at crack initiation locations. The 0.1 mm undercut size induced the high values of stresses, while the no undercut condition exhibits the lowest values. The intermediate range of stresses between the zero and 0.1 mm undercut sizes occurred in the 0.25 mm undercut case.

7.4.2. Probabilistic Fatigue Resistance Life Predictions

In Table 7.8 of the 6.4 mm weld size, the total fatigue life of the concave weld profiles (e.g. cases 2 and 3) are generally larger than the total fatigue life of convex weld profiles (cases 1, 7 and 8). It is affected by many variables such as: the weld profile size, the shear and tension leg sizes, the initial undercut condition and the applied stress range during propagation. In case 7, crack initiation life should not be ignored as it comprised a significant portion of the fatigue life as both the maximum size of shear leg size and weld throat size led to the short total fatigue life in general. Moreover, due the variations of weld profile sizes, the percentage of crack initiation life to total fatigue life ranges between 1.93% and 17.8% for 6.4 mm fillet weld.

In general, variations in initial weld under cut, weld size have a great influence on the fatigue life prediction especially in the fatigue crack initiation phase. Other parameters like residual stresses, final crack size, material properties have lesser effect. Moreover, the geometry of the detail and the direction of loading could have an effect on the fatigue life prediction. Further investigations for other types of initial weld flaws could be studied.

7.4.3. Probability of Failures and Reliability Indices

The probability of failures of the weld detail, for the eight weld size cases of nominal size 6.4 mm, were predicted by defining the limit state function in equation (7.1), the probabilistic number of cycles for fatigue resistance (N_r) and applied number of cycles (N_a) due to probabilistic stress ranges which was predicted earlier in Chapter 4.

In Figure 7.6, it was observed that the weld sizes of cases 2 and 5 have more fatigue remaining life than the other cases for 6.4 mm weld size. This can be related to the degree of weld concavity in these two particular cases, when compared to the other cases. The two curves intersect with the minimum reliability index of 1.65, which was used also by Kwon and Frangopol (2010) in a range of 15 - 20 years. However, it is always a good practice to have inspection on critical weld details every 3 – 5 years. In case 7, where the fatigue life of weld resistance was less than one million cycle, immediate actions are required regarding the improving of fatigue life using one or more of the post-weld treatment techniques discussed in Chapter 2. In less than 5 years, cases 1 and 8 need fatigue life improvement. Other weld size cases: 4, 3 and 6 necessitated fatigue life improvement using the mentioned methods in Chapter 2 after 7, 8 and 12 years respectively.

In summary, the fatigue life reliability indicates that the concave weld profiles could generally induce fatigue life that last more than the convex ones for the 6.4 mm weld. Furthermore, the fatigue life reliability emphasized the need of fatigue life improvements, which in some cases is required immediately, or in a range of five years. The study developed reliability index versus time for each weld size case to illustrate clearly which weld details have larger fatigue life than others and which welds that require immediate actions. From Figure 7.6, one can observe few weld profiles illustrated a prolonged fatigue life without any anticipated repairs throughout the service life of the detail. However, the good practice in bridge maintenance requires periodic inspections from three to five years to allow for early detection of fatigue cracks and then start implementing the appropriate repair procedures.

8. SUMMARY, CONCLUSIONS AND FUTURE RECOMMENDATIONS

8.1. Summary

This research focused on the reliable prediction of fatigue life for welded detail in steel bridges taking into account the fatigue loading and resistance. This was achieved by four research objectives. The first objective was the implementation of the weight-in-motion (WIM) databases received from two provinces (Ontario and Quebec) and one territory (Northwest Territories) in Canada to calibrate the current fatigue truck factor and equivalent number of cycles due to truck passage, N_d, used in the Canadian Highway Bridge Design Code (CHBDC) (CSA 2006). This calibration was based on dual slope fatigue design (S-N) curves, which is currently applied in CSA-S16-09 (CSA 2009). The second objective was the establishment of a methodology to transform actual truck data received from the same sources in Canada into stress range histograms, which could be modeled probabilistically for fatigue life reliability predictions. The third objective was to investigate experimentally and numerically the weld toe grinding as a method of fatigue life improvement of severe welded details "Category E" in existing steel bridges. Finally, the study aimed to develop a procedure for the assessment of fatigue life reliability prediction for cruciform welded detail. This assessment employed previous experimental and literature data of fatigue material properties for fatigue crack initiation and propagation stages.

The collected WIM data from Ontario, Quebec, and NWT in Canada was employed in the calibration of fatigue truck factor, reduction factor and equivalent stress cycles. For calibration purposes, gross errors that represent unphysical data (GVW $\leq$ 0 and speed $\leq$ 0) in WIM data were first removed. Then, the study implemented WIM filtration criteria based on several researches in the United States, Europe and South Africa on the received WIM data in addition to the current truck limitations in Canada (TAC 1991). Load histories at critical locations in one, two and five span bridge with spans range from 2.0 m to 70.0 m were developed using the influence lines. The research used rainflow cyclic counting method to transform the bending moment loading histories into bending moment range spectra. These histograms used both single and dual slope fatigue design curves to predict the fatigue truck factors for each bridge span length and configuration based on equating the fatigue damage from actual trucks and design trucks. Recommended values for fatigue truck factor and reduction factor were presented. The study also validated the current equivalent number of cycles based on the new recommended

truck factors and single slope fatigue design curves. Moreover, new values for equivalent stress cycles were presented using dual slope fatigue design curves. These values are used to estimate the annual number of cycles due to truck passage for fatigue life reliability.

For the reliability-based approach of the fatigue life prediction, load range spectrums must be defined in probabilistic distributions. The study only considered the WIM from Ontario and Quebec for the probabilistic load history and spectrum prediction as their results in fatigue truck calibration were almost the same compared to the NWT WIM data, which comprised a lot of light weight vehicles which will have no effect on the fatigue life. The bending moment range histograms, predicted for the fatigue truck calibration, were employed for one, two and five-span bridges for spans that range from 6.0 m to 60.0 m. By assuming appropriate built-up steel sections, the study converted these moment range histograms into stress range histograms. Finally, the stress range histograms are fitted into suitable probabilistic distributions with defined parameters (e.g. mean, standard deviation, etc.) for various span lengths.

The study investigated the effect of weld toe grinding as a tool for post-weld treatment to improve the fatigue life. The weld toe grinding aimed to relieve the stress concentrations at toes due to the welding processes by producing a favourable weld shape and by removing harmful defects and undercuts at the weld toe. Full-scale fatigue tests on severe structural welding detail (Category-E) were carried out to investigate the effect of weld toe grinding effect on the fatigue life improvement.

The fatigue lives from the full-scale fatigue test results, were predicted using deterministic approaches. Finite element models were developed to assess the effect of no flaw, spherical/elliptical flaws and residual stresses on energy-based method parameters in the fatigue life initiation prediction. Several numerical methods to illustrate the crack initiation and propagation lives were assessed. These methods took into account extreme flaw crack sizes, absence or presence of crack closure (residual stresses) and threshold stress intensity factor range, and absence or presence of crack closure. The study employed the fatigue material properties of base and weld metal already assessed in previous research work at the University of Alberta since there was no change in the material type. As a result, the study determined the most suitable deterministic fatigue life method to validate the developed model against the test results of the full-scale specimens, which was used in the probabilistic prediction.

Fatigue life predictions using probabilistic approaches were carried out on a cruciform weld detail from literature. The results indicated the significant effect of the weld size profile whether: convex, concave or straight along with the tension leg weld size on the predicted fatigue life resistance of the investigated details especially in the fatigue crack initiation stage. Another important factor that affected the fatigue life resistance is the initial weld undercut size. For the probabilistic fatigue life prediction using Monte-Carlo Simulation, the study modeled the effective input parameters in its probabilistic forms, while other parameters that have minor effect on the results were in its deterministic forms.

The current research work focused on the development of a reliability-based approach to account for loading and fatigue resistance uncertainties for steel welded details in aging steel highway bridges. The study developed a procedure to estimate the fatigue loading cycles due to the truck traffic by using the probabilistic distributions with its defining parameters and average daily truck traffic (ADTT) for Quebec WIM data. The reliability approach to predict the remaining fatigue life of the cruciform detail was developed for simple span bridge of 36.0 m length from WIM Quebec-Batiscan. The effective input parameters of the fatigue life prediction for the load and the resistance were modeled in their probabilistic forms. By applying the fatigue limit state; this study predicted the probability of failures and reliability indices for each case of the weld profile of the investigated cruciform welded detail.

To keep the scope of the research focused, the study considered several assumptions and limitations. First of all; it assumed a step size of 1.0 m to predict the loading histories using WIM truck data (Axle weight and axle spacing) at critical locations for all bridge span lengths. Secondly, the loading histories considered one passing truck at a time and did not take into account multiple presences of more than one truck. The study ignored the dynamic effects including the pavement roughness in the fatigue truck calibration, which could result in a decrease in the fatigue truck factor (Hong *et al.* 2010). Then, the study implemented the procedure to assess the tolerances in WIM measurement for Class 9 trucks only due to the lack of information of static weights for the rest of the truck classes. Afterwards, the deterministic fatigue life prediction assumed that crack will initiate from the center of the bottom flange. It also considered one weld flaw shape either spherical or elliptical and did not take into account other shapes or multiple flaws. Furthermore, the probabilistic fatigue life prediction of the bridge detail focussed on fatigue category C only. It also considered the variations in initial weld

undercut with maximum size of 0.25 mm (W59 2013) and weld profiles of nominal size of 6.4 mm only. Finally, the study considered fatigue mode I loading that controls crack behaviour in the propagation stage (Broek 1989).

8.2. Conclusions

The following conclusions can be drawn from the work described above:

The study introduced screening criteria to be implemented on received WIM data based on previous researches and taking into account the current regulations for truck weights and dimensions in Canada. It also emphasized the importance of conducting the proper pre-screening procedure to ensure the quality of WIM data involved in the fatigue truck calibration and load history prediction by getting rid of any encountered unrealistic data and implementing specific screening criteria. The outcomes of fatigue truck calibration illustrated that two parameters affected the fatigue truck factor: the span length for both single and dual slope fatigue curves; the fatigue detail category influences truck factor for short spans and dual slope curves only. In bridge span lengths less than 12.0 m, there is a great variability in truck factors values. Then, this variability decreases from span lengths 12.0 m to 30.0 m. The fatigue truck factor is almost constant in most cases for span lengths beyond 30.0 m. Consequently, the study suggested three fatigue truck factors for three different span ranges to account for this variation due to span lengths for single and dual slope fatigue design curves. Using the same concept (truck factor vs span range), equivalent numbers of stress cycles are introduced for the same bridge span ranges. The study recommended new values for the fatigue truck factor, reduction factor and the equivalent stress cycles due to the passage of design truck for various bridge span ranges using single and dual slope fatigue design curves, which could be implemented in CSA-S6-06 (CSA 2006).

The variability in truck loads should be incorporated into a reliability-based approach to represent the loading portion of the fatigue limit state. Most realistic results are obtained through WIM data on specific highways, which are known to have heavy truck traffic. The study assessed the measurement tolerances for WIM from Ontario and Quebec using ASTM E1318 (2009). It was found that the measurement tolerances in WIM measurements are within the standard limits. For fatigue life reliability assessments, stress range histograms, using Ontario and Quebec WIM data, were developed in their probabilistic forms (e.g. mean, standard

deviation, type of the probabilistic distribution). These probabilistic models were defined for span length that ranged from 6.0 m to 60.0 m for midspan and at support sections in one, two and five bridge spans.

In the experimental program, one ground specimen showed a significant improvement in fatigue life (around 60%) compared to the non-ground specimen, which matched the expected increase in fatigue life in literature. However, some adverse effects in the fatigue life using weld-toe grinding could result from weld imperfections or unevenness in weld profile. As a result, the fatigue life of the other ground specimen did not improve since these stress raisers acted as potential crack initiation sites and crack propagation occurred faster.

The deterministic fatigue life prediction is best represented with an energy-based approach for crack initiation life and a linear elastic fracture mechanics approach, including the threshold stress intensity factor range and crack closure, for the crack propagation life. An initial spherical flaw size of 0.1 mm with no residual stresses led to the most accurate prediction of fatigue resistance of the tested specimens.

In the probabilistic fatigue life prediction of welded steel details, the results showed that fillet weld size, profiles as well as weld undercuts affected the predicted fatigue life of critical details. In general, convex weld profiles induced higher stresses and plastic strain energies, when compared to the concave weld profiles. Moreover, the 0.1 mm weld undercut size induced the higher values of maximum stresses and plastic strain energy densities compared to the 0.25 mm undercut size or no undercut at all.

The developed reliability-based analysis allowed for the prediction of the remaining fatigue life of steel detail. For eight different weld profiles in 6.4 mm nominal size, the study illustrated the reliability indices versus time to determine the consequence of failure, inspection management, crack growth rates and redundancies. The study employed Monte Carlo Simulation to solve the limit state function.

In general, for welded details, the total fatigue life is primarily governed by crack propagation. Approximations that simplify the shape of flaws and the distribution of residual stresses are therefore adequate for the fatigue life prediction of welded details.

8.3. Recommendations

Dual slope fatigue design curves should be introduced in the Canadian Highway Bridge Design Code (CHBDC). Moreover, fatigue truck factors should take into account the bridge span lengths and presented for three bridge span ranges: span length < 12.0 m, 12.0 m ≤ span length ≤ 30.0m and span length > 30.0 m. The study predicted the load histories using a step size of 1.0 m for various bridge span lengths. This step could have an effect on the accuracy of the developed load histories using influence lines especially for the short bridge spans (2.0 m to 6.0 m). Further investigations are required to increase the fatigue truck calibration accuracy for such spans by employing step size < 1.0 m. Future studies should take into account the dynamic effects such as pavement roughness for better prediction of the fatigue truck calibration.

Bridge owners should provide static weight measurements for the same trucks, predicted from the WIM data, to assess the systematic and random errors in WIM data more precisely. Moreover, WIM databases should be recorded annually on specific locations which could experience a high traffic demand to predict the traffic growth. Finally, bridge owners should enforce rules for recording the total time taken in WIM monitoring, as this will assist in predicting the ADTT, which will be used to determine the actual number of cycles using probabilistic stress range histograms

More full-scale fatigue tests should be carried out to quantify the effect of grinding of fatigue life improvement. More refined welds should be fabricated to reduce the effect of unevenness and irregularities that might induced during the welding process.

The initial flaw size proved to be the most the influencing parameter affecting the fatigue life of any bridge detail. More comprehensive investigations are required to characterize the shape of weld flaws, two or more initial flaws, and flaws due to mechanical damage. The crack propagation model in this study assumed mode I loading (tensile). However, some structural details are subjected to other loading modes. Especially the effect of mode III loading (tearing), which might be present in some bridges due to e.g. out-of-plane distortions, requires investigation.

More studies are required to assess the effect of weld profiles of weld nominal sizes bigger than 6.4 mm on energy parameters (plastic strain energy density and maximum stresses). Thus, the effect of its variability on the prediction of crack initiation life should be properly assessed. This

research covered the cruciform details for probabilistic fatigue life prediction; more investigations are required for other bridge weld details.

LIST OF REFERENCES

AASHTO (2007). “LRFD bridge design specifications”, American Association of State Highway and Transportation Officials, 4th Edition. With Interims, Washington, D.C.

AASHTO/AWS (2008). “Bridge welding code. AASHTO/AWS D1.5M/D1.5”, American Association of State Highway and Transportation Officials, Washington, D.C./American Welding Society, Miami, USA.

Ackermann, G., Theyse, H., Kannemeyer, L. and AS, C.V. (2008). “Current status of weigh-in-motion in sub Sahara Africa”. Proc. of the International Conference on Heavy Vehicles, May 19-22, Paris.

Agerskov, H. and Nielsen, J.A. (1999). “Fatigue in steel highway bridges under random loading”. J. Struc. Engrg., 125(2), 152-162.

Anderson, T. L. (2005). “ Fracture mechanics, fundamentals and applications”. 3rd Edition, CRC Press, Boca Raton, USA.

Ang, A. H.-S. and Cornell, A.M. (1974). “Reliability bases of structural safety and design”. J. Str. Div., 100, ST9, 1755 – 1769.

Ang, A. H-S. and Tang, W.H. (1984). “Probability concepts in engineering planning and design, Vol. II: Decision, risk, and reliability”. John Wiley and Sons, New York, USA.

Aoki, T., Nakano, K., Fukuhara, H., Okada, A., Kobayashi, S., Kimura, K. and Inagaki, M. (1986). “Fatigue life and corrosion fatigue life prediction of welded joints of structural steel containing planar defects”. Trans. of the Iron and Steel Institute of Japan, 26(11), 977-984.

ASTM Designation E1318 (ASTM 2009). “Standard specification for highway weigh-in-motion WIM systems with user requirements and test method”. American Society for Testing and Materials, Philadelphia, USA.

ASTM Designation E1049-85E1 (ASTM 2011). “Standard practices for cycle counting in fatigue analysis”. American Society of Testing Materials, West Conshohocken, PA, USA.

AWS 5.20/5.20 M (2005). “Specifications for carbon steel electrodes for flux cored arc welding”. American Welding Society, Miami, USA.

AWS D1.1/D1.1M (2008). “Structural welding code – Steel”. American Welding Society, Miami, USA.

Banz, A. and Nussbaumer, A. (2001). “Fiabilité des ponts métalliqués vis á vis de l’état limite combine fatigue et rupture” (Reliability of steel bridges under the combined limit state of fatigue and fracture). Report 446, ICOM Steel Structures Institute, Swiss Federal Institute of Technology, Lausanne, Switzerland.

BD 77/98 (1999). “Assessment of steel highway bridges for residual fatigue life”. Draft Highways Agency Standard, London.

Bergan, A.T., Berthelot, C. F. and Taylor, B. (1997). "Effect of weigh-in-motion accuracy on weight enforcement efficiency, International Road Dynamics". Technical Paper: http://www.irdinc.com/english/html/tech-ppr/index.htm, June 1, 2005.

Bignonnet, A., Lieurade, H.P., Picouet, L. and Castex, L. (1987). "Shot peening of welded joints and residual stress relaxation during fatigue". 3rd Int. Conf. on Shot Peening, 585-594.

Bokalrud, T. and Karlsen, A. (1982). "Probabilistic fracture mechanics evaluation of fatigue failure from weld defects in butt weld joints". Conf. on Fitness for Purpose Validation of Welded Construction, 1, The Welding Institute, Cambridge, UK.

Bowman, M.D. and Quinn, B.P. (1994). "Examination of fillet weld strength". AISC Engrg. J., 31(3), 98-108.

Bremen, U (1989). "Amelioration du comportement à la fatigue d'assemblages sou-dés : étude et modelisation de l'effet de contraintes residuelles". EPFL Thesis No. 787, Lausanne, Switzerland.

Broek, D. (1989). " The practical use of fracture mechanics". 2nd Printing, Kluwer Academic Publishers. Dordrecht, The Netherlands.

Brückner, A. and Munz, D. (1982). "Curve fitting to defect size distributions for the calculations of failure probabilities". Nuclear Engineering and Design, 74, 75-78.

BSI 7910 (2005). "Guide to methods for assessing the acceptability of flaws in metallic structures". British Standard Institute, London, UK.

Butler, L.J. and Kulak, G. L. (1971). "Strength of fillet welds as a function of direction of load". Welding J., Welding Research Supplement, 36(5), 231s-235s.

Butler, L.J., Pal, S. and Kulak, G.L. (1972). "Eccentrically loaded welded connections". J. Str. Div., ASCE, 98, ST5, 989-1005.

Carper, K. (1998). : "Failures in architecture & engineering: What are the lessons?", EPFL Conferences, Lausanne, Switzerland.

Chan, K.S. and Miller, A.K. (1982). "Prediction of fatigue failure in structural alloys: Initiation and crack propagation". Int. Symp. for Testing and Failure Analysis, ASM International, Metals Park, OH, 272-279.

Chen, H., Grondin, G.Y. and Driver, R. (2005). "Fatigue resistance of high perfomance steel". Structural Engineering Report No. 258, Dept. of Civ. and Envir. Engrg., University of Alberta, Edmonton, Canada.

Cheng, W. and Finnie, I. (1993). "Measurement of residual stress distributions near the toe of an attachment welded on a plate using the crack compliance method". Engrg. Fracture Mech., 46, 79-91.

Cheng, X., Fisher, J. W., Prask, H. J., Gnaupel-Herold, T, Yesn, B. T., and Roy, S. (2003) "Residual stresses modification by post-weld treatment and its beneficial effect on fatigue strength of welded structures". Int. J. of Fatigue, 25, 1259-1269.

Cheung, M.S. and Li, W.C. (2003). "Probabilistic fatigue and fracture analyses of steel bridges". Struc. Safety, 23, 245-262.

Clark, P.J. (1971). "Basis of design for fillet welded-joints under static loading". Proc. of Conf. on Improving Welded Product Design, The Welding Institute, Cambridge, England, 85-96.

Cornell, C.A. (1969). "A probability-based structural code". J. of the American Concrete Institute, 66(12), 974 – 985.

Coughlin, R. and Walbridge, S. (2010). "Fatigue correction factors and design S-N curves for welded aluminum highway bridge structures". Proc., 8th Int. Conf. on Short and Medium Span Bridges. Niagara Falls, Canada.

CSA-W59-13 (2013). "Welded steel construction (Metal Arc Welding)". Canadian Standards Association International, Mississauga, Canada.

CSA-S6-06 (2006). "Canadian Highway Bridge Design Code". Canadian Standards Association International, Mississauga, Canada.

CSA-S16-09 (2009). "Limit States Design of Steel Structures". Canadian Standards Association International, Mississauga, Canada.

Cui, W. (2002). "A state-of-the-art review on fatigue life prediction methods for metal structures". J. Marine Science and Tech., 7, 43-56.

Davies, P. and Sommerville, F. (1987). "Calibration and accuracy testing of weigh-in-motion systems". Transportation Research Record, 1123, Transportation Research Board, Washington, D.C., 122–126.

DNV 30.6 (1992). "Structural reliability analysis of marine structures". Det Norske Veritas, Classification Notes No. 30.6, Høvik, Norway.

DNV-RP-C203 (2010). "Fatigue design of offshore steel structures". Det Norske Veritas, Høvik, Norway.

Dowling, N.E. (1999). "Mechanical behavior of materials: Engineering methods for deformation, fracture, and fatigue". 2nd Edition, Prentice Hall, Upper Saddle River, USA.

Ellyin, F. (1997). "Fatigue damage, crack growth and life prediction". Chapman and Hall, London, New York.

EN 25817 (1992). "Arc welded joints in steel – guidance on quality levels for imperfections". European Committee for Standardization, Brussels, Belgium.

Engesvik, K.M. and Moan, T. (1983). "Probabilistic analysis of the uncertainty in the fatigue capacity of welded joints". Engrg. Fracture Mech., 18(4), 743-762.

European Convention of Constructional Steelwork (ECCS) (2005). "Assessment of existing steel structures, remaining fatigue life". Technical Committee 6 – Fatigue.

Farkhideh, N. (2012). "Evaluation of weigh-in-motion systems in Alberta". M.Sc. thesis, University of Alberta, Edmonton, Canada.

Fisher, J.W., Mertz D.R. and Zhong, A (1983). "A steel bridge members under variable amplitude long life fatigue loading". NCHRP 267. Washington: Transportation Research Board.

Galambos, T.V. and Ravindra, M.K. (1978). "Properties of steel for use in LRFD". J. of Structural Div., 104, 1459-1468.

Gurney, T.R. (1979a). "An analysis of some fatigue crack propagation data for steel subjected to Pulsating Tension Loading". Welding Research International, 9(4), 45 – 59.

Gurney, T.R. (1979b). "Fatigue of welded stuctures". 2nd Edition, Cambridge University Press, Cambridge, UK.

Higgins, T.R. and Preece, F.R. (1969). "Proposed working stress for fillet welds in building construction". Engrg. J. AISC, 6(1), 16-20.

Health and Safety Executive (HSE) (1999). "Review of probabilistic inspection analysis methods". Offshore Tech. Rep. 1999/061, Aker Offshore Partner, Sandsli, Norway.

Hong, H. P., Goda, K., Lam, C. and Au A. (2010). "Assessment of fatigue reliability of steel girder bridges". Proc. 8th Int. Conf. on Short and Medium Span Bridges. Niagara Falls, Canada.

Joint Committee on Structural Safety (JCSS) (2001). "Probabilistic model code, Part 3 – Resistance models". Federal Institute of Technology, Zurich, Switzerland.

Josi, G. and Grondin, G.Y. (2010). "Reliability-based management of fatigue failures". Structural Engineering Report No. 285, Dept. of Civ. and Envir. Engrg., University of Alberta, Edmonton, Canada.

Kirkhope, K.J., Bell, R., Caron, L., Basu, R.I. and Ma, K.-T (1999). "Weld detail fatigue life improvement techniques. Part 1: review". Marine Structures, 12, 447 -474.

Kulak, G.L. and Grondin, G.Y. (2006). "Limit state design in structural steel". 8th Edition, Canadian Institute of Steel Construction, Willowdale, Canada.

Kwon, K. and Frangopol, D. M. (2010). "Bridge fatigue reliability assessment using probability density functions of equivalent stress range based on field monitoring data". Int. J. of Fatigue, 32, 1221 – 1232.

Lagoda, T. (2008). “Lifetime estimation of welded joints”. Springer-Verlag, Berlin Heidelberg: Springer Publications.

Lawrence, F.V. (1981). “The Predicted influence of weld residual stresses on fatigue crack initiation”. Industrial Diamond Review, 53-60.

Lotsberg, I., Sigurdsson, G., and Wold, P.T. (2000). “Probabilistic inspection planning of the Åsgard A FPSO hull structure with respect to fatigue”. J. Offshore Mech. and Arctic Engrg., 122, 66 – 72.

Lukic, M. and Cremona, C. (2001). “Probabilistic assessment of welded joints versus fatigue and fracture”. J. Struc. Engrg., 127(2), 211-218.

Maddox, S J. (1991). “Fatigue strength of welded structures”. 2nd Edition, Woodhead Publishing Ltd., Cambridge, UK.

Matsuishi, M. and Endo, T. (1968). “Fatigue of metals subjected to varying stress”. Japan Soc. Mech. Engineering.

Melchers, R.E. (1999). “Structural reliability analysis and prediction - 2nd Edition”. John Wiley and Sons Ltd., Chichester.

Metropolis, N. (1987). “The beginning of the Monte Carlo method”. Los Alamos Science, 1987, Special Issue.

Miazaga, G.S. and Kennedy, D.J.L. (1989). “Behavior of fillet welds as a function of the angle of loading”. Canadian J. Civil Engrg., 16(4), 583-599.

Miner, M.A. (1945). “Cumulative damage in fatigue”. Trans. ASME, 67, A159-64.

Moan. T. and Song, R. (2000).“Implications of inspection updating on system fatigue reliability of offshore structures”. J. Offshore Mech. and Arctic Engrg., 122, 173-180.

Mohr, W. C, Tsai, C., Tso. C-M. (1995). “Fatigue strength of welds with profile and post-weld improvements”. Proc. of 4th Int. Conf. Offshore Mech. and Arctic Engrg., Copenhagen, Denmark.

Ng, A.K.F., Driver, R.G. and Grondin, G.Y. (2002). “Behaviour of transverse fillet welds”. Structural Engineering Report No. 245. Dept. of Civil and Envir. Engrg., University of Alberta, Edmonton, Canada.

O’Brien, E.J., and Enright, B. (2013). “Using weigh-in-motion data to determine aggressiveness of traffic for bridge loading”. J. Bridge Engrg., 18(3), 232-239.

Oehme, P. (1989). “Schäden an stahltragwerken – eine Analyse (Damage analysis of steel structures)”, IABSE Proceedings, paper No. 139/89.

Ohta, A., Soya, I., Nishijma, S. and Kosuge, M. (1986). “Statistical evaluation of fatigue crack propagation properties including threshold stress intensity factor”. Engrg. Fracture Mech., 24(6), 789 – 802.

Paris, P. and Erdogan, F. (1963). “A critical analysis of crack propagation laws”. Trans. ASME, 85, 528 – 534.

Pelphrey, J., Higgins, C., Sivakumar, B., Groff, R., Hartman, B.H., Charbonneau, J.P., Rooper, J.W. and Johnson, B.V. (2008). “State-specific LRFR live load factors using weigh-in-motion data”. J. Bridge Engrg., 13(4), 339-350.

Porter-Goff, R.F.D., Free, J.A. and Tsiagbe, W.Z. (1988). “Residual stresses in welded tubular nodes”. In: Fatigue of offshore structures, W.D. Dover and G. Glinka (Eds.), 285-295.

Prozzi, J.A. and Hong, F. (2007). “Effect of weigh-in-motion system measurement errors on load-pavement impact estimation”. J. Transp. Engrg., 133 (1), 1-10.

Radaj, D. (1990). “Design and analysis of fatigue resistance welded structures”. Abington Publishing, Cambridge, UK.

Radaj, D. and Sonsino, C.M. (1998). “Fatigue assessment of welded joints by local approaches”. Abington Publishing, Cambridge, England.

Righiniotis, T.D., and Chryssanthopoulos, M.K. (2003). “Probabilistic fatigue analysis under constant amplitude loading”. J. of Constr. Steel Research, 59, 867-886.

Righiniotis, T.D., and Chryssanthopoulos, M.K. (2004). “Fatigue and fracture simulation of welded bridge details through a bi-linear crack growth law”. J. of Struct. Safety, 26, 141-158.

Righiniotis, T.D. (2004). “Influence of management actions on fatigue reliability of a welded joint”. Int. J. Fatigue, 26, 231-239.

Sarihan, V. (1994). “Energy based methodology for damage and life prediction of solder joints under thermal cycling”. IEEE Transactions on Components, Packaging and Manufacturing Technology, Part B, Advanced Packaging, 17(4), 626-631.

Shantz, C. (2010). “Uncertainty quantificattion in crack growth modeling under multi-axial variable amplitude loading”. Ph.D. Thesis, Vanderbilt University, Nashville, Tennessee, USA.

Shetty, N.K. and Baker, M.J. (1990). “Fatigue relibaility of tubular joints in offshore structures: Reliability analysis”. Proc. of the 9th Int. Conf. on Offshore Mechanics and Arctic Engineering-OMAE, 2, 33-40.

Simonen, F. A. (1995). “Non-destructive examination reliability. In: Probabilistic structural mechanics handbook”. C. Sundarajan (Editor), Chapan & Hall, New York, USA, 238-260.

Smith, I.F.C. and Hirt, M.A. (1985). “A review of fatigue strength improvement methods”. Canadian J. Civil Engrg., 12, 166-183.

Smith, I.F.C. and Smith, R.A. (1982). “Defects and crack development in fillet welded joints”. Fatigue Engrg. Materials and Str., 5, 151-165.

Smith, K. N., Watson, P. and Topper, T. H. (1970). “A stress-strain function for the fatigue of materials”. J. of Materials, 15(4), 767-778.

Snyder, R. E., Likins, G. E. Likins and Moses, F. (1985). “Loading spectrum experienced by bridge structures in the United States, FHWA/RD, Report-85/012, FHWA, U.S. Department of Transportation (1985).

Sivakumar, B., Ghosn, M., Moses, F., Lichtenstein Consulting Engineers Inc., and Paramus, NJ (2008). “Protocols for collecting and using traffic data in bridge design, NCHRP (Web-only Document 135). Final report for NCHRP project 12-76, Tranportation Research Board.

Stacey, A., Barthelemy, J.-Y., Leggatt, R H. and Ainsworth, R.A. (2000). “Incorporation of residual stresses into the SINTAP defect assessment procedure”. Engrg. Fracture Mech., 67, 573-611.

Straub, D. and Faber, M.H. (2004). “Systems effects in generic risk-based inspection planning”. J. Offshore Mech. Arctic Engrg., 126, 265-271.

Transportation Association of Canada (TAC) (TAC 1991). “Memorandum of understanding respecting a federal-provincial-territorial agreement on vehicle weight and dimensions”. Council of Ministers Responsible for Transportation and Highway Safety, Transportation Association of Canada, Ottawa.

Vårdal, O.T., Moan, T. and Hellevig, N.-C. (1999). “Comparison between observed and predicted characteristics of fatigue cracks in North Sea jackets”. Proc. of the Annual Offshore Technology Conf., 3, 243-252.

Wang, T.-L., Liu, C., Huang, D. and Shahawy, M. (2005). “Truck loading and fatigue damage analysis for girder bridges based on weigh-in-motion data”. J. Bridge Engrg., 1, 12-20.

Walbridge, S. (2005). “A Probabilistic study of fatigue in post-weld treated tubular bridge structures”. Ph.D. Thesis No. 3330, Swiss Federal Institute of Technology, Laussane, Switzerland.

Weisstein, E.W. (2003). “Normal sum distribution. Math World – A Wolfram Web Resource”. Wolfram Research Inc., Champaign, USA.

Wright, W. (1996). “Post-weld treatment of a welded bridge girder by ultrasonic hammer peening”. Internal Research Report, Federal Highway Administration, Turner Fairbank Highway Research Center, McLean, VA, USA.

Yazdani, N. and Albrecht, P. (1990). “Probabilistic fracture mechanics applications to highway bridges”. Engrg. Fracture Mech., 37(5), 969-985.

Yin, Y., Grondin, G.Y. and Elwi, A.E. (2006). “Fatigue crack behaviour in mine excavator”. Structural Engineering Report No. 265, Dept. of Civ. and Envir. Engrg., University of Alberta, Edmonton, Canada.

Zhi, X., Shalaby, A., Middleton, D. and Clayton, A.(1999). “Evaluation of weigh-in-motion in Manitoba”. Canadian J. of Civ. Engrg., 26, 655-666.

APPENDIX A

Probability Density Functions

Probability density functions

The probability density functions (pdf), $f_x(x)$, and cumulative distribution functions, $F_x(x)$, used in the present work are:

- Exponential: Exp(λ)

$$f_x(x) = \frac{1}{\lambda}.e^{-x/\lambda}$$

$$F_x(x) = 1 - e^{-x/\lambda} \qquad \text{(A.1)}$$

- Normal: N(μ,σ)

$$f_x(x) = \frac{1}{\sqrt{2\pi}\sigma}.e^{-\frac{1}{2}\left(\frac{x-\mu}{\sigma}\right)^2}$$

(A.2)

$$F_x(x) = \int_{-\infty}^{x} \frac{1}{\sqrt{2\pi}\sigma}.e^{-\frac{1}{2}\left(\frac{y-\mu}{\sigma}\right)^2} dy \qquad \text{(no closed form solution)}$$

- Lognormal: LN(μ,σ)

$$f_x(x) = \frac{1}{\sqrt{2\pi}x\varepsilon}.e^{-\frac{1}{2}\left(\frac{\ln x-\lambda}{\varepsilon}\right)^2} \qquad \text{(A.3)}$$

$$F_x(x) = \int_{-\infty}^{x} \frac{1}{\sqrt{2\pi}y\varepsilon}.e^{-\frac{1}{2}\left(\frac{\ln y-\mu}{\sigma}\right)^2} dy$$

Where $\lambda = E\left[ln(X)\right]$ and $\varepsilon^2 = Var\left[ln(X)\right]$

The lognormal distribution can be expresses as a normal distribution by putting

$$x = ln(x)$$

$$\mu = ln(\alpha) - \frac{1}{2}ln\left(1 + \left(\frac{\beta}{\alpha}\right)^2\right) = ln(\alpha) - \frac{1}{2}\sigma^2$$

$$\sigma = \sqrt{ln\left(1 + \left(\frac{\beta}{\alpha}\right)^2\right)}$$

In equation (A.2), where $\alpha = E[X]$ (mean value) and $\beta = \sqrt{Var[X]}$ (standard deviation). The parameters of the lognormal distribution as used in the present work always refer to α, β (mean values and standard deviation) and not λ, ε.

- Weibull: $W(\theta, \tau)$

$$f_x(x) = \frac{\tau}{x}.\left(\frac{x}{\theta}\right)^{\tau}.e^{-\left(\frac{x}{\theta}\right)^{\tau}} \qquad \text{(A.4)}$$

$$F_x(x) = 1 - e^{-\left(\frac{x}{\theta}\right)^{\tau}}$$

APPENDIX B

Probabilistic crack propagation parameters proposed in the literature

Reference	Distribution for C	m	Remarks
Bokalrud and Karlsen (1982), DNV 30.6 (1992)	LN($3.47\text{x}10^{-13}$, $2.06\text{x}10^{-13}$)	3.1	Steel used for non-corrosive environment; based on 2207 measurements of various steel types with $0.10 \leq R \leq 0.85$
Shetty and Baker (1990)	LN($2.02\text{x}10^{-13}$, $5.05\text{x}10^{-14}$)	3.0	Steel used in air: average yield strength of 380 MPa
Lotsberg *et al.* (2000)	LN($6.31\text{x}10^{-13}$, $2.59\text{x}10^{-13}$)	2.88	Steel used in air; $R \geq 0.5$
Moan and Song (2000)	LN($1.10\text{x}10^{-13}$, $5.98\text{x}10^{-14}$)	3.10	Tubular steel in offshore structures
Banz and Nussbaumer (2001)	LN($1.89\text{x}10^{-13}$, $4.73\text{x}10^{-14}$)	3.0	Common bridge steel with nominal yield strength of approximately 350 MPa
Cheung and Li (2003)	LN($1.26\text{x}10^{-13}$, $7.94\text{x}10^{-14}$)	3.0	Common bridge steel
BSI (2005)	LN($3.98\text{x}10^{-13}$, $1.4\text{x}10^{-13}$) LN($5.86\text{x}10^{-13}$, $3.52\text{x}10^{-13}$)	2.88 2.88	Steels in air; $R < 0.5$ Steels in air; $R \geq 0.5$
Walbridge (2005)	LN($3.61\text{x}10^{-13}$, $2.15\text{x}10^{-13}$)	3.0	Common tubular bridge steel with nominal strength of approximately 350 MPa

APPENDIX C

MATLAB Code for Prediction of Load Histories, Rainflow Analysis and Probabilistic Prediction of Fatigue life

Matlab Code for prediction of load histories for one span

```
function [MYtotal,time] = my(L,increment,filenamexx);
tic
load ([filenamexx]);
MYtotal = [];
xx=size(inputs);
Ptotal=inputs(:,1:2:xx(2));
Stotal=inputs(:,2:2:xx(2));
increment=1;
max_length = ceil(L + sum(Stotal'));

for count = 1: length(max_length)
My =[];
   for n = 1:max_length(count)+1
P = Ptotal(count,:);
S = Stotal(count,:);

for i = 1:length(P)
X(i) = (((n-1)*increment)-[sum(S(1:i-1))]);
end

Y = zeros(1,length(X));
Y((X./L)<=0) = 0;
Y(((X./L)>0)&((X./L)<=0.5)) = (X(((X./L)>0)&((X./L)<=0.5))./2);
%Y(((X./L)>0.5)&((X./L)<1)) = ((1-X(((X./L)>0.5)&((X./L)<1)))./2);
Y(((X./L)>0.5)&((X./L)<1)) = (1 -(X(((X./L)>0.5)&((X./L)<1)))./L).*(L/2);
Y((X./L)>=1) = 0;


My(n) = sum(P.*Y);

end
MYtotal = [ MYtotal My];
end
MYtotal = MYtotal';
time = toc;


for L=2:2:70;
   [MYtotal,time]=my(L,1,'ontario')
   CZ=L/2;
   eval (['save' ' span' num2str(L) '.txt' ' MYtotal' ' -ascii'])
end
```

Sample Matlab Code for prediction of load Spectrum using rainflow analysis

```
function [no,xo]=rfdemo2(ext)
% function rfdemo2(ext)
%
% RFDEMO1 shows cycles extracted from signal
% using rainflow algoritm. Good for very long
% time signals (100 000 points).
%
% INPUT:  ext - option; number, vector with turning
%              points or pure signal. Default ext=10000.
%
% OUTPUT: no enable.
%
% SYNTAX:
%        >>rfdemo2
%        >>rfdemo2(50000)
%        >>rfdemo2(my_time_signal)

% By Adam Nies³ony
% ajn@po.opole.pl

load span70.txt;
s=span70;
error(nargchk(0,1,nargin))

if nargin==0,
   % turning points from 10000 random numbers
   ext=sig2ext(s);
end

ext=sig2ext(ext);
rf=rainflow(ext);
figure, rfhist(rf,30,'ampl')
%figure, rfhist(rf,30,'mean')
%figure, rfmatrix(rf,30,30)
[no,xo]=rfhist(rf,30,'ampl')
```

Sample Matlab Code for probabilsitic prediction of fatigue life

```
%Ntotal is the primary m-file
%input "Ntotal(x)" where x is the number of random
%sets that need to be generated

function Ntotal_NP(repetitions)

max = repetitions;                                  %max number of new values



t = 32.00;                                          % thickness
b = -0.059;                                         % fatigue strength exponent in crack initiation
calculation
c = -0.63;                                          % fatigue ductility exponent in crack initiation calculation
m = 3.0;                                            % exponent in crack propagation


% mean values and standard deviations of RVs; lognormal transformed to
% normal

m_ln_a_init = 0.1;                                  % initial crack size
s_ln_a_init = 0.04;
s_a_init = sqrt(log(1+(s_ln_a_init/m_ln_a_init)^2));
m_a_init = log(m_ln_a_init)-s_a_init^2/2;

% Crack initiation
m_ln_sigma_f = 630;                                 % strength coefficient
s_ln_sigma_f = 30;
s_sigma_f = sqrt(log(1+(s_ln_sigma_f/m_ln_sigma_f)^2));
m_sigma_f = log(m_ln_sigma_f)-s_sigma_f^2/2;

m_ln_epsilon_f = 0.34;                              % ductility coefficient
s_ln_epsilon_f = 0.07;
s_epsilon_f = sqrt(log(1+(s_ln_epsilon_f/m_ln_epsilon_f)^2));
m_epsilon_f = log(m_ln_epsilon_f)-s_epsilon_f^2/2;

m_ln_E = 207000;                                    % modulus of elasticity
s_ln_E = 5000;
s_E = sqrt(log(1+(s_ln_E/m_ln_E)^2));
m_E = log(m_ln_E)-s_E^2/2;

m_ln_delta_m = 50;                                  % stress range
s_ln_delta_m = 8;
s_delta_m = sqrt(log(1+(s_ln_delta_m/m_ln_delta_m)^2));
m_delta_m = log(m_ln_delta_m)-s_delta_m^2/2;

% Crack propagation
m_ln_smax = 375;                                    % maximum load stress in crack propagation
s_ln_smax = 26;
s_smax = sqrt(log(1+(s_ln_smax/m_ln_smax)^2));
m_smax = log(m_ln_smax)-s_smax^2/2;
```

```
m_ln_smin = 96;                                          % minimum load stress in crack propagation
s_ln_smin = 24;
s_smin = sqrt(log(1+(s_ln_smin/m_ln_smin)^2));
m_smin = log(m_ln_smin)-s_smin^2/2;

m_sres = 0.1;                                            % residual stress in crack propagation
s_sres = 0.0001;

m_ln_alpha = 0.5;                                        % crack aspect ratio a/c
s_ln_alpha = 0.16;
s_alpha = sqrt(log(1+(s_ln_alpha/m_ln_alpha)^2));
m_alpha = log(m_ln_alpha)-s_alpha^2/2;

m_ln_af = 16;                                            % final crack size
s_ln_af = 0.01;
s_af = sqrt(log(1+(s_ln_af/m_ln_af)^2));
m_af = log(m_ln_af)-s_af^2/2;

m_ln_C = 2.7E-13;                                        % fatigue propagation constant C
s_ln_C = 1.4E-13;
s_C = sqrt(log(1+(s_ln_C/m_ln_C)^2));
m_C = log(m_ln_C)-s_C^2/2;

m_ln_delta_K_th = 60;                                    % threshold stress intensity factor
s_ln_delta_K_th = 6;
s_delta_K_th = sqrt(log(1+(s_ln_delta_K_th/m_ln_delta_K_th)^2));
m_delta_K_th = log(m_ln_delta_K_th)-s_delta_K_th^2/2;

for i = 1:max                                            % loop as many times as required

   matrix_value = 0;                                     % initialize storage matrix placeholder
   matrix_value = matrix_value + 1;                      % increment matrix place holder

   % random number generator(s)

   % crack initiation
   XDe = rand;
   Xsigma_f = rand;
   Xsigma_max = rand;
   Xepsilon_f = rand;
   Xdelta_m = rand;
   XE = rand;

   %crack propagation
   Xsmax = rand;
   Xsmin = rand;
   Xsres = rand;
   Xa_init = rand;
   Xalpha = rand;
   Xaf = rand;
   XC = rand;
   Xdelta_K_th = rand;
```

```
   delta_m = exp(icdf('normal',Xdelta_m,m_delta_m,s_delta_m));
   sigma_f = exp(icdf('normal',Xsigma_f,m_sigma_f,s_sigma_f));                    %inverse cumulative distr.
generator(s)
   epsilon_f = exp(icdf('normal',Xepsilon_f,m_epsilon_f,s_epsilon_f));                    %format ->
icdf('name',Xname,A,B)
   E = exp(icdf('normal',XE,m_E,s_E));                                    %'name' is distribution type normal
distribution
                                                    %'Xname' is random variable
   smax = exp(icdf('normal',Xsmax,m_smax,s_smax));                    %'A' is mean'B' is std. dev.
   smin = exp(icdf('normal',Xsmin,m_smin,s_smin));
   sres = icdf('normal',Xsres,m_sres,s_sres);
   a_init = exp(icdf('normal',Xa_init,m_a_init,s_a_init));
   alpha = exp(icdf('normal',Xalpha,m_alpha,s_alpha));
   af = exp(icdf('normal',Xaf,m_af,s_af));
   C = exp(icdf('normal',XC,m_C,s_C));
   delta_K_th = exp(icdf('normal',Xdelta_K_th,m_delta_K_th,s_delta_K_th));



   if a_init > 0.1
      m_ln_De = 0.00015-0.0005*(a_init-0.1);                    % strain amplitude
   else
      m_ln_De = 0.00003+0.0013*a_init;
   end
   s_ln_De = 0.05*m_ln_De;
   s_De = sqrt(log(1+(s_ln_De/m_ln_De)^2));
   m_De = log(m_ln_De)-s_De^2/2;

   if a_init > 0.1
      m_sigma_max = 453.33-326.36*(a_init-0.1);                    % maximum stress in crack initiation
   else
      m_sigma_max = 294.87+1584.6*a_init;
   end
   s_sigma_max = 0.1*m_sigma_max;

   De = exp(icdf('normal',XDe,m_De,s_De));
   sigma_max = icdf('normal',Xsigma_max,m_sigma_max,s_sigma_max);


   a0 = a_init;


   A1max = (300/smax-1)/9.525;                    % A1 used to calculate stress gradient factor for
max stress
   A1min = 0;                                    % A1 used to calculate stress gradient factor for min
stress
   A1res = 0;                                    % A1 used to calculate stress gradient factor for res
stress


   %matrixA(1,matrix_value) = De;                    %places values into matrix for storage
```

```
   %matrixA(2,matrix_value) = sigma_f;                    %format -> matrixA(x,y)
   %matrixA(3,matrix_value) = sigma_m;                    %'matrixA' is name of matrix to store in
   %matrixA(4,matrix_value) = b;                          %'x' is row to store in
   %matrixA(5,matrix_value) = epsilon_f;                  %'y' is the column to store in which is
incremental with loop
   %matrixA(6,matrix_value) = c;
   %matrixA(7,matrix_value) = Ds;
   %matrixA(8,matrix_value) = a_init;
   %matrixA(9,matrix_value) = alpha;
   %matrixA(10,matrix_value) = af;
   %matrixA(11,matrix_value) = C;
   %matrixA(12,matrix_value) = m;
   %matrixA(13,matrix_value) = t;
   %matrixA(14,matrix_value) = delta_K_th;


   Ninit(i,1) = min(IS(b,epsilon_f,c,sigma_f,sigma_max,E,De,delta_m),10000000);          %crack
initiation uses randomly generated a_init as a0
   Nprop(i,1) = Npropagation(A1max,A1min,A1res,t,a0,af,alpha,C,delta_K_th,smax,smin,sres,m);    %crack prop
uses calculated atrans as a0

   Ntotal(i,1) = min(Ninit(i,1) + Nprop(i,1),10000000);          %combining total cycles


end

save Ninit -ascii Ninit                          %saves Ninit values to file called Ninit
save Nprop -ascii Nprop                          %saves Nprop values to file called Nprop
save Ntotal -ascii Ntotal                        %saves Ntotal values to file called Ntotal
```

APPENDIX D

Sample calculation for the design of built-up section and the prediction of stress ranges from moment ranges

Design Assumption

Span length = 6.0 m

Moment due to live load is the maximum moment for a simple span due to Ontario WIM data

Deck slab thickness = 200 mm

Asphalt thickness = 90 mm

Unit weight of concrete γ_c = 24.5 kN/m3

Unit weight of asphalt γ_c = 23.5 kN/m3

Fy = 350 MPa

Preliminary Proportioning of Built-up Section

Dead load = 0.2 x 24.5 x 1.0 + 0.09 x 23.5 x 1 = 8 kN/m'

Moment due dead load = 8 x 62 / 8 = 36 kN.m

Max. Moment for one span due to WIM trucks (kN.m) using Ontario truck data = 434.2 kN m (From the prediction of load history).

Mmax (ultimate) = 1.2 MD.L + 1.7 ML.L

= 1.2 x 36 + 1.7 x 434.2 = 781.3 kN m

The web height $h \simeq \left[\frac{M}{F_y}\right]^{1/3} \simeq \left[\frac{781.3 \times 10^6}{350}\right]^{1/3}$ =705 mm

Take the web height h = 750 mm

Assume minimum web thickness = 14 mm

$$A_f = \frac{M_f}{Fy.h} = \frac{781.3x106}{350x750} = 2977 \text{ mm2}$$

Assume the flange thickness is 20 mm and the flange width is 150 mm

Actual flange area = 20 x 150 = 3000 mm2 > 1977

Check of local buckling of web

$$\frac{h}{w} = \frac{750}{14} = 53.5 \le \frac{83000}{F_y} = 237$$

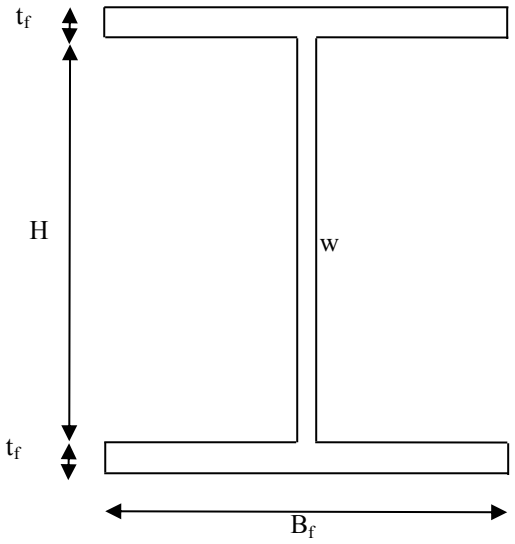

The stress range, $\Delta\sigma$, can be predicted from the moment range, ΔM , predicted from the rainflow of the moment history in Appendix C by defining the moment of inertia, I_{xx} , as follows:

$$\Delta\sigma = \frac{\Delta M}{I_{xx}}.y$$

In this sample, the ΔM = 3.617 kN.m, I_{xx} = 1381737500 mm4, y = 385 mm

Therefore, $\Delta\sigma$ = 1 MPa

APPENDIX E

Welding Procedure Specification

Welding procedure specification

Welding procedure

The welding of the wide flange beam and end plates of the large scale specimens was done by one welder according to the following procedure:

Electrode:	Arcair® DC copeerclad Pointed Electrode
	4.7 X 305 mm
	Carbon / graphite electrode with copper coating
Voltage:	~ 9.0 V
Amperage:	~ 300 A
Air Pressure:	~ 275 kPa (-40 psi)

Welding procedure Specification

The welding of the specimens described in Chapter 4 (pad for chemical analysis, welded plates), of the three test assemblies (three wide flange beam and three end plates) for the large scale tests presented in Chapter 4 was performed by one welder using the flux cored arc welding (FCAW) process and the following procedure:

Position:	Flat
Electrode:	Stein-Megafil® 713R (seamless rutile flux cored wire) with rapidly solidifying slag)
	AWS 5.20 [2005]: E491T1
Diameter:	1.2 mm (0.045 in.)
Voltage	~ 30.0 V
Wire feed speed:	~ 190 mm/s (~ 450 ipm), resulting in a current of ~ 300 A
Electrode extension:	~ 25 mm
Current and Polarity:	DCEP
Transfer:	Spray
Travel Speed:	~ 3.4 mm/s (~8 ipm), with stringer beads (no weaving)
Shielding Gas:	25% CO2 – 75% Ar (flow rate ~ 15 L/min)
Preheat Temp.	Min. 20°C
	Max. 230°C
Cooling Rate	Slow cool
Cleaning	Brushing and if needed gridning

APPENDIX F

Different Weld Profiles and Undercut Conditions for the Eight Cases of Weld Sizes Employed in the Finite Element Analysis

6.4 MM WELD SIZE

Different weld sizes cases for fillet weld size 6.4 mm as indicated above.

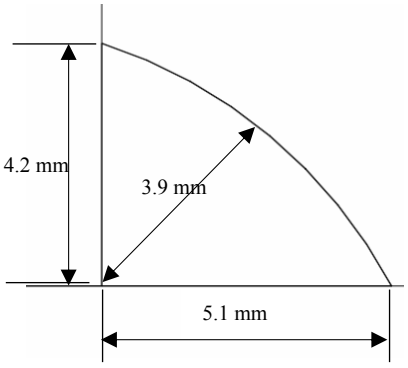

(a) No Under-cut

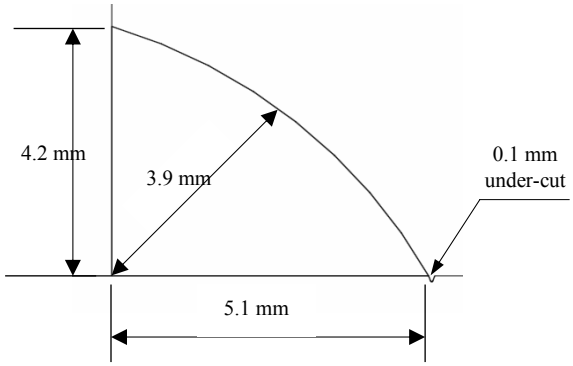

(a) 0.1 mm under-cut

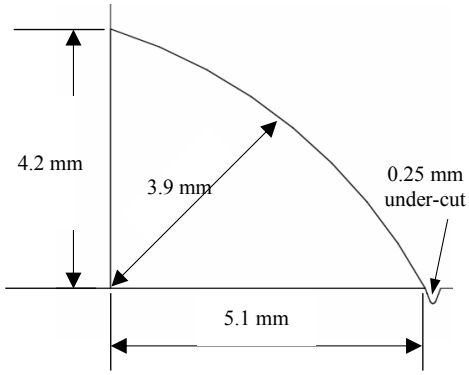

(c) 0.25 mm under cut

Figure F.1 *– Case 1 weld dimensions used in finite element model for nominal fillet weld 6.4 mm.*

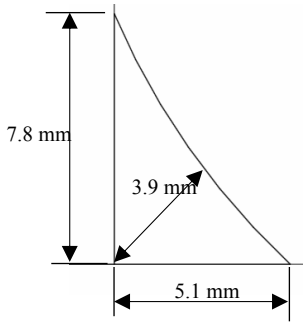

(a) No Under-cut

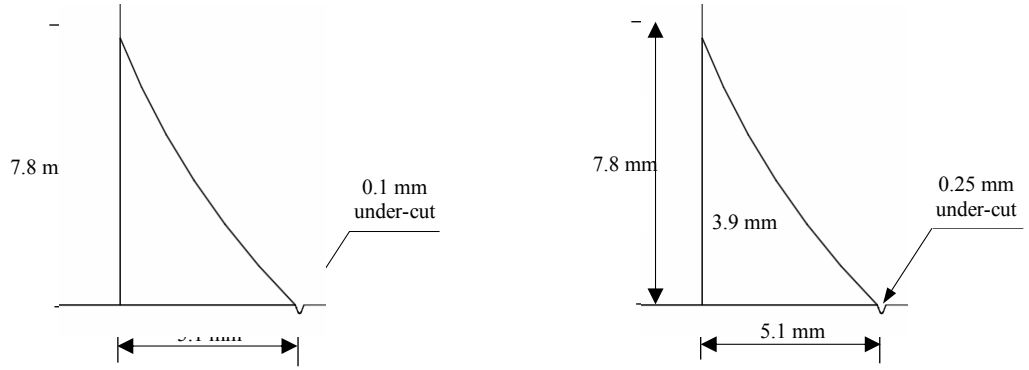

(b) 0.1 mm under-cut (c) 0.25 mm under cut

Figure F.2 *– Case 2 weld dimensions used in finite element model for nominal fillet weld 6.4 mm.*

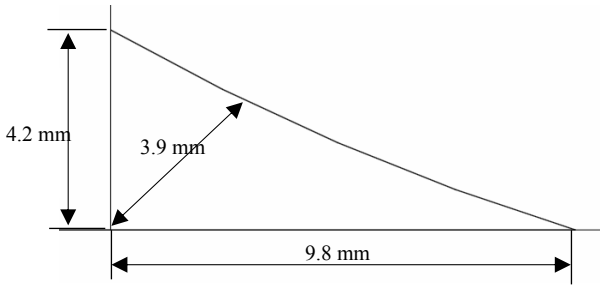

(a) No Under-cut

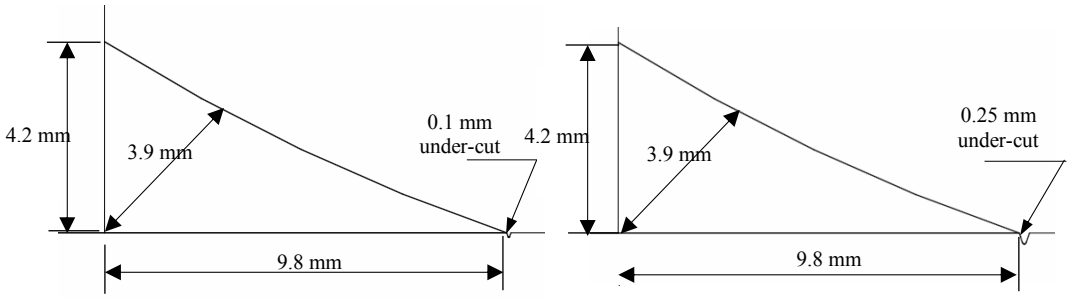

(b) 0.1 mm under-cut (c) 0.25 mm under cut

Figure F.3 *– Case 3 weld dimensions used in finite element model for nominal fillet weld 6.4 mm.*

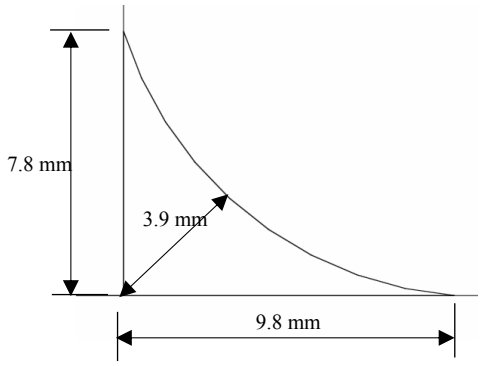

(a) No Under-cut

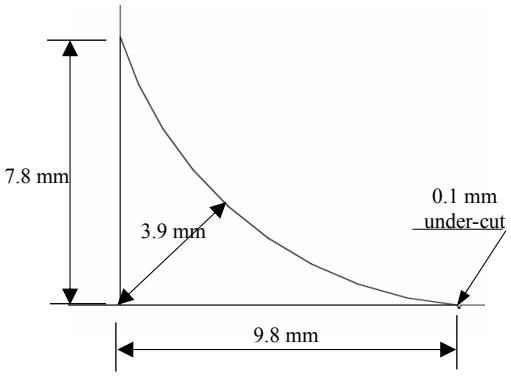

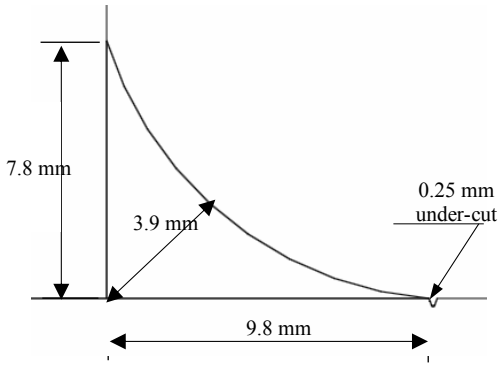

(b) 0.1 mm under-cut (c) 0.25 mm under cut

Figure F.4 *– Case 4 weld dimensions used in finite element model for nominal fillet weld 6.4 mm.*

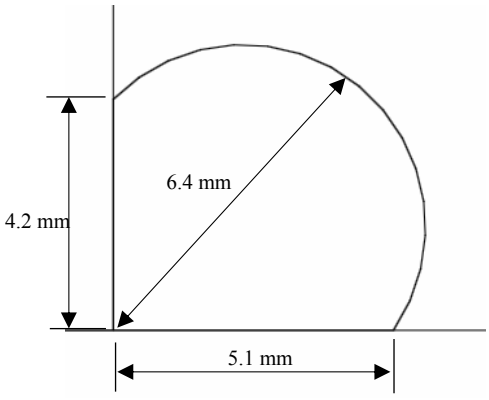

(a) No Under-cut

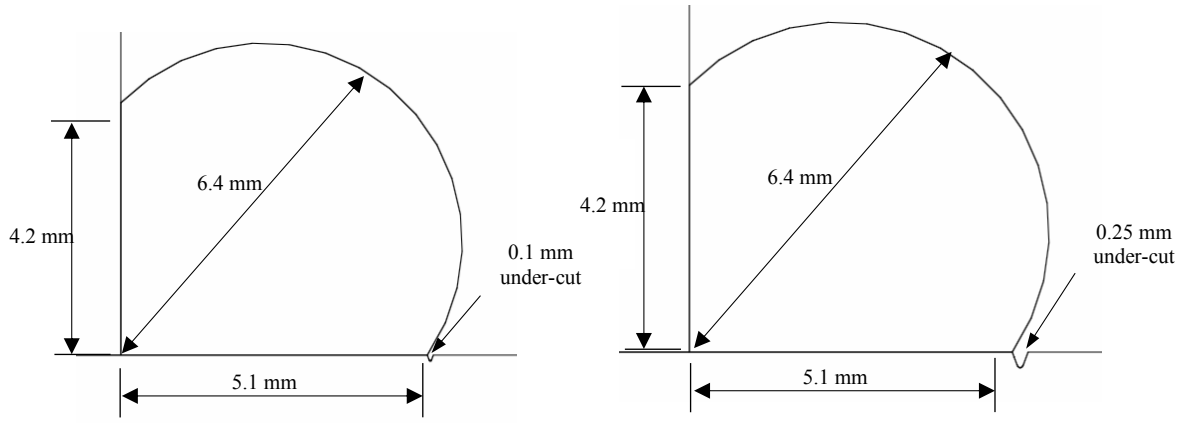

(b) 0.1 mm under-cut (c) 0.25 mm under cut

Figure F.5 *– Case 5 weld dimensions used in finite element model for nominal fillet weld 6.4 mm.*

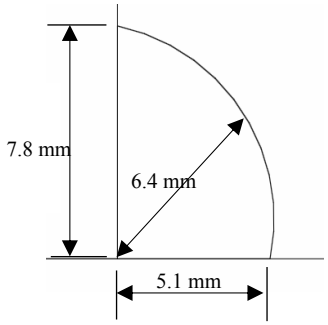

(a) No Under-cut

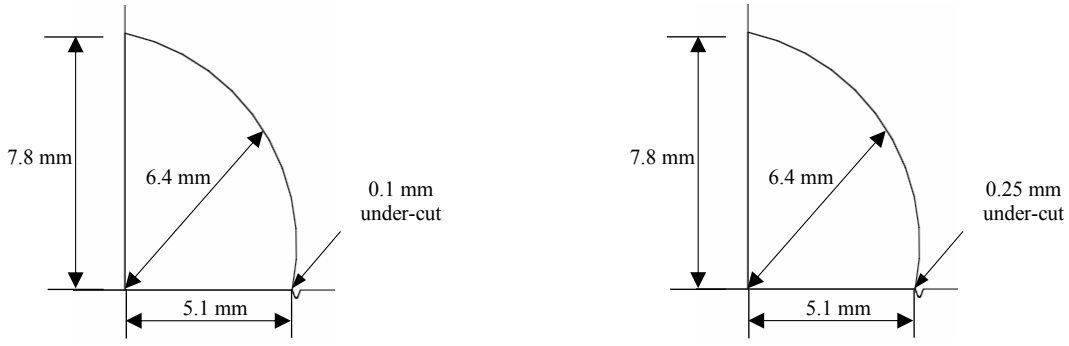

(b) 0.1 mm under-cut (c) 0.25 mm under cut

Figure F.6 *– Case 6 weld dimensions used in finite element model for nominal fillet weld 6.4 mm.*

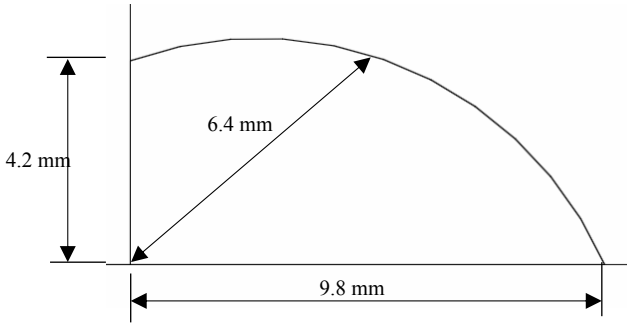

a) No Under-cut

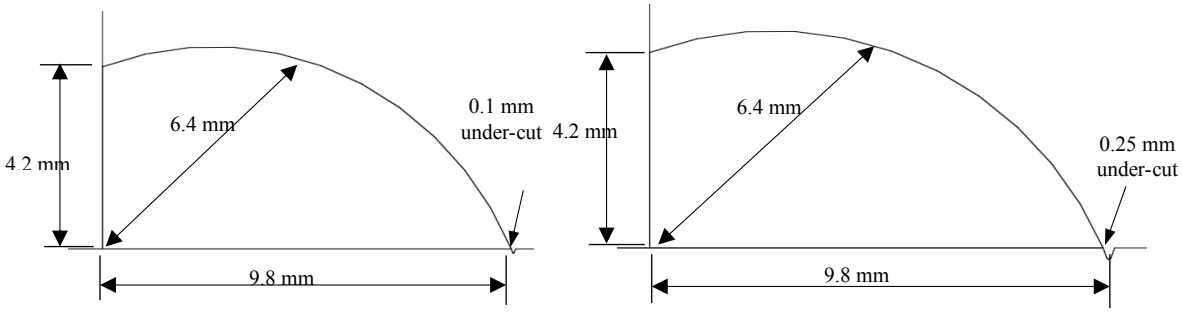

(b) 0.1 mm under-cut (c) 0.25 mm under cut

Figure F.7 *– Case 7 weld dimensions used in finite element model for nominal fillet weld 6.4 mm.*

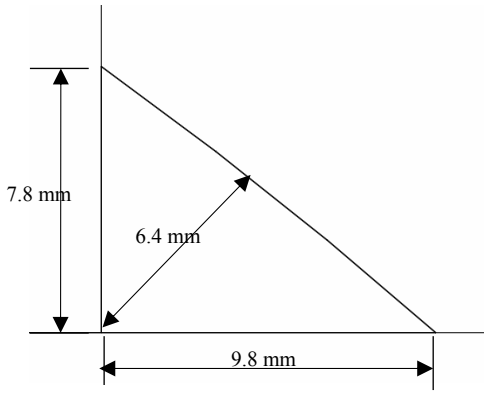

a) No Under-cut

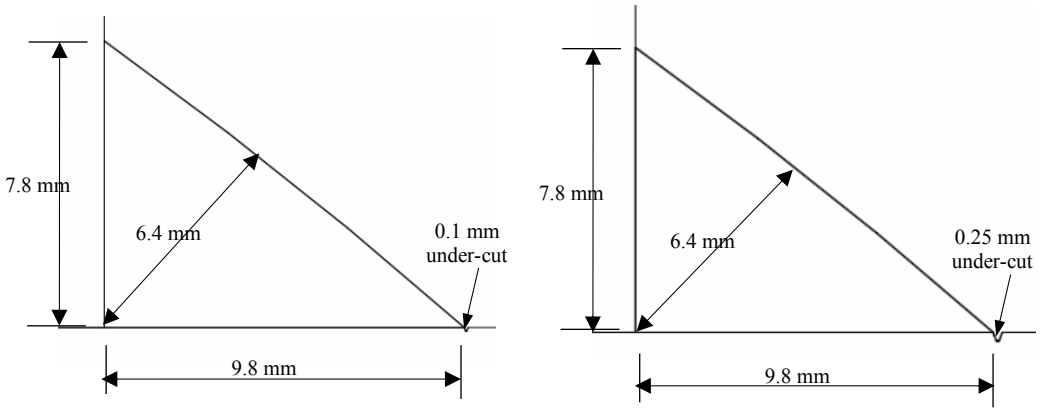

(b) 0.1 mm under-cut (c) 0.25 mm under cut

Figure F.8 *– Case 8 weld dimensions used in finite element model for nominal fillet weld 6.4 mm.*

APPENDIX G

The relationships between energy parameters and initial flaw for other cases of weld size 6.4 mm from Finite Element Analysis

Nominal 6.4 mm Weld Size - Case 1

Stress Range 25 MPa

$$\Delta W^p = 1.5x10^{-4} - 0.0005(a_{init} - 0.1) \quad \text{for } a_{init} > 0.1 \text{ mm}$$

$$\Delta W^p = 3.0x10^{-5} + 0.0013a_{init} \quad \text{for } a_{init} \le 0.1 \text{ mm}$$

$$\sigma_{max} = 453.33 - 326.36\left(a_{init} - 0.1\right) \quad \text{for } a_{init} > 0.1 \text{ mm} \qquad \text{(G.1)}$$

$$\sigma_{max} = 294.87 + 1584.6a_{init} \quad \text{for } a_{init} \le 0.1 \text{ mm}$$

Stress Range 50 MPa

$$\Delta W^p = 0.00027 - 0.0013(a_{init} - 0.1) \quad \text{for } a_{init} > 0.1 \text{ mm}$$

$$\Delta W^p = 0.00003 + 0.0029a_{init} \quad \text{for } a_{init} \le 0.1 \text{ mm}$$

$$\sigma_{max} = 522.693 - 290.97\left(a_{init} - 0.1\right) \quad \text{for } a_{init} > 0.1 \text{ mm} \qquad \text{(G.2)}$$

$$\sigma_{max} = 356.76 + 1659.3a_{init} \quad \text{for } a_{init} \le 0.1 \text{ mm}$$

Stress Range 75 MPa

$$\Delta W^p = 0.00047 - 0.0023(a_{init} - 0.1) \quad \text{for } a_{init} > 0.1 \text{ mm}$$

$$\Delta W^p = 0.00006 + 0.0046a_{init} \quad \text{for } a_{init} \le 0.1 \text{ mm}$$

$$\sigma_{max} = 578.44 - 301.21\left(a_{init} - 0.1\right) \quad \text{for } a_{init} > 0.1 \text{ mm} \qquad \text{(G.3)}$$

$$\sigma_{max} = 399.85 + 1785.9a_{init} \quad \text{for } a_{init} \le 0.1 \text{ mm}$$

Nominal 6.4 mm Weld Size - Case 2

Stress Range 25 MPa

$$\Delta W^p = 0.00023 - 0.0007(a_{init} - 0.1) \quad \text{for } a_{init} > 0.1 \text{ mm}$$

$$\Delta W^p = 0.00002 + 0.0017a_{init} \quad \text{for } a_{init} \le 0.1 \text{ mm}$$

$$\sigma_{max} = 476.34 - 184.18\left(a_{init} - 0.1\right) \quad \text{for } a_{init} > 0.1 \text{ mm} \qquad \text{(G.4)}$$

$$\sigma_{max} = 277.78 + 1985.6a_{init} \quad \text{for } a_{init} \le 0.1 \text{ mm}$$

Stress Range 50 MPa

$$\Delta W^p = 0.00035 - 0.0015(a_{init} - 0.1) \quad \text{for } a_{init} > 0.1 \text{ mm}$$

$$\Delta W^p = 0.00003 + 0.0033a_{init} \quad \text{for } a_{init} \le 0.1 \text{ mm}$$

$$\sigma_{max} = 548.1 - 217.99\left(a_{init} - 0.1\right) \quad \text{for } a_{init} > 0.1 \text{ mm} \qquad \text{(G.5)}$$

$$\sigma_{max} = 336.2 + 2119 a_{init} \quad \text{for } a_{init} \le 0.1 \text{ mm}$$

Stress Range 75 MPa

$$\Delta W^p = 0.00039 - 0.0011(a_{init} - 0.1) \quad \text{for } a_{init} > 0.1 \text{ mm}$$

$$\Delta W^p = 0.00006 + 0.0031 a_{init} \quad \text{for } a_{init} \le 0.1 \text{ mm}$$

$$\sigma_{max} = 605.91 - 277.17\left(a_{init} - 0.1\right) \quad \text{for } a_{init} > 0.1 \text{ mm} \qquad \text{(G.6)}$$

$$\sigma_{max} = 379.81 + 2261.1 a_{init} \quad \text{for } a_{init} \le 0.1 \text{ mm}$$

Nominal 6.4 mm Weld Size - Case 3

Stress Range 25 MPa

$$\Delta W^p = 0.00006 - 0.0004(a_{init} - 0.1) \quad \text{for } a_{init} > 0.1 \text{ mm}$$

$$\Delta W^p = 0.0006 a_{init} \quad \text{for } a_{init} \le 0.1 \text{ mm}$$

$$\sigma_{max} = 383.16 - 242.82\left(a_{init} - 0.1\right) \quad \text{for } a_{init} > 0.1 \text{ mm} \qquad \text{(G.7)}$$

$$\sigma_{max} = 169.14 + 2140.2 a_{init} \quad \text{for } a_{init} \le 0.1 \text{ mm}$$

Stress Range 50 MPa

$$\Delta W^p = 0.00015 - 0.0005(a_{init} - 0.1) \quad \text{for } a_{init} > 0.1 \text{ mm}$$

$$\Delta W^p = 0.0012 a_{init} \quad \text{for } a_{init} \le 0.1 \text{ mm}$$

$$\sigma_{max} = 466.57 - 323.71\left(a_{init} - 0.1\right) \quad \text{for } a_{init} > 0.1 \text{ mm} \qquad \text{(G.8)}$$

$$\sigma_{max} = 234.72 + 2318.5 a_{init} \quad \text{for } a_{init} \le 0.1 \text{ mm}$$

Stress Range 75 MPa

$$\Delta W^p = 0.00027 - 0.0013(a_{init} - 0.1) \quad \text{for } a_{init} > 0.1 \text{ mm}$$

$$\Delta W^p = 0.0023 a_{init} \quad \text{for } a_{init} \le 0.1 \text{ mm}$$

$$\sigma_{max} = 531.75 - 403.23\left(a_{init} - 0.1\right) \quad \text{for } a_{init} > 0.1 \text{ mm} \qquad \text{(G.9)}$$

$$\sigma_{max} = 272.79 + 2590 a_{init} \quad \text{for } a_{init} \le 0.1 \text{ mm}$$

Nominal 6.4 mm Weld Size - Case 4

Stress Range 50 MPa

$$\Delta W^p = 0.00016 - 0.0004(a_{init} - 0.1) \quad \text{for } a_{init} > 0.1 \text{ mm}$$

$$\Delta W^p = 0.0017 a_{init} \quad \text{for } a_{init} \le 0.1 \text{ mm}$$

$$\sigma_{max} = 337.16 + 228.31(a_{init} - 0.1) \quad \text{for } a_{init} > 0.1 \text{ mm} \quad \text{(G.10)}$$

$$\sigma_{max} = 171.08 + 1660.9a_{init} \quad \text{for } a_{init} \le 0.1 \text{ mm}$$

Stress Range 75 MPa

$$\Delta W^p = 0.000208 + 0.00008(a_{init} - 0.1) \quad \text{for } a_{init} > 0.1 \text{ mm}$$

$$\Delta W^p = 0.0023a_{init} \quad \text{for } a_{init} \le 0.1 \text{ mm}$$

$$\sigma_{max} = 392.807 + 235.87(a_{init} - 0.1) \quad \text{for } a_{init} > 0.1 \text{ mm} \quad \text{(G.11)}$$

$$\sigma_{max} = 218.37 + 1744.4a_{init} \quad \text{for } a_{init} \le 0.1 \text{ mm}$$

Nominal 6.4 mm Weld Size - Case 5

Stress Range 25 MPa

$$\Delta W^p = 0.00006 - 0.0001(a_{init} - 0.1) \quad \text{for } a_{init} > 0.1 \text{ mm}$$

$$\Delta W^p = 0.00002 + 0.0004a_{init} \quad \text{for } a_{init} \le 0.1 \text{ mm}$$

$$\sigma_{max} = 462.275 - 382.55(a_{init} - 0.1) \quad \text{for } a_{init} > 0.1 \text{ mm} \quad \text{(G.12)}$$

$$\sigma_{max} = 314.64 + 1476.3a_{init} \quad \text{for } a_{init} \le 0.1 \text{ mm}$$

Stress Range 50 MPa

$$\Delta W^p = 0.00008 - 0.0002(a_{init} - 0.1) \quad \text{for } a_{init} > 0.1 \text{ mm}$$

$$\Delta W^p = 0.00005 + 0.0005a_{init} \quad \text{for } a_{init} \le 0.1 \text{ mm}$$

$$\sigma_{max} = 541.635 - 407.45(a_{init} - 0.1) \quad \text{for } a_{init} > 0.1 \text{ mm} \quad \text{(G.13)}$$

$$\sigma_{max} = 376.77 + 1648.7a_{init} \quad \text{for } a_{init} \le 0.1 \text{ mm}$$

Stress Range 75 MPa

$$\Delta W^p = 0.00023 - 0.0007(a_{init} - 0.1) \quad \text{for } a_{init} > 0.1 \text{ mm}$$

$$\Delta W^p = 0.0001 + 0.0012a_{init} \quad \text{for } a_{init} \le 0.1 \text{ mm}$$

$$\sigma_{max} = 602.96 - 454.39(a_{init} - 0.1) \quad \text{for } a_{init} > 0.1 \text{ mm} \quad \text{(G.14)}$$

$$\sigma_{max} = 418.35 + 1846.1a_{init} \quad \text{for } a_{init} \le 0.1 \text{ mm}$$

Nominal 6.4 mm Weld Size - Case 6

Stress Range 25 MPa

$$\Delta W^p = 0.000031 - 0.00009(a_{init} - 0.1) \quad \text{for } a_{init} > 0.1 \text{ mm}$$

$$\Delta W^p = 0.00003 + 0.0002 a_{init} \quad \text{for } a_{init} \le 0.1 \text{ mm}$$

$$\sigma_{max} = 466.6 - 331.62\left(a_{init} - 0.1\right) \quad \text{for } a_{init} > 0.1 \text{ mm} \qquad \text{(G.15)}$$

$$\sigma_{max} = 330.05 + 1365.5 a_{init} \quad \text{for } a_{init} \le 0.1 \text{ mm}$$

Stress Range 50 MPa

$$\Delta W^p = 0.000098 - 0.00002(a_{init} - 0.1) \quad \text{for } a_{init} > 0.1 \text{ mm}$$

$$\Delta W^p = 0.00007 + 0.0007 a_{init} \quad \text{for } a_{init} \le 0.1 \text{ mm}$$

$$\sigma_{max} = 533.35 - 389.49\left(a_{init} - 0.1\right) \quad \text{for } a_{init} > 0.1 \text{ mm} \qquad \text{(G.16)}$$

$$\sigma_{max} = 381.1 + 1522.5 a_{init} \quad \text{for } a_{init} \le 0.1 \text{ mm}$$

Stress Range 75 MPa

$$\Delta W^p = 0.00026 - 0.0004(a_{init} - 0.1) \quad \text{for } a_{init} > 0.1 \text{ mm}$$

$$\Delta W^p = 0.0001 + 0.0016 a_{init} \quad \text{for } a_{init} \le 0.1 \text{ mm}$$

$$\sigma_{max} = 598.195 - 476.95\left(a_{init} - 0.1\right) \quad \text{for } a_{init} > 0.1 \text{ mm} \qquad \text{(G.17)}$$

$$\sigma_{max} = 422.25 + 1759.5 a_{init} \quad \text{for } a_{init} \le 0.1 \text{ mm}$$

Nominal 6.4 mm Weld Size - Case 7

Stress Range 25 MPa

$$\Delta W^p = 0.00025 - 0.0005(a_{init} - 0.1) \quad \text{for } a_{init} > 0.1 \text{ mm}$$

$$\Delta W^p = 0.00003 + 0.0018 a_{init} \quad \text{for } a_{init} \le 0.1 \text{ mm}$$

$$\sigma_{max} = 397.89 + 107.07\left(a_{init} - 0.1\right) \quad \text{for } a_{init} > 0.1 \text{ mm} \qquad \text{(G.18)}$$

$$\sigma_{max} = 308.67 + 892.23 a_{init} \quad \text{for } a_{init} \le 0.1 \text{ mm}$$

Stress Range 50 MPa

$$\Delta W^p = 0.00034 - 0.0006(a_{init} - 0.1) \quad \text{for } a_{init} > 0.1 \text{ mm}$$

$$\Delta W^p = 0.00003 + 0.003 a_{init} \quad \text{for } a_{init} \le 0.1 \text{ mm}$$

$$\sigma_{max} = 459.47 + 96.927\left(a_{init} - 0.1\right) \quad \text{for } a_{init} > 0.1 \text{ mm} \qquad \text{(G.19)}$$

$$\sigma_{max} = 360.57 + 989.08 a_{init} \quad \text{for } a_{init} \le 0.1 \text{ mm}$$

Stress Range 75 MPa

$$\Delta W^p = 0.0005 - 0.001(a_{init} - 0.1) \quad \text{for } a_{init} > 0.1 \text{ mm}$$

$$\Delta W^p = 0.00006 + 0.0043 a_{init} \quad \text{for } a_{init} \le 0.1 \text{ mm}$$

$$\sigma_{max} = 521.13 + 26.473\left(a_{init} - 0.1\right) \quad \text{for } a_{init} > 0.1 \text{ mm} \quad \text{(G.20)}$$

$$\sigma_{max} = 403.04 + 1180.9 a_{init} \quad \text{for } a_{init} \le 0.1 \text{ mm}$$

Nominal 6.4 mm Weld Size - Case 8

Stress Range 25 MPa

$$\Delta W^p = 0.0002 - 0.001(a_{init} - 0.1) \quad \text{for } a_{init} > 0.1 \text{ mm}$$

$$\Delta W^p = 0.0022 a_{init} \quad \text{for } a_{init} \le 0.1 \text{ mm}$$

$$\sigma_{max} = 469.91 - 231.37\left(a_{init} - 0.1\right) \quad \text{for } a_{init} > 0.1 \text{ mm} \quad \text{(G.21)}$$

$$\sigma_{max} = 267.24 + 2026.7 a_{init} \quad \text{for } a_{init} \le 0.1 \text{ mm}$$

Stress Range 50 MPa

$$\Delta W^p = 0.00037 - 0.0013(a_{init} - 0.1) \quad \text{for } a_{init} > 0.1 \text{ mm}$$

$$\Delta W^p = 0.00004 + 0.0032 a_{init} \quad \text{for } a_{init} \le 0.1 \text{ mm}$$

$$\sigma_{max} = 556.24 - 361.43\left(a_{init} - 0.1\right) \quad \text{for } a_{init} > 0.1 \text{ mm} \quad \text{(G.22)}$$

$$\sigma_{max} = 325.93 + 2303.2 a_{init} \quad \text{for } a_{init} \le 0.1 \text{ mm}$$

Stress Range 75 MPa

$$\Delta W^p = 0.00051 - 0.0019(a_{init} - 0.1) \quad \text{for } a_{init} > 0.1 \text{ mm}$$

$$\Delta W^p = 0.00005 + 0.005 a_{init} \quad \text{for } a_{init} \le 0.1 \text{ mm}$$

$$\sigma_{max} = 481.88 - 472.85\left(a_{init} - 0.1\right) \quad \text{for } a_{init} > 0.1 \text{ mm} \quad \text{(G.23)}$$

$$\sigma_{max} = 370.66 + 2530.7 a_{init} \quad \text{for } a_{init} \le 0.1 \text{ mm}$$